



AALBORG UNIVERSITY
DENMARK

Aalborg Universitet

Sensor Based Welding Automation Modelling System

Including a Specially Developed Low-cost Temperature Imaging System

Kjeldsen, Hans Christian Elm

Publication date:
2007

Document Version
Publisher's PDF, also known as Version of record

[Link to publication from Aalborg University](#)

Citation for published version (APA):

Kjeldsen, H. C. E. (2007). *Sensor Based Welding Automation Modelling System: Including a Specially Developed Low-cost Temperature Imaging System*. Denmark.

General rights

Copyright and moral rights for the publications made accessible in the public portal are retained by the authors and/or other copyright owners and it is a condition of accessing publications that users recognise and abide by the legal requirements associated with these rights.

- Users may download and print one copy of any publication from the public portal for the purpose of private study or research.
- You may not further distribute the material or use it for any profit-making activity or commercial gain
- You may freely distribute the URL identifying the publication in the public portal -

Take down policy

If you believe that this document breaches copyright please contact us at vbn@aub.aau.dk providing details, and we will remove access to the work immediately and investigate your claim.

Sensor Based Welding Automation Modelling System

Including a Specially Developed Low-cost Temperature Imaging
System

Hans Christian Kjeldsen Orye
M.Sc. M.Eng.

Ph.D Thesis
December 2005

Supervisors:

Hans Holm, Professor, Ph.D.
Department of Production, Aalborg University
Denmark

Jens Klæstrup Kristensen, Professor, Ph.D.
Technical Vice President, Welding and Production Innovation
FORCE Technology, Brøndby, Denmark

Bjørn Langeland, Associate Professor, Ph.D.
Department of Production, Aalborg University
Denmark

Opponents:

Ole Madsen, Associate Professor, Ph.D.
Department of Production, Aalborg University
Denmark

Torben A. Andersen, Senior Vice President
Odense Steel Shipyard, Lindø, Odense
Denmark

Herschel B. Smartt, Senior Scientist, Dr.
Idaho National Engineering Laboratory
Idaho, USA

Department of Production, Aalborg University, Denmark
FORCE Technology, Brøndby, Denmark
Copyright ©



Danish Summary

Denne rapport beskriver en ny mulig arkitektur af et temperatur-tilbagekoblings-system, der bl.a. kan anvendes til lukket sløjfe styring af robotiseret lysbuesvejsning. Arkitekturen er baseret på et offline svejse planlægningssystem og et online svejse styresystem. Offline svejse planlægningssystemet genererer en reference som følges af online lukket-sløjfe styresystemet. Hovedmålet med denne arkitektur er, at udvikle en metode der muliggør automatisk design af online lukket-sløjfe styresystemet. Dette styresystem kan bruges til styring af tykpladet metal geometrier, og systemet tilbagekobler temperaturer på overfladen af geometrien. Temperaturerne er tilbagekoblet ved hjælp af et temperatur vision system.

Denne rapport beskriver også udviklingen af temperatur vision systemet, som er baseret på et lavpris CCD-chip kamera. Under udviklingen af dette temperatur vision system er en metode til at måle temperaturer emittansuafhængigt udviklet og testet.

Det samlede system er til sidst testet med et meget positivt resultat.

English Summary

The report describes a possible architecture of a thermal feedback system for closed loop control of robotic arc welding. The architecture is based on an off-line planning system for welding and an on-line welding control system, where the off-line planning system builds the reference to be followed by the on-line closed loop system. The main aim of this architecture is to develop a method by which thermal feedback welding control systems can be designed automatically. This control system is meant for control of welding of thickwalled sheet metal geometries and the system feeds back the temperatures on the surface of the geometry. The temperature is fed back by a temperature imaging system.

The report also describes the development of the temperature imaging system, which is based on a low cost CCD-array camera. During the development of this temperature imaging system a method to measure the temperature independently of the emittance is developed and tested.

The full system is finally tested with a very positive result.

Preface

This thesis is the result of three years research work carried out at the Department of Production, Aalborg University, Denmark and FORCE Technology, Brøndby, Denmark and constitutes one for the requirements in order to acquire an industrial Ph.D. degree. The thesis is addressed to the opponents of the thesis, FORCE Technology, Aalborg University and others with interest in methods for closed loop welding on application of temperature distribution models as well as the imaging system, which was developed to measure these temperature distributions.

The research work documented in this thesis was carried out in the period from October 1999 to November 2002 and was sponsored partly by Danish Academy of Technical Sciences (ATV), Lyngby, Denmark and partly by FORCE Technology, Brøndby, Denmark.

Formalities

This thesis consists of a main report and 14 appendixes and enclosures. The development of the imaging system is documented in the appendixes. A summary of this work is given in the main report.

Throughout this thesis, words of special interest for the context are enhanced by use of *italic*.

Acknowledgements

I would first of all like to thank my supervisor at Aalborg University, Professor Hans Holm, for his always very inspiring, profound and enthusiastic help. I would also like to thank my industrial supervisor from FORCE Technology, Professor Jens Klæstrup Kristensen, for his inspiring help and support not at least in the final part of the documentation period.

Also thanks to Erling Rask who helped with the preliminary experiments in the laboratory of Institute for Production, Aalborg University. Thanks to Kim Hardam Christensen who was a great help in the design of the communication between the X-Y table and the weld machine, which was an important part of the on-line system. Thanks to Kjeld Petersen who was a great help in the design of the temperature imaging system. I would also like to express my thanks to Research

Preface

and Development manager Torben Funder-Kristensen at Danfoss A/S who offered me very good working conditions which enabled me to finalise this thesis.

I finally owe my wife Helena thousand loving thanks for always supportive attitude and patience despite that many holidays, weekends and evenings have been spent on this thesis.

Sønderborg, December 2005

Hans Christian Orye

Contents

DANISH SUMMARY	III
ENGLISH SUMMARY	V
PREFACE.....	VII
CONTENTS.....	IX
1. BACKGROUND AND INTRODUCTION.....	1
1.1. WHY NUMERICAL CONTROLLED WELDING?.....	1
1.2. WAMOS STARTING POINT.....	2
1.2.1. <i>Model Properties</i>	2
1.2.2. <i>Off-line Programming</i>	3
1.2.3. <i>Close Loop Welding Execution</i>	4
1.2.4. <i>Motivation for Closed-Loop Welding Temperature Control</i>	4
1.3. THE WAMOS-SYSTEM	6
1.3.1. <i>The off-line System</i>	8
1.3.2. <i>The On-line System</i>	13
1.3.3. <i>Combining the Off-line and the On-line System</i>	14
1.3.4. <i>Philosophy and Hypotheses of the WAMOS-System</i>	14
1.3.5. <i>The Quality Reference</i>	16
1.4. NATIONAL AND INTERNATIONAL WORK	17
1.4.1. <i>Work in Denmark Outside Department of Production, Aalborg University, Relevant to the WAMOS-Method</i>	17
1.4.2. <i>International Work Related to the WAMOS-Method</i>	18
1.4.3. <i>National and International Work Related to the Developed Temperature Imaging System</i>	21
2. PROBLEM STATEMENT.....	25
2.1. CHOICE OF METHOD.....	26
2.2. THE STEPS OF THE <i>WAMOS-METHOD</i>	27
2.3. PRELIMINARY PROJECT DECISIONS	28
3. INPUT AND OUTPUT VARIABLES.....	31
3.1. DETERMINATION OF INPUT VARIABLES.....	32
3.2. DETERMINATION OF OUTPUT VARIABLES	33
3.3. CHOICE OF INPUT AND OUTPUT VARIABLES	34

4. OFF-LINE PREPARATION SYSTEM	43
4.1. THE OFF-LINE SYSTEM	44
5. OFF-LINE IDENTIFICATION.....	49
5.1. INITIATING REQUIREMENTS.....	49
5.2. IDENTIFICATION OF $G_M(s)$ BASED ON $G_S(s)$	51
5.2.1. Selection of the Parameter α	53
5.2.2. Choose the Degree of Numerator and Denominator	55
5.2.3. Calculate $G_M(s)$	56
6. DESIGN OF ON-LINE CONTROLLER.....	59
6.1. THE P-CONTROLLER.....	59
7. TEMPERATURE IMAGING SYSTEM.....	65
7.1. TEMPERATURE IMAGING SYSTEM DESIGN.....	65
7.1.1. Choice of camera.	66
7.1.2. Optical design	69
7.1.3. Raw Images of the Temperature Imaging System	74
7.1.4. Position of the camera.....	76
7.2. EMITTANCE INDEPENDENT MEASUREMENTS.....	80
7.3. CALIBRATION OF THE TEMPERATURE IMAGING SYSTEM.....	82
7.4. TEMPERATURE MEASUREMENTS COMPARED TO OFF-LINE SIMULATIONS .	84
7.5. COMPONENTS OF THE TEMPERATURE IMAGING SYSTEM.....	86
8. ON-LINE WELD EXECUTION SYSTEM	89
8.1. EXPERIMENTAL EQUIPMENT	90
9. EXPERIMENTS.....	93
9.1. OFF-LINE PREPARATION EXPERIMENTS	94
9.2. FIRST WELD-TEST	103
9.3. SECOND WELD-TEST	108
9.4. THIRD WELD-TEST	115
9.5. DISCUSSION OF THE EXPERIMENTAL RESULTS	122
10. CONCLUSION	123
10.1. CONTRIBUTIONS FROM AND ACHIEVEMENTS OF THE PROJECT.....	123
10.2. USABILITY OF THE <i>WAMOS-METHOD</i> AND SYSTEM	126
10.3. USABILITY OF THE TEMPERATURE IMAGING SYSTEM	128
10.4. FUTURE WORK AND PERSPECTIVES	128
BIBLIOGRAPHY.....	131

Appendices and Enclosures

A. INPUT FILE	137
B. PROGRAM CODE OF THE OFF-LINE PREPARATION SYSTEM...	141
C. OFF-LINE IDENTIFICATION - MATLAB CODE	147
C.1. THE MAIN PROGRAM	148
C.2. OFF-LINE IDENTIFICATION PROGRAM.....	150
D. ON-LINE CONTROLLER – MATLAB CODE.....	155
E. CAMERA TESTS.....	159
E.1. TEST OF CAMERA INPUT - OUTPUT LINEARITY	159
E.2. SMEARS EFFECT	160
F. SPECTRAL RADIANCE FROM A GTAW ARC	161
F.1. SELF-MADE MEASUREMENTS PERFORMED AT AAU	161
<i>F.1.1. Spectral Radiance, Visible Electrode</i>	<i>162</i>
<i>F.1.2. Spectral Radiance, Not Visible Electrode</i>	<i>163</i>
F.2. SELF-MADE MEASUREMENTS PERFORMED AT FORCE.....	164
F.3. FORMER MEASUREMENTS PERFORMED AT FORCE.....	165
F.4. THEORETICAL FIGURES OF THE SPECTRAL RADIATION IN PURE ARGON .	165
F.5. THEORETICAL FIGURES OF THE SPECTRAL RADIANCE FOR ARGON IN AIR SURROUNDINGS.....	167
G. OPTICAL CALCULATIONS	171
H. EMITTANCE INDEPENDENT TEMPERATURE IMAGING SYSTEM...	179
H.1. PROOF OF HOW TO PERFORM TEMPERATURE MEASUREMENTS INDEPENDENT OF THE FACTOR OF EMITTANCE	180
H.2. OPTICAL DESIGN OF THE EMITTANCE INDEPENDENT CAMERA	183
I. CALIBRATION OF THE TEMPERATURE IMAGING SYSTEM.....	193
I.1. CALIBRATION IN A FURNACE	194
<i>I.1.1. Calibration By Means of an Iron Plate</i>	<i>196</i>
<i>I.1.2. Calibration By Means of a Platinum Plate.....</i>	<i>198</i>
I.2. CALIBRATION ON A NON-MOVING WELD	202
I.3. CALIBRATION ON A MOVING WELD.....	203
J. TEMPERATURE MEASUREMENTS COMPARED TO OFF-LINE SIMULATIONS	205
K. JOURNAL PAPER (2003)	209
L. CONFERENCE PAPER (2002)	215
M. EXAMPLES OF JOINTS.....	223
N. DATA SHEETS OF THE CHOSEN CAMERA	225

1. Background and Introduction

During the last century a dominating development in industrial manufacturing has been braking down geographical and cultural barriers for economy, manufacturing and transport. In parallel to this the ruling industry management-philosophies have, to a large extent, divided the management part from the actual production, which means the production can in fact be placed anyplace where the necessary infrastructure is available. Many examples of moving-out productions to countries and areas where the salary is low but which still have sufficient infrastructure have as a consequence been seen.

The different societies have, however, not been able to reduce the national and geographical constraints to the same degree. Therefore, it is still so that e.g. Denmark is completely dependent on a production and employment within the borders of Denmark in order to maintain and develop the ordinary standard of living and welfare.

This conflict demands a strong Danish effort and is the initiating motivation for this Welding Automation MOdelling System (WAMOS).

1.1. Why Numerical Controlled Welding?

There are six main reasons for choosing numerically controlled welding for manual welding:

1. The influence of labour cost is greatly reduced, which means that the production may be placed also in high income areas as e.g. Denmark or Europe.
2. Some welding tasks are impracticable without use of numerical welding.
3. By numerically controlled welding, the quality of the weld is improved.
4. By numerically controlled welding, weld quality repeatability is improved.
5. Numerically controlled welding can run at a higher velocity than manual welding.
6. Welding by numerically controlled equipment does not have to be interrupted due to welder fatigue.

These five points together constitute a wide-ranging improvement of the production when choosing numerically controlled welding.

1.2. WAMOS Starting Point

Based on the above argumentation for putting an effort into numerically controlled welding (Section 1.1) a retrospect of the work at Department of Production, Aalborg University within numerically controlled welding is now presented. This ends with the motivation for closed-loop welding temperature control.

1.2.1. Model Properties

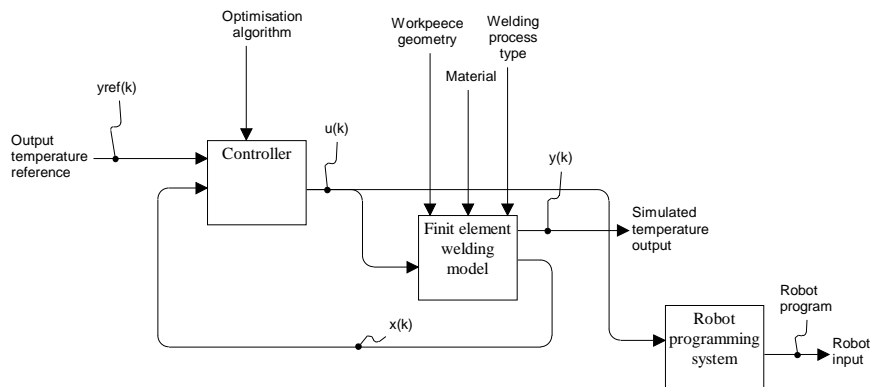
Since 1988 the Department for Production, Aalborg University has been working with development of methods for programming and control of robotic welding. The original control development was focused on gain scheduling based on parameterised models of which all the parameters are determined by regression analysis based on the Taguchi method. The programming development was based on weld process models, which were developed by regression analysis based on the Taguchi method. The regression analysis was based on performance of welding experiments [Madsen, 1992], [Lauridsen, 1992], [Andersen, 1997A] and [Andersen, 1997B]. On one hand regression models have proven to be applicable. On the other hand the Taguchi method has, however, shown to be a very resource demanding method, which requires a substantial amount of experiments to identify the model parameters. This is a problem when the models generated by the Taguchi method are often rather specific models, i.e. their range of validity with respect to e.g. variations in groove geometry and posture is unsatisfactorily limited. A small variation in workpiece geometry forces the welding planner to provide new welding process models. In productions with a large variety of groove geometries the need for weld process models is consequently large. In many cases the investment needed to produce the necessary models required to enable computer automated welding is so big that it becomes prohibitive for their generation.

During the development of the parameterised process models experiments were made to test the geometric limits of the models. It was during these experiments visually possible to discover that the temperature distribution in the workpiece became uneven when the geometry was changed causing the weld process to turn out with deficits. This experience, together with the conflict that the parameterised process model used only works under limited geometry variations though the geometry varies considerably in most production environments, made the research team look for a new type of model.

The choice fell on a finite-element model. By developing a finite-element model, which is capable of calculating the temperature distribution in the workpiece to be welded, it is now possible to simulate the heat distribution. Using a finite-element model has the advantage that the correctness of the model is in principle independent of the workpiece geometry on which the model is applied. By choosing a finite-element model, the number of welding experiments necessary to automate welding programming for a wide variety of welding tasks, was therefore expected to be considerably reduced compared with the number of experiments necessary to automate welding programming based on the above discussed parameterised process models. It should also be emphasised, that the above-discussed process models are confined to be applied only when a welding can be carried out through steady state or quasi-steady states. Contrary to parametric process models finite-element models apply to modelling welds, which are performed in transient state, as well as to modelling welds, which are carried out in steady state.

1.2.2. Off-line Programming

The finite-element model is meant to form the basis of a weld *planning system* (Figure 1-1).



$u(k)$:

Input variables:

- Power
- Position of torch
- Orientation of torch
- Velocity of torch
- Orientation velocity of torch
- Filler wire speed

$y(k)$:

Simulated realised output temperatures.

$x(k)$:

Simulated temperatures chosen to be fed back including output temperatures.

Figure 1-1 The weld *planning system*.

A weld planning is performed by letting a controller control the weld process simulation. The simulation system above (Figure 1-1) is established by means of a finite-element model. The controller ensures that the simulation output trajectory $y(1) \dots y(k) \dots y(N)$ is as close to the desired simulation output trajectory $y_{\text{ref}}(1) \dots y_{\text{ref}}(k) \dots y_{\text{ref}}(N)$ as possible.

Hereby a trajectory of inputs $U(1) \dots U(k) \dots U(N-1)$ is generated. As this input trajectory is the one that best possibly creates the desired simulated welding process output, this input trajectory should be applied to the physical equipment, which again generates the input trajectory to the physical weld execution. Therefore this input trajectory should be embedded into the program, which executes an open-loop physical welding. Controlling a finite-element model introduces the possibility of controlling the weld based on a reference. The reference could e.g. be a desired temperature distribution at the bottom of the workpiece including full penetration. By means of the temperature distribution profile reference it is possible to define the desired weld quality. The *planning system* schedules the weld-task based on the predefined temperature quality reference.

1.2.3. Close Loop Welding Execution

As the *planning system* is based on a finite-element model that calculates the temperature distribution in the full geometry of the workpiece at every time-step (t) the temperatures at the surface of the workpiece constitute part of these temperatures. By saving the calculated temperatures of that surface in which the arc touches the workpiece an estimate of what the temperature distribution should appear like on the surface of the workpiece is generated. It is now obvious that this scheduled surface temperature profile could be compared to the actually archived surface temperature distribution by the automatic welding equipment. This idea of comparing measured surface temperature distributions with simulated distributions fostered the idea of generating an on-line control-system and was hereby the genesis of the WAMOS-system and is in this work named the *proposed weld-system architecture*.

1.2.4. Motivation for Closed-Loop Welding Temperature Control

The motivation for developing a temperature feedback welding execution control-system emerges because conditions under which weldings are expected in industrial shop floors do often differ from the conditions assumed in the models which form the basis for creation of the welding process input trajectory.

The following types of deviations are types of deviations, which can be compensated for by feeding back temperature measurements to a compensation control-system:

1. Workpiece displacement.

In relation to the model by which the off-line generated robot program has been generated the workpiece is displaced. This causes a weld torch path error; but temperature distribution feedback and control may compensate for that path error.

2. Grove geometry deviations.

The geometry of the physical weld groove differs from the geometry of the weld groove of the model used for off-line programming. Temperature distribution feedback and control may compensate for that difference.

The difference may be differences in groove gap, groove angle, preparation misalignment, and solid workpiece cross sectional area or groove nose height.

3. Weld sequence changes.

The sequence in which a series of weld seams are planned to be welded may have been changed during the execution for instance in order to minimise distortion.

This may cause the initial temperature of a given groove to differ from that planned.

Temperature distribution feedback and control may compensate for that.

4. Heating from neighbour welds.

The heating from a neighbour weld of a groove may differ from that planned for instance due compensated welding trajectories of the neighbour seam.

Temperature distribution feedback and control may compensate for that.

5. Preheating deviation.

For workpieces to be preheated in order to ensure proper metallurgical quality of the welds the preheating may differ from that planned.

In that case temperature distribution feedback and control may compensate for that.

If automatic welding is carried out without geometry sensor feed forward or temperature sensor feedback precaution to ensure required weld quality is often taken by adding more heat and reinforcement metal than required from a point of view of workpiece strength. This results in significantly reduced productivity and in larger workpiece distortions than necessary. Hence lack of use of geometry feed forward and temperature feedback prohibits, such

trust in off-line optimised weld trajectories, that they can be used as basis for optimally performed weld execution.

Hence development of temperature feedback control methods will support off-line generated weld trajectory optimisation. As many good control results have been reported on geometry feed forward control (See [Madsen, 1992], and [Andersen, 20001]) this work has been focussed on temperature feedback control.

1.3. The WAMOS-System

In this section, an introduction to the WAMOS-system is given. This introduction is meant to give an understanding of the elements in the WAMOS-system and the philosophy of the system. First, a general introduction to the system is given followed by a description of the off-line part of the system (Section 1.3.1), then the on-line part of the system (Section 1.3.2), and subsequently with the combination of the two systems (Section 1.3.3). This is continued by the philosophy and hypothesis of the WAMOS-system (Section 1.3.4) and by a discussion of the welding quality reference (Section 1.3.5).

The main aim of the WAMOS project is to reach a method by which thermal feedback welding control-systems can be designed. The proposed method enables on-line feedback control of the weld quality of the internal of thick walled workpieces. This is expected to be possible even though the temperature in the internal of the workpiece cannot be measured during the process. This expectation is justified below. It is, however, first to be mentioned that it is possible to measure the temperatures of the surfaces of the workpiece during the process. The surface on which the welding process is carried out has therefore been chosen as surface for temperature feedback of the process. Consequently, a camera is planned to be mounted on the welding robot. This surface temperature feedback is achievable by means of a camera, which is able to measure the temperature of the surface of the workpiece. This camera is developed in the WAMOS project to fulfil the difficult task to measure the surface temperature profile under and around the very strong electric arc. The camera is actually a conventional and very cheap CCD-chip based black and white camera. By replacing the conventional CCD-chip filter with a special and more suitable band-pass filter and by developing specially designed optics for heat measurements, it is possible to obtain rather good surface temperature profile images. In Chapter 7 the camera is described in further details.

The reason why, on-line control of the internal of thick-walled workpieces becomes possible, as mentioned above, by feeding back the surface

temperatures only, is that an off-line generated surface temperature reference (Figure 1-2) has been generated.

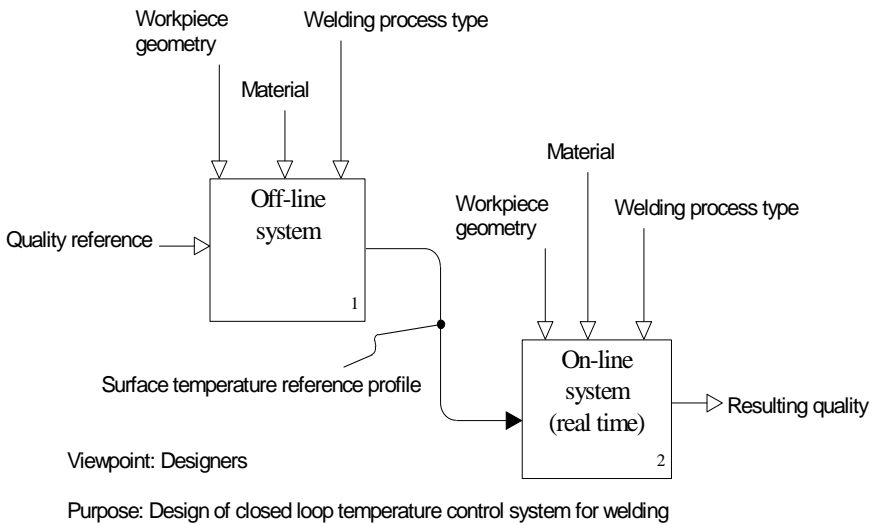


Figure 1-2 Overall view of the *proposed weld-system architecture for thermal feedback welding control.*

The surface temperature reference is generated by the off-line system, which uses the finite-element model to simulate the process by calculating the temperatures of the internal of the workpiece. As reference for the off-line system a desired temperature profile is defined, which enables the user to obtain a desired weld quality during the weld process. This temperature profile (off-line reference) could define the desired temperatures on the backside of the workpiece, i.e. the side of the workpiece where measurement of the surface temperatures to ensure full penetration is normally not possible. The defined reference temperature profile for the off-line system represents the quality which is gained firstly by the off-line *planning system* and succeedingly by the on-line closed-loop execution system.

When controlling the temperatures inside the workpiece by simulating the process using the finite-element method the theoretical temperatures in all the node points are known, also the nodes on the surface. The temperature of the nodes on that surface, where the arc touches the workpiece and where temperatures can be measured by the CCD-camera, are saved as output from the off-line *planning system* and are used as reference temperature input in the on-line system. In the on-line system the off-line generated surface temperature is used as temperature reference and compared to the surface temperatures measured by the temperature-measuring CCD-camera.

Hence the surface temperature reference for the on-line system has been generated in the off-line *planning system* by recording that surface temperature trajectory which results from a temperature distribution

1. Background and Introduction

trajectory from the internal of the workpiece which ensures a desired weld quality (for instance that the seam bottom temperature has reached a maximum which is above the melting point temperature). It is therefore expected that:

1. when welding the workpiece in such a way that the achieved surface temperature trajectory is the same as the off-line generated surface reference temperature trajectory,
2. then the temperature trajectory of the internal of the physical workpiece will equal corresponding the temperature trajectory of the off-line modelled workpiece from which the reference surface temperature trajectory was generated.

A surface temperature trajectory of the physical workpiece which is equal to the surface reference trajectory may be generated by many different weld power input trajectories each resulting in different temperature trajectories of the internal of the workpiece. Such trajectories subsequently result in different weld qualities. However, if the welding control vector is started in the physical welding in the same way as it has been planned in the off-line system then the temperature trajectory of the internal of the workpiece is expected to develop as the temperature trajectory of the internal of the off-line workpiece model. This is because the on-line control-system maintains a surface temperature trajectory, which equals the reference surface temperature trajectory.

The *proposed weld-system architecture* for thermal feedback welding control can be divided into two sub-systems (Figure 1-2):

An **off-line** *planning system* (Section 1.3.1).

An **on-line** executing disturbance-compensating control-system (Section 1.3.2).

1.3.1. The off-line System

The off-line *planning system* is based on a reference model, a controller and a finite-element model. The reference model, which serves as input is composed of a quality reference, the workpiece geometry and material data. The output is a surface temperature reference, which is to be used by the on-line closed-loop system (Figure 1-3).

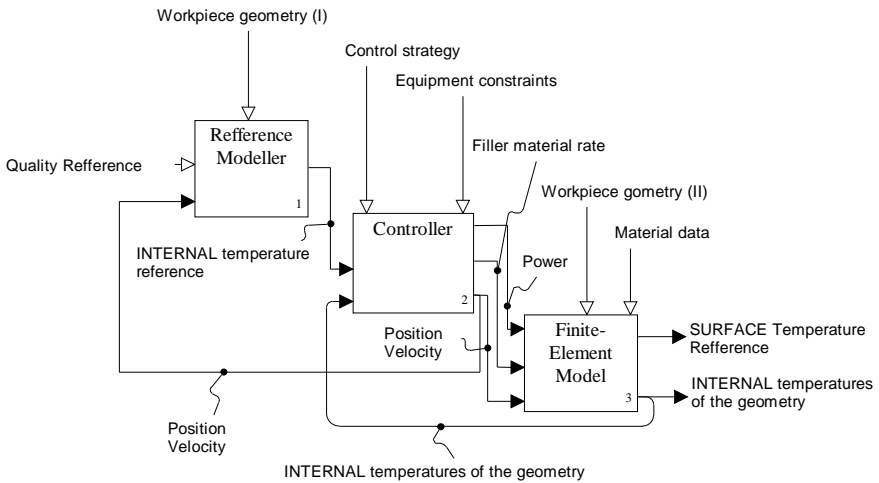


Figure 1-3 Architecture of the off-line *planning system*.

This off-line *planning system* contains all the elements necessary for planning the motion and power trajectories. This type of planned trajectories can be used directly in an on-line open-loop execution system.

Because the off-line system is capable of simulating the trajectories and the temperature in the full geometry, it is also capable of generating a reference for the on-line closed-loop system, which receives a sensor feedback on the selected surface temperature output of the system. As the off-line *planning system* generates the on-line reference based on knowledge of the internal workpiece temperatures and its surface temperatures, it is natural to store some of those temperatures as reference for the on-line closed-loop system. The simulated temperatures to be stored are the temperatures of the surface of the workpiece as those temperatures are comparable with the temperatures measured by the camera in the on-line closed-loop sensor feedback execution system. When using this temperature field, information from the off-line *planning system* is transferred to the on-line closed-loop system. The knowledge lying implicitly in these heavily calculated temperature states is transferred to and used in the on-line system. When comparing the on-line sensor feedback with a signal based on knowledge from the off-line system, not only the temperature in the surface of the workpiece is expected to be sustained but also, to a large extent, the internal temperatures of the workpiece.

The controller for the off-line *planning system* could take many different forms. Presently, the controller is based on a simple search algorithm, which searches for the largest error between the desired reference temperatures and the achieved simulated temperatures. The controller includes equipment constraints as maximum velocity and acceleration of the robot to be controlled and max and minimum power of the welding equipment to be controlled in the on-line system. Based on the search algorithm and the

1. Background and Introduction

different constraints, the controller finds its path through the weld-task and minimises the error in accordance with the defined off-line temperature reference input, derived from e.g. the ISO standard terms. The output of the controller is the position, the velocity and the welding power.

Instead of sending the position and the velocity to the robot and the power request to the welding equipment as in the physical on-line system, a finite-element model is fed with this input. The purpose of feeding a FE model with the input is to simulate the controlled welding process. The FE model's control-input is the input, which brings the welding process nearest possible to its desired state. The best input possible for the on-line weld execution system is generated in the form of the output surface temperature distribution from the simulated off-line control-system. Hereby does the off-line *planning system* work as an *off-line preparation system*, which performs the preparation for the physical on-line closed-loop system.

One of the key parts in the off-line system is the model. To plan a weld trajectory based on this system requires a model, which describes the process sufficiently well. The question of, what is sufficiently well, will have to be answered by testing the model at different stages. Presently, a non-linear model has been developed at the Department of Production, Aalborg University. The model is based on a non-linear model of heat conduction, on a linear model of the radiation and convection, and on a simplification of the model of the weld pool to heat conduction in solid material. The heat source is modelled as a Gaussian heat distribution. Because of the chosen modelling method and the architecture of the system it is possible to use this off-line system with arbitrary workpiece geometry. This control-system is continuously adapting the control variables to the states of the workpiece. This is done through the use of the reference heat profile of the bottom of the workpiece (Figure 1-4), which is compared with the achieved heat distribution at the bottom of the workpiece in the FE model. The off-line system will then use optimal control to compute a new set of adapted welding control variables.

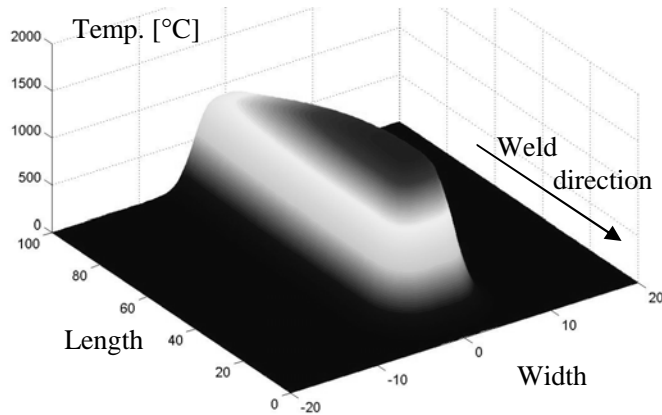


Figure 1-4 Off-line quality reference. The desired temperature distribution in the bottom of the workpiece. In this case the workpiece is a plate where the desired temperature distribution ensures full penetration [Terp, 1999].

Based on the desired temperature or quality reference (Figure 1-4) and the calculated internal and surface temperatures of the geometry, the controller (Figure 1-3) calculates the error temperature profile of the bottom for each time-step (Figure 1-5).

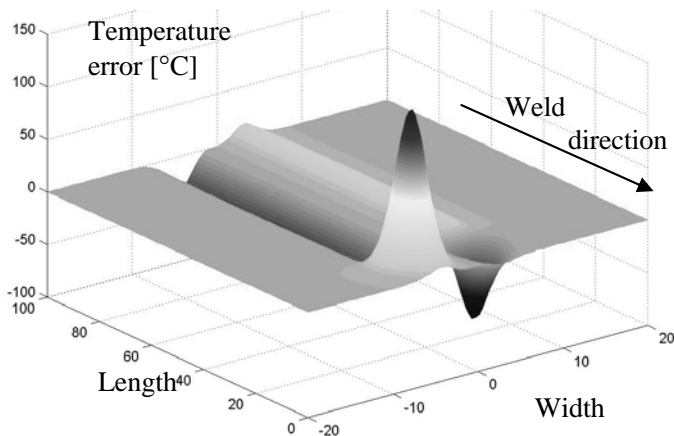


Figure 1-5 The error temperature profile illustrates the error between the off-line quality reference and the finite-element calculated temperature distribution in the bottom of the workpiece [Terp, 1999].

Based on the error temperature profile the controller generates the input settings for the coming time-step. This estimated new path (or coming position) and heat input is sent to the finite-element program, which calculates the effect of the new position and heat input. The finite-element system works as a model, which simulates the actual world and calculates for each time-step the internal temperatures of the geometry to be welded (Figure 1-6).

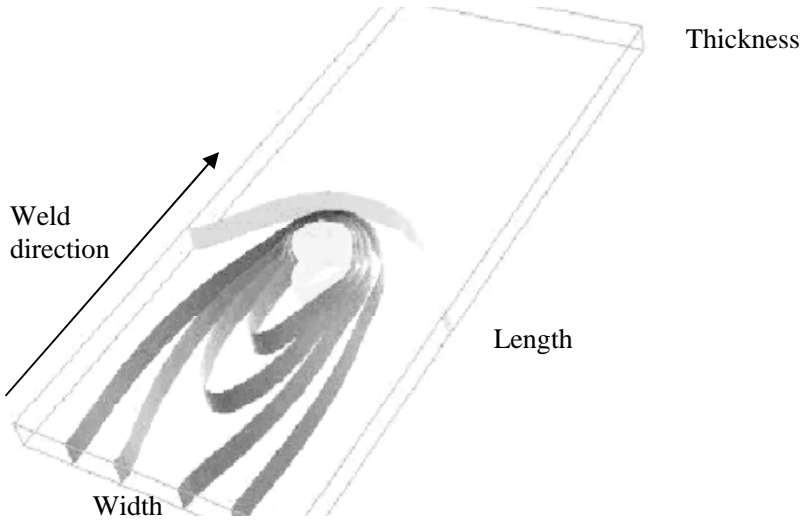


Figure 1-6 Temperature isotherms illustrating the temperature distribution in the full geometry at a given time-step calculated by the finite-element system in the off-line simulation system [Terp, 1999].

Some of these internal temperatures are fed back to the reference modeller and compared to the quality reference. The loop is now closed.

The off-line system does not use a predefined weaving pattern but creates its own arbitrary weaving path in accordance with the optimal control strategy.

Using the presented architecture for the off-line process *planning system* (Figure 1-3) enables use of planning and programming open-loop robotic welding execution as well as closed-loop robotic weld execution. Since a finite-element program carries out the simulation, the trajectories of the temperatures of the surface where the arc touches the workpiece constitute part of those temperatures, which are simulated (Figure 1-7).

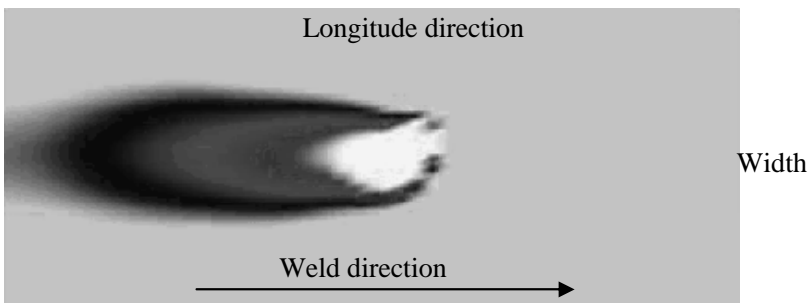


Figure 1-7 The temperature distribution at the surface of the workpiece, the surface where the arc touches the plate. This surface temperature distribution generated by the off-line system is used as reference in the on-line system.

These simulated surface trajectories form good temperature reference trajectories for a physical closed-loop welding control-system (the on-line system), which feeds back measured temperatures from the surface of the workpiece (Figure 1-8), where the arc touches the workpiece and where CCD-camera measuring is possible.

1.3.2. The On-line System

The on-line system is a control-system comparable with the off-line system. The main difference is that the on-line system does not have a control loop around a finite-element model describing the world but it has a loop around the actual world itself. The actual world is in the on-line system called Joining Material (Figure 1-8).

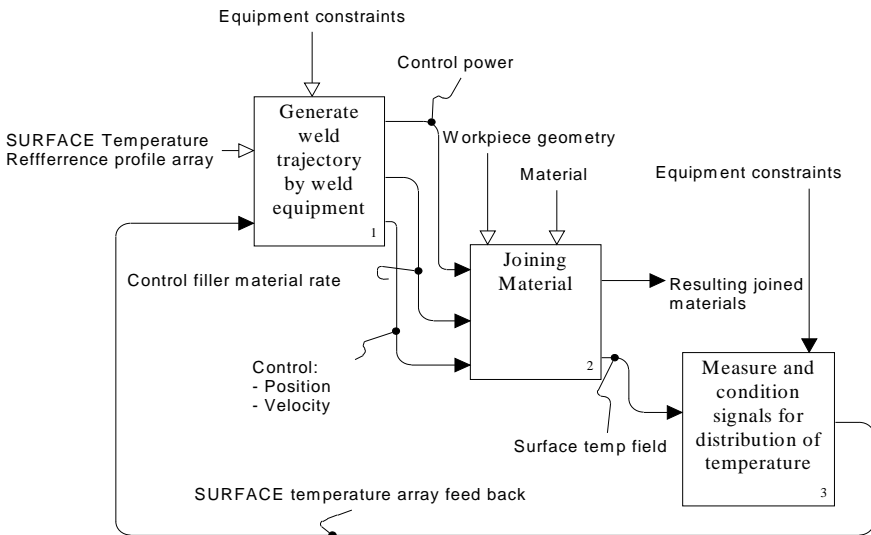


Figure 1-8 Architecture of the on-line control-system, which is real-time controlling the physical welding procedure.

A CCD-camera, which captures the surface temperature profile around and underneath the electric arc, generates the feedback in the on-line feedback system. The camera is placed under the “measure and condition signals for distribution of temperature” box of Figure 1-8, which delivers the feedback to the controller placed in the “generate weld trajectory by weld equipment” box of Figure 1-8. This feedback surface temperature profile is compared with the surface temperature reference profile previously simulated by the off-line system. Based on the error between those two temperature profiles the controller in the “generate weld trajectory by weld equipment” box of Figure 1-8 now generates a new path, set point and heat input for the coming time-step. The robot and the weld equipment carry out this weld job and the material is joined. Then the camera measures the feedback again and the whole procedure is repeated. This loop will continue for every time-step till welding is completed.

In the off-line system a finite-element model of the heat conduction was used. A simplified version of the off-line model is used for the design of the on-line state space control-system for real-time closed-loop control of welding (Chapter 6). Using a simplification of the FE model enables use of a well-understood control-system design method for design of the real-time control-system (Chapter 5 and 6).

In the off-line system the controller attempts to reach the desired temperature distribution in the bottom of the workpiece contrary to the on-line control-system, which attempts to reach the desired temperature distribution at the surface where the arc touches the workpiece.

1.3.3. Combining the Off-line and the On-line System

Both the off-line and the on-line system can be used independently but the largest advantage of the WAMOS-method comes from the combination of the off-line and the on-line system. The off-line system is a heavy control-system, which is planning the weld task based on advanced physical finite-element calculations. Whereas the on-line system is a fast real-time system performing the weld-task based on the knowledge from the off-line system. The off-line system is used for a two-fold purpose. One is to prepare the on-line welding by generating the surface temperature control reference. The other one is to serve as a tool for design of the control laws by which the on-line control-system is to be operated. Based on the off-line generated surface temperature reference and the off-line generated on-line controller the on-line system performs the welding based on closed loop control.

1.3.4. Philosophy and Hypotheses of the WAMOS-System

Combining the slow finite-element based off-line system with the much faster real-time controlled on-line system gives the possibility to specify the desired welding quality as a temperature profile or temperature distribution anywhere in the workpiece. If the workpiece is based on two plates, which are to be welded as a butt joint*, then this quality reference could be the temperature distribution on the backside of the workpiece to ensure full penetration. Based on this temperature distribution reference (quality reference) the off-line system schedules the weld-task. During this planning simulation the welding torch position, the power input, and the temperature distribution in the full geometry of the workpiece is calculated at every time-step. The output used for the on-line system is the temperature distribution in the surface where the arc touches the workpiece. This output is stored for every time-step and used as reference in the on-line system (Figure 1-2).

* Butt joint is defined in enclosure A

The real-time running on-line system controls the actual weld by comparing the on-line generated surface temperature reference with the actual surface temperature distribution measured by the developed camera. The hypothesis is: If the on-line system can obtain the same surface temperature profile as calculated by the off-line system, then the temperature isotherms in the internal of the workpiece will be just as calculated in the off-line model.

The controller in the on-line system is designed based on the off-line system. The controller is built from a simple transfer-function where the transfer-function is generated based on the off-line system. The transfer-function is generated by applying the simulation with one or more step-input(s). The number of step-input(s) is decided from the number of desired control variables. The idea is to apply the step-input in the off-line simulation environment at every *weld-step*.

The definition of the designation, a *weld-step*, used in the context above is: A *weld-step* is a welding where the geometry and the remaining process parameters have a specific size. When the weld reaches a corner, the corner is designated a new *weld-step* to the extent variables and parameters are constant during the corner welding and the string to be welded after the corner is designated a new *weld-step*. Every time the geometry or the remaining process parameters change and hence causes a significant influence on the variables of the control-system the weld will be designated as a new *weld-step*.

One or more transfer-functions are generated for each of the *weld-step*. Based on these off-line generated transfer-function(s) corresponding controller(s) are generated for every *weld-step*. The generation of the transfer-functions and the corresponding controllers are done by use of theory from Dieter Franke [Franke, 1993].

Because, one or more transfer-functions are generated for each *weld-steps*, when welding, even simple workpieces, often many transfer-functions and their respective controllers are needed. This fact could be seen as a problem if the transfer-functions were to be built based on real world experiments but in this case they are automatically built based on the off-line system. It is mainly in this step the WAMOS-system is distinguished from other methods for control of welding e.g. control by parameterised process models (Section 1.2). This method for generating on-line controllers based on the knowledge in the off-line system is in this project identified and elaborated. This method is through out the rest of this report designated the *WAMOS-method*.

The different controllers built by the off-line system are used in the on-line system at the respective *weld-steps*. Therefore, during continuous welding the on-line system has to change controller at every *weld-step* e.g. when welding in a corner or when the local geometry changes. This approach of

1. Background and Introduction

generating many specific controllers instead of a few general controllers became possible because of the off-line system and the newly developed theory of Dieter Franke.

Now to summarise: The off-line system generates based on a quality reference (Figure 1-4) a surface temperature profile for each time-step (Figure 1-7). This surface temperature reference is saved and used as reference in the on-line system. The off-line system also generates the controller, for each of the *weld-steps*, to be used in the on-line system.

The philosophy of the WAMOS-system is: *The off-line system could be regarded as a transformation engine, which transforms the quality reference to welding rules in the form of on-line controllers and a surface temperature reference distribution, which is comparable to the actual temperature distribution measured by the camera in the on-line control-system.*

The hypothesis of the WAMOS-system: *If the on-line system is capable of reaching the same surface temperature as simulated in the off-line system, and if the on-line system is started with the same inputs and states as used in the off-line generated optimal trajectory then the internal temperatures of the geometry of the physical workpiece should be the same as simulated. Hereby a control link from the desired bottom temperature reference to the on-line control-system, which creates the actually archived bottom temperature, has been established.*

1.3.5. The Quality Reference

Welding quality is defined by the quality of a weld after end of welding. Apart from the direct influence of weld defects like e.g. cracks and pores this quality is for example measured by various mechanical and corrosion test methods. For steel structures especially hardness, tensile strength, impact toughness and fatigue strength are often considered as is also the resulting distortion. While the fatigue strength mainly is governed by the weld geometry most other mechanical properties are dependent on the material composition and the resulting microstructure. The microstructure is on its side controlled by the composition and the thermal cycle resulting from the welding process and especially the temperature cooling rate is of high importance. Material composition is decided in advance where temperature cooling rate and weld geometry are process dependent factors. To reach the desired welding quality has during the last two decades until today in far majority been based on an understanding of the influence of various microstructures, hardness models, the welder's experience and experiments. It is well know that the temperature distribution in the weld has a major impact on the strength characteristics and distortion quality of the welding. Nevertheless the welding society today has no or only little experience in specifying welding quality based on requests to temperature distribution. Besides the *WAMOS-method* no other method is known to enable the user on

beforehand to define the desired welding quality in temperature distribution terms. By defining the desired temperature distribution (the quality reference) the WAMOS-system facilitates the possibility to define different requests related to the temperature and temperature changes in the weld. For instance, it enables specifications of the heat-affected zone (haze zone) or the size and position of the weld pool to ensure a high strength welding or to minimize the heat input to minimize distortion.

As the welding society is not familiar with defining requirements to the welding by defining a desired temperature distribution this task will require some education of the future user. It is, however, believed that it is going to be easier to specify the temperature reference (the quality reference) than to specify the actual welding parameters, which is the practice today. This is substantiated by the facts that:

1. The relation between temperature distribution trajectory and resulting weld quality in strength and distortion terms are better understood than the relation between on one hand weld control variables and weld parameters and on the other hand weld quality in terms of strength and distortion. Deciding the quality reference in temperature distribution terms is actually physically understandable whereas deciding the weld parameters requires a big quantity of practical experience.
2. The material structure and properties obtained by different cooling rates is already for most steel types described by regression analysis based hardness models.

Though the new discipline to define a quality reference will require a new way of thinking it is, however, expected to be a change for the better.

1.4. National and International Work

In this section relevant nationally and internationally published work, which is comparable to the developed *WAMOS-method* and the developed temperature-measuring camera system, is presented.

1.4.1. Work in Denmark Outside Department of Production, Aalborg University, Relevant to the *WAMOS-Method*

To the knowledge of the writer there is no person in Denmark who pursues the use of an off-line planning system combined with an on-line executing disturbance-compensating control-system. The most related work known takes place at Department of Manufacturing Processes, Danish Technical University (DTU). In this work neural network is used to control the wire feed speed, the weaving amplitude and the welding current in butt joint

welding of plate geometries. The process used is gas metal arc welding (GMAG) where the width of the gap, which is measured by a laser scanner in front of the process, is used as input to the neural network [Christensen, 2003]. Force Technology is presently continuing this work with the aim of being able to weld a full V-groove i.e. as well the root pass as the filler passes. [Klæstrup Kristensen, 2005]. Force is furthermore developing a new concept in which knowledge based and empirically based models are combined into a hybrid model. In this way it is possible to take advantage of the best properties of each model type [Klæstrup Kristensen, 2005] and [Weiss, 2004].

1.4.2. International Work Related to the *WAMOS-Method*

Though much literature search has been done no research activity has been identified, which pursues the use of an off-line planning system combined with an on-line executing disturbance-compensating control-system.

In the off-line system the goal is to obtain a virtual automatic welding trajectory planning system. By such a system such reference trajectories are produced, which are used by the on-line closed-loop welding execution control-system, which has to perform the planned welding.

In the on-line system it is wanted to develop methods by which closed-loop (sensor based) welding disturbance-compensating control can be performed. Such closed-loop control-systems must enable the best possible pursuit of optimised trajectories, which are planned by the off-line system.

Though no organizations or authors have been found, who pursue the combination of an off-line planning system and an on-line executing disturbance-compensating control-system, two Swedish authors and five American authors have been identified who pursue sub elements of the WAMOS-system.

The two Swedish authors both work with Volvo Aerospace. One of the writers has developed an off-line simulation system comparable to the WAMOS off-line system ([Ericsson, 2002] and [Ericsson, 2001]). The other writer has developed a system for measuring the temperature distribution based on an Infra Read (IR) camera [Henrikson, 2002]. Their off-line trajectory planning system presently works for gas tungsten arc welding (GTAW). The main aim of the system is to minimise the number of trials on complex geometries by simulating the distortion and the temperature distribution. In short the system is based on the following steps (Figure 1-9):

1. The component to be manufactured is created in a CAD/CAM system.
2. The model in step one is imported to the Robot simulation system (IGRIP) and the finite-element analysis system (FEA) software, either using a direct translator or by using a neutral file format, such as IGES or STEP. In the Robot simulation software a model of the work cell is

- created. A welding program (including robot motion, weld speed, arc current, etc.) is developed. Check for collisions are also made.
3. The welding variables, i.e., robot co-ordinates, weld speed and arc current, are exported from the Robot simulation software to the FEA analysis software. Hence no computer controlled weld trajectory optimization is performed with respect to joint strength.
 4. Thermal histories and residual stresses are predicted in the FEA software. An optimization of weld velocity is performed to generate the lowest component deformation while keeping full penetration. Hence only one control variable is comprised by the optimization with respect to torsion.
 5. The optimized welding parameters are exported to the Translator where a translation of the program to a specific robot programming language is made.
 6. The final program is downloaded to the manufacturing equipment (Irb and weld controller systems).

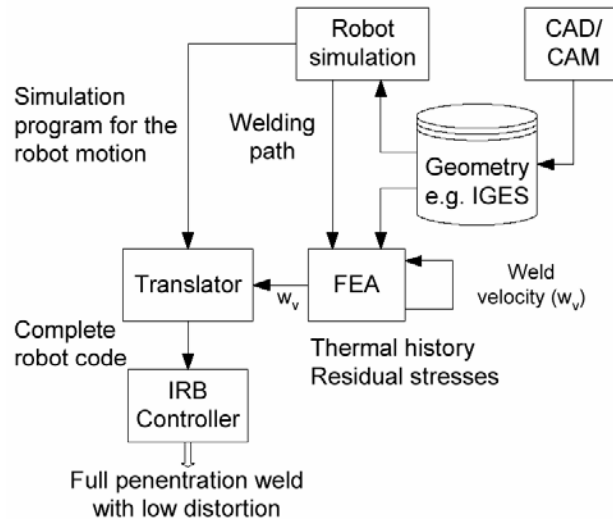


Figure 1-9 The overall architecture of the Swedish off-line trajectory planning simulation system [Ericsson, 2001].

They do not mention how they achieve full penetration. It is therefore not known which type of control-system they have incorporated or if they are using trial and error. It is thus not clear, how their on-line control strategy should adapt to a workpiece geometry change, nor how the trajectory preparation should adapt to a workpiece geometry change.

From the point of view of the objectives of this thesis it is interesting that [Ericsson, 2001, 2002] apparently plans the weld trajectory such that distortions of the workpiece are minimised. Minimisation of workpiece distortions is one of the objectives of this thesis. This distortion minimisation

1. Background and Introduction

is meant to be achieved by enabling heat input minimised weld temperature trajectories to form the reference for execution of the welding.

Such trajectories leave very little space for weld disturbances, because such weldings are performed so close to the limit of permissible penetration geometry qualities that small disturbances e.g. in groove shape may cause penetration deficiencies. Therefore welding with minimised induction of energy into the workpiece is only economically accomplished if they are performed under closed-loop (sensor feedback) control for compensation of disturbances to the optimal weld trajectory.

The Swedish writers have also developed a temperature imaging system [Henrikson, 2002] based on an IR camera, which is for validation of their off-line planning system. The temperature imaging system is apparently not meant for on-line control of disturbances as in the WAMOS on-line system. They have not mentioned on-line control by means of the camera and the temperature imaging system presently works as a delayed data collecting system, which enables the writer to analyse the images after end welding, not real-time. To get around changing emissivity due to the changing surface structure they soot the workpiece before the weld experiment. This solution would for cost reasons not be applicable in an industrial environments. Also the fact they use an IR camera makes the system very expensive and heavy. These indications all substantiate the belief that the camera is not meant for a disturbance-compensating control-system.

Four of the five American authors identified do finite difference thermal diffusion modelling in order to use it for manual weld-trajectory preparation. Only the most recent authors of those do three-dimensional modelling. None of the Americans try to do the trajectory planning automatically. They do not even mention it ([Doumanidis, 2001], [Doumanidis, 1999], [Korizis, 1999], [Doumanidis, 1998], [Moore, 1997], [Moore, 1996], [Kovacevic, 1996] and [Kovacevic, 1995]).

Three of the five authors have developed thermal feedback closed-loop control based on application of a time series model (a so called ARMA model) ([Doumanidis, 2001], [Doumanidis, 1998] and [Kovacevic, 1996]). Their goal is to ensure the overall geometric, material and mechanical integrity of the joint. They do, however not account for the control objectives, nor for how they might relate these to a control criterion. It is thus not clear, how their control strategy should adapt to a workpiece geometry change, nor how the trajectory preparation should adapt to a workpiece geometry change.

The fourth author Kevin L. Moore (et al.) focuses his control development efforts to achieve constant material and power induction into the workpiece by GMAW-process ([Moore, 1996] and [Moore, 1997]), so he does not yet

exploit the knowledge stored in his thermal conduction model to design a control-system, by which he can control the distribution of the power, he induces into his workpiece.

The fifth American author has built an on-line system, which performs real-time disturbance-compensation control of a GTAW welding process as in the WAMOS on-line control-system. The author controls the weld based on a single input single output (SISO) state space control-system where an IR spot sensor feeds back the temperature behind the tail of the weld. The structure of this on-line system is much alike the structure of the WAMOS on-line system. The WAMOS on-line system is, however, a multiple input multiple output (MIMO) system. The control objective in the work of the fifth American is full penetration. This author has also made experiments very similar to the experiments made during this WAMOS project (see Chapter 9). The experiments were, however, only based on a single input single output (SISO) control-system. The control reference is made based on experiments only and there is not accounted for any off-line trajectory planning [Fan, 2002].

There are several papers describing the use of temperature-measuring camera systems in laser welding applications (e.g. [Brüggemann, 1996]). None of these writers are, however, found to pursue the two-fold objective of the WAMOS project. One reason for the relatively high effort spent on camera systems in laser welding compared to that spent in industry using the more widespread welding process gas metal arc welding (GMAW) and GTAW welding is that laser welding is performed automatically, only. Another reason is that the laser beam is easily filtered off the sensor compared with filtering the undesired radiation from the electrode in e.g. GTAW welding off the sensor.

In the following national and international work related to the developed temperature imaging system is presented.

1.4.3. National and International Work Related to the Developed Temperature Imaging System

In addition to the developed *WAMOS-method*, a temperature imaging system has been developed based on a CCD-chip camera.

In this work the three main objectives are as follows:

1. To make use of a Low-cost CCD-chip based camera instead of an IR camera.
2. Off filtration of undesired radiation from the gas tungsten arc and the tungsten electrode.

3. Emittance independent temperature measurements *

Though much literature search has been done no research activity has been identified, which pursues all three objectives.

To Make Use of a Low-cost CCD-chip Based Camera Instead of an IR Camera

Though several writers discuss the use of CCD-chip based cameras for locating the joint, detecting the joint start and end, tracking the seam, measuring the joint size, measuring the weld bead profile, monitoring the weld pool behaviour etc. (e.g. [Lucas, 2000] and [Smith, 1996]) no writers were found who pursue the objective to use a Low-cost CCD-chip based camera for measuring the temperature in and around a GTAW or GMAW welding arc. CCD-cameras or IR cameras have in several cases been used in laser welding applications (e.g. [Lhospitalier, 1999]). Although laser welding will also involve a hot light emitting plume that possibly even may turn into a plasma, laser welding does opposed to arc welding not have a wide arc and a light-emitting electrode, which must be off filtered to measure the temperature in and around the weld. The fact that GTAW welding has been used in this project only makes the undesired electrode radiation stronger compared to other arc welding methods.

The idea to use a CCD-camera came from a French writer ([Renier, 1998] and [Renier, 1996]). Also he used the camera for laser welding (YAG welding).

Off Filtration of Undesired Radiation From the Gas Tungsten Arc and the Tungsten Electrode

Concerning the off filtration of undesired radiation from the gas tungsten arc and the tungsten electrode one writer has been identified [Farson, 1998]. Similarly to the WAMOS project Farson uses a band-pass filter to off filter radiation from the arc. Farson also uses a shielding plate. The shielding plate is working as a wall between the electrode and the camera to avoid direct radiation into the camera from the electrode and arc (Figure 1-10).

* To measure the temperature independently of the emissivity coefficient (See Appendix H).

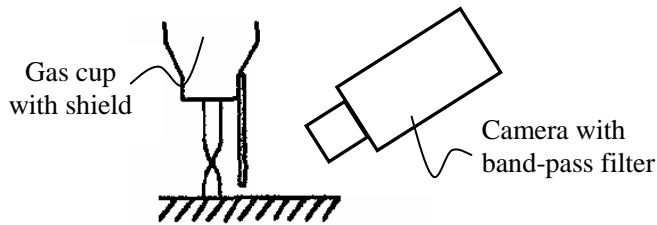


Figure 1-10 Shielding plate attached to gas cup [Farson, 1998].

Though the paper only documents the spectral lines of the gas tungsten arc from 200 nm to 1000 nm the band-pass filter, with a width of 15.2 nm, chosen in Farsons work is placed at 1064 nm. The combination of a band-pass filter and shielding enabled Farson to make temperature measurements 12 mm behind and 5 mm to the side of the arc centre point from 450 C° to 900 C°. In Farsons work an IR spot sensor has been used and the sensor is calibrated based on measurements from thermocouples. Though thermocouples have been used for calibration the dilemma of changing emissivity is however not mentioned.

An analysis of the GMAW spectrum has also been identified [Agapiou, 1999]. This paper presents measurements of the spectrum of the light emitted from a GMAW welding arc for the purpose of designing a laser based seam tracking sensor based on CCD technology. The paper, however, only documents the spectral radiation from 150 nm to 970 nm. An old analysis of the optical emission from weld arcs (Ar-O₂ shield gas and CO₂ shield gas) and their effects on the performance of welding robot vision systems has also been identified [Alan, 1985]. In this paper the spectral radiation is documented from 610 nm to 920 nm.

Emittance Independent Temperature Measurements

It is a fact that the coefficient of emissivity varies from material to material. It is also a fact that the surfaces of the elements to be welded in heavy metal industry are not always clean. The surfaces contain oil, dust, soot rust, etc.. Despite these facts only one writer has been identified who pursues the goal to perform temperature measurements independently of the conditions of the metal sheet plates to be welded [Sato, 1997]. This Japanese writer has identified that if the temperature is measured by ultra violet (UV) thermal radiation then the measurements are less dependent on the coefficient of emissivity. The writer uses a CCD-chip camera with a band-pass filter at 350 nm having a width of 90nm. In this work it was concluded that absolute temperature measurements could be performed with this set-up without any emissivity correction. The writer performed this experiment with success on laser welding and GTAW welding. The laser welding was performed on the same side as the camera was measuring whereas the GTAW welding experiments were performed on the side of the plate opposite to the camera.

1. Background and Introduction

By measuring on the opposite side of where the gas Tungsten arc is active the writer avoided the problematic to off filtering the radiation of the arc and the radiation from the electrode.

Also an Italian writer has pursued the goal to enable absolute temperature measurements independently of the coefficient of emission. This writer has improved the measurement accuracy of the temperature of a flame from a military jet engine to build an absence flame alarm [Parenti, 1994]. The writer uses a CCD TV colour camera to measure the absolute temperature of the flame by combining the radiation intensity measured by two different colours of the camera. By measuring the radiation from one point of the flame by two different colours in the camera the writer has a measure of the radiation radiated from one point measured in two different wavelengths. Combining the intensities measured in two different wavelengths of the same point Planck's law opens the possibility to eliminate the coefficient of emission. By this method the Italian writer has enabled absolute temperature measurements independently of the coefficient of emission. This is a technique also used in some commercial pyrometers.

Based on this introduction to the WAMOS project the actual problem to be solved is formulated in the following chapter.

2. Problem Statement

The main goal of this project is to develop a design method, the WAMOS-method, by which real-time welding control-systems can be designed. The by the WAMOS-method designed control-systems must enable real-time controlled welding of thickwalled material by feeding back temperatures from the surface of the material. The temperatures are fed back by means of a temperature sensitive camera.

By means of the WAMOS-method, developed in this project, the proposed weld-system architecture (Section 1.3) will be tested in accordance with the hypothesis (Section 1.3.4):

The hypothesis of the WAMOS project: If the on-line system is capable of reaching the same surface temperature as simulated in the off-line system then the internal temperatures of the geometry should be the same as simulated. Hereby a control link from the desired bottom temperature, the off-line quality reference, to the on-line control-system and back to the actually archived bottom temperature has been established.

This hypothesis is tested by performing thermal feedback closed-loop welding experiments on a workpiece with nominal weld groove geometry and on a workpiece with characteristic geometric disturbances (Chapter 9).

The main objective of this proposed system and developed *WAMOS-method* is to reduce the cost and improve the robustness and quality of automatic welding. The system is also expected to enable more complex welds to be coped with as well as a wider variety of welding situations compared to present weld-systems (See Section 1.2). Finally desired weld properties may be obtained through an intelligent choice of the initial reference temperature profile.

All this is expected by the use of a combined *off-line preparation system* and an on-line execution system for automatic preparation and execution of robotic welding (See Section 1.3).

An extraordinary goal has been to develop an imaging system based on a CCD-chip-camera. The temperature imaging system must enable measurement under and around the arc. The system must measure temperatures at 1530 °C (melting point of metal) and at least 100 degrees down.

2. Problem Statement

The temperature imaging system developed is based on the cheap CCD-chip technology instead of the much more expensive IR camera technology, which typically is used for temperature measurements.

The temperature measurement capability of the temperature imaging system is investigated by calibrating its output on a temperature reference (Appendix I). The temperature imaging system is further evaluated by comparing the surface temperature distribution measured by the camera with the corresponding simulated surface temperature distribution generated by the *off-line preparation system*.

Based on this problem formulation and the introduction (Chapter 1) the choice of method for design of real-time control-systems is chosen in the following section.

2.1. Choice of method

In the introduction the idea of combining an off-line system based on a heavy, geometry independent finite-element model and on an on-line system based on several small and fast models was introduced and argued.

The approach of generating many specific controllers instead of a few general controllers became possible because of the availability of the off-line system and the newly developed theory of Dieter Franke [Franke, 1993]. Dieter Franke describes a method by which it is possible fully automatically to identify a transfer-function. The identification can be based on the *output* measured on a system, which has been, subject to application of a step-input. Dieter Franke also describes a method by which it is possible to generate the control feedback matrices based on the transfer-function identified.

These two methods together make it possible fully automatically to generate many specific controllers from the more general and heavy finite-element model.

Because the Dieter Franke method makes it possible easily and fully automatically, to generate a controller by means of a finite-element model it is chosen to use the method of Dieter Franke as part of the *WAMOS-method*.

The *WAMOS-method* is a sequential method and in the following section the steps of the *WAMOS-method* are listed and referred to the coming chapters. The list of steps in the *WAMOS-method* is followed by a presentation of the major delimitations made in this project.

2.2. The Steps Of the *WAMOS-method*

The in this project proposed method, by which real-time control-systems can be designed for welding of thickwalled materials, is sequential. This sequence can be regarded as the recipe of the *WAMOS-method*. To maintain the general view of the *WAMOS-method* the main steps of this sequence are introduced below. These steps will be further elaborated in the coming chapters:

1. **Control variables.** The first step is to determine the *input* to the weld process, \underline{U} , and the *output* to be controlled, \underline{Y} . The *input*, \underline{U} , is a vector of *controlling* variables, e.g. current, welding speed and weaving width. The *output*, \underline{Y} , is a vector of *measurable* variables, e.g. the temperature at the surface of the workpiece where the arc touches it. The choice of the *input* variables is mainly based on the equipment available. These controlling variables are used both in the off- and on-line system. The *input* and *output* variables are determined in Chapter 3.
2. **Off-line simulation.** After determination of the control variables the next step is to do two different off-line simulations by the *off-line preparation system*.
 - 2.(a) **The first simulation** performed has the purpose to plan the welding task based on a predefined temperature distribution quality. The *output* of this off-line simulation is the temperature distribution of the surface where the arc touches the plate. One temperature distribution profile at every time-step, t . This sequence of off-line generated surface temperature distributions is used as reference in the on-line system. This simulation is named the *reference-generating simulation*. The length of one *reference-generating simulation* depends on how much the parameters, which are influencing the weld, are changed. One *reference-generating simulation* is regarded as one *weld-step*.
 - 2.(b) The first simulation generates the on-line reference. **The second simulation** is needed in order to generate the on-line controller. To generate the on-line controller a precise but simple transfer-function is needed. This transfer-function is generated based on off-line identification [Franke, 1993]. To off-line identify a transfer-function a set of data is needed and it is exactly this set of data, which is generated, in the second simulation a simulation must be made for each *input* variable. Each of the desired on-line control variables is in the off-line simulation system one by one given a step-input. Now saving the step-input and the corresponding surface temperature response for each of the step-inputs enables generation of the needed set of data. To insure a precise transfer-function it is important to introduce this step-input under the same conditions as used in the *reference-generating simulation*, 2.(a). This means to introduce the step-input on the same welding task as the one just simulated in the *reference-generating simulation*, 2.(a). This simulation is named *step-input simulation* and the data generated in this simulation is used in the off-line identification. Off-line simulations are elaborated in Chapter 4.

2. Problem Statement

3. **Off-line identification.** After generating the on-line reference and the dataset needed to identify the transfer-functions, the next step is to identify the transfer-functions. By use of off-line identification, it is possible to identify simple but precise transfer-functions of a partial performance of the general and far more complex finite-element model. This or these simple transfer-functions are like the finite-element model able to describe dynamic properties of the system. However, in a much more limited working domain. These transfer-functions are placed in a matrix named the *transfer-function matrix*. The *transfer-function matrix* is used for design of the on-line controller. The off-line identification is elaborated in Chapter 5.
4. **Design of on-line controller.** Based on the off-line identified *transfer-function matrix* the *control-matrices* are designed. As the *transfer-function matrix* also the controller is working in a limited working domain only. Therefore, a new controller is to be made for every *reference-generating simulation* where instance the geometry changes. The design of the on-line controller is done off-line. It is elaborated in Chapter 6.
5. **On-line system.** By achievement of the off-line generated on-line temperature reference and the off-line generated on-line controller the preparation for the on-line system is now completed. When the on-line system is in action it continuously compares the achieved surface temperature with the reference surface temperature. Based on the error between the actual and the desired surface temperature the off-line generated controller calculates the coming path and power *input*. This loop continues for every time-step and is succeedingly continued with the next *weld-step* until end weld-task*. One weld-task contains one or more *weld-steps*.

The imaging system is described in Chapter 7 and the full on-line executing system is presented in Chapter 8. In Chapter 9 the weld experiments made to test the on-line WAMOS-system and hence the *WAMOS-method* are presented followed by the conclusion in Chapter 10.

Before the WAMOS-system is elaborated in more details in the coming chapters some delimitations to the project are made.

2.3. Preliminary Project Decisions

To develop a new method which generates welding control-systems is a rather difficult task. Therefore, to improve the chance of reaching a successful result within the given time of the project the following decisions were made. The principle when making these decisions is to make the system as simple as possible while maintaining the possibility of demonstrating the capabilities and perspectives of the *proposed weld-system architecture* and *WAMOS-method*. In

* One weld-task is defined sequentially as one start of welding, followed by one or more weld-strings and one stop of welding.

consequence of this project principle it was decided to implement the architecture confining the implementation to:

- **GTAW welding.** The welding control-system is based on an automated gas tungsten arc welding (GTAW) process.
- **Base material.** Structural steel is selected as it is very typical for the welding industry needing this kind of automation and at the same time from a welding point of view is quite a challenging material.
- **No filler material.** There will be no use of filler material.
- **Bead on plate.** As no filler material is added the process will be performed as bead on plate welding.
- **Linear MIMO proportional-controller.** The controller in the on-line control-system to be designed in this project (Chapter 6) is a linear MIMO proportional-controller (P-controller).

Note that none of these decisions introduce delimitations to the *WAMOS-method*. They only apply delimitations to this project. Though no other controller but the P-controller is demonstrated in this project the *WAMOS-method* does open the possibilities of automatically building PD-, PI, or PID-controller, if necessary or desirable. The *WAMOS-method* also opens the possibilities of using other welding types than GTAW welding and filler material.

To design the on-line control-system the *input* and *output* variables of the system must be determined. This is done in the following chapter partly based on experience and partly based on temperature measurement experiments by means of the developed imaging system. Determination of the *input* and *output* variables constitute the first step of the proposed *WAMOS-method*.

3. Input and Output Variables

The thermal feedback welding control-system to be designed (Chapter 3 to Chapter 6) is a linear Multiple Input Multiple Output (MIMO) control-system. The system is designed based on the theory of [Franke, 1993]. This control-system basically consists of the following elements (Figure 3-1):

- A *reference*, $\underline{W}(s)$, which is the off-line simulated surface temperatures;
- the *error*, $\underline{E}(s)$, which is the difference between the *reference*, $\underline{W}(s)$, and the *output*, \underline{Y} ;
- the *input*, \underline{U} , which is a vector of *controlling* variables, e.g. current, welding speed and weaving amplitude;
- the *output*, \underline{Y} , which is a vector of *measurable* variables, e.g. the actually achieved temperature at the surface of the workpiece, where temperature can be measured;
- *forward-regulation*, \underline{V} , which ensures a correct *input*, \underline{U} , though the *error* is small or zero;
- the *control-matrix*, \underline{K}_p , which is the controlling matrix;
- and the *model* of the physical system, $\underline{G}_M(s)$, which is generated on basis of the off-line finite-element model. The physical system is named $\underline{G}_S(s)$.

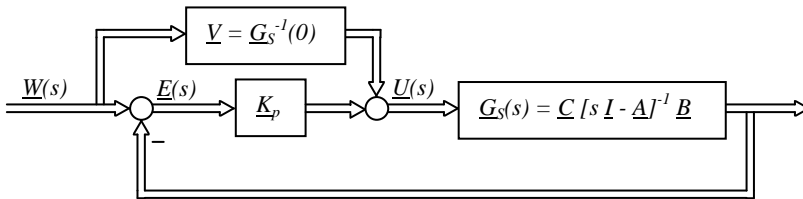


Figure 3-1 The block diagram of the physical system and controller. The controller depicted is the linear MIMO P-controller, which is used in the on-line system [Franke, 1993, page 108].

To design the on-line control-system a *model* of the physical system, in form of *transfer-functions*, must be established. Before establishment of the *transfer-functions*, the *input*, and *output* variables must be determined. To demonstrate the possibility of generating a MIMO control-system, based on the in this project proposed *WAMOS-method*, a 2x2 control-system is established. The two times two *input* and *output* variables are chosen in this chapter.

3.1. Determination of Input Variables

The choice of *input* variables for the on-line system is made among the following *input* variables, which are regarded reasonable when performing automatic GTAW welding:

- *Current*
- *Weld gun position*
- *Weld gun orientation*
- *Filler wire speed*

The welding gun position includes *travel speed*, *voltage* and the *weaving pattern* as the *weaving amplitude*.

The physical experiments performed in this project were performed on a cnc controlled x- y- table at FORCE Technology (Chapter 8). The workpiece to be welded is moved in the horizontal coordinate plane by the x- y- table while the welding gun and the camera are positioned in a fixed position during the experiments (Figure 3-2). That fact sets some natural limits on the choice of *input* variables. The *weld gun orientation* and the *voltage* are therefore not applicable as *input* variables and because of the preliminary project decision, not to use base material, the *filler wire speed* is also excluded as *input* variable.

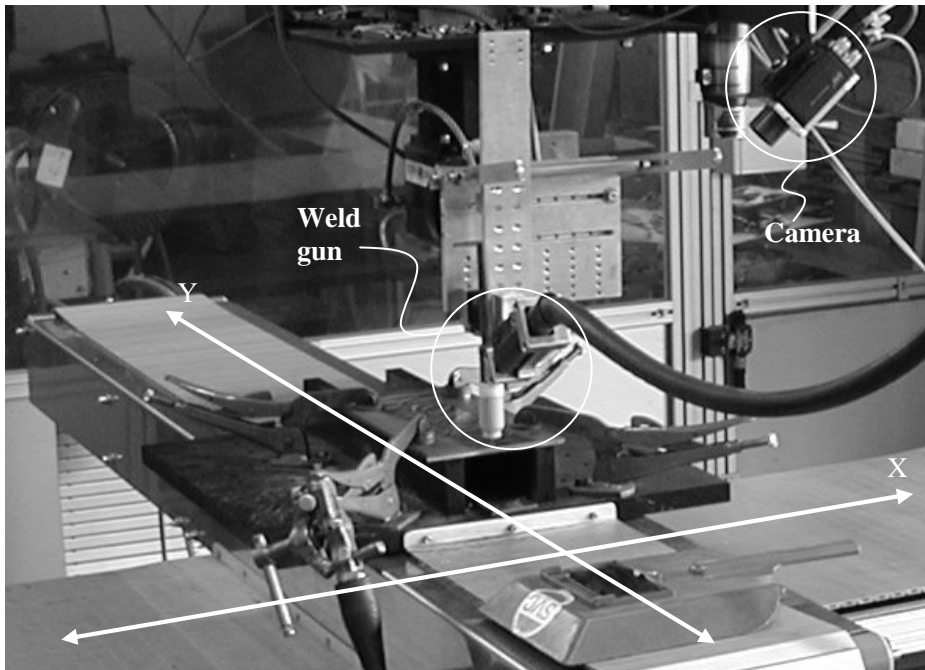


Figure 3-2 Cnc controlled x- y- table on which the experiments were made. The camera and weld gun were fixed on the same spatial position whereas the table was moving.

Based on the equipment available and the preliminary project decisions the two *input* variables are to be chosen among: *Current*, *travel speed*, and *weaving amplitude*.

The final choice of *input* variables among the three above mentioned variables is made together with the choice of *output* variables (Section 3.3). To decide the *input* variables together with the *output* variables enables us to choose a set of *input* and *output* variables, which matches. Before choosing the final set of *input* and *output* variables a set of possible *output* variables is established.

3.2. Determination of Output Variables

The choice of *output* variables is, due to the *proposed weld-system architecture* of the WAMOS-system, limited to a choice among the temperatures on the surface of the geometry. These surface temperatures (*output* variables) are measured by the imaging system. The imaging system to be developed in Chapter 7 is capable of measuring temperatures from 1530 °C to 1350 °C. That corresponds to the geometry range from the border of the weld pool and out to, as far as the temperature gets below 1350 °C. The position of the camera determines whether the temperatures on the tail or at the side of the weld pool are to be measured. When the camera measures from the side of the weld pool the temperatures at the tail are measured at the highest precision. Opposite when the camera measures from behind the weld pool the temperatures at the side of the weld pool are measured at the highest precision (Section 7.1.4). In the control-system, which is to be developed and tested the camera is positioned on the side of the weld pool meaning that the temperatures of the tail of the weld pool is measured by high precision. This decision was primarily based on two considerations: Firstly, due to smaller temperature gradients at the tail of the weld pool compared to the gradients of the side of the weld pool. The temperature field at the tail of the weld pool is much larger than the temperature field at the side of the weld pool. Choosing the tail gives a wide range of possible *output* variables. Also the position of the temperature measurement point at the tail are further away from the arc compared to the position of the temperature measurement point at the side of the weld pool which lead to more precise measurements because of less noise from undesired radiation (Section 7.1.4). Secondly, it was experienced that *output* variables based on temperatures on the tail of the weld matched the above chosen possible *input* variables better than *output* variables based on temperatures from the side of the weld.

The two *output* variables to be chosen in the following section will be based on *temperatures from 1530 °C to 1350 °C* or *gradients* at the tail of the weld.

In the following section the final set of *input* and *output* variables is decided based on experiments.

3.3. Choice of Input and Output Variables

In this section the final set of variables, two *input* and two *output* variables, is chosen based on experiments. To improve the controllability of the system the following two criteria are used: Firstly, the two *input* variables each must have a strong but significantly different influence on the process. Secondly, *output* variables are preferred where only one of the *outputs* changes significantly when one of the *inputs* is changed, and where the other *output* variable changes when the second *input* variable is changed. In other words, the purpose of the experiments is to identify a pair of *input* and *output* variables, which is decoupled.

Based on Section 3.1 - 3.2 the *input* variables to choose among are: *Current*, *travel speed*, and *weaving amplitude*. Due to the capabilities of the temperature imaging system (Chapter 7) the *output* variables must be based on *temperatures from 1530 °C to 1350 °C* measured at the tail of the weld or *gradients* measured at the tail of the weld.

The experiments performed to determine the variables were carried out using the following constant parameters (Table 3-1).

Constant parameters	Value
Material type	Grade S235
Size of workpiece	300x150x6 mm
Electrode type	WT-20
Electrode thickness	2,4 mm
Electrode angle	60°
Stickout	4,3 mm
Tip to workpiece distance	2,7 mm
Gas (pure argon)	10 l/min
Work angle	0°
Travel angle	0°
Camera position and angle	Side, 45 Grades

Table 3-1 These constant parameters are used in the experiments made to determine the *input* and *output* variables.

The parameters to be varied (variables) are listed in Table 3-2.

Variable parameters	Varied values
<i>Current</i>	150 A to 250 A
<i>Travel speed</i>	2 mm/sec. to 5 mm/sec.
<i>Weaving amplitude</i>	0 mm to 3 mm

Table 3-2 In the experiments which are used to determine the final set of *input* and *output* variables these three possible *input* variables are varied.

By means of the constant parameters (Table 3-1) and by varying the three possible variables (Table 3-2) several experiments were performed. In each of the

experiments the surface temperature images were recorded. These recorded surface temperature images were afterwards analysed to identify a proper set of *input* and *output* variables. During the process of analysing the recorded surface temperature images a wide range of possible *output* variables were tested. Because of the large amount of tests only the chosen set of variables is presented and argued in this report. The chosen set of *input* and *output* variables is (Table 3-3):

Couple	<i>Input</i> variables	<i>Output</i> variables
A	<i>Current</i>	<i>Average temperature</i>
B	<i>Weaving amplitude</i>	<i>Approximated width of the weld</i>

Table 3-3 The chosen set of *input* and *output* variables. Couple a; the *current* is meant to be coupled with the *average temperature* Couple b; the *weaving amplitude* is meant to be coupled with the *approximated width of the weld*. Couple a and b are to a large extent decoupled.

Among the three possible *input* variables the variable, *welding velocity* was excluded. This exclusion was due to difficulties in identifying a change in *temperature* or *temperature gradient* due to the change in *welding velocity* whereas the change in *temperature* or *temperature gradient* would be better decoupled from a change in *current* or *welding amplitude*.

The two remaining *input* variables, *current* and *weaving amplitude* were chosen as the two *input* variables to be used in this WAMOS test system because two appropriate *temperature output* variables were discovered, which relatively decoupled describe the state of each of the two *input* variables.

To verify that the set of two *input* and two *output* variables contains two couples which to a large extent are decoupled from each other and that the chosen *input* variables both have a strong influence on the process the chosen set of *input* and *output* variables is in the following investigated by introducing a step-input to the two *input* variables. First a step-input to the first *input* variable, *current* is applied followed by a step-input to the second *input* variable, *welding width*. For both of these two step-input cases the two chosen *outputs* are generated and plotted. The travel speed is 2 mm/sec..

First, based on a step-input to *current* (Figure 3-3) the two chosen *output*, *average temperature* and the *approximated width* are illustrated respectively in Figure 3-4 and Figure 3-5. The *average temperature* is measured as the average pixel value in the rectangle behind the weld pool. The estimation of the *approximated width* is done by calibrating the average temperature along the grey line to the width of the pool. The *input*, *current* and the *output*, *average temperature* are coupled and named couple “a” (Table 3-3). The *weaving amplitude* is coupled to the *approximated width* of the weld pool and is named couple “b”.

In Figure 3-3 an image taken by the imaging system of the weld before and after the step-input to *current* is depicted. In Figure 3-3-A the *current* is 178 amp. and after a step-input the *current* is 222 amp., see Figure 3-3-B. Both before (Figure

3. Input and Output Variables

3-3-A) and after (Figure 3-3-B) the step-input the *average temperature* and the *approximated width* are measured at every time-step. These measurements are illustrated in Figure 3-4 and Figure 3-5.

The temperature images given in this report are all generated by the developed imaging system (Chapter 7). The presented images (Figure 3-3 A and B) are the raw images captured by the camera. The tail of the weld pool can be seen to the left. The black cone in and below the weld is the gas nozzle and the white light above is undesired reflected radiation, mainly from the electrode. The pictures taken by the imaging system are further elaborated in Chapter 7.

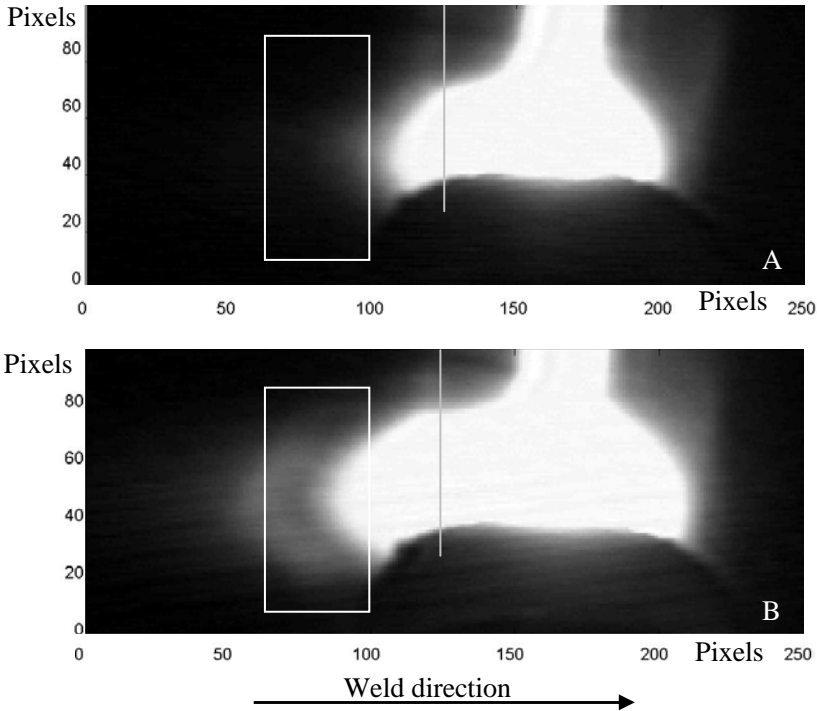


Figure 3-3 shows the image taken by the imaging system before (A) and after (B) a step-input to the *current* is introduced. In image (A) the *current* is 178 amp. and in image (B) the *current* is 222 amp.. The white rectangle illustrates the area where the *average temperature* is measured and the grey line illustrates the line along which the *approximated width* is calculated.

The measured *average temperature* and *approximated width* during the above experiment (Figure 3-3) are illustrated below (Figure 3-4 and Figure 3-5). The *average temperature* is calculated as the average pixel value of the pixels within the white rectangle (Figure 3-3). At the time 0 the welding is activated with the starting *current* of 178 amp.. The step-input is activated after 45 seconds where the *current* is change to 222 amp. The *weaving amplitude* constantly is 0 mm.

The following figure shows the reaction on the *average temperature* when a step-input to the *current* is introduced (Figure 3-4). The *average temperature* is plotted for every time-step.

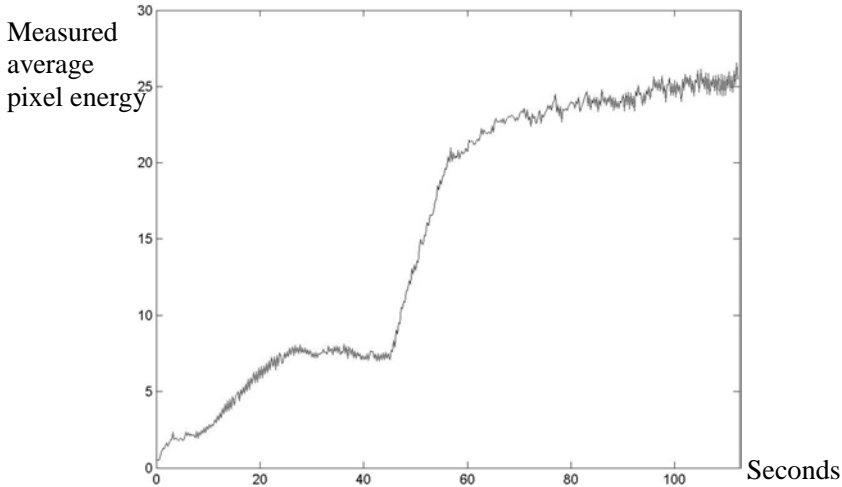


Figure 3-4 Step-input on the *input variable, current* at time 45 seconds. The *current* is changed from 178 amp. to 222 amp. and the first *output*, the *average temperature* is measured at every time-step. The *average temperature* is measured as the average pixel value within the white rectangle depicted in Figure 3-3.

In Figure 3-4 it is clear that the step-input introduces a significant and consistent change in the *average temperature output*. In the same step-input experiment the *approximated width* of the weld pool is measured. This *approximated width* is plotted in Figure 3-5.

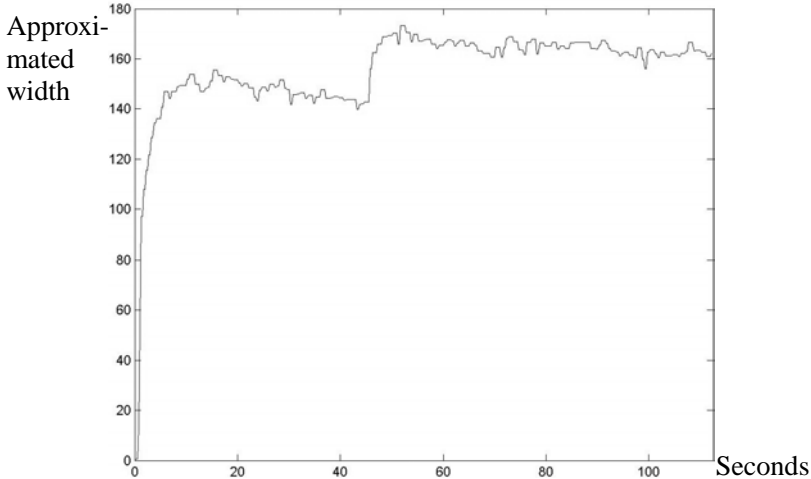


Figure 3-5 The second *output*, the *approximated width* is here plotted in its full length. After 45 seconds the step-input is applied by changing the *input variable, current* from 178 amp. to 222 amp.. The *output* is measured as the average pixel value along the grey line depict in Figure 3-3.

3. Input and Output Variables

Estimation of the *approximated width* is done by calibrating the average temperature along the grey line (Figure 3-3) to the width of the weld pool. The above illustration (Figure 3-5) shows, as desired, that the *approximated width output* does only introduce a small significant and persistent change on account of the step-input to the *current*.

Below is an image of the workpiece, on which the step-input to *current* was introduced (Figure 3-6).

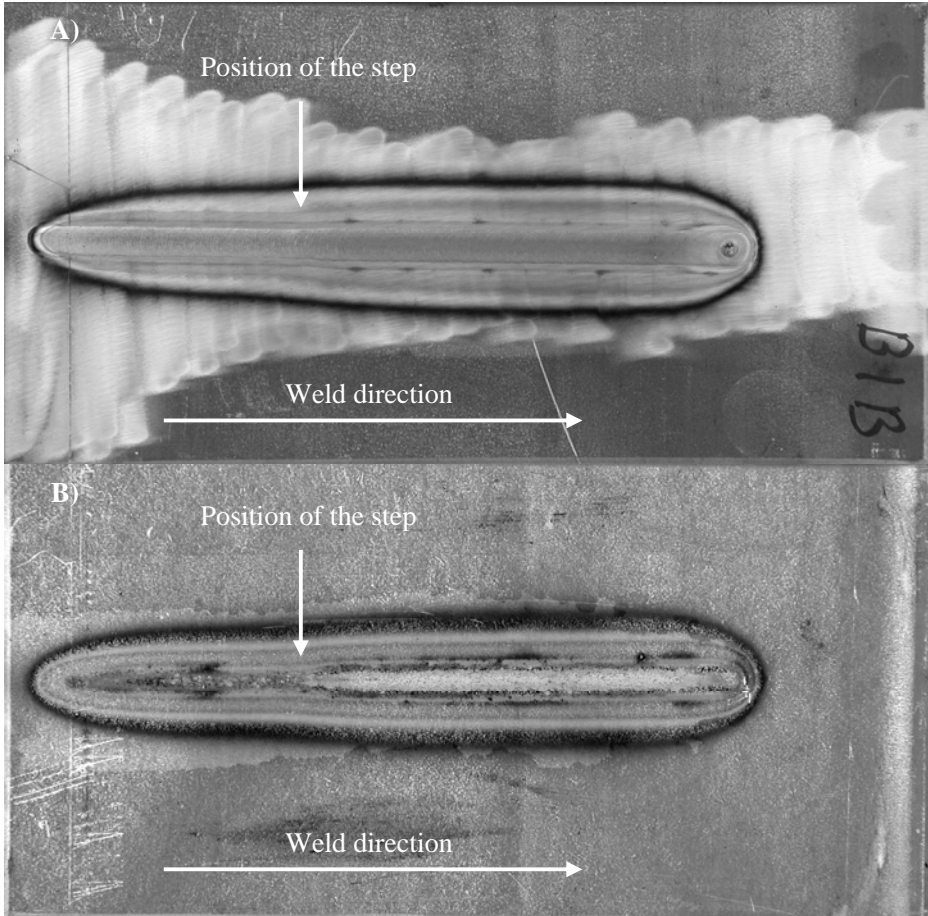


Figure 3-6 A picture of the workpiece which was introduced to the step-input on the *current*. A) is front side of the workpiece and B) is the backside.

In Figure 3-7 is shown the image effect when a step-input to the *weaving amplitude* is introduced. The two images illustrated in the figure are captured by the imaging system at the highest weaving amplitude (A) and the lowest one (B) during the change experiment. The *output* measurements are performed identically to the measurements performed in the first experiment above.

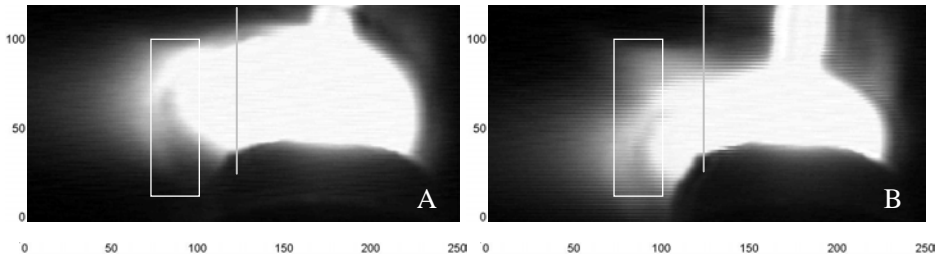


Figure 3-7 illustrates two images taken by the imaging system after the step-input on the *weaving amplitude* is introduced. Image (A) captures the weld when the *weaving amplitude* has the highest amplitude and (B) when it has the lowest amplitude.

All the experiments performed run with four time-steps per second (4 Hz) and the weaving frequency is set to 2 Hz. The imaging system is set to capture the weld only when the weaving amplitude is in high and low position (Section 8.1), one image per time-step. The *average temperature* calculated for every time-step is illustrated below (Figure 3-8).

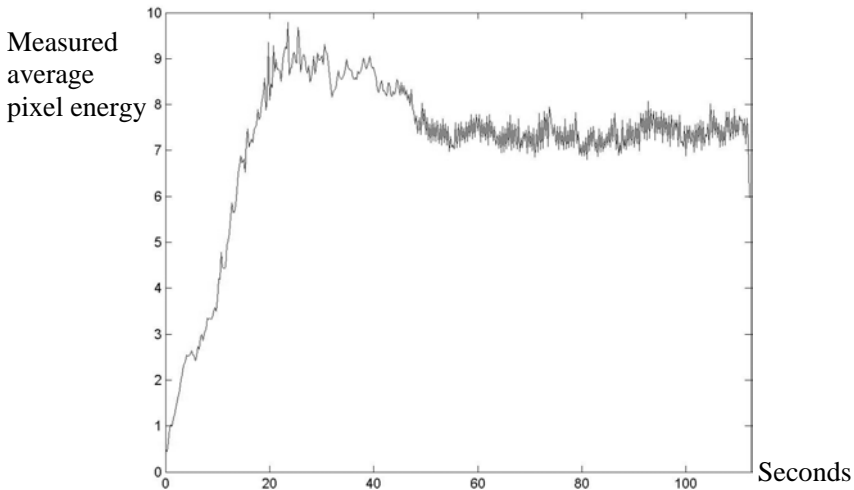


Figure 3-8 The first *output*, the *average temperature* is here plotted in its full length. After 45 seconds the step-input is introduced and the *input* variable, *weaving amplitude* is changed from 0 mm to 3 mm.

The step-input to the *weaving amplitude* is, as in the first experiment, introduced after 180 time-steps. Before the step-input the *weaving amplitude* is 0 mm and doing the step-input it is changed to 3 mm. In this experiment the *current* constantly is 178 amp.. The above illustration (Figure 3-8) shows, as desired, that the *average temperature output* only gets a small significant change on account of the step-input on the *current*.

To generate the *approximated width* the average pixel value along the grey line (Figure 3-7) is used. To use this as a measure of the width of the weld pool when

3. Input and Output Variables

weaving, the measurements performed when the torch is positioned at one lateral of the extreme points of the weaving motion (Figure 3-7-A) are used only. That is every two of the grabbed images. To stabilize the estimate further the last two measurements of the *approximated width* (where the weld is in top position) are compared and the largest one is chosen. In practise this is done by comparing the measurements of the past four time-steps and chose largest measurement value. This is done for every time-step.

The *approximated width* calculated for every time-step is illustrated in Figure 3-9:

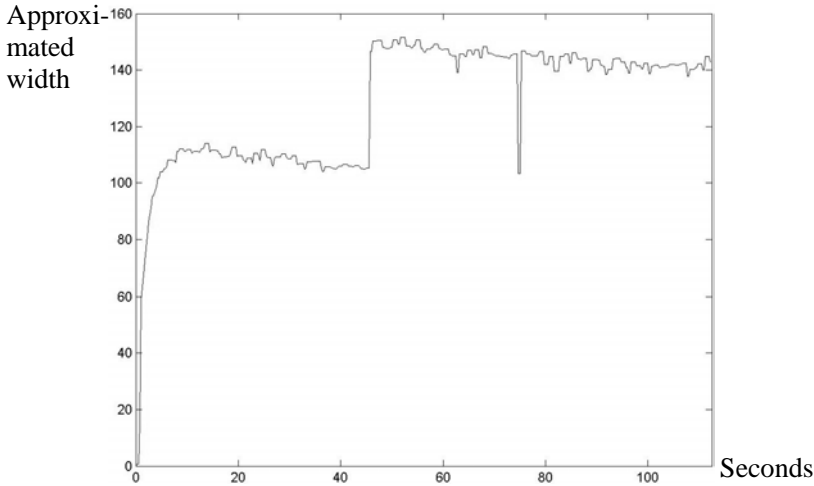


Figure 3-9 The second output, the *approximated width* is here plotted in its full length. After 45 seconds the step-input is applied and the *input variable, weaving amplitude* is changed from 0 mm to 3 mm.

From this graph (Figure 3-9) it appears that the step-input on the *weaving amplitude* has a significant effect on the measured *approximated width*.

Below an image of the workpiece, on which the step-input on the *weaving amplitude* was introduced, is shown (Figure 3-10)

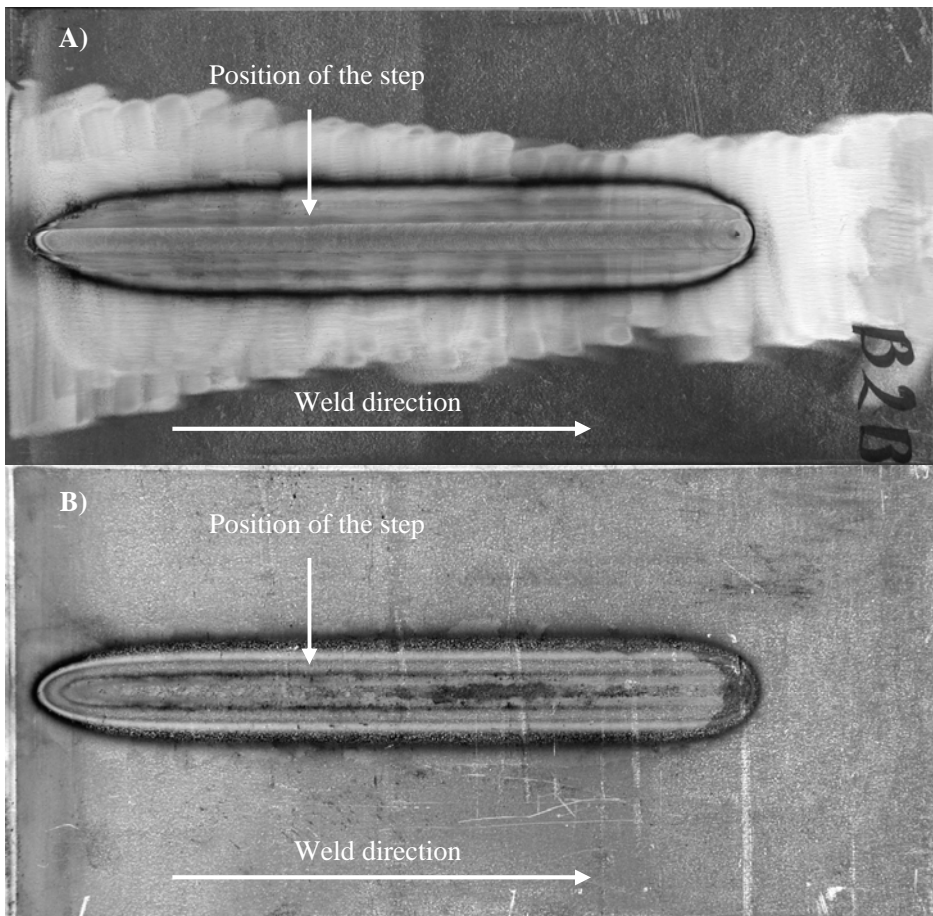


Figure 3-10 An picture of the workpiece which was introduced to the step-input to the *weaving amplitude*. A) is front side of the workpiece and B) is the backside.

Based on these figures it is clear that the chosen set of two *input* and two *output* variables contains two couples which to a wide extent are decoupled from each other and the chosen *input* variables both have a strong influence on the process.

In Chapter 9 it is though concluded that to decouple the couple of variables should only be one part of a larger goal, which is to identify output variables that are closely linked to the desired weld quality criteria. These weld criteria could be full penetration, restrictions to the haze zone, and/or weld pool width, or more generally spoken: The output variables should be as closely linked to the desired *quality reference* (see Figure 1-4) as possible. A frequently useful *quality reference* is a desired temperature distribution in the workpiece.

The process to identify a proper set of *output* and *input* variables may be difficult to automate. It is though expected that to identify a set of *output* and *input* variables is only needed once for every set of weld criteria.

3. Input and Output Variables

Also this trouble is reduced when using a systematic feedback system design method as the feedback amplifications determined for the welding MIMO system are such determined that the effect of the undesired couplings are minimized.

In Chapter 5 the off-line identification of the finite-element model is performed based on this chosen set of *input* and *output* variables but first an introduction to the simulation system, which contains the finite-element model, is given.

4. Off-line Preparation System

In this chapter the off-line simulation system is presented. The off-line system is meant to be used as an *off-line preparation system*, which is used to generate the *reference* for the on-line system. This simulation is named the *reference-generating simulation*. It is also meant to generate a set of data from which the on-line controller is built (Chapter 5 and 6). This simulation is named the *step-input simulation*.

The off-line simulation system is in this and the following chapters named the *off-line preparation system* whereas in the prior chapters it was named the off-line *planning system* (see Section 1.3.1). The reason for this shift in name is that the off-line system initially was developed mainly for the purpose to off-line plan or schedule trajectories and execute them in an open-loop execution system. The development of this off-line *planning system* is performed by Christian Blicher Terp, Department of Production, Aalborg University, Denmark (See [Terp, 1999]), and sponsored by Odense Staalskibsværft A/S, Denmark, STVF (the National Technical Research Counsel of Denmark), and Department of Production at Aalborg University, Denmark. The *off-line preparation system* of the WAMOS *method* is based on this previously developed off-line *planning system* of Christian Terp and additional new program code, which together enable us to carry out *reference-generating simulations* and *step-input simulations*. As described in Section 1.3.1 the off-line system is meant to be able to plan the full welding including an arbitrary weaving path based on a, by the user, predefined *quality reference* (Figure 1-2). The previously developed off-line *planning system* is at this date close at fulfilling this goal for a few welding categories as horizontal and upside down GMAW and GTAW welding. However, as this project is meant to test if the use of a combined off- and on-line control-system for automatic control of welding is at all feasible and as project recourses are limited, a simplified version of the desired full-scale *off-line preparation system* is made. An introduction to this simplified version of the *off-line preparation system* is given below.

Because the imaging system and the finite-element model of the *off-line preparation system*, within the project time, has not been calibrated to correspond each other, the *reference-generating simulations* and the *step-input simulations* are not used in the final experiments of this report when the WAMOS-*method* is validated (Chapter 9xx). This limitation should not have any consequence on the validation of the WAMOS-*method*. It however makes the validation easier as it is

4. Off-line Preparation System

not necessary to take the finite-element model correctness into account when evaluating the *WAMOS-method*.

4.1. The off-line system

The current *off-line preparation system* is like the *planning system* in Figure 1-3 based on a controller and a finite-element model. The *step-input simulation* does however not use the Reference Modeller and a feedback of the internal temperatures of the geometry. The *off-line preparation system* is for both the *reference-generating simulation* and for the *step-input simulation* supplied with a “file generation” procedure that extracts the temperatures needed to build the on-line controller and the *reference*. The architecture used for the step-input simulation is illustrated in (Figure 4-1).

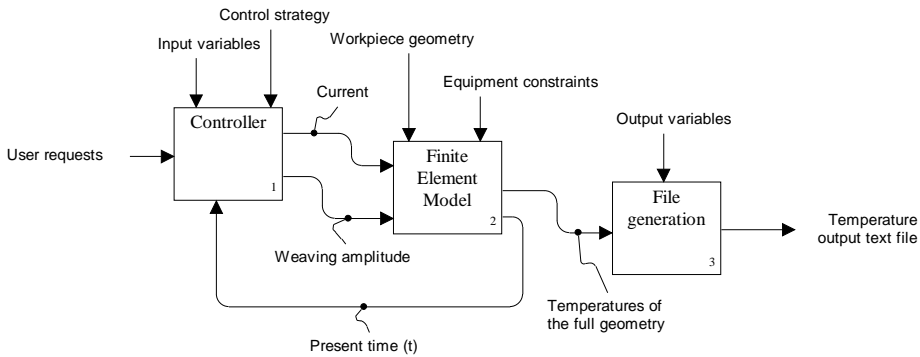


Figure 4-1 The *off-line preparation system* architecture used for the *step-input simulation*.

The controller of the *off-line preparation system* could take many different forms. Presently, the controller is programmed to feed the finite-element model with the desired *input* at every time-step (t). The controller includes the “*input variables*” and the “*control strategy*”. There are two control strategies one for the *reference-generating simulation* and one for the *step-input simulation*. For the *reference-generating simulation* the “*quality reference*” of Figure 1-3 could be the off-line *quality reference* profiles (Figure 1-4) which is given as input for the Reference Modeller (Figure 1-3). For the *step-input simulation* the “*user request*” would be the desired *current* and *weaving amplitude* both before and after the step-input. At every time-step the controller sends the *current* and *weaving amplitude* to the finite-element model, which calculates the temperature in the full geometry of the workpiece. Beside the *current* and *weaving amplitude* the finite-element model is fed with “*workpiece geometry*” and “*equipment constraints*”. These constraints could be maximum velocity and acceleration of the robot that is to be controlled in the on-line system, together with other constraints relating to the welding equipment. These constraints are given to the system at the beginning of every

simulation by use of an *input* file, which contains all the needed figures (Appendix A).

Since a finite-element programme calculates the temperatures in the full geometry of the workpiece the temperatures of the surface where the arc touches the workpiece constitute part of these simulated temperatures (Figure 4-2). The “file generation” function of Figure 4-1 extracts for every time-step these surface temperatures needed for the on-line system and stores them in a “temperature output text file”. The file generation program is programmed to maintain the same field of view as the camera in the on-line system. This field of view is like the on-line system centred on the centre of the weld pool and the temperature field extracted has the same resolution as the temperature field captured by the camera (Figure 4-3).

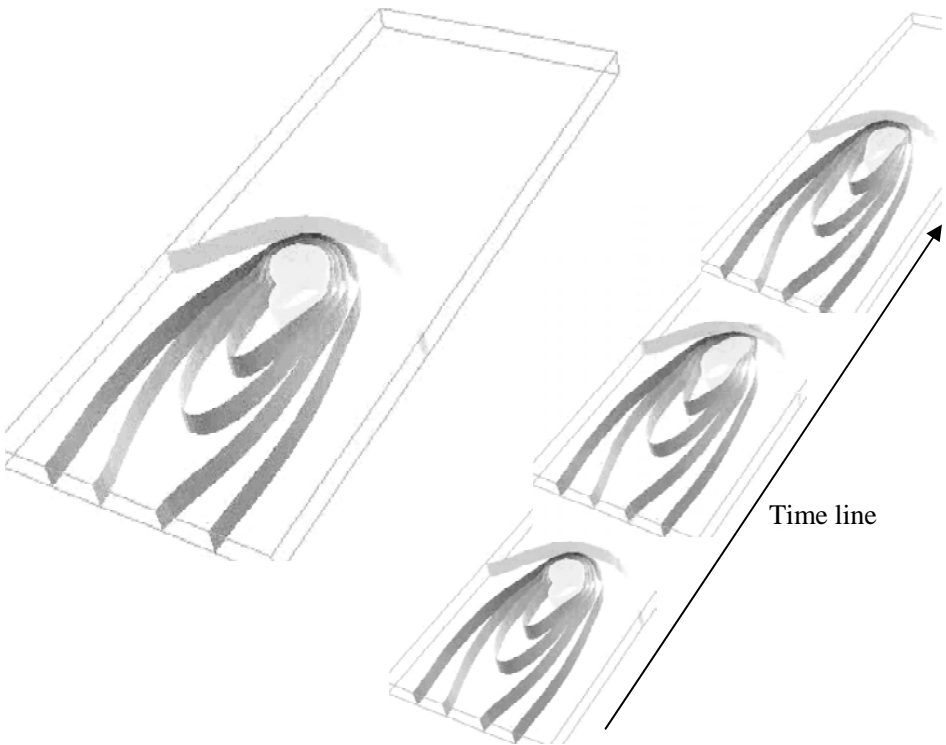


Figure 4-2 Temperature profile generated by the *off-line preparation system* which shows the temperature isotherms in the full geometry of the workpiece. At the right of the figure the temperature isotherms are showed at different time-steps.

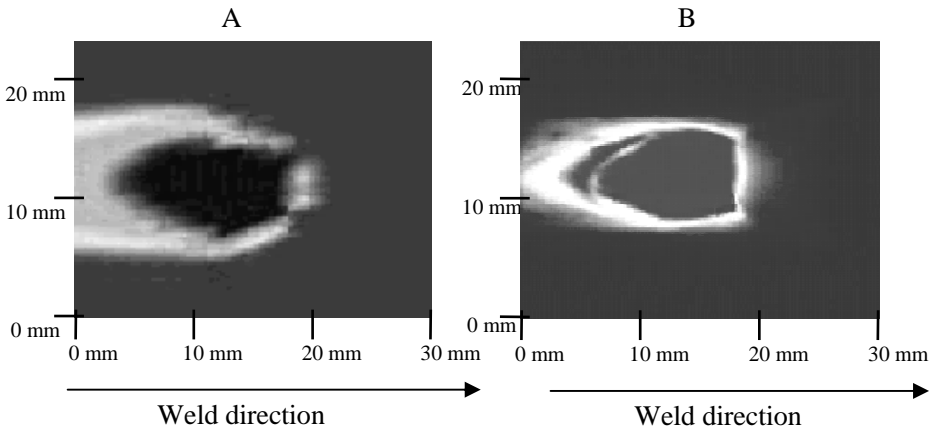


Figure 4-3 Field of view generated in the *off-line preparation system* (A) and the field of view of the camera in the *on-line system* (B).

The “file generation” program is fed with the “*output variables*”, which in this case is the two *output variables*, *average temperature* and *approximated width* of the weld, chosen in Chapter 3.

One of the key parts of the *off-line preparation system* is the model. To plan a welding trajectory based on this system requires a model, which describes the process sufficiently well. The question about, what is sufficiently well, will have to be answered by testing the model at different stages. Presently, a non-linear model has been developed. The model is based on a non-linear model of the heat conduction, on a linear model of the radiation and convection, and on a simplification of the model of the weld pool into heat conduction in solid material. The heat source is modelled as a Gaussian heat distribution. Because of the chosen modelling method and the architecture of the system it is possible to use this off-line system with arbitrary workpiece geometry (see [Terp, 1999] and [Kjeldsen, 2000]).

The program code of the finite-element model and the additional code are programmed in Diffpack. Diffpack is a programming language suited for building finite-element or finite-difference models. Diffpack is based on C++ structure and classes and is therefore quite similar to C++. Because the code of the finite-element model has not been generated in this project and because of its length it is not presented in this report. However, the additional code, which is generated in this project, can be seen in Appendix B. For further information of the code of the finite-element model please see [Terp, 1999] and [Kjeldsen, 2000].

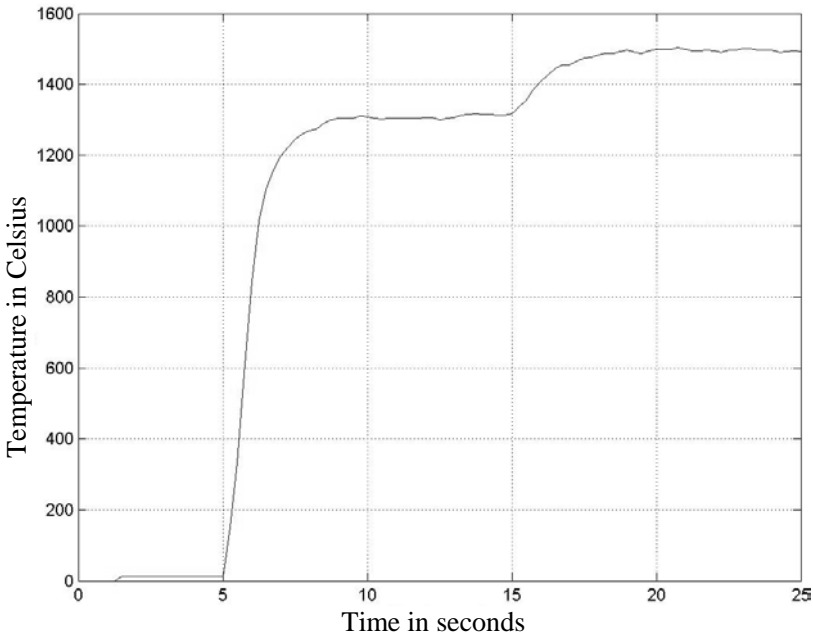


Figure 4-4 Step-input of the *input* variable, *current*. The temperature plot is generated based on the off-line produced data generated by the *off-line preparation system*.

Based on this *off-line preparation system* it is now possible to perform the *reference-generating simulation* and the *step-input simulation*. Figure 4-4 illustrates the response to a step-input applied to the *input* variable, *current* generated by means of the *off-line preparation system*. The first 5 seconds no energy is applied. After 5 seconds the *current* is turned on to 178 amps and after 15 seconds the step-input is applied (from 178 to 222 amps). The ordinate is the simulated *average temperature output* and the abscissa is the time in seconds. This simulation is made under similar conditions as in the physical experiments illustrated in Chapter 3 and 9. Figure 4-4 should therefore be comparable to Figure 3-4. However, as the plots in Chapter 3 and 9 are based on raw images captured by the imaging system and not images calibrated to fit the model of the *off-line preparation system* the scales of the two ordinates are not comparable.

The reason why the factor of proportionality between Figure 4-4 and Figure 3-4 is different is because the imaging system only measures radiation intensities and only for temperatures above 1350 °C. The relation between radiation and temperatures is given by Planck's law (Eq. 7.1).

Because of time limitations it was decided not to calibrate the finite-element model and the imaging system to correspond each other. The *reference-generating simulation* and the *step-input simulation* of the *off-line preparation* are therefore not used in the final experiments of this report when the *WAMOS-method* is validated in Chapter 9. The *off-line preparation system* is not used because

4. Off-line Preparation System

experiments (See [Kjeldsen, 2002] and Appendix J) showed deviations between the surface temperature profiles, which were calculated by the finite-element model and the surface temperature profiles which were measured by the developed temperature imaging system.

In future versions of the WAMOS-system when the model of the *off-line preparation system* and the measurements of the temperature imaging system are calibrated to correspond to each other the *off-line preparation system* will be used to generate the data needed for building the controller and for the *reference* of the on-line system. However in the rest of this report welding experiments are performed to generate the data needed of the *off-line preparation system*. These actual weld experiments will be named the *off-line preparation experiments*. The *off-line preparation experiments* are used to perform both *step-input experiments* and *reference-generating experiments* as substitute for respectively the *step-input simulations* and the *reference-generating simulation*. In the *off-line preparation experiments* the temperature imaging system measures the surface temperatures by which the model for the design of the on-line control-system is to be built as well as the temperatures for estimation of the *reference* needed for the on-line system. As the *off-line preparation system* is not used in this thesis Figure 4-4 is only to be regarded as an example of the capabilities of the *off-line preparation system*.

The *off-line preparation experiments* that are used as substitute for the *off-line preparation system* were presented in Chapter 3.3 (Figure 3-4, 3-5, 3-8, and 3-9). The *output* data generated in these experiments is meant to be used in the calculations presented in the following chapter. In the following chapter the identification of simple models is described. Those models are to be identified on basis of the step-input and the *output* data presented in Chapter 3.3.

5. Off-line Identification

To build the on-line weld execution control-system a model of the plant is needed. For this purpose the finite-element model of the off-line system is regarded as too heavy. Identification of a more simple model is therefore wanted. The identification method chosen for this purpose is an off-line identification method of parameterised models by [Franke, 1993, page 69]. This method only requires the process signals from a single step-input ($h(s)$) to identify one transfer-function ($G_M(s)$) that describes the relationship between one *input* variable ($u(t)$) and one *output* variable ($y(t)$).

The reason why it has been chosen to use this identification method is that the system identification can be done by applying a step-input function to the system to be identified. The reason for wanting to apply a step function signal to the input of the system to be identified is that this type of signal is easy to generate. Most system identification literature recommends not using step input functions as system excitation signal. This is because application of this type of signal inabilities the applied identification equations to determine an appropriate order of the system model. Therefore the method of [Franke, 1993], which avoids this problem has been chosen for this project.

By means of off-line identification, it is possible to identify simple but specific and precise sets of transfer-functions based on the general and far more complex finite-element model. This or these simple transfer-functions are like the finite-element model able to describe the dynamic properties of the system. The working domain for each of these specific transfer-functions is though much more limited than the working domain of the finite-element model. The off-line identification therefore has to be performed for every *weld-step* (see definition of *weld-step* in Section 1.3.4).

This method, which enables off-line identification of one or more transfer-functions, constitutes part of the *WAMOS-method*.

5.1. Initiating requirements

Before using this method the *input* and *output* signals, respectively $u(t)$ and $y(t)$, must be recorded. This is done by applying a step-input to each of the *inputs*, one at a time, and measure each of the *outputs* for every step-input. The *input* signal

5. Off-line Identification

could be a step-input on the welding current, the welding speed or the arc voltage etc. The *output* could be the temperature of a given point at the surface of the workpiece or temperature gradients.

In Chapter 3 the following control system variables were defined (Table 5-1):

Couple	Input variables	Output variables
a	Current	Average temperature
b	Weaving amplitude	Approximated width of the weld

Table 5-1 The chosen set of input and output variables. Couple a; the current and the average temperature. Couple b; the weaving amplitude and the approximated width of the weld.

Based on a step function signal on the *input* variables and the measured *output* a model on the following transfer-function form is to be identified (Eq.5.1):

$$G_M(s) = \frac{b_0 + b_1s + \dots + b_ms^m}{s^q(1 + a_1s + \dots + a_ns^n)}; \quad m \leq n + q \quad 5.1$$

where the coefficients a_n and b_m are to be estimated.
 m, n and q are integers.

It is required that the system to be identified at least is roughly describable by a transfer-function ($G_M(s)$), that the system is time invariant and approximately linear. It is assumed that the process signals of $u(t)$ and $y(t)$ reach a steady state value.

The fundamental idea of the method is an approximation that says that, if the transfer function behaviour of two systems, coincide in a finite number, N , of points, the input/output behaviour of the two systems can be approximated with only one transfer-function. (Eq. 5.2).

$$G_M(k\alpha) = G_S(k\alpha); \quad k = 1, 2, \dots, N \quad 5.2$$

where N is an integer that designates the total number of points where the two transfer-functions coincide. The size of N is $N = n + m + 1$,

$$s = k\alpha,$$

k is an integer which designates the sample support-point number in the *step-input simulation* of the *off-line preparation system*,

α is a parameter which emphasises steady state or transient state properties of the transfer-function to be identified. The size of α must be selected. The selection process is described in the following section (Section 5.2.1).

The mathematical proof for equation 5.2 is elaborated in [Franke, 1993].

$G_M(s)$ is the model to be identified of the system of transfer-function $G_S(s)$. $G_S(s)$ is in the WAMOS-system the finite-element model of the *off-line preparation system*. First a step-input is applied to $G_S(s)$. The model $Y_{G_M}(s)$ is identified based on the corresponding *output*. This identification of $Y_{G_M}(s)$ is based on equation 5.2, which in this specific situation can be written as:

$$Y_{G_M}(k\alpha) = G_S(h : k\alpha); \quad k = 1, 2, \dots, N \quad 5.3$$

where h designates that $G_S(s)$ has been subject to a step-input.

$Y_{G_M}(k\alpha)$ has the same form as $G_M(k\alpha)$ (Eq. 5.1):

$$Y_{G_M}(s) = \frac{b_0 + b_1s + \dots + b_ms^m}{s^q(1 + a_1s + \dots + a_ns^n)}; \quad m \leq n + q \quad 5.4$$

The relation ship between $G_M(k\alpha)$ and $Y_{G_M}(k\alpha)$ is:

$$h(s)G_M(s) = Y_{G_M}(s) \quad 5.5$$

To generate $G_M(k\alpha)$ based on $Y_{G_M}(k\alpha)$, $Y_{G_M}(k\alpha)$ is multiplied $h(s)^{-1}$:

$$G_M(s) = h(s)^{-1}Y_{G_M}(s) \quad 5.6$$

5.2. Identification of $G_M(s)$ based on $G_S(s)$

First the steps required, to identify $Y_{G_M}(k\alpha)$ based on a step-input to $G_S(s)$, are introduced.

5. Off-line Identification

Based on Eq. 5.3 and Eq. 5.4 one can generate the following equation:

$$b_0 + b_1 k\alpha + \dots + b_m (k\alpha)^m = \hat{G}_s(k\alpha) \cdot [1 + a_1 k\alpha + \dots + a_n (k\alpha)^n] \quad 5.7$$

where $\hat{G}_s(k\alpha) = (k\alpha)^q G_s(k\alpha)$

This equation can be rewritten as:

$$b_0 + b_1 k\alpha + \dots + b_m (k\alpha)^m - \hat{G}_s(k\alpha) \cdot a_1 k\alpha - \dots - \hat{G}_s(k\alpha) \cdot a_n (k\alpha)^n = \hat{G}_s(k\alpha) \quad 5.8$$

and in matrix notation where k varies from 1 to N (Eq. 5.9):

$$\begin{bmatrix} 1 & \alpha & \dots & \alpha^m & -\alpha \cdot \hat{G}_s(\alpha) & \dots & -(\alpha)^n \cdot \hat{G}_s(\alpha) \\ 1 & 2\alpha & \dots & (2\alpha)^m & -2\alpha \cdot \hat{G}_s(2\alpha) & \dots & -(2\alpha)^n \cdot \hat{G}_s(2\alpha) \\ \cdot & \cdot & & \cdot & \cdot & & \cdot \\ \cdot & \cdot & & \cdot & \cdot & & \cdot \\ \cdot & \cdot & & \cdot & \cdot & & \cdot \\ 1 & N\alpha & \dots & (N\alpha)^m & -N\alpha \cdot \hat{G}_s(N\alpha) & \dots & -(N\alpha)^n \cdot \hat{G}_s(N\alpha) \end{bmatrix} \begin{bmatrix} b_0 \\ b_1 \\ \vdots \\ b_m \\ a_1 \\ \vdots \\ a_n \end{bmatrix} = \begin{bmatrix} \hat{G}_s(\alpha) \\ \hat{G}_s(2\alpha) \\ \cdot \\ \cdot \\ \hat{G}_s(N\alpha) \end{bmatrix} \quad 5.9$$

where $b_0 \dots b_m$ and $a_1 \dots a_n$ are the coefficients of $G_M(s)$ that are to be identified. This equation is called the *synthesis equation*.

The identification of $Y_{G_M}(s)$, based on a step-input to the system $G_s(s)$, is carried out through the following three steps:

1. Choose the parameter α
2. Choose the degree of the numerator, m , and the denominator, n , in $Y_{G_M}(s)$ (Eq. 5.4)
3. Calculate $Y_{G_M}(s)$ and hence $G_M(s)$

The result of step 1 is dependent on step 2 and the other way around.

This identification implies that the observed progress of the system reaches a stationary state. Therefore q of Eq. 5.4 is 0 (see [Franke, 1993, page 71]).

The three steps above are described in the following three sections.

5.2.1. Selection of the Parameter α

The dynamic properties of the identified transfer-function are influenced by the parameter α . A high α value gives a fast reacting system with a large steady state (SS) error whereas a small α gives a slow reacting system with a small SS error.

The parameter α is defined by the Faust equation (Eq. 5.10) (see [Franke, 1993, page 63]):

$$\alpha = \frac{\text{value}}{t_e} \quad 5.10$$

where t_e is defined as the time when the time response is in SS, i.e. t_e is settling time.

In Figure 5-1 α is varied from $0.5/t_e$ to $5/t_e$. $n = 1$ and $m = 2$ for all the curves.

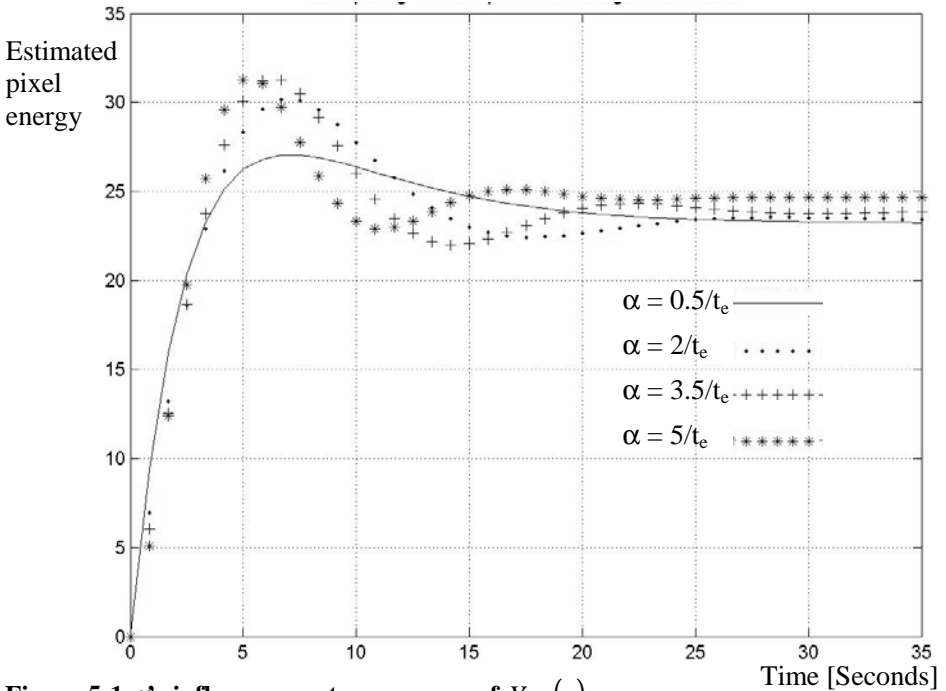


Figure 5-1 α 's influence on step response of $Y_{G_M}(s)$.

$\alpha = 3.5/t_e$ is a common average value of α named the standard α value

The source data, $y(t)$, of which the estimate of $Y_{G_M}(s)$, for different α values, have been generated, is plotted below (Figure 5-2).

5. Off-line Identification

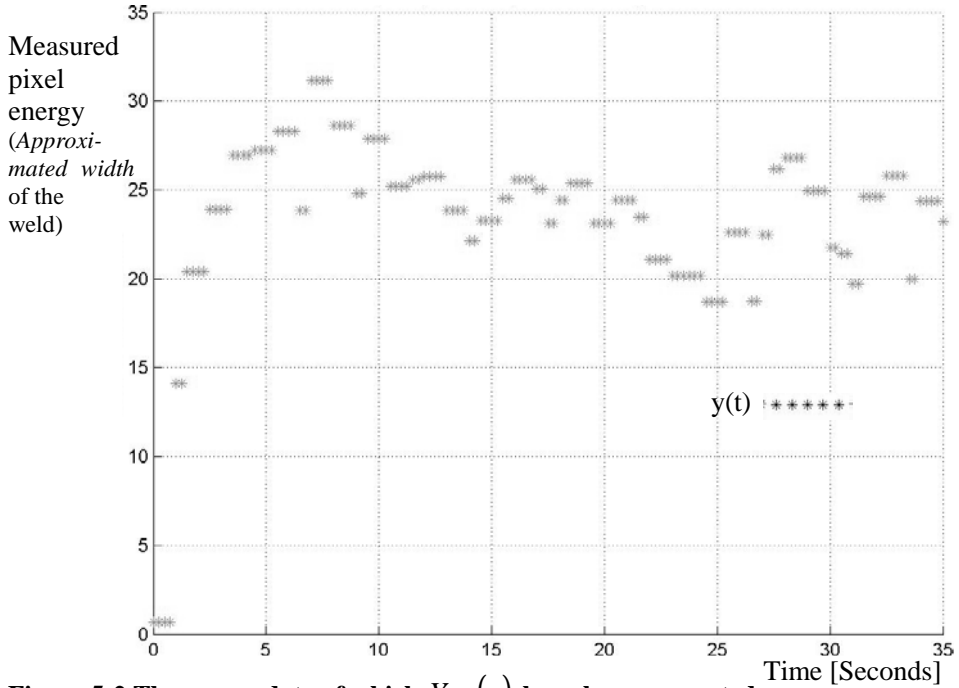


Figure 5-2 The source data of which $Y_{G_M}(s)$ have been generated.

The source data plotted above (Figure 5-2) is an extract of the full *output* data, *approximated width* of the weld pool, generated when applying a step function to the *input* variable *current*. The full *output* data is plotted in Chapter 3 (Figure 3-5). Figure 5-2 only shows the weld pool width reaction to the step-input from when the step-input is introduced to 35 seconds after the step-input. That is in Figure 3-5 from 45 seconds to 80 seconds. To narrow down the data window the *output* data have been displaced 142 in measured pixel energy. The *output* data in Figure 5-2 therefore start at approximately 0 when the step-input is initiated. The input generated by the controller must be augmented with the step-input (Section 8.1, Figure 9-6). Narrowing the data window is done to get a more simple and exact transfer-functions.

The optimal value of α might vary from *weld-step* to *weld-step* e.g. if the plate thickness changes. To estimate an optimal value of α automatically requires as a minimum to measure the time, t_e , from the step-input is applied to the process is in SS. Such an estimation can be done automatically. It is hence believed that the estimation of α can be done fully automatically.

After α is defined the degree of the numerator and denominator must be chosen.

5.2.2. Choose the Degree of Numerator and Denominator

The degree of the numerator and denominator of Eq. 5.4 is to begin with chosen based on a set of rules (Table 5-2).

a	If the slope is positive at time $t = 0$. Then the difference between n and m is supposed to be 1, ($n - m = 1$).
b	If the slope is zero at time $t = 0$. Then the difference between n and m is supposed to be 2 or 3, ($n - m = 2$ or 3).
c	If $y(0) \neq 0$. Then the size of m should equal n , ($m = n$).

Table 5-2 A set of rules that are used to choose the difference in degree between the numerator and denominator [Franke, 1993, page 71].

In the data of Figure 5-2 the difference between n and m should be one.

After this rough choice a more visual evaluation of the numerator and denominator degree must be done. In Figure 5-3 the numerator and the denominator degree are varied. In all cases the difference is one and α is $3,5/t_e$.

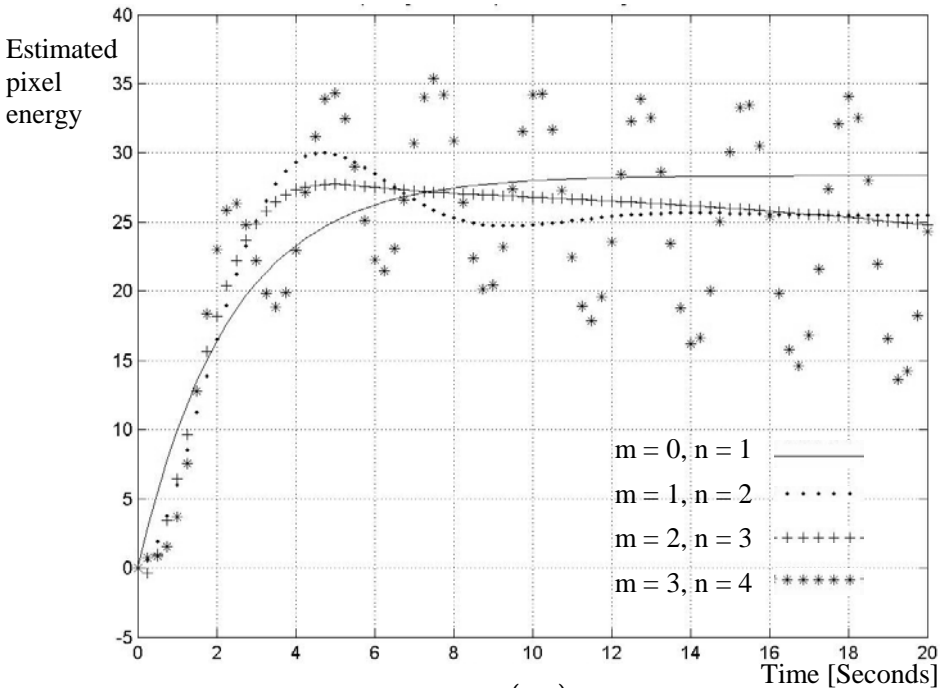


Figure 5-3 The influence of m and n on $Y_{G_M}(k\alpha)$ when α is $3,5/t_e$.

In the case when the numerator and denominator exceed respectively 2 and 3 the system becomes unstable. A numerator and denominator of respectably 0 and 1 or 1 and 2 can, in the present weld-system, in most cases be used with success.

5. Off-line Identification

In the following a suggestion how to estimate the numerator and denominator automatically is outlined:

1. Fix the difference between the numerator and denominator by means of the three rules above (Table 5-2).
2. Calculate the SS value of $Y_{G_M}(s)$ and compare it to the SS value of the source data, $y(t)$. Do this for different values of degree of numerator and denominator and choose the best fitting. The difference between the values of the nominator and denominator must apply to step one.
3. Check the value of the output fluctuations as time tends to infinity. If it does fluctuate then repeat step two and three where a smaller degree of numerator and denominator must be chosen.

When the parameters α , n and m have been chosen $Y_{G_M}(s)$ and hence $G_M(s)$ is to be calculated.

5.2.3. Calculate $G_M(s)$

The coefficients $b_0 \dots b_m$ and $a_1 \dots a_n$ of $Y_{G_M}(s)$ (Eq. 5.4) are found by means of the *synthesis equation* (Eq. 5.9). The unknowns of the *synthesis equation* are α and $\hat{G}_s(k\alpha)$, where $\hat{G}_s(k\alpha) = (k\alpha)^q G_s(k\alpha)$ (Eq. 5.7). To calculate the coefficients $b_0 \dots b_m$ and $a_1 \dots a_n$ of $Y_{G_M}(s)$ the parameter α and $G_s(k\alpha)$ must be identified first.

The identification of the parameter α was described in Section 5.2.1. The identification of $G_s(s)$ is described below.

The transfer-function of $G_s(s)$ of a given system is defined by the following relation:

$$G_s(s) = \int_0^{\infty} w(t) e^{-st} dt \quad 5.11$$

where $w(t)$ is the response of the system to an input, which is $\delta(t)$ (the unit impulse function). The Laplace transform of the response of a system to a given signal $p(t)$ is defined by the following relation:

$$Y(s) = \int_0^{\infty} g_s(t) e^{-st} dt \quad 5.12$$

where $g_s(t)$ is the response of the system to that given input signal $p(t)$.

If the response $h_s(t)$ of a step-input is used (E.g. Figure 5-2) the Laplace transform of that response $h_s(t)$ equals to $H_S(s)=G_S(s)/s$ in the Laplace-domain. Based on a single step-input it is possible to write $G_S(k\alpha)$ as:

$$G_S(k\alpha) = k\alpha \cdot H_S(k\alpha) = k\alpha \cdot \int_0^{\infty} h_s(t) e^{-k\alpha t} dt \quad 5.13$$

At time t_e the value of the step-input is $h_s(\infty) = b_0$:

$$G_S(k\alpha) = k\alpha \cdot \int_0^{t_e} h_s(t) e^{-k\alpha t} dt + k\alpha h_s(t_e) \int_{t_e}^{\infty} e^{-k\alpha t} dt$$

$$\Downarrow$$

$$G_S(k\alpha) = k\alpha \cdot \int_0^{t_e} h_s(t) e^{-k\alpha t} dt + h_s(t_e) e^{-k\alpha t_e} ; \quad k = 1, \dots, N \quad 5.14$$

The trapezoidal rule, for numerical integration, has the following form [Franke, 1993, page 73]:

$$\int_a^b f(t) dt \approx T \sum_{i=1}^{M-1} f(a + iT) + \frac{T}{2} [f(a) + f(b)]; \quad T = \frac{b-a}{M} \quad 5.15$$

where M is the number of steps between the boundaries a and b . T is the sampling time. Based on the trapezoidal rule the numerical integration of Eq. 5.14 is as in Eq. 5.16:

$$\int_0^{t_e} h_s(t) e^{-k\alpha t} dt \approx T \sum_{i=1}^{M-1} h_s(iT) e^{k\alpha iT} + \frac{T}{2} [h_s(0) + h_s(t_e) e^{-k\alpha t_e}] \quad 5.16$$

Since the values of $h_s(t)$ are known from the step-input applied on the *off-line preparation system* (e.g. Figure 5-2) it is now possible to calculate $G_S(k\alpha)$ (Eq. 5.14) and $Y_{G_M}(s)$ (Eq. 5.9) and hence $G_M(k\alpha)$ numerically.

If the WAMOS weld control-system were a single-input-single-output (SISO) system only one transfer-function G_M is required. However, a multiple-input-multiple-output (MIMO) WAMOS weld control-system is required. It is therefore necessary to identify more transfer-functions. In the final experiments of Chapter 9 a 2x2 MIMO control-system is tested. To build a controller for this 2x2 MIMO

5. Off-line Identification

control-system four transfer-functions are required. Each of these four transfer-functions $Y_{G_{M1,1}}$, $Y_{G_{M1,2}}$, $Y_{G_{M2,1}}$, and $Y_{G_{M2,2}}$ are identified separately based on each of their step-output. All of the transfer-functions of the MIMO control-system are placed in a matrix (Eq. 5.17):

$$\underline{Y}_{G_M}(s) = \begin{bmatrix} Y_{G_{M1,1}}(s) & Y_{G_{M1,2}}(s) \\ Y_{G_{M2,1}}(s) & Y_{G_{M2,2}}(s) \end{bmatrix} \quad 5.17$$

To get $\underline{G}_M(s)$, $\underline{Y}_{G_M}(s)$ of Eq. 5.17 is applied to $U(\delta)^{-1}$ (Eq. 5.6):

$$\underline{G}_M(s) = h(s)^{-1} \underline{Y}_{G_M}(s) \quad 5.6$$

$\underline{G}_M(s)$ is named the *transfer-function matrix*.

The Matlab program that performs the off-line identification of the transfer-functions can be seen in Appendix C.

In this chapter a method was given which enables off-line identification of the transfer-functions required to build the WAMOS weld controller. To calculate $\underline{G}_M(s)$ can be performed numerically and therefore automatically. The only bottleneck is the selection of the parameters α , n , and m . A suggestion to how to select these three parameters automatically is given. It is hence believed that the estimation of $\underline{G}_M(s)$ can be done fully automatically.

In the next chapter (Chapter 6) it is described how the WAMOS weld controller is built based on the identified transfer-functions.

6. Design of On-line Controller

In this chapter a method, which enables generation of the on-line controller for the WAMOS-system, is presented.

The method used to build the on-line controller is based on the theory of [Franke, 1993, page 102-213]. Dieter Franke describes a method by which it is possible to identify transfer-functions and generate the control feedback matrices based on the transfer-functions identified.

Because Dieter Franke method makes it possible, to generate a controller by means of a the knowledge contained in a finite-element model it is chosen to use the method of Dieter Franke as a part of the *WAMOS-method*.

Another advantage by the method of Dieter Frank is that the method opens up the possibility to influence the behaviour of the controller by means of a transfer-function matrix, $\underline{F}_W(s)$. Based on this wish matrix, $\underline{F}_W(s)$, it is possible to describe the desired behaviour of the system in terms of transfer-functions. To express the desired behaviour in terms of transfer-functions is desirable because the behaviour of a transfer-function is well understood and comprehensible. The same method is used for both SISO and MIMO control-systems.

The method of [Franke, 1993, page 102-213] enables design of a SISO and MIMO P-, PI-, PD-, as well as a PID-controller. Due to time restrictions has only the design of MIMO P-controller been tested in this work.

In the following the [Franke, 1993, page 102-213] theory of the P-controller is elaborated.

6.1. The P-controller

The structure of the P-controller is illustrated in the figure below (Figure 6-1). To avoid the steady state *error* that occur when the P-control-system is in SS the *forward-regulation* gain $\underline{V} = \underline{G}_s^{-1}(0)$ is implemented.

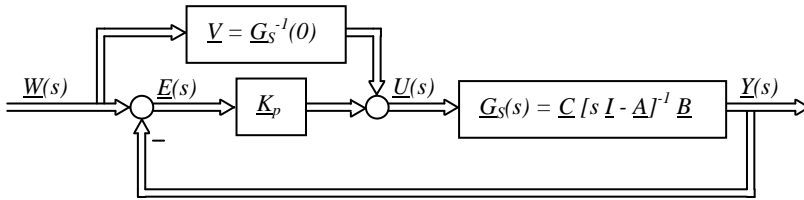


Figure 6-1 Block diagram structure of the P-controller in continues time.

To find the gain matrix \underline{K}_p the system equation (Eq. 6.1) and the control vector of the system (Eq. 6.2) is used:

$$\underline{Y}(s) = \underline{G}_s(s)\underline{U}(s) \tag{6.1}$$

$$\underline{U}(s) = \underline{V}\underline{W}(s) + \underline{K}_p [\underline{W}(s) - \underline{Y}(s)] \tag{6.2}$$

Based on these two equations the first step is to identify $\underline{G}_w(s)$ (see Figure 6-2).

$\underline{G}_w(s)$ is the close loop transfer-function of the system. The P-control-system of Figure 6-1 can be simplified to the block diagram below where $\underline{G}_w(s)$ is the close loop transfer-function of the system (Figure 6-2).

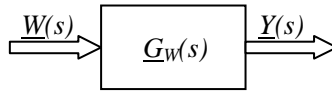


Figure 6-2 Simplified block diagram of the P-control-system.

The close loop system equation for this system (Figure 6-2) is:

$$\underline{Y}(s) = \underline{G}_w(s)\underline{W}(s) \tag{6.3}$$

To identify $\underline{G}_w(s)$, $Y(s)$ must be derived from Eq. 6.1 and 6.2:

$$\underline{Y}(s) = \underline{G}_s(s)[\underline{V}\underline{W}(s) + \underline{K}_p [\underline{W}(s) - \underline{Y}(s)]] \tag{6.4}$$

⇕

$$\underline{Y}(s) = [\underline{I} + \underline{G}_s(s)\underline{K}_p]^{-1} \underline{G}_s(s)[\underline{V} + \underline{K}_p]\underline{W}(s) \tag{6.5}$$

From Eq. 6.3 and Eq. 6.5 it is clear that $\underline{G}_W(s)$ is:

$$\underline{G}_W(s) = [I + \underline{G}_S(s)\underline{K}_P]^{-1} \underline{G}_S(s)[\underline{V} + \underline{K}_P] \quad 6.6$$

The goal is to design $\underline{G}_W(s)$ such that the weld process archives the desired behaviour. To describe the desired behaviour a wish transfer-function matrix $\underline{F}_W(s)$ is introduced (Eq. 6.7).

$$\underline{F}_W(s) = \text{diag}[F_{W1}(s), \dots, F_{Wp}(s)] = \begin{bmatrix} F_{W1}(s) & & 0 \\ & \ddots & \\ 0 & & F_{Wp}(s) \end{bmatrix} \quad 6.7$$

where p is an integer. $\underline{F}_W(s)$ has the same size as the identified *transfer-function matrix* $\underline{G}_M(s)$. In the final experiments Chapter 9 $\underline{F}_W(s)$ is a 2x2 matrix.

To choose $\underline{F}_W(s)$ is an interactive process and is the designer's possibility to influence the result of the controller behavior. To choose $\underline{F}_W(s)$ usually is a compromise between a desired fast reacting control-system and the equipment constraints.

To ensure that the closed-loop transfer-function $\underline{G}_W(s)$ archives the desired behaviour $\underline{F}_W(s)$, $\underline{G}_W(s)$ is set to equal $\underline{F}_W(s)$:

$$\underline{G}_W(s) = \underline{F}_W(s); \quad k = 1, 2, \dots, N \quad 6.8$$

As in the identification of the transfer-functions (Chapter 5) the design of the control-matrix also relies on the approximation that says that, two different transfer-functions only have to contain the same behaviour in some known points to describe the same overall *input/output* behaviour (Eq. 6.8).

In Eq. 6.6 $\underline{G}_W(s)$ is derived. To archive the desired behaviour of the closed-loop system, $\underline{F}_W(s)$ is set equal to $\underline{G}_W(s)$:

$$\underline{F}_W(s) = [I + \underline{G}_S(s)\underline{K}_P]^{-1} \underline{G}_S(s)[\underline{V} + \underline{K}_P] \quad 6.9$$

To identify the gain matrix it is simply to isolate \underline{K}_P of Eq. 6.9:

$$\underline{K}_P = [\underline{F}_W(s)\underline{G}_S^{-1}(s) - \underline{V}][I - \underline{F}_W(s)]; \quad \underline{V} = \underline{G}_S^{-1}(0) \quad 6.10$$



$$\underline{K}_P = \left[\underline{F}_W(s) \underline{G}_S^{-1}(s) - \underline{G}_S^{-1}(0) \right] \left[I - \underline{F}_W(s) \right] \quad 6.11$$

The proportional gain matrix \underline{K}_P (Eq. 6.11) is derived in continuously time but as the system is to be computer controlled the control equation should be in discrete time. The discrete version of the proportional gain matrix \underline{K}_P is shown in Eq. 6.12 [Franke, 1993, Chapter 6]:

$$\underline{K}_P = \left[\underline{F}_W(s) \underline{G}_S^{-1}(s) - \underline{G}_S^{-1}(0) \right] S_{WZ}^{-1} \left(e^{\alpha T} \right) \quad 6.12$$

where T is the time-step length and $S_{WZ}^{-1} \left(e^{\alpha T} \right)$ is a constant to be calculated mainly based on the z transform of $\underline{F}_W(s)$ [Franke, 1993, Chapter 6].

$\underline{G}_S(s)$ of Eq. 6.12 in principle describes the full behaviour of the true system and is not known in the present weld-system. It is here the *transfer-function matrix* $\underline{G}_M(s)$ is used. $\underline{G}_M(s)$ was identified in Chapter 5 and describes the behaviour of the weld-system in a limited but specifically desired working domain.

To identify the gain matrix K_P of Eq. 6.12, $\underline{G}_S(s)$ is substituted by $\underline{G}_M(s)$:

$$\underline{K}_P = \left[\underline{F}_W(s) \underline{G}_M^{-1}(s) - \underline{G}_M^{-1}(0) \right] S_{WZ}^{-1} \left(e^{\alpha T} \right) \quad 6.13$$

To calculate the gain matrix K_P a Matlab program is developed. This program can be viewed in Appendix D.

By means of the method of Dieter Franke it is possible to generate the control-matrix fully automatically. The wish transfer-function matrix, $\underline{F}_W(s)$, that enables the user to specify the desired behaviour of the control-system might require some experience. One advantage, by the use of $\underline{F}_W(s)$, is that it, by the use of $\underline{F}_W(s)$, is possible for the designer to set-up requirements to the system in the time response domain.

To set-up the wish transfer-function matrix $\underline{F}_W(s)$ in principle is an interactive process and is at the moment not automated. One way to build the wish transfer-function matrix $\underline{F}_W(s)$ automatically could be by means of the *off-line preparation system*. To choose $\underline{F}_W(s)$ usually is a compromise between a desired fast reacting control-system and the equipment constraints. In the *off-line preparation system* parameters like workpiece thickness, travel speed and equipment constraints are known. It would therefore stand to reason to define a wish transfer-function matrix $\underline{F}_W(s)$ in the *off-line preparation system*. The wish transfer-function matrix $\underline{F}_W(s)$

should be generated for every *weld-step* along with the *reference-generating simulations* and the *step-input simulations*.

In this chapter the method for generating the gain matrix was elaborated. In the next section the developed temperature imaging system is described. This is followed by a general description of the structure of the physical on-line system, which was used to test the controller and hence the *WAMOS-method*. The test results are presented in Chapter 9.

7. Temperature Imaging System

The temperatures on the surface of the geometry, of which the arc is active, are used as feedback for the WAMOS-system. To feedback these temperatures a system that measures the surface temperatures is required. In this chapter the developed temperature imaging system for surface temperature measurements around the weld pool of the gas tungsten arc welding (GTAW) process is described.

The temperature imaging system is developed to fulfil the difficult task that it is to measure the surface temperature profile under and around the electric arc. The camera is based on a conventional low-cost charge-coupled device (CCD) chip. The camera is a inexpensive black and white camera. By replacing the conventional CCD-chip filter with a dedicated and more suitable filter, and by developing special designed optics for heat measurements, it is possible to obtain surface temperature profile images.

In the following, the choice of camera is described, the specially developed optical system for the low-cost CCD-camera is described, calibration of the camera is described and measurements performed by the developed temperature imaging system are presented.

7.1. Temperature Imaging System Design

The temperature imaging system described below is designed to measure temperatures just outside the weld pool, in a temperature range from roughly 1350°C to the melt temperature, approximately 1530°C. The reasons for choosing this temperature range are:

- The heat conduction in the weld pool of the present finite-element model is approximated to heat conduction in solid-state material. The simulated surface temperature profile of the weld pool is therefore not comparable to the actual temperatures of the weld pool. The surface temperature imaging system is therefore not designed for temperature measurements in the weld pool, that is temperatures above 1530°C.
- Also, when going from the solid-state to liquid-state the emittance factor of the workpiece material changes. The change in the factor of emittance results in less emitted radiation just as the state is changed from solid-state to liquid-state. This is though the temperature rises.

7. Temperature Imaging System

- To measure low temperatures (e.g. below 1350 °C) and to react on those temperatures would give a longer response time.

The temperature range was therefore chosen from roughly 1350°C to the melt temperature, approximately 1530°C.

7.1.1. Choice of camera.

The temperature of an object may be determined from the electromagnetic radiation emitted from the object within the spectrum illustrated in Figure 7-1.

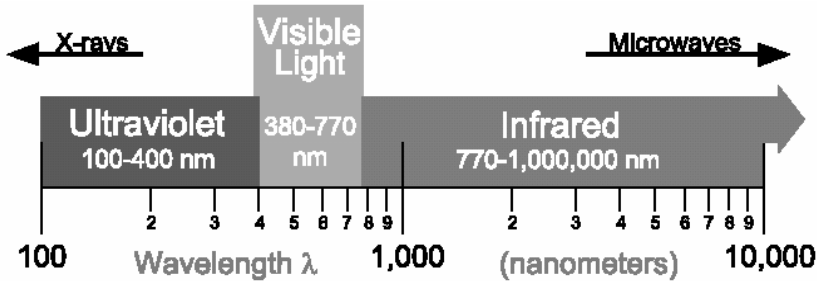


Figure 7-1 The electromagnetic spectrum.

Planck's law describes the connection between the radiation from an object and the temperature of the object (Eq. 7.1).

$$E_1 = \varepsilon \cdot \frac{C_1}{\lambda_1^5} \cdot \frac{1}{e^{\frac{C_2}{\lambda_1 T}} - 1} \quad 7.1$$

Where E is the energy emitted in the wavelength (λ) from an given object, ε is the factor of emittance, T is the absolute temperature in Kelvin, and C1 and C2 are constants.

According to (Eq. 7.1) the peak in the emitted radiation moves towards smaller wavelengths as the temperature of the object rises. This can be seen in Figure 7-2, which is calculated based on Eq. 7.1.

It follows from Figure 7-1 and Figure 7-2 that a significant emission is occurring within the visible region once the temperature is above approximately 1000 °K. It is therefore chosen to base the measurements on a charge-coupled device (CCD) chip based camera, because it is very cheap and capable to measure visible and near-infrared light. The theoretical sensitivity of a silicon-based chip is shown in Figure 7-3.

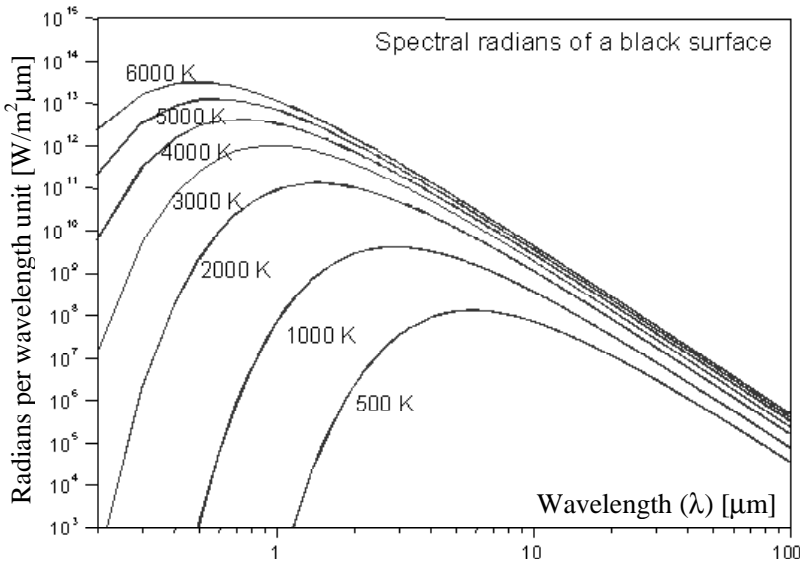


Figure 7-2 Intensity of the emitted radiation of a black surface as a function of wavelength and temperature.

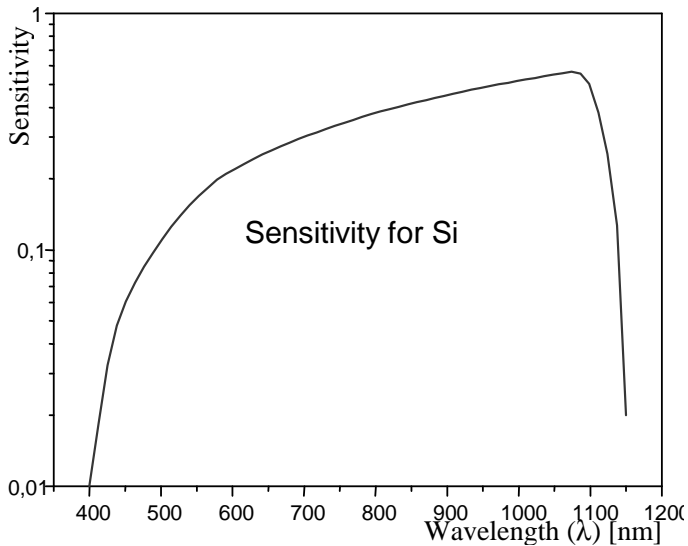


Figure 7-3 Theoretical sensitivity for silicon.

Though the sensitivity of a silicon-based chip theoretically is highest at approximately 1100 nm, real CCD-chips are typically not very sensitive at wavelengths above 700 nm.

The camera finally chosen was a CV-M10 RS Progressive Scan Monochrome camera. The main reason for choosing this CCD-camera is its ability to measure

relatively long wavelengths compared to other CCD-cameras at the same price level. The official nominal sensitivity of the camera including a lens optimised for visible light is shown in Figure 7-4. Here, the camera seems to have virtually no sensitivity above 1000 nm.

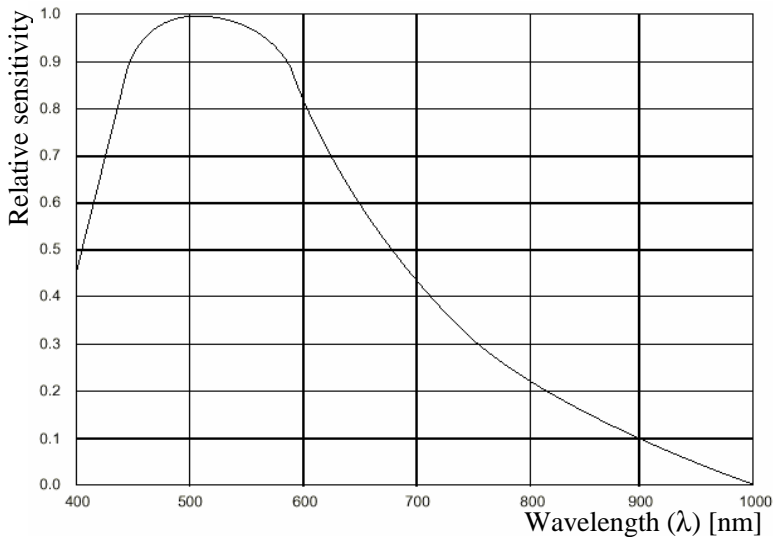


Figure 7-4 Nominal spectral sensitivity characteristic of a CV-M10 RS Progressive Scan Monochrome camera. The curve includes lens characteristics, but excludes light source characteristics.

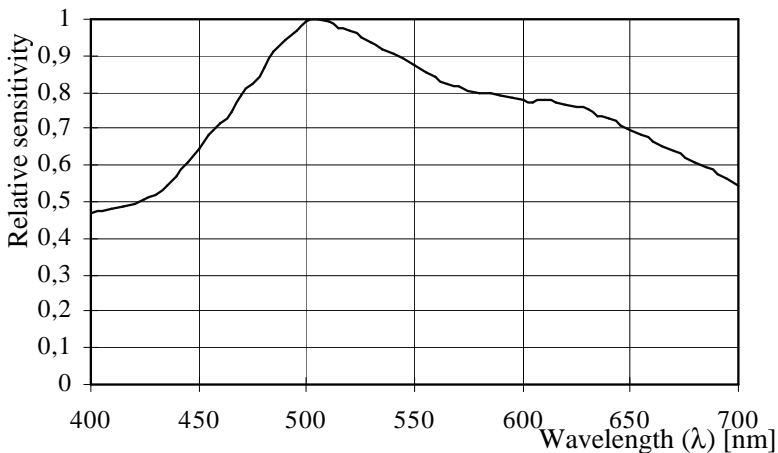


Figure 7-5 True spectral sensitivity characteristics of the CCD-chip of the CV-M10 RS Progressive Scan Monochrome camera (without lens characteristics).

The actual response characteristics of the camera measured without lens however shows a slightly different response (Figure 7-5). Most notable is that the relative sensitivity was found to be approximately 20% higher at 700 nm in the true spectral sensitivity characteristic than in the nominal spectral sensitivity

characteristic. The actual camera sensitivity for wavelengths above 700 nm is therefore also expected to be higher than stated in the official nominal spectral sensitivity chart (Figure 7-4) and expected to be sensitive above 1000 nm.

The datasheets of the chosen camera can be viewed in Enclosure B. Before the camera was used the camera was tested in relation to the camera *input/output* linearity. This test is described in Appendix E.1.

After a camera is chosen for the temperature imaging system, the optical design of the camera is described in the following section.

7.1.2. Optical design

The most difficult task in the development of the low-cost temperature imaging system for surface temperature measurements underneath a GTAW welding arc, is the optical design. The main purpose of the optics is twofold: One, to focus the waves emitted from the surface area of the workpiece onto the chip. Two, to off-filtrate the not desired radiation sources. In the design of the optics one has to be aware of three main radiation sources. Emitted radiation from:

- The workpiece on which the welding process is running (desired).
- The arc (noise).
- The Tungsten electrode tip (noise).

The emitted radiation from the workpiece surface on which the weld process is active is the desired radiation. Based on this radiation it is possible to estimate the temperature of the workpiece. However, as the light from the arc and the electrode is far more intensive than the light from the plate, it becomes a very important issue to off-filtrate the not desired light, which originates from the Tungsten electrode tip and the arc.

The undesired radiation from the arc is characterized by a unique pattern of spectral lines typical of the atoms or ions forming the arc-plasma. Each line corresponds to a jump between two electronic energy levels. A large part of this emission occurs in the visible and especially in the ultraviolet range. The main substance in the plasma of the GTAW welding of a steel workpiece is argon from the shielding gas, but also e.g. iron, manganese, copper, aluminium, tungsten, nitrogen and oxygen typically constitute small parts of the atmosphere. As metals are easily ionised these ions are together with argon-ions the main contributors to the emission spectrum. The radiation of the arc is thus dominated by this pattern of spectral lines, but it contains also a weak background of ordinary heat radiation from the welding plume as such. Due to this nature of the spectrum it is in theory possible to find a set of wavelengths where the arc does not contain spectral lines.

To gather knowledge of the spectral radiance of the present process, different sources were used:

- Self-made measurements by two different sensors both capable to measure the spectral lines from 150 nm to 800 nm. These measurements are figured in Appendix F.
- Earlier measurements made at FORCE Technology, which show the spectral lines from 200 nm to 1100 nm (Figure 7-6).
- Theoretical figures of the spectral radiation.

Earlier measurements made at FORCE Technology show the spectral lines from 200 nm to 1100 nm. These measurements show low radiation activity from 500 nm to 700 nm, around 900 nm, around 960 nm and from 980 nm to 1050 nm, as shown in Figure 7-6.

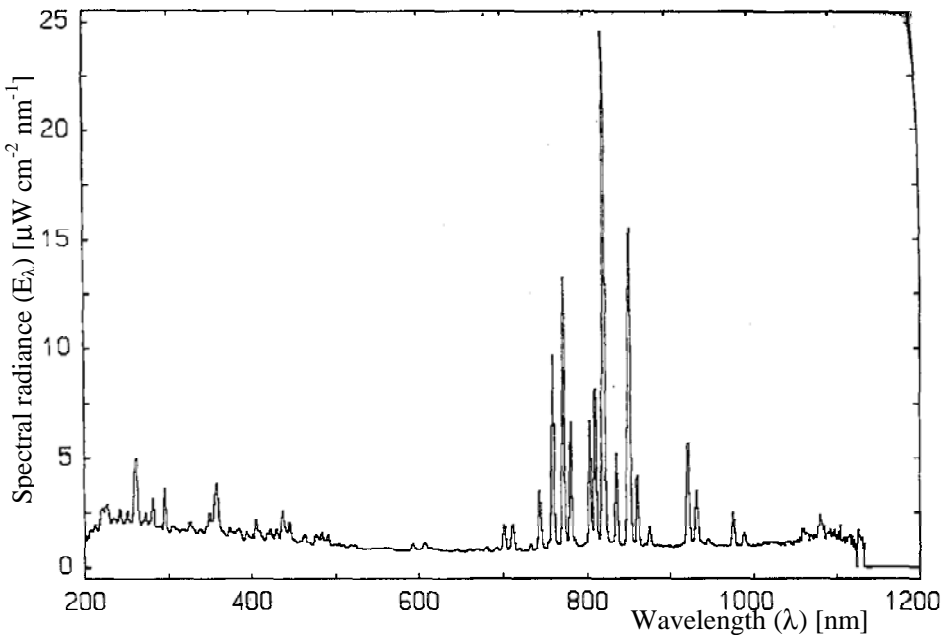


Figure 7-6 Spectral radiance of a GTAW arc in 99% argon.

As the conditions for the above measurements were not ideal for the present application, dedicated measurements have also been made as a part of this project. Based on the total set of measurements, the wavelength range from 500 to 700 nm turned out to be a possible area in which to place a band-pass filter (Appendix F). Therefore a band-pass filter at 640 nm with a width of 40 nm was tested. Due to rather low signal to noise ratio this band-pass filter is not used in the following WAMOS experiments. A filter similar to this filter is however used in Appendix I where the possibility to perform temperature measurements, that are independent of the factor of emittance is verified experimentally. In Appendix H the possibility to perform temperature measurements independently of the emittance is verified theoretically.

In the wavelength range from 800 nm to 1100 nm the signal is stronger (Figure 7-2). Therefore various theoretic literatures discussing the spectral lines in this field have been investigated. Due to measurements, theory and experiments the position of the band-pass filter in-between 980 nm and 1050 nm was of special interest. One of the references illustrates, by a drawing, the spectral radiation of pure Argon up till 1000 nm [A. I. of P. H.]. The drawing is shown in Figure 7-7. This figure shows roughly no radiation above 978 nm. A table in the same reference does, however, show a peak at 1047 nm.

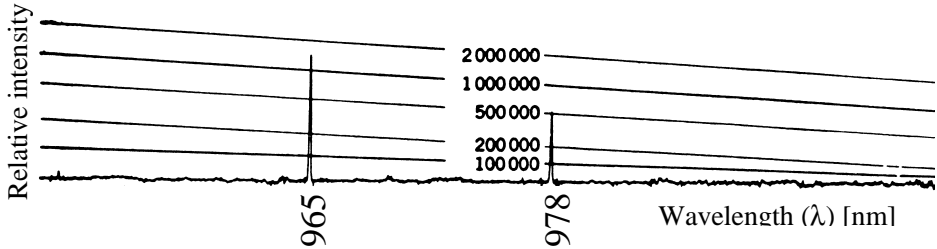


Figure 7-7 The theoretic spectrum of pure Argon in the range from 950 nm to 1000 nm [A. I. of P. H.]. The scale of the ordinate is relative intensity.

A second reference that shows the spectral lines of an argon arc in air surroundings gives the results shown in Table 7-1 [CRC, 1979].

Relative intensity	Wavelength (λ) [nm]
25000	965
4500	978
180	1005
30	1033
100	1047
1600	1047

Table 7-1 Figures of the theoretic spectrum for Argon in air from [CRC, 1979].

The two references used above also state that pure iron and tungsten do not contribute with spectral lines above 950 nm. It has, therefore, been chosen to use a band-pass filter centred at 1010 nm with a width of 40 nm, as shown in Figure 7-8.

However, according to Table 7-1 a weak but undesired spectral line occurs at 1005 nm.

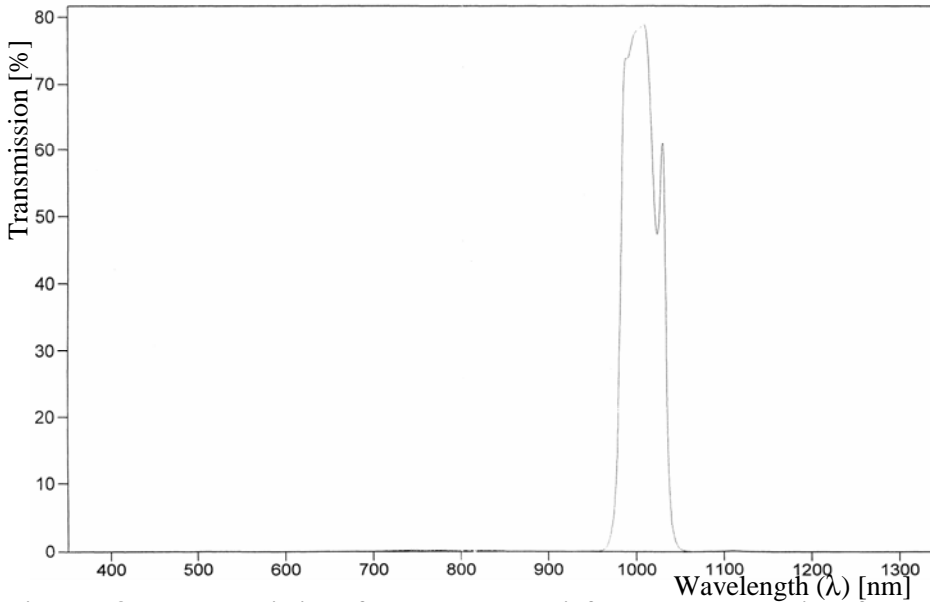


Figure 7-8 The transmission of the chosen near infrared band pass interference filter at 1010 nm and width 40 nm.

The purpose of the band-pass filter is to block the undesired radiation from the arc. Neither the radiation from the arc, nor from the electrode is desired. Contrary to the radiation from the arc, the radiation from the tungsten electrode tip is not characterized by spectral lines. The radiation from the tungsten electrode is characterized by Planck's blackbody radiation. The temperature at the tip of the electrode is during the welding process approximately 3000°C. The radiation from the electrode tip will therefore always at any wavelength be stronger than the radiation from the workpiece (Figure 7-2). It is therefore not possible to use the same filtration technique to off-filtrate the undesired radiation from the electrode as used when off-filtrating the undesired plasma radiation of the arc.

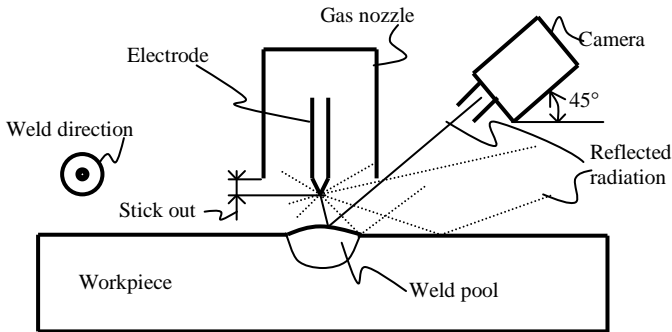


Figure 7-9 The camera is by means of the gas cup shielded from direct radiation from the electrode tip.

Though, if the stick out of the electrode is small and the position of the camera is high then the gas nozzle will shield the camera from direct radiation from the electrode, as shown in Figure 7-9. This will protect the camera from direct radiation from the electrode and minimize the risk of smears effect on the chip. Smears effect is the capacity coupling, which arises when the CCD-chip is over-exposed. The “smears” effect is visible as lines in the images (See Appendix E.2).

Hiding the electrode under the gas nozzle is though not enough. The welding bead and the workpiece surface reflects a substantial part of the radiation of the hidden electrode into the camera. To minimize the noise from the undesired reflected radiation of the electrode, one must pick the position of the camera with thoughtfulness. When the surface temperature of the workpiece is measured in front or at the tail of the welding pool, the camera should be placed at the side of the welding gun orthogonal to the welding direction (Figure 7-9). At this position the noise from reflection of the electrode (and the arc) is minimal. Opposite, when the surface temperature of the surface of the workpiece is to be measured at the side of the weld pool one should place the camera in front of or behind the welding gun to avoid most reflection.

To minimize the undesired reflected radiation from the electrode even further, an interference filter that passing through light with only a selected polarization has been applied to the optical set-up (Figure 7-11). This eliminates some of the reflected radiation and by Brewster’s law [Pedrotti, 1995] it is possible to calculate the angle θ where the reflected radiation is fully polarized and therefore theoretical may be fully blocked by the interference filter. This angle θ is approximately 56 degrees when the atmosphere is Argon and the reflection plate is Iron (Figure 7-10).

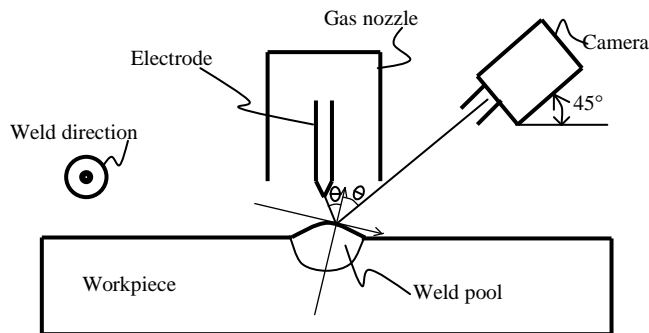


Figure 7-10 When the angle θ is 56 degrees the reflection in theory is completely off-filtrated by use of an interference filter.

To obtain the highest effect possible of the interference filter, the angle of the camera should therefore be 34 degrees. Such a sharp angle would, however, give very deform images. It is therefore chosen to place the camera in an angle of 45 degrees.

7. Temperature Imaging System

Behind the interference filter and band-pass filter a proper lens is placed, which is coated to allow penetration of short waved infrared waves. Finally, to minimize the amount of diffuse waves in the optical set-up, a 1 mm pinhole has been placed in front of the optic and the optical frame etc. have been coated black. The distance from the lens to object (the workpiece) is in this set-up 400 mm.

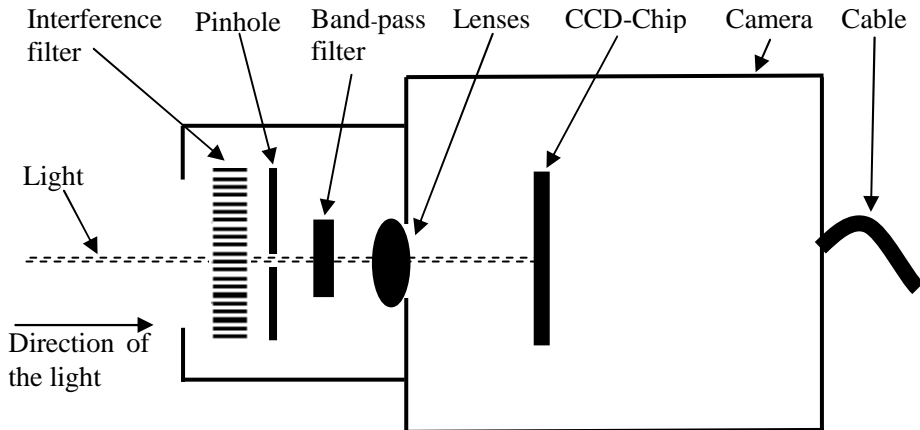


Figure 7-11 The optical set-up of the camera.

In the process of choosing all the elements required in the optical design a calculation spreadsheet involving all the elements in the optical set-up was made. These calculations were made in the mathematical program MathCad and can be viewed in Appendix G.

In Appendix G the shutter time is set to 1/120 sec. The shutter time is the time in which the chip is disposed to light. The resolution of this camera is calculated to 0.11 x 0.11 mm. The definition of resolution is here defined as the area of the object that one pixel measures. If the travel speed during a weld experiment is 5 mm/sec. and the shutter time of the camera is 1/120 sec. then the camera moves 0.042 mm per shut. That is a little more than 1/3 of the resolution of one pixel. The shutter time and resolution is therefore satisfyingly proportionalised.

7.1.3. Raw Images of the Temperature Imaging System

In this section surface temperature images measured by the above-described surface temperature imaging system are illustrated.

The images depict are raw images where the shutter time is varied from 1/1000 of a sec. to 1/60 of a sec.. Varying the shutter time enables the imaging system to measure in higher and lower temperature ranges (Figure 7-12 to Figure 7-14) and gives a good sense of the capabilities of the camera. The images are all captured in the same GTAW welding process. The travel speed is 0 and the welding process is in quasi-stationary state. All the images are captured from the side in an angle of 45° relative to the vertical workpiece and the gas nozzle is positioned horizontal (see Figure 7-9).

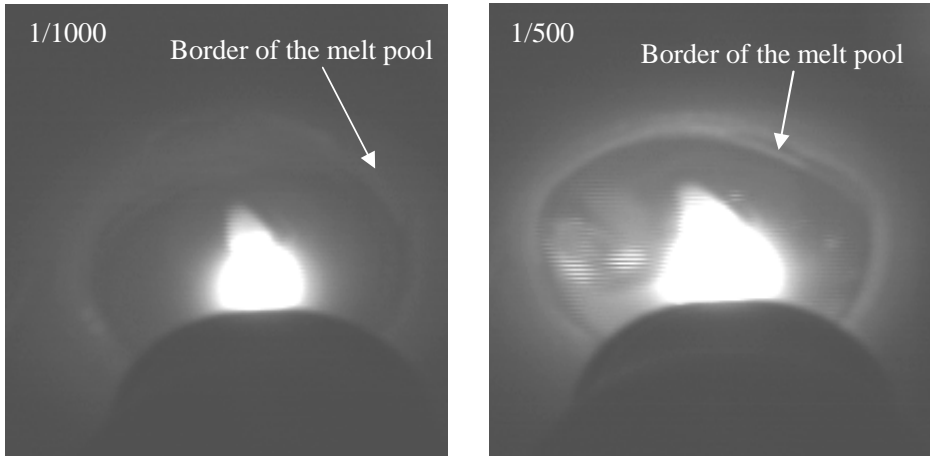


Figure 7-12 Captured with a shutter speed of 1/1000 and 1/500 of a sec.

In these images (Figure 7-12 to Figure 7-14) the white area is the area where the camera pixels are saturated. The saturation is partly due to the high temperatures in the middle of the melt pool and undesired radiation from the arc. The black cone in and below the weld is the gas nozzle. The Wolfram tungsten electrode is hidden behind the gas nozzle. None of these images are calibrated to an absolute temperature scale.

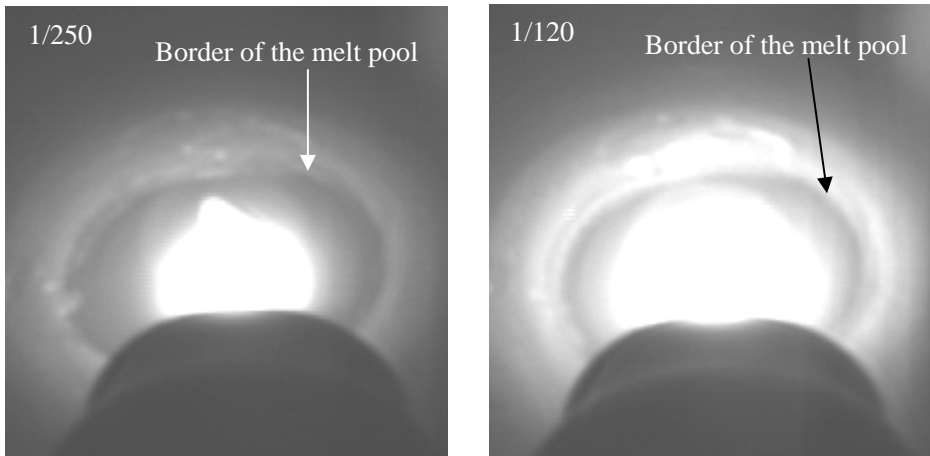


Figure 7-13 Captured with a shutter speed of 1/250 and 1/120 of a sec.

The higher the shutter speed is the larger the saturated area is. When the shutter speed is 1/60 the saturated area has expanded into the non-melted part of the material where it interrupts the desired temperature measurements. In Appendix G the optimal shutter speed is calculated to 1/120 of a second. The measurements (Figure 7-12 to Figure 7-14) consolidate the calculated shutter speed. A shutter speed of 1/120 sec enables temperature measurements from just above the melting

point to 200°C below the melting temperature. In the following part of this rapport the shutter speed of 1/120 sec. is used.



Figure 7-14 Captured with a shutter speed of 1/60 of a sec.

When interpreting these temperature images generated by the temperature sensitive imaging system one has to be aware that the dark areas not necessary are shadow areas but areas with relative lower emitted radiation. It is tempting to imagine a three dimensional geometry based on the grey tone pattern in these images. This is however not the correct way to interpret these temperature images. The white areas are areas emitting more radiation whereas the dark areas are emitting less radiation.

In the next section the optimal position of the camera in relation to the arc is discussed.

7.1.4. Position of the camera

All the radiation emitted from the radiating arc and electrode has despite the present filtration (Section 7.1.2) not been 100% off-filtrated. To minimise the undesired radiation further the position of the camera must be chosen with care.

Below an image is figured (Figure 7-15) which is captured from the side of the welding where the travel speed is 4.5 mm per sec. In this picture the white area is the area where the camera pixels are saturated. The tail of the weld pool can be seen to the left. The black cone in and below the weld is the gas nozzle and the white light above is undesired reflected radiation, mainly from the electrode.

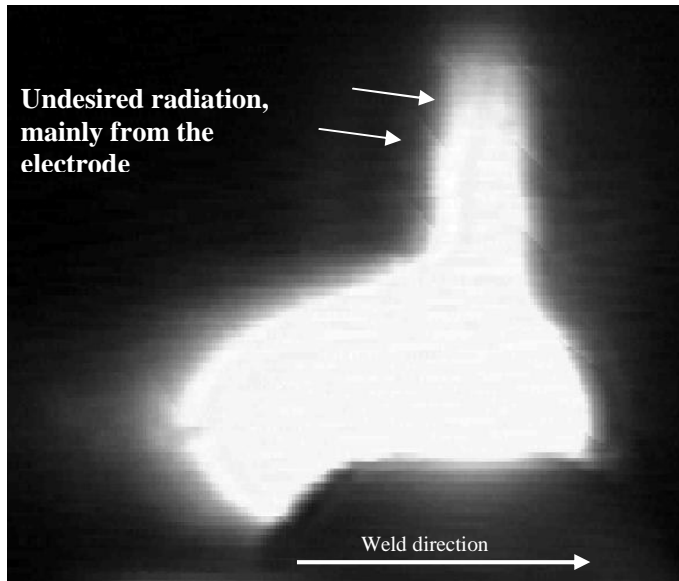


Figure 7-15 Image captured from the side of the weld. This picture has not been calibrated to fit a temperature scale.

In the figure above (Figure 7-15) it is easy to identify the undesired radiation from the electrode. There is no doubt that the light above the weld is not a part of the weld.

In the following two images, captured under the same conditions as the image above (Figure 7-15), the surface temperature profile has been captured from behind the weld in an angle of 45 degrees (Figure 7-16). Opposite the image above (Figure 7-15) the two images below are depict in 3 dimensions (3D). The first two dimensions are the width and length where the third dimension is the intensity of the emitted radiation. The areas lying high are areas that are hotter than the low areas. The grey tone is here only used to enlarge the visual effect of the temperature field.

In Figure 7-16 one can identify a temperature hill. This hill is mainly due to reflection of undesired radiation from the electrode. At the border of the weld pool where the material goes from melted to solid state, the surface of the melted and the surface of the solid material is most often not the same level. Sometimes the border of the melted pool is higher than the solid material and opposite. This geometrical height difference creates a hill along the weld pool. Along this geometrical hill the angle of the surface changes. Some surface angles reflect the emitted radiation from the electrode better than other angles. This differentiation in the reflect ability along the weld pool border generates a hill effect in the measured intensity of radiation. By choosing the correct camera angle it is possible to minimise this undesired reflection from the electrode substantially.

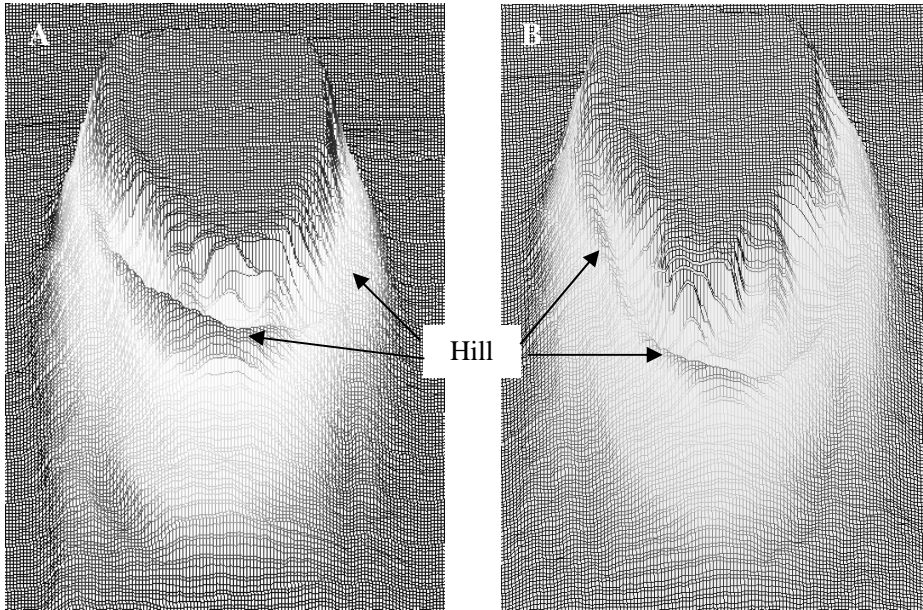


Figure 7-16 Two images captured of the same quasi-stationary process at two different time-steps.

When calibrating the camera to an absolute temperature scale (Section 7.3) the radiation energy in the bottom of the “valley” just before the hill of high radiation is used as calibration value. The reason for this is that it is assumed that the undesired reflection from the electrode here is close to zero and that the temperature here is at the melting point. The fact that the temperature here is known and the undesired reflected radiation here is assumed to be minimal makes it an applicable calibration point.

In Chapter 3 the *input* and *output* variables were chosen. The *output* variables were chosen to be the *average temperature* of the weld tail and the *approximated width* of the weld (Table 3.3). For both of these *output* variables it is important that the noise from the arc and the electrode is minimised.

Two factors were taken into consideration when choosing the position of the camera:

- To enable measurement of the optimal *output* variable (Chapter 3).
- To minimise the noise from the electrode and argon arc.

The temperatures to be measured by the imaging system are temperatures from 1350°C to 1530°C. Of the temperatures in this temperature span are the temperatures at the tail of the weld most far away from plasma arc. Hence are the temperature measurements at the tail of the weld less influenced by the arc. It is therefore natural to perform the measurements at the tail of the weld.

To measure temperatures at the tail of the weld without the nozzle shading for the tail of the weld, gives two possible positions of the camera. One, measuring behind the weld. Two, measure from one of the sides of the weld.

To measure from behind the weld will however maximise the undesired reflected radiation emitted from the electrode (See Figure 7-15 and Figure 7-16). The undesired reflection at the tail of the weld is much lower when the camera is placed at the side. The position of the camera is therefore chosen to be on the side of the weld.

The optimal angle from the workpiece to the camera was in Section 7.1.2 chosen to be 45° (Figure 7-10). This decision was a compromise between the interference filtration and optical resolution.

In the remaining of this report the temperature profiles depict are measured from the side and in a camera to workpiece angle of 45 degrees.

Below in Figure 7-17 and Figure 7-18 is respectively the undesired reflection of the electrode and the undesired radiation of the plasma arc visualised. This is done by depicting the pixel energy though the centre of the weld of five in a row made measurements (Figure 7-18). The pixels values illustrated are the pixels values along the black line sketched in Figure 7-17. The five pixel energy intensity measurements of Figure 7-18 are made while shutting off the argon arc. The first three measurements are with the arc on, while the argon arc is turned off in the two last measurements. The time between each of the measurement is 1/10 of a second. A pixel energy value of approximately 245 equals the melting temperature of the iron workpiece (Figure 7-18). When the pixel energy value is above 245 the CCD-chip is saturated. There are therefore, in this measurement, no pixel energy values higher than 245.

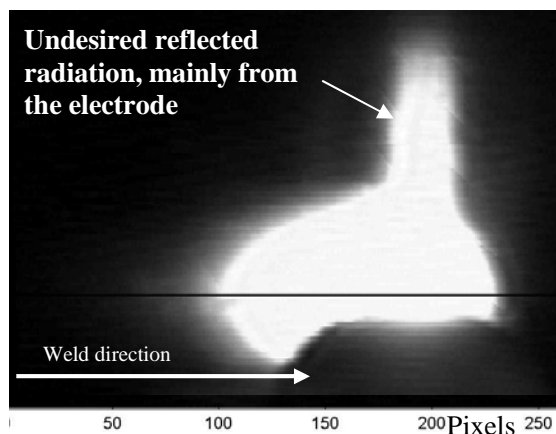


Figure 7-17 The pixel energy along the black line in the centre of the weld is depict in Figure 7-18.

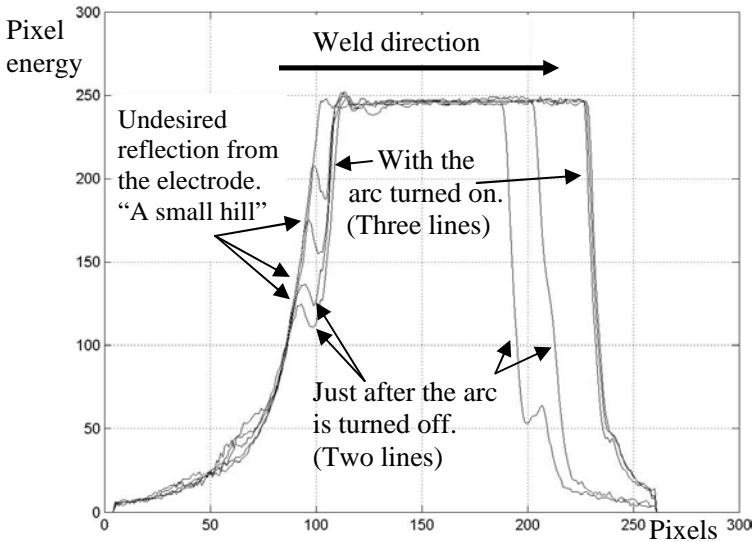


Figure 7-18 Five measurements of the pixel energy along the centre of the weld. The travel speed is remained on 4,5 mm per sec. One pixel equals to 0,1 mm.

After shutting off the arc the pixel energy falls distinctly in the front of the weld. At the tail of the weld the drop in pixel energy is less distinct. The large drop in the front of the weld is mainly due to two reasons: One, that the weld is moving forward causing high temperature gradients. Two, that the front of the weld is positioned much closer to the centre of the arc than the tail of the weld is. At the tail of the weld the noise from the arc does not seem to have a significant effect. The undesired reflection of the electrode is though visible at the tail. The undesired reflection from the electrode can be seen as a small hill at the tail of each measurement (Figure 7-16).

In this section it was concluded that the most optimal position of the camera is on the side of the weld in an angle of 45 degrees from the workpiece to the camera. In the next section the possibility to create a temperature imaging system, which is independent of the factor of emittance, is discussed.

7.2. Emittance independent measurements

The theory, which enables us to measure the surface temperature by means of a vision camera, is Planck's law (Eq. 7.1).

$$E_1 = \varepsilon \cdot \frac{C_1}{\lambda_1^5} \cdot \frac{1}{e^{\frac{C_2}{\lambda_1 T}} - 1} \quad 7.1$$

Where E is the energy emitted in the wavelength (λ) from an given object, ε is the factor of emittance, T is the absolute temperature in Kelvin, and C_1 and C_2 are constants.

To measure the temperature, T , by means of the energy emitted, E , the wavelength, λ , and the factor of emittance, ε , must be known. A suitable band-pass filter easily controls the wavelength whereas the factor of emittance is not so easily controlled. The factor emittance varies along the workpiece. The factor of emittance changes if the workpiece is dirty or contains spots of rust.

Because the WAMOS-system is meant for use in the heavy metal industry such as shipyards, where the nature of the surface of the workpieces to be welded are changing substantially, a special effort has been placed in gaining a method, by which it is possible to measure the temperature independently of the factor of emittance, ε .

In the search for possible ways to perform emittance independent surface temperature measurements by means of the conventional vision camera it was natural to look at Planck's law of radiation (Eq. 7.1). During this process it was discovered that it theoretically is possible to measure the temperature independent of the factor of emittance. Both, how this is possible and the mathematical proof for this is demonstrated in Appendix H.

The idea is to measure the temperature in two different wavelengths. Planck's law opens up this possibility if the temperature to be measured is not too high (e.g. below 3000°C), see Eq. 7.2.

$$T = \frac{C_2 \cdot \left(\frac{1}{\lambda_2} - \frac{1}{\lambda_1} \right)}{\ln \left(\frac{E_1 \cdot \lambda_1^5}{E_2 \cdot \lambda_2^5} \right)} \quad 7.2$$

Based on Eq. 7.2 it is possible to calculate the absolute temperature by means of two measurements of the energy emitted from an object. Because the energy is measured in two different wavelengths (λ_1 and λ_2), this measurement is independent of the factor of emittance, ε .

When using the camera C_2 , λ_1 and λ_2 are known constants. Eq. 7.2 is therefore simplified to a function of E_1 and E_2 :

$$T \left\{ \begin{matrix} E_1 \\ E_2 \end{matrix} \right\} = \frac{C_a}{\ln \left(\frac{E_1 \cdot C_b}{E_2} \right)} \quad 7.3$$

7. Temperature Imaging System

Based on the above equation (Eq. 7.3) it is clear that the temperature, T , is based on the proportion of the measured energy E_1 and E_2 . Therefore the camera system is supposed to measure the emitted energy of one point in two different wavelengths. How to measure the emitted energy of one point in two different wavelengths can be seen in Appendix H.

Because the temperature estimation theoretically is based on proportions, a table containing different proportions and their matching temperature could give us the absolute temperature based on a camera measurement in the two wavelengths. Using a table containing proportions and their respective absolute temperatures would give a simple and applicable system. The camera system first measures the two energy levels then divides them, and based on this division the absolute temperature is achieved from the table containing proportions and their respective absolute temperatures. This table could be generated based on a calibration or theoretically. See the calibration of the emittance independent temperature imaging system in Appendix I.1.

Despite the possibility to measure the surface temperature independent of the factor of emittance it is decided not to use this possibility. This is due to insufficient filtration. When performing emittance independent measurements two band-pass filters are required. The filters chosen in this project is a filter centred at 640 nm with a width of 40 nm and a filter centred at 1010 nm with a width of 40 nm (Appendix F). The filter centred at 1010 nm performs satisfactorily, whereas the filter centred at 640 nm performs poorly. It was therefore chosen to continue the experiments of the WAMOS-system based on the emittance dependent temperature imaging system where the band-pass filter centred at 1010 nm was used only.

The clear effect of the emittance independent temperature imaging system is however tested and shown in Appendix I.1.2. This test is though based on two former band-pass filters that have been tested earlier in the project.

In the following section the emittance dependent temperature imaging system is calibrated.

7.3. Calibration of the Temperature Imaging System

The calibration of the emittance dependent temperature imaging system was done based on three different methods:

1. Calibration in a furnace and by means of thermocouples.
2. Calibration on a non-moving weld and by means of thermocouples.
3. Combined theoretical and physical calibration on a moving weld.

The first two methods turned out to be inadequate for calibration of the temperature imaging systems, whereas the third method performs satisfactorily. The emittance dependent temperature imaging system is therefore calibrated by means of the third method. Only the third method, which combines theoretical and physical calibration on a moving weld, is presented in this section. All three methods are explained in Appendix I.

The calibration of the emittance dependent temperature imaging system was done based on an active and moving weld where the melting point is used as temperature reference. By means of one reference temperature and Planck's law it is possible to calibrate the temperature imaging system. The melting point of the workpiece is on the boarder of the weld and has a temperature of 1530 °C. The position and the measured vision value of the melting point can be identified from stored camera measurements after an ended calibration welding.

Based on the emitted radiation of the workpiece it is, by Planck's law, possible to calculate the absolute temperature (Eq. 7.4):

$$T = \frac{C_2}{\lambda} \cdot \frac{1}{\ln\left(\frac{\varepsilon \cdot C_1}{E \cdot \lambda^5} + 1\right)} \quad 7.4$$

Where C_1 , C_2 , and λ are known constants and ε is dependent on the surface of the given workpiece. This expression can be simplified to (Eq. 7.5):

$$T = C_A \cdot \frac{1}{\ln\left(\frac{C_C}{Value_{pixel}} \cdot C_B + 1\right)} \quad 7.5$$

Where C_A is based on the constants C_2/λ and C_B is based on the constants C_1/λ^5 . $Value_{pixel}$ is the value measured by the temperature imaging system at the identified melting point. C_C is a correction constant that describes the difference in emitted energy compared to the measured temperature value, $Value_{pixel}$. The factor of emittance, ε , constitute a part of the correction constant C_C (Eq. 7.5):

This correction constant C_C is the constant that is to be identified in the calibration process of the emittance dependent temperature imaging system. As C_A and C_B are based on known constants and the $Value_{pixel}$ is measured at the temperature $T = 1530^\circ\text{C}$ the calibration constant, C_C , is computable (Eq. 7.6).

$$C_C = \frac{Value_{pixel}}{C_B} \cdot \left(e^{C_A \frac{1}{T}} - 1\right) \quad 7.6$$

7. Temperature Imaging System

In a calibration test on a workpiece similar to the one used in the final experiments (Chapter 9) the measured value of the temperature imaging system was measured to 142. Based on this figure the constant C_C is by Eq. 7.6 calculated to 0,0333.

By means of the calculated constant, C_C , and Eq. 7.5 the relation between measured pixel values and the absolute temperature is drawn (Figure 7-19).

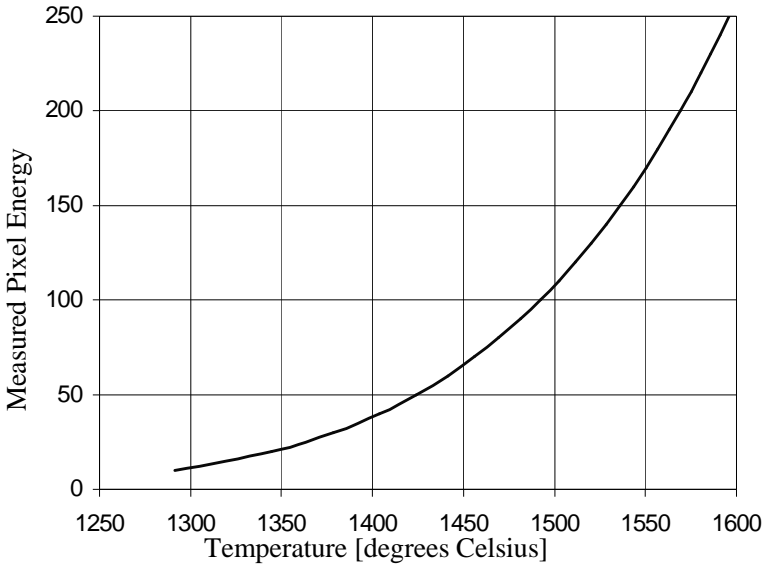


Figure 7-19 depicts the relation between the measured pixel value and the corresponding calibrated absolute temperature.

This calibration is used in the following section where measured surface temperatures of an actual performed weld experiment are compared to surface temperatures of the corresponding simulated weld experiment. The calibration procedure is described in more details in Appendix I.3.

7.4. Temperature Measurements Compared to Off-line Simulations

In Appendix J measurements performed by the emittance dependent temperature imaging system are compared to thermal simulations generated by the finite-element model of the *off-line preparation system*. The comparison is made on the basis of the width of the weld and the gradients at the side of the weld pool, only, as these are regarded as crucial parameters in avoiding welding defects like e.g. lack of fusion and/or penetration. The finite-element model of the *off-line preparation system* has been calibrated. The finite-element model is calibrated to fit the height and the width of these post-process macro cross sections at a welding *current* of 143 amps.

The temperature measurements that are compared to off-line simulations in appendix J shows that the width of the simulated weld is 8.7 mm and the width measured by the temperature imaging system on a corresponding actual weld process is 10 mm. 0.05 second after the arc is shut off the width measured by the temperature imaging system, was though measured to 8.7 mm which equals the width of the simulated weld. Macro cross sections of the workpiece made subsequently shows that the width of the physical weld is 8.7 mm.

The gradients were also compared. The gradients were measured as the distance from where the temperature on the side of the weld is 1500°C to where the temperature is 1400°C. This distance was for the simulated weld measured to 0.15 mm and for the actual weld, measured by the temperature imaging system, measured to 0.9 mm. Because the gradient does not change after the arc is turned off, this inconsistency is concluded not to be due to the disturbing arc (See Appendix J). The error might come from either undesired radiation from the electrode or an incorrect simulation model.

Because of this inconsistency in temperature and temperature gradient measured by the temperature imaging system and gradients simulated by the *off-line preparation system*, it is decided not to use the *off-line preparation system* when the WAMOS-system and hence the *WAMOS-method* is tested in Chapter 9.

As replacement for the *reference-generating simulation* and the *step-input simulation* of the *off-line preparation system* actual weld experiments are performed to generate the data needed. In these *reference-generating experiments* and *step-input experiments* the temperature imaging system measures the workpiece surface temperature distribution on which the on-line model is to be built as well as the *reference* temperatures needed for the on-line system. The actual welding experiments used as substitute for the *step-input simulations* was presented in Chapter 3.3

Because the temperature imaging system based on an actual welding is used as substitute for the *off-line preparation system* it is not necessary to calibrate the emittance dependent temperature imaging system to absolute temperatures. To use absolute temperatures, when the on-line control-system compares the actual archived surface temperature profiles to the temperature profiles of the *reference-generating experiment*, would not be of any use only serve as an extra complexity. Non-calibrated measurements of the temperature imaging system are therefore used when testing the WAMOS-system (Chapter 9).

Though deviations for both the developed camera and the simulation were identified, a promising correspondence was demonstrated. The deviation was in Appendix J concluded to be due to lacking filtration of the arc and limitations to the simulation model of the *off-line preparation system*.

In the next section the physical structure of the temperature imaging system is described.

7.5. Components of the Temperature Imaging System

The temperature imaging system is physically based on an optic and a camera which is connected to a computer by means of a cable and a frame grabber. The software that controls the camera and generates the *input* for the controller of the WAMOS-system is programmed in the program WIT. WIT is a programming language similar to Lab View and HP VEE. WIT is an icon-based programming language optimised for image analysis. The programming is in practical based on connecting different *Operators* (icons) by *Links* (lines) (Figure 7-20).

Each of the *operators* is based on C code. It is therefore possible to build new *operators* or change in existing *operators*.

By means of additional software that follows with the camera it is possible to control the exposure, gain, shutter time etc..

In the WAMOS-system the WIT program not only controls the temperature imaging system it also controls all the equipment of the WAMOS-system. The full on-line WAMOS system is presented in the following chapter (Chapter 8).

In this chapter the temperature imaging system was described, calibrated and tested. Two systems were described: One temperature imaging system, which is dependent on the factor of emittance, and one system, which is independent of the factor of emittance. Both of the temperature imaging systems were tested and performed well. In Appendix I.1.2 it was visually illustrated that the temperature measurements of the emittance independent temperature imaging system were warring less due to emittance changes of the workpiece than the emittance dependent temperature imaging system. Despite the capability of the emittance independent imaging system it was decided not to use the emittance independent temperature imaging system in the final experiments. This is due to poor filtration of one of the bandpass filters. The temperature imaging system which is dependent on the factor of the emittance is instead used in the final experiments (Chapter 9). The emittance dependent imaging system is capable to measure temperatures from 1350 °C to 1530 °C.

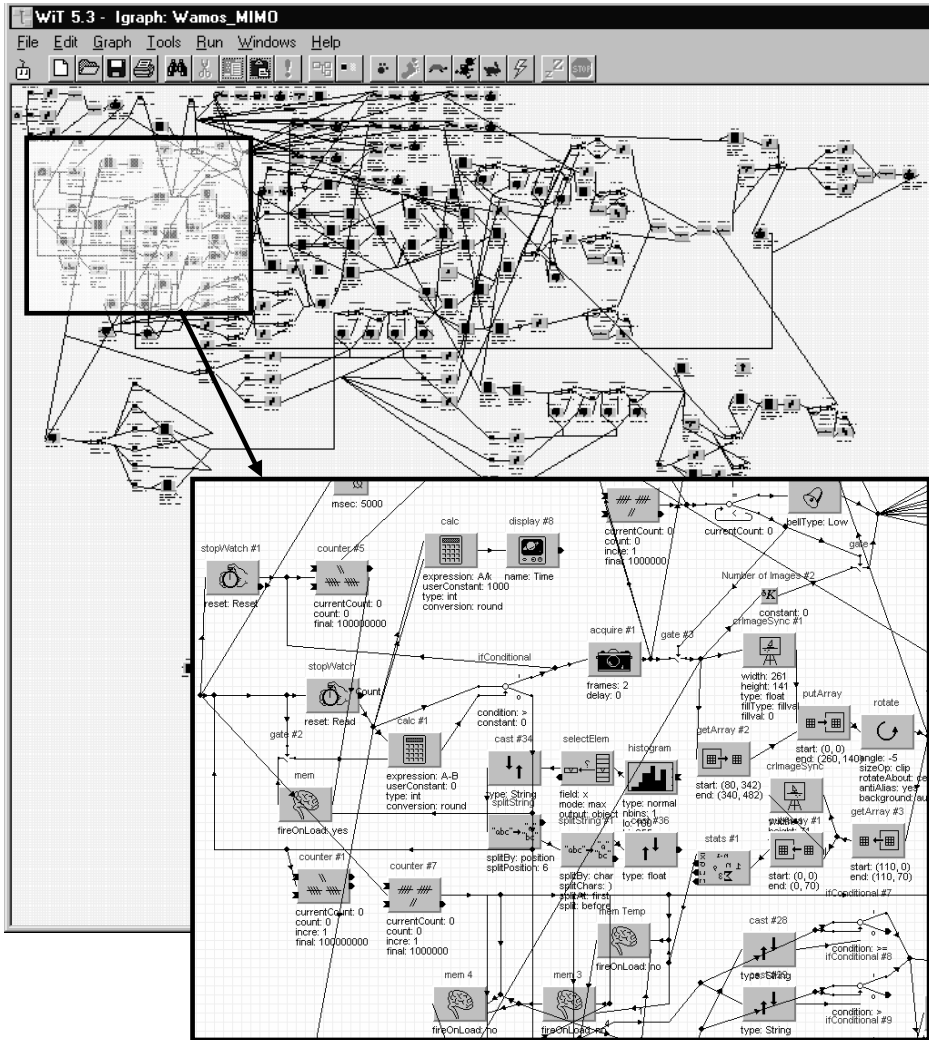


Figure 7-20 The whole temperature vision program programmed in WIT is visualised above and below an enlarged segment of the program is visualised.

In Section 7.4 off-line simulated surface temperatures were compared to corresponding surface temperature measurements of the emittance dependent temperature imaging system. This comparison demonstrated a promising correspondence between the simulated and actual measured temperatures but also some inconsistencies were demonstrated. Because of these inconsistencies it was concluded not to use the *off-line preparation system* for the *reference-generating simulation* when testing the WAMOS-system and hence the *WAMOS-method* in Chapter 9.

7. Temperature Imaging System

As replacement for the *reference-generating simulation* actual welding experiments are performed to generate the data needed of the *off-line preparation system*. Because the imaging system is used as a substitute for the *off-line preparation system* it is not necessary to calibrate the emittance dependent imaging system to absolute temperatures. Non-calibrated measurements of the imaging system are therefore used when testing the WAMOS-system.

In the following chapter the equipment used to test the WAMOS-system and hence the *WAMOS-method* is presented.

8. On-line Weld Execution System

Based on the off-line generated *reference* (Chapter 4), the controller built in Chapter 6, and the imaging system developed in Chapter 7 the on-line weld execution system becomes a reality.

In this chapter the on-line weld execution system is introduced. In this introduction to the on-line weld execution system the elements of the on-line weld execution system and their coherence are described. In Chapter 9 the results of the on-line weld execution system are presented.

The architecture of the on-line system is depicted in Figure 8-1.

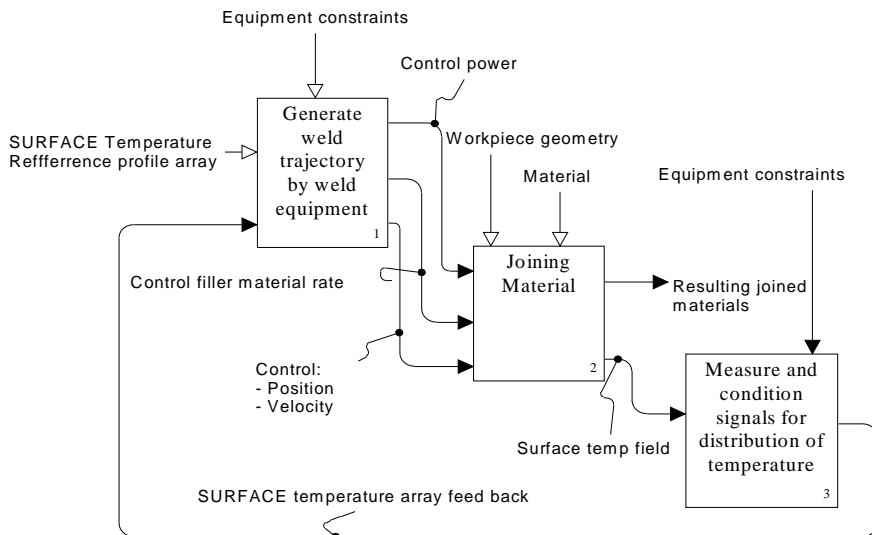


Figure 8-1 Architecture of the on-line control-system, which is real-time controlling the physical welding procedure.

Three main boxes describe the architecture of the on-line system. This architecture was described in Section 1.3.2.

In the following section a general description of the experimental equipment is given.

8.1. Experimental Equipment

To verify the design of the on-line control-system and hence the *WAMOS-method* setting up a physical real-time weld equipment was required. This real-time weld execution system is based on two computers, a x-y table, a weld machine, and the vision camera. In this report the on-line system is described in broad terms only. The general architecture is illustrated in Figure 8-2.

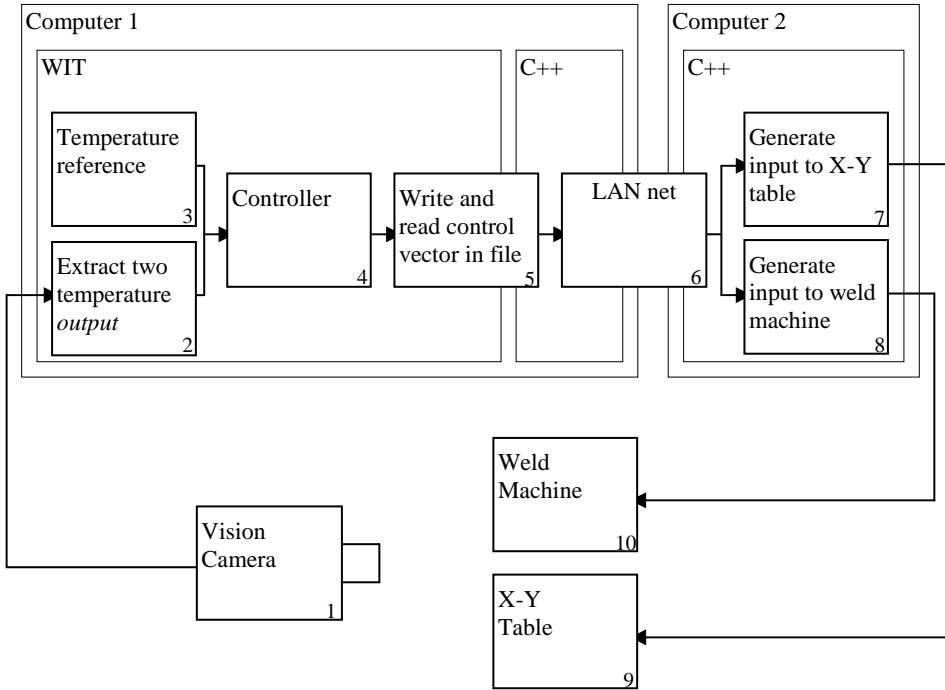


Figure 8-2 The general architecture of the physical on-line weld execution system.

Two computers control the on-line system. Computer 1 is a Pentium 800 MHz with two processors where Computer 2 is a Pentium 500 MHz with one processor. On these two computers three main programs are running. On Computer 1, which is the main computer, a WIT program and a C++ program are running. On Computer 2 one C++ program is running. A LAN connection is connecting these two computers.

One of the two programs that run on Computer 1 is written in WIT code. WIT is an icon-based programming language optimised for image analysis. The WIT program was introduced in Section 7.5 The program WIT was from the beginning chosen to be the main program of the system as the image analysis is the most resource requiring process of the on-line weld execution system. The other two programs of respectively Computer 1 and Computer 2 are written in traditional C++ code.

To give a general understanding of the system the content of the boxes numbered 1-10 is gone through:

Box 1 the “Vision Camera” is the CCD-camera and the in Chapter 7 designed emittance dependent optic. The camera is linked to and controlled by the “WIT” program of “Computer 1”

Box 2 the “Extract two temperature *output*” is the part of the WIT program that controls the camera. For each time-step the WIT program captures an image. From this temperature image the WIT program extracts the two temperature *output*, \underline{Y} . Before the extracted temperatures are used in the “Controller” box 4 the temperatures are subtracted with the displacement made during the off-line identification of the transfer-functions. This displacement of the *output* data was done to narrow the data window and hereby get more exact and simple transfer-functions (Section 5.2.1). These two temperatures are in box 4 the “Controller” compared to the “Temperature reference” Box 3.

Box 3 the “Temperature reference” is the temperature *reference* that is calculated in the *off-line preparation system*. The *reference* data is also subtracted with the displacement made during the off-line identification of the transfer-functions (see Eq. 9.9. and 9.10). This temperature *reference* is in the final experiments a constant and is for every experiment manually written into the code.

Box 4 the “Controller” is the P-controller. Based on the “Temperature reference” and the *output* the P-controller calculates the *input* vector, \underline{U} , of the physical system for every time-step. This *input* vector is added with the step-input values $\underline{U}(\delta)$. This is due to the displacement carried through during the off-line identification of the transfer-functions.

Box 5 the “Write and read control vector” writes the *input* vector to a file that is placed on “Computer 1”. Before writing the *input* vector the *input*, *weaving amplitude input*, is transformed to an absolute position. The value of the *input*, *current*, is remained the same as in the *input* vector. This is all done in the WIT program. While the WIT program for every time-step writes the transformed *input* vector to the file a C++ program reads from the file. The C++ program constantly checks if the file has been updated. If that is the case it will read the transformed *input* vector from the file.

Box 6 the “LAN net”. When the C++ program reads the file a server program sends the *input* vector by means of a LAN connection to “Computer 2”. On “Computer 2” a C++ client program receives the *input* vector and distributes the vector to respectively the program that generates the input for the x-y table, box 7, and the program that generates the input for the weld machine, box 8.

Box 7 the “Generate input to x-y table” program receives for every step-input the desired absolute position of the x-y table. To ensure that the x-y table is in the

8. On-line Weld Execution System

desired position at next time-step the required acceleration and velocity is calculated. This desired position, velocity, and acceleration is, by means of a wire connection and the software that came with the x-y table, communicated to the x-y table, box 9.

Because of the method used to measure the *output* variable, the *approximated width* of the weld, it is required that the x-y table is at the extreme point of the weaving when every new time-step is initiated. This is because temperature imaging system, which is a part of the WIT program, is programmed to capture the new temperature profile when the x-y table and hence the weld is at the extreme point of the weaving (Section 3.3).

Box 8 the “Generate input to the weld machine” program receives for every step-input the desired *current*. This desired *current* is, by means of a wire connection and the software that came with the weld machine, communicated to the weld machine, box 10.

Box 9 the “x-y table” is a CNC controlled table owned by FORCE Technology. The x-y table is controlled by two Packerhauser servos of the type HDX 92E4-44S1. The resolution of the servo is $\pm 0,014$ mm. The x-y table is illustrated in Figure 3-2.

Box 10 the “Weld Machine” is a Migatron BDH 320 weld machine owned by FORCE Technology. The machine is a 320 amps digital GTAW machine.

The control-system runs with four time-step per second (4 Hz) and the weaving frequency is 2 Hz. The temperature imaging system is set to capture the weld only in high and low position of the *weaving amplitude* that is when the weld is at the extreme point of the weaving (Section 3.3). To stable lice the estimate of the *output* variable, *approximated width* of the weld, the measurement of the past four time-step are compared and the largest figure is chosen. The *output* variable, *average temperature*, is used directly, for every time-step, without any stabilisation.

There are of cause many details in the design of the automatic weld execution system, on which the *WAMOS-method* is tested, that have not been mentioned. As these details have not been found necessary for the proper understanding of the work of this thesis it is chosen to describe only the most important information flow in and between the programs of the on-line control-system. In theory the *WAMOS-method* is independent of the design of the automatic weld execution system. The program code of the automatic weld execution system is therefore also not illustrated in this thesis.

In the next chapter the final experiments, where the WAMOS-system and hence the *WAMOS-method* is tested, are presented.

9. Experiments

In this chapter the WAMOS-system and hence the *WAMOS-method* is tested. The test is based on five weld experiments performed on the on-line weld execution system described in Chapter 8.

As discussed in Chapter 4 it was because of time limitations decided not to calibrate the finite-element model and the imaging system to correspond each other. Consequently the *reference-generating simulation* and the *step-input simulation* of the *off-line preparation* are therefore not used here, but instead welding experiments are performed to generate the data needed of the *off-line preparation system*. These actual weld experiments are named the *off-line preparation experiments*. However, in future versions of the WAMOS-system when the model of the *off-line preparation system* and the measurements of the temperature imaging system are calibrated to correspond to each other the *off-line preparation system* will be used to generate the data needed for building the controller and for the *reference* of the on-line system.

The five experiments performed are therefore two *off-line preparation experiments* used to build the P-controller including the on-line reference and three experiments used to test the P-controller of the on-line weld execution system.

The two *off-line preparation experiments* are performed based on the *input* and *output* variables of Chapter 3 and as described in Chapter 4. The P-controller of the on-line weld execution system is established based on the outcome of the two *off-line preparation experiments* as described in the theory of Chapter 5 and 6.

The established P-controller is tested on three weld geometries. Test one: On a geometry that is analogous to the geometry for the two *off-line preparation experiments*. Test two and three: On a geometry that is analogous to the geometry of the two *off-line preparation experiments* where a step-input on respectively the width and thickness of the geometry is introduced.

The weld parameters under which the experiments have been carried through are given below in Table 9-1.

Constant parameters	Value
Material type	Grade S235
Size of workpiece	300x150x6 [mm]
Electrode type	WT-20
Electrode thickness	2,4 [mm]
Electrode angle	60 [°]
Electrode stickout	4,3 [mm]
Tip to workpiece distance	2,7 [mm]
Gas (pure argon)	10 [l/min]
Work angle	0 [°]
Travel angle	0 [°]
Camera position and angle	Side, 45 Grades
Travel speed	2 [mm/sec.]
Variable parameters	Value
<i>Current</i>	0 to 315 [A]
<i>Weaving amplitude</i>	0 to 3 [mm]

Table 9-1 The experimental weld parameters of the weld experiments performed to test the WAMOS-system and hence the *WAMOS-method*.

Based on the above weld parameters the five weld experiments, meant to test the WAMOS-system and hence the *WAMOS-method*, are presented in the following sections (Section 9.1 to Section 9.4).

9.1. Off-line Preparation Experiments

The first step is to perform the two *off-line preparation experiments*, which is required, to build the P-controller. These two experiments are carried through under the constant parameters given in Table 9-1. In the first experiment a step-input is applied on the *input* variable *current*. In this experiment the *current* initiates at 178 amps. After 45 seconds the step-input is applied by changing the *current* from 178 amps to 222 amps. The *weaving amplitude* is kept constant at 1.5 mm during this experiment. In the second experiment a step-input is applied on the *input* variable *weaving amplitude*. In this experiment the *current* is kept constant at 178 amps and the weaving amplitude is initiated at 0 mm. The step-input is again applied after 45 seconds where the *weaving amplitude* is changed from 0 to 1.5 mm. In both experiments the *output* variables *average temperature* and *approximated width* of the weld are measured. It is these four *outputs* that are used to build the P-controller. In all experiments of this chapter one second equals four time-steps.

In Figure 9-1 the outcome of the two *step-input experiments* are illustrated by the four *output curves*. The same four curves are in fact also depicted in Chapter 3. In Chapter 3 the *input* and *output* variables are determined. A natural way to illustrate the chosen *input* and *output* variables is to exemplify the chosen variables on the actual system and under the same conditions as the weld experiments that are used to test the WAMOS-system. The verification of the chosen *input* and *output* variables of Chapter 3 is therefore done on the same *step-input experiments* as which are depict below (Figure 9-1).

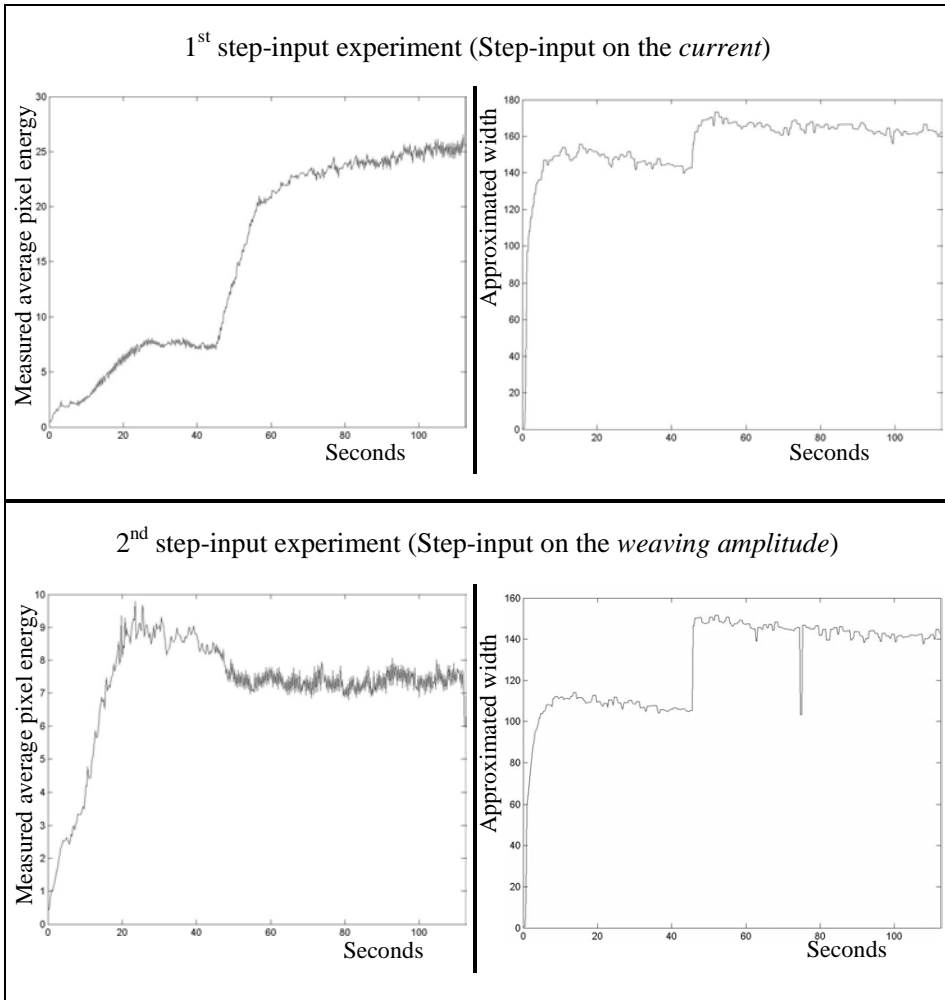


Figure 9-1 The *output* of the two *step-input experiments*.

The *output* data depict in Figure 9-1 is the full *output* data of the two step-input experiments. The *output* data used to build the P-controller is however only an extract of these four *outputs*. The extract is from when the step-input is introduced to 35 seconds after the step-input was introduced. That is in Figure 9-1 the data

9. Experiments

from 45 seconds to 80 seconds. To narrow the data window the *output* data of the four graphs have been displaced along respectively the “measured average pixel energy” axis and the “approximated width” axis. The *output* data depict in Figure 9-2 therefore starts at approximately 0 when the step-input is initiated. To carry through a displacement of the *output* data of the step-input experiment implies that the *input* data must be displaced to their initiating values. To use a control-system, which is build, based on data, which have been displaced, implies that the *output* data and the *input* data of the on-line system for every time-step must be displaced in the opposite direction (See Section 8.1 or Figure 9-6).

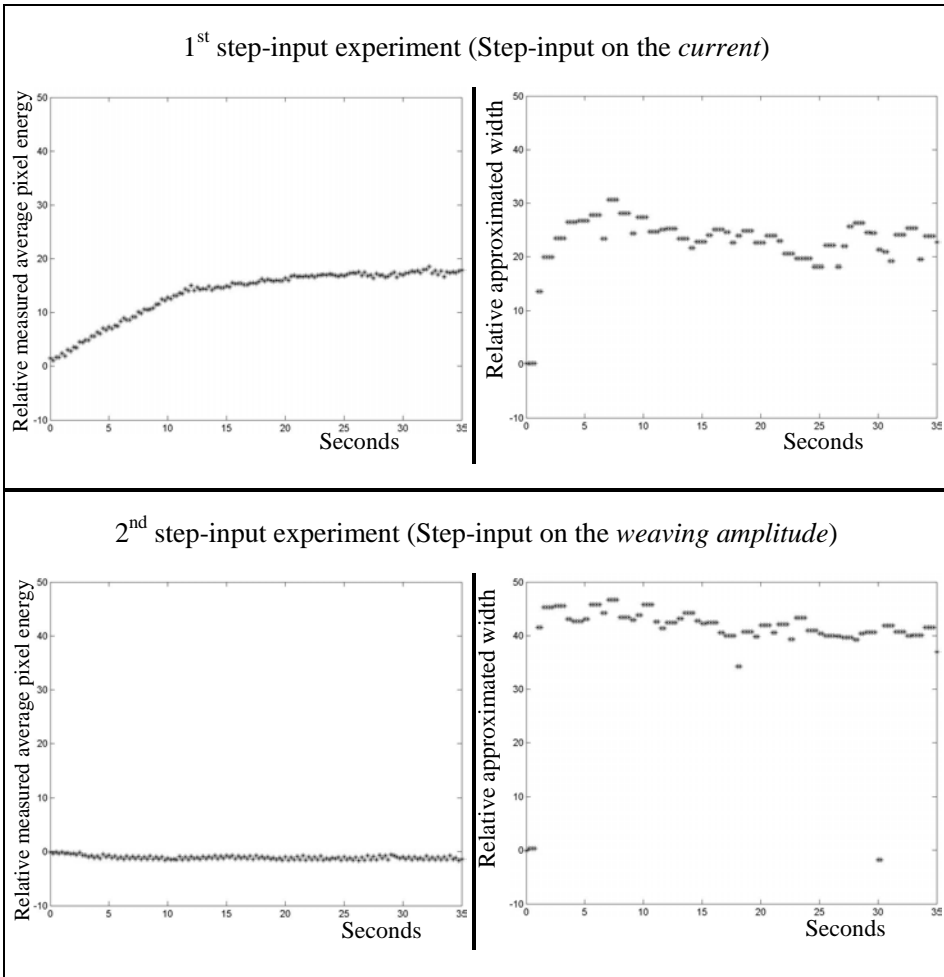


Figure 9-2 The *output* data used to build the P-controller.

Images of the two workpieces on which the *step-input experiments* were carried through can be seen in Figure 3.6 and Figure 3.10.

Based on the four output dataset that are illustrated in Figure 9-2 the respective four transfer-functions are to be identified. The identification is done in accordance to the three identification steps described in Section 5.2.

First, the parameter α for each of the four transfer-functions must be chosen. The α values chosen is the standard α value (Section 5.2.1):

$$\underline{\alpha} = \begin{bmatrix} 3.5/te & 3.5/te \\ 3.5/te & 3.5/te \end{bmatrix} \quad 9.1$$

Where te is the time when the time response is in SS which in this case is approximately 35 seconds after the step-input. te is therefore 35.

Secondly, the degree of the numerator, m , and the denominator, n , for each of the four transfer-functions must be chosen. The degree is chosen in accordance to the rules of Table 5-2:

$$m = \begin{bmatrix} 0 & 0 \\ 0 & 0 \end{bmatrix} \quad 9.2$$

$$n = \begin{bmatrix} 1 & 1 \\ 1 & 1 \end{bmatrix}$$

Finally, identify the four transfer-functions, $\underline{Y}_{G_M}(s)$, and hence the *transfer-function matrix*, $\underline{G}_M(s)$ must be identified.

The transfer-functions are identified based on the parameters above the step-input data-output and the theory of Chapter 5. The four transfer-function are given in Eq. 9.3.

$$\underline{Y}_{G_M}(s) = \begin{bmatrix} \frac{19.0}{10.3s+1} & \frac{25.0}{1.61s+1} \\ -1.25 & 42.6 \\ \frac{4.60s+1}{1.07s+1} & \end{bmatrix} \quad 9.3$$

The step responses of the four transfer-functions are illustrated in Figure 9-3 together with the response of the respective four *output* data ranges of Figure 9-2.

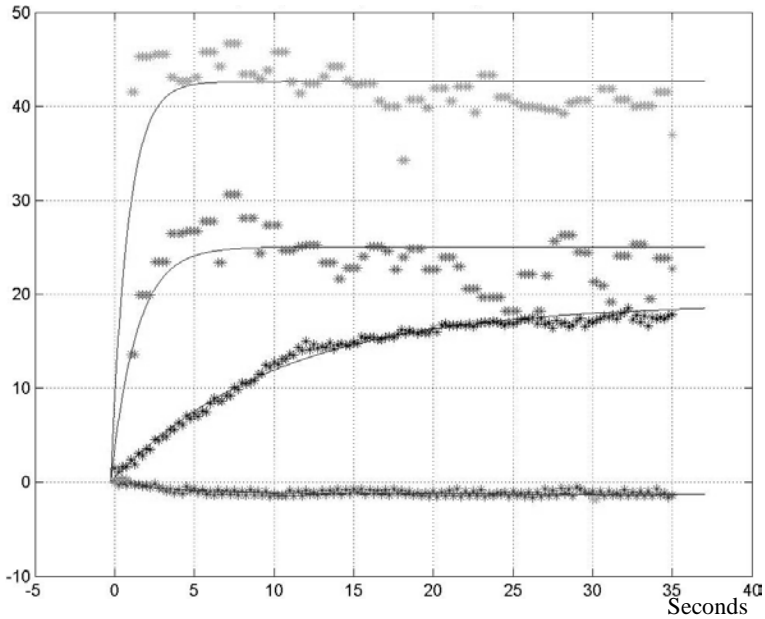


Figure 9-3 The step response of the four identified transfer-functions illustrated together with the actual *output* data.

Based on the identified transfer-functions, $\underline{Y}_{G_M}(s)$, the *transfer-function matrix*, $\underline{G}_M(s)$, is calculated by means of $\underline{Y}_{G_M}(s)$ and $\underline{h}(s)$ (See Eq. 5.6). $\underline{h}(s)$ is the *step-input matrix* and it contains the values of the step-input that was applied in the *step-input experiments*. The two step-input applied was: First, a step-input on the *input variable current*. That was from 178 amps to 222 amps, which is a step on the *current* of 44 amps. Secondly, a step-input on the *input variable weaving amplitude*. That was from 0 mm weaving to 1.5 mm weaving which is a step of 1.5 mm *weaving amplitude*. The step-input matrix can therefore be written as:

$$\underline{h}(s) = \begin{bmatrix} 44 & 0 \\ 0 & 1.5 \end{bmatrix} \tag{9.4}$$

In the above two *step-input experiments*, on which the on-line controller is build, the initiating *input* values of the two experiments were not the same as the initiating *weaving amplitude* of the first step-input experiment was 1.5 mm, whereas it in the second experiment was 0 mm. Strictly spoken it is only correct to vary the initiating values when the system to be identified is perfectly linear which for the present system is not the case for large input variations. The present small variation is however not considered in practice to have significant influence and it is therefore chosen to ignore this minor flaw in the experimental data.

Based on the step-input matrix, $\underline{h}(s)$, and the identified transfer-functions, $\underline{Y}_{G_M}(s)$, the *transfer-function matrix*, $\underline{G}_M(s)$, can be calculated by means of Eq. 5.5.

$$\underline{G}_M(s) = \begin{bmatrix} \frac{0.432}{10.4s+1} & \frac{0.569}{1.61s+1} \\ \frac{-0.832}{4.60s+1} & \frac{28.4}{1.07s+1} \end{bmatrix} \quad 9.5$$

By means of the *transfer-function matrix* the next step is to build the controller. That is the gain matrix K_P together with the *forward-regulation* gain, \underline{V} . The *forward-regulation* gain is easily calculated by means of $\underline{G}_M(s)$ (see Section 6.1).

$$\underline{V} = \underline{G}_M^{-1}(0) = \begin{bmatrix} 2.23 & -0.0446 \\ 0.653 & 0.0339 \end{bmatrix} \quad 9.6$$

To calculate the gain matrix K_P a wish transfer-function matrix, $\underline{F}_W(s)$, must be set up (see Eq. 6.7). Setting up the wish transfer-function matrix is the designer's possibility to influence the behaviour of the control-system. To choose $\underline{F}_W(s)$ usually is a compromise between a desired fast reacting control-system and equipment constraints. In the final experiments the following wish transfer-function matrix was chosen:

$$\underline{F}_W(s) = \begin{bmatrix} \frac{0.2}{s+0.2} & 0 \\ 0 & \frac{0.2}{s+0.2} \end{bmatrix} \quad 9.7$$

The two chosen transfer-functions were of first order because of two reasons. First, all the identified transfer-functions were of first order. Secondly, to keep the calculations as simple as possible. The reason, why the coefficients of both the transfer-functions were chosen to be 0.2, was mainly to slow down the system. When the coefficients are 0.2 the transfer-function step response demonstrates a settling time that is comparable to the settling time of the physical system when it was applied to a step-input on the *current* (see Figure 9-2). The step response of the chosen transfer-functions is depict in Figure 9-4.

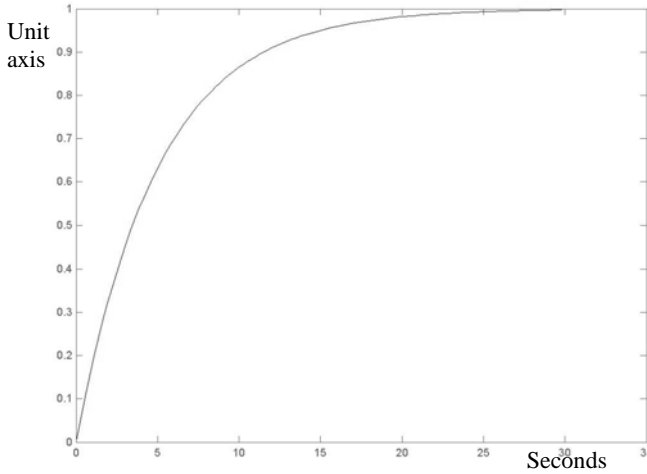


Figure 9-4 Step response of the wish transfer-functions.

By means of the $\underline{F}_W(S)$ and $\underline{G}_M(S)$ and the theory of Chapter 6 it is possible to calculate the gain matrix \underline{K}_P :

$$\underline{K}_P = \begin{bmatrix} 2.29 & -0.0374 \\ 0.0033 & 0.0276 \end{bmatrix} \quad \mathbf{9.8}$$

The last step of the *off-line preparation experiments* is to perform the *reference-generating experiment* to build the reference.

Instead of performing a separate *reference-generating experiment* it is chosen to use the first 45 seconds of the “1st *step-input experiment*”(Figure 9-1). The 1st *step-input experiment* is therefore divided into two stages. The first stage (0 seconds to 45 seconds) is used as the *reference-generating experiment* and the second stage (45 seconds to 112 seconds) is used as the *step-input experiment*. First stage starts after 0 seconds where the *current* and *weaving amplitude* is changed from respectively 0 amps and 0 mm to 178 amps and 1.5 mm. The second stage starts after 45 seconds where the *current* and *weaving amplitude* is changed from respectively 178 amps and 1.5 mm to 222 amps and 1.5 mm. See the output of the *reference-generating experiment* in Figure 9-5.

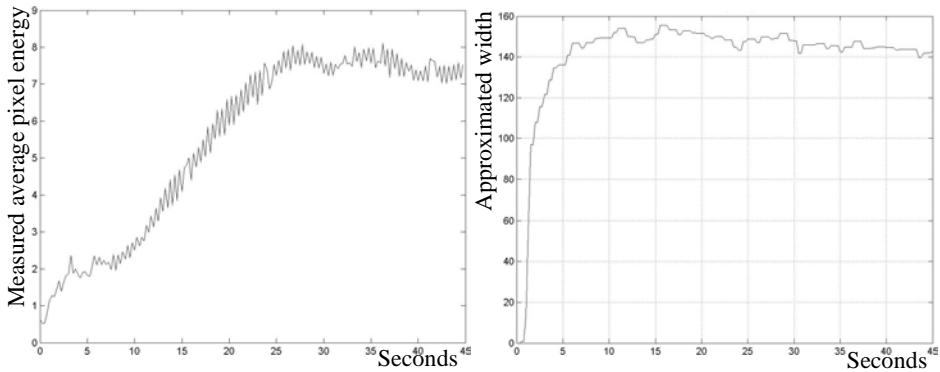


Figure 9-5 The output of the reference-generating experiment.

The *reference-generating experiment* is therefore based on an experiment where the current and weaving amplitude is changed from respectively 0 amps and 0 mm to 178 amps and 1.5 mm. The reference is meant to be the SS output values of this *reference-generating experiment* (Figure 9-5). The true reference is:

$$\begin{bmatrix} 7.25 & 147 \end{bmatrix} \quad \mathbf{9.9}$$

However, as the step-output datasets of the two *step-input experiments* were displaced (Figure 9-2), the constant reference values are changed to:

$$W(s) = \begin{bmatrix} 0 & 0 \end{bmatrix} \quad \mathbf{9.10}$$

that is because the output data sets that are used to build the on-line controller (Figure 9-2) have been displaced so that they initiated from zero. Because the controller is based on data, which were displaced, the *input* data and *output* data of the controller must be displaced equivalently opposite. The *output* of the vision system therefore must be subtracted with $[7.25, 147]$ before the controller processes it and the output of the controller must be added with $[178, 1.5]$ before the controller output is used as *input* for the weld equipment (Figure 9-6).

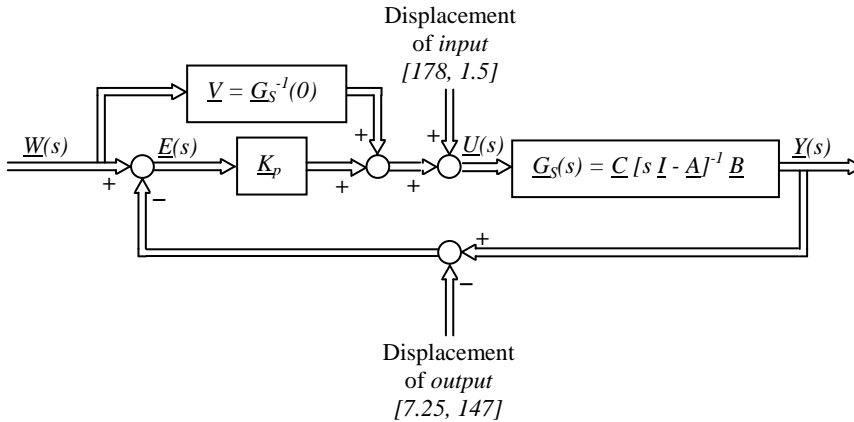


Figure 9-6 Modified block diagram of the on-line weld execution control-system.

All the parameters needed for the on-line weld execution control-system have now been calculated. The steps necessary to calculate the parameters all have the potential to be carried through automatically in a finite-element based *off-line preparation system*. The necessary steps of a potential finite-element based *off-line preparation system* are:

1. Choose a proper step-input, $h(s)$.
2. Carry through *step-input simulation*.
3. Carry through *reference-generating simulation*.
4. Choose *alfa*.
5. Choose the numerator and denominator degrees.
6. Choose a proper wish matrix, $\underline{E}_W(s)$.

To decide a proper step-input, $h(s)$, do not seem to be critical and might therefore very well be done automatically. To carry through simulations is already done. It is though, due to poor calibration, not used in the present experiments. The *alfa* values chosen in this section were the standard *alfa* value. The numerator and denominator degree values chosen in this section were chosen in accordance with the rules of Table 5-2. These rules can be applied fully automatically. To set-up the wish transfer-function matrix $\underline{E}_W(s)$ in principle is an interactive process and is at the moment not automated. One way to build the wish transfer-function matrix $\underline{E}_W(s)$ automatically could be by means of the *off-line preparation system*. To choose $\underline{E}_W(s)$ usually is a compromise between a desired fast reacting control-system and the equipment constraints. In the *off-line preparation system* parameters like workpiece thickness, travel speed and equipment constraints are known. It would therefore stand to reason to define a wish transfer-function matrix $\underline{E}_W(s)$ in the *off-line preparation system*. This method for building dedicated control-systems might therefore very well be done fully automatically.

The next step is to test the weld system and hence the *WAMOS-method* by means of three tests. First an experiment where the controller is tested on a standard workpiece on which no disturbances is applied. This workpiece is similar to the workpiece on which the step-input experiments were carried out. Secondly an experiment on a workpiece where the width halfway is changed from 150 mm to 15 mm. Thirdly an experiment where the workpiece thickness halfway is changed from 6 mm to 3 mm. These three experiments are carried through in the following three sections. First the controller is tested on a standard workpiece on which no disturbances are applied.

9.2. First Weld-test

In the first weld-test the P-controller is tested on a workpiece similar to the workpieces on which the *off-line preparation experiments* were carried through. The purpose of this test is to see how the control-system reacts compared to the *reference-generating experiment* (Figure 9-5). The experiment is performed with the parameters given in Table 9-1 and based on the controller, which were designed in Section 9.1.

The *output* measured by the temperature imaging system is given in Figure 9-7.

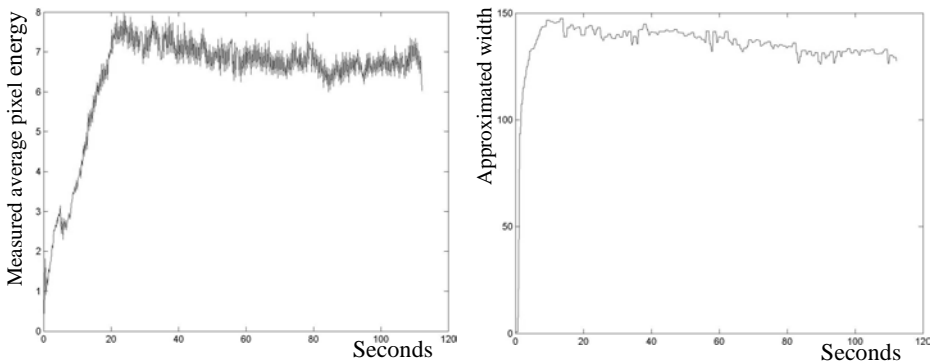


Figure 9-7 Measured output of the first weld-test. Left, average temperature. Right, approximated width of the weld.

On the left the measured *average temperature* is depicted. This temperature should be compared to the reference temperature, which is 7.25. On the right the measured *approximated width* is depicted. This width should be compared to the reference width, which is 147. Why the measurements, from after 20 seconds, for both of the measured *outputs* have a tendency to decrease is not fully understood, but it may be due to distortions of the plate as this influences the arc length and thereby the arc voltage and power. This decreasing tendency has been seen in all experiments carried out with constant weld parameters.

9. Experiments

The error between the measured *output* of Figure 9-7 and the reference (Eq. 9.9) is given in Figure 9-8. In Figure 9-9 the *input* values generated by the P-controller are depicted.

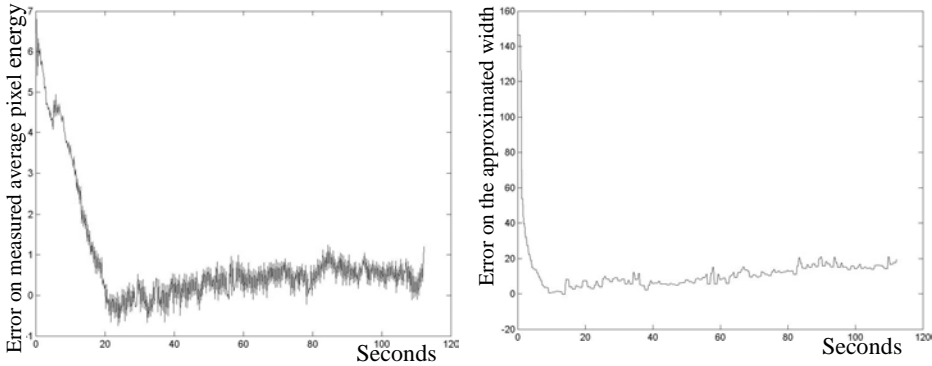


Figure 9-8 The error of the first weld-test. Left, the reference temperature subtracted by the *average temperature*. Right, the reference width subtracted by the *approximated width*.

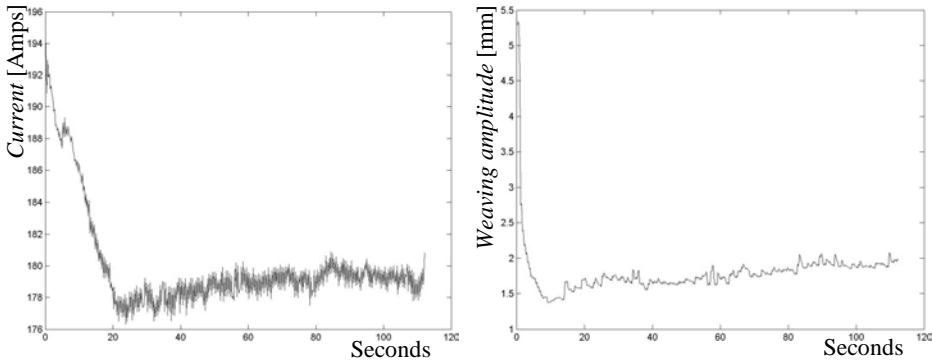


Figure 9-9 The *input* of the first weld-test. Left, the *current* applied to the weld equipment. Right, the *weaving width* applied to the weld equipment.

The left plot of Figure 9-9 shows the *current inputs*, which were applied to the weld equipment. This *current input* is, when a steady state (SS) situation is achieved, expected to be 178 amps, which it also is. The *weaving amplitude* ends, in correspondence with the decreasing measured width of Figure 9-7, a bit high. It was expected at 1.5 mm, which is where it is after 10 sec. It however slowly increases during the experiment and ends at 2 mm, which is 0.5 mm higher than expected.

In the next figure the measured *average temperature* of the first weld-test is plotted together with the measured *average temperature* of the *reference-generating experiment* (Figure 9-10).

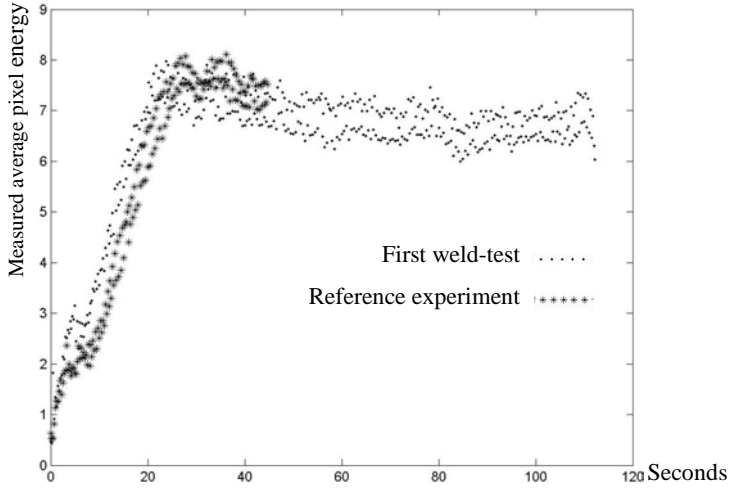


Figure 9-10 The measured average temperature of the first weld-test and the measured average temperature of the reference-generating experiment.

In Figure 9-10 it is especially in the first 20 seconds of the weld visible that the response of the controller based first weld-test is only a little faster than the reference-generating experiment, which was based on constant parameters. The reason for this rather slow response is the control gains of matrix, K_P (Eq. 9.8), and hence the choice of the wish transfer-function, \underline{F}_W (Eq. 9.7). If the wish transfer-function had been $1/(s+1)$ instead of $0.2/(s+0.2)$ then the K_P matrix would

have been $\begin{bmatrix} 20.3 & -0.0374 \\ 0.278 & 0.0276 \end{bmatrix}$ instead of the present $\begin{bmatrix} 2.29 & -0.0374 \\ 0.0033 & 0.0276 \end{bmatrix}$.

That would have given a more aggressive response. In the next figure the measured approximated width of the first weld-test is plotted together with the measured approximated width of the reference-generating experiment (Figure 9-11).

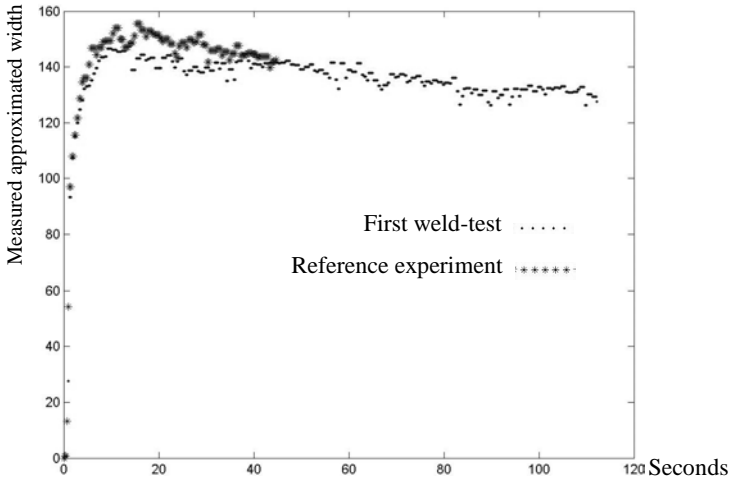


Figure 9-11 The measured *approximated width* of the first weld-test and the measured *approximated width* of the reference-generating experiment.

In Figure 9-11 the two responses are quite similar. The most distinct difference is that the *reference-generating experiment* 10 to 35 seconds from start has a slightly higher measured *approximated width* than the controller based first weld-test. The reason for that minor deviation has not been determined although it may be due to the fact that the chosen method, by which the width of the weld was measured, for the same true weld width is somewhat dependent of the weaving amplitude of the x- y- table. This might also explain the slightly high weaving amplitude of Figure 9-9. The choice of measuring technique is therefore maybe not optimal, and a more reliable output that also would relate better to the weld width and depth might be to measure the weld pool length instead of the average temperature behind the tail. This is discussed further towards the end of part 9.3.

In Figure 9-12 a cross section images of respectively the *reference-generating experiment* and the first weld-test is pictured. Both of the cross section images are made when the process is in steady state (SS), 30 seconds from start.

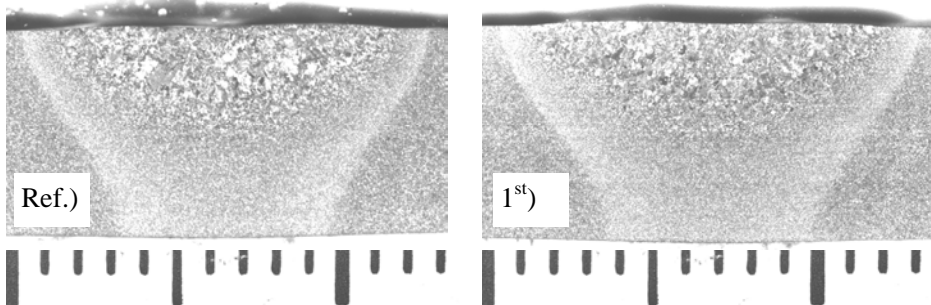


Figure 9-12 Images of the cross section made 30 seconds from the start. Ref.) is the *reference-generating experiment* and 1st) is the first weld-test.

In the cross section images of Figure 9-12 the width of the material, which have been melted, is about 0.5 mm wider in the first weld-test than in the *reference-generating experiment*. That is a deviation of about +5%. Also the width of the heat affected zone (HAZ) in the top of the cross sections is 0.5 mm wider in the first weld-test than in the *reference-generating experiment*. There is no difference in the width of the HAZ zone in the bottom of the two cross sections and there is found no deviation in the penetration depth of the two experiments.

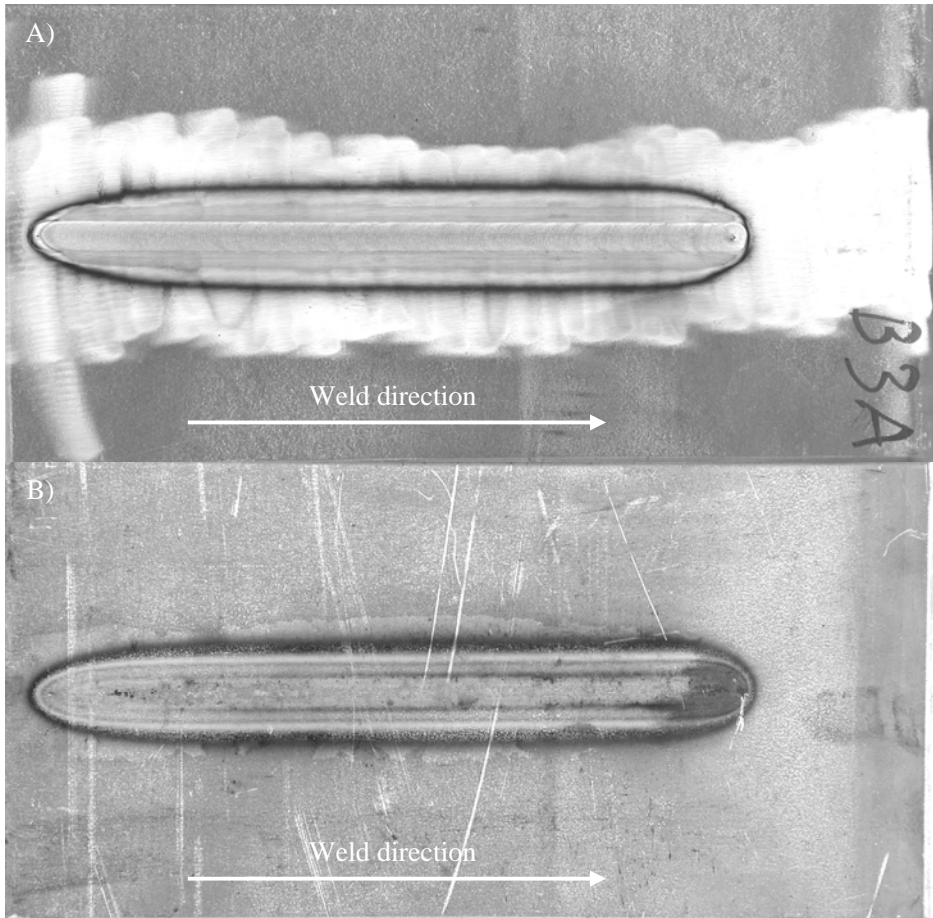


Figure 9-13 The workpiece on which the first weld-test is carried through. A) is the front side of the workpiece and B) is the backside.

In Figure 9-13 the workpiece on which the first weld-test were carried through is pictured. The front side of the workpiece has, before welding, been brushed by means of a wire brush. The two pictures of Figure 9-13 can be compared to the pictures of the *reference-generating experiment* (Figure 3-6). Remark that the weld zone of Figure 9-13 only is comparable with Figure 3-6 from the start of the *reference-generating experiment* till the position of the step of Figure 3-6. The two

weld zones of Figure 3-6 and Figure 9-13 look similar just as it was visualised by the cross section images of Figure 9-12.

The result of the first weld-test showed good agreement between the *reference-generating experiment* and the first weld-test. The controller based first weld-test shows a faster response than the corresponding *reference-generating experiment* response, which was run with constant weld parameters. The test also indicates that the method used to measure the output variable approximated width of the weld is not the best solution. In the next section the results of the second weld-test is discussed.

9.3. Second Weld-test

In the second weld-test the workpiece is applied with a disturbance on the width of the workpiece. The width of the workpiece is at the middle of the workpiece changed from 150 mm to 15 mm (Figure 9-14). The thickness is however kept the same.

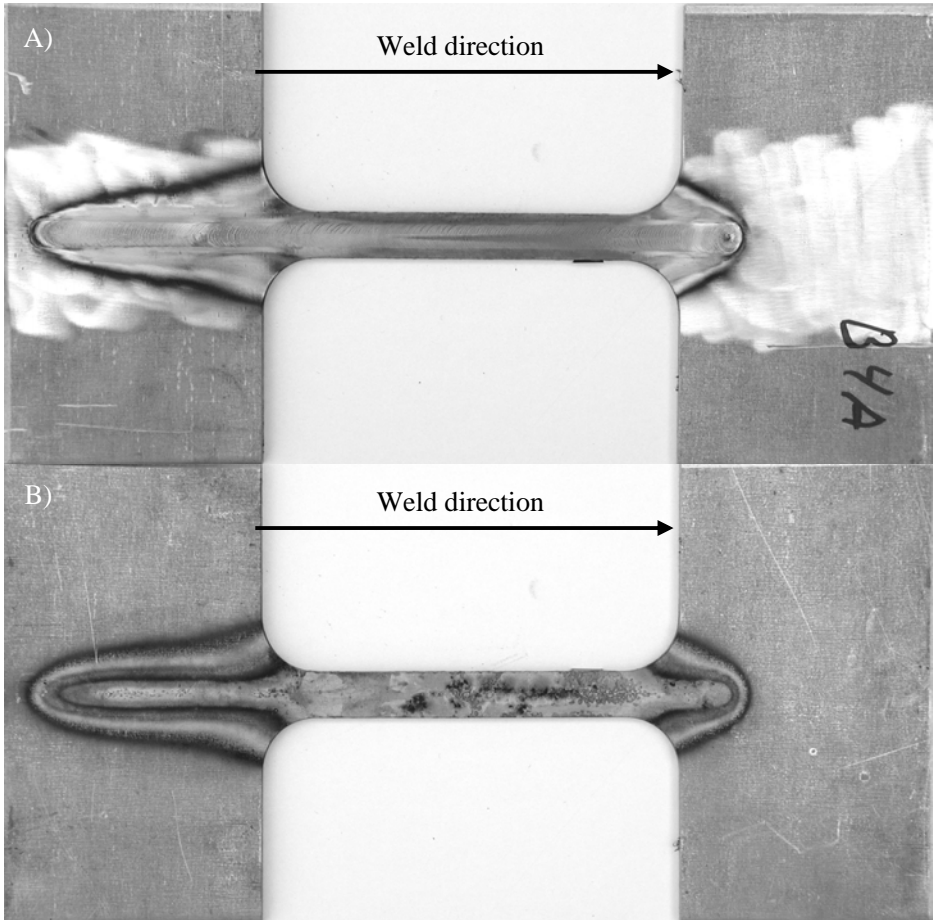


Figure 9-14 The workpiece on which the second weld-test were carried through. A) is the front side of the workpiece and B) is the backside.

The purpose of this test is to see how the control-system reacts on a significant change of the workpiece width. The result is compared to the *reference-generating experiment* (Figure 9-5). The experiment is performed with the parameters given in Table 9-1 and based on the same controller used in the first weld-test, which was designed in Section 9.1.

The *output* measured by the temperature imaging system is given in Figure 9-15.

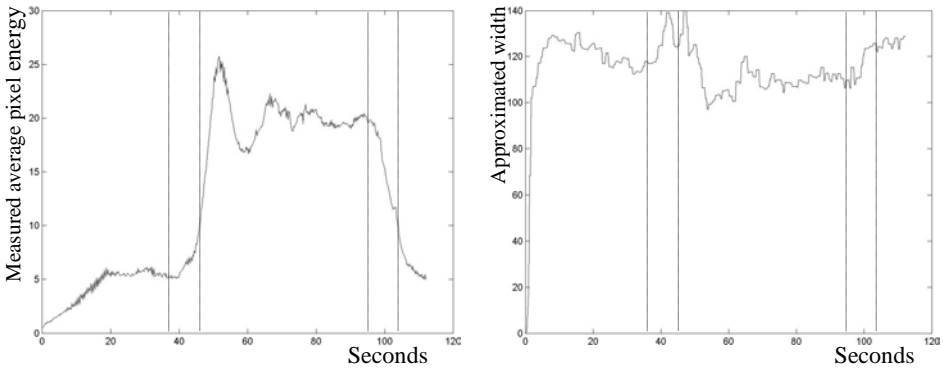


Figure 9-15 Measured output of the second weld-test. Left, average temperature. Right, approximated width of the weld.

The *average temperature* plot on the left should be compared to the reference temperature, which is 7.25 (Figure 9-15). The *approximated width* on the right should be compared to the reference width, which is 147. The time at which the width of the workpiece starts to narrow down is at 37 seconds and it is fully narrowed down after 45 seconds. The time at which the width of the workpiece starts expanding again is after 96 seconds and it is fully expanded to the standard width after 104 seconds. The dashed lines of Figure 9-15 to Figure 9-17 indicate these steps.

The error between the measured *output* of Figure 9-15 and the reference (Eq. 9.9) is given in Figure 9-16. In Figure 9-17 the *input* values generated by the P-controller are depicted.

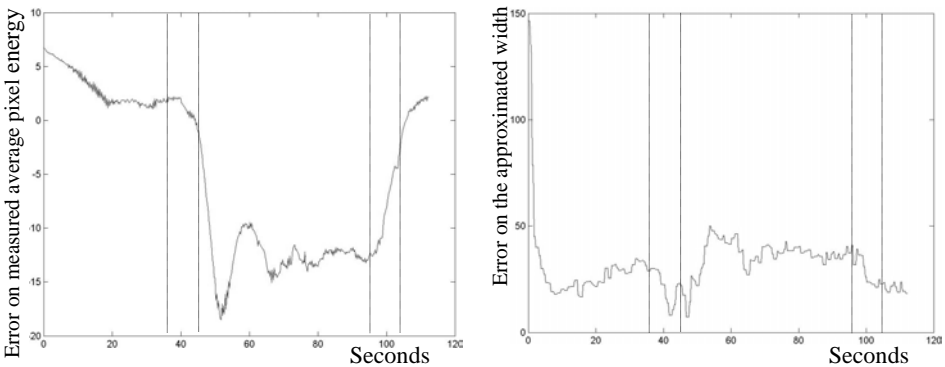


Figure 9-16 The error of the second weld-test. Left, the reference temperature subtracted by the average temperature. Right, the reference width subtracted by the approximated width.

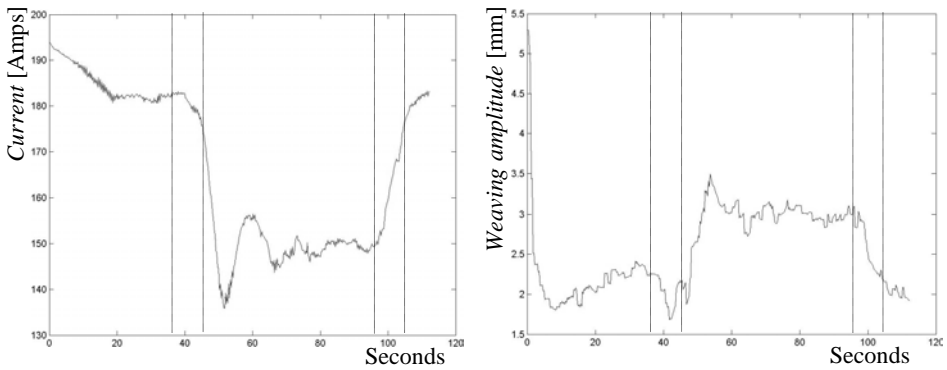


Figure 9-17 The *input* of the second weld-test. Left, the *current* applied to the weld equipment. Right, the *weaving width* applied to the weld equipment.

In the left plot of Figure 9-15 it is clearly seen that the *average temperature* is higher than the reference temperature from when the width of the workpiece narrows down to it expands again. When evaluating the true temperature change it must however be taken into account that a very small temperature change may result in quite large measured pixel energy change (see Figure 7-19).

The right plot of Figure 9-15, which shows the *approximated width* of the weld, does however not show a similar deviation. The *approximated width* of the weld truly expands when the width of the workpiece starts to narrow down, but shortly after the *approximated width* is measured to be less than before the workpiece started to narrow down. The decrease occurs because the *current* at this time is turned down due to a high *average temperature*. The low *current* causes the width of the weld pool to reduce. The weaving amplitude is consequently increased to compensate (See Figure 9-17). When the width of the workpiece again retains to its standard width the *average temperature* and the *approximated width* also retains to their values as they were before the width of the workpiece narrowed down (Figure 9-15).

The measured values of the *average temperature* and the *approximated width* before and after the workpiece geometry width disturbance are for both cases a bit lower than the reference. The *input* variables *current* and *weaving amplitude* are therefore correspondingly higher before and after the workpiece geometry width disturbance. The reason for that is not clear, but such minor deviations may come from a small disposition of the equipment compared to the workpiece. In the relative simple set-up, which was used in the experiments, there was no automatic check or calibration of the weld gun position and hence the tungsten tip to workpiece distance or the position of the camera, and factors like that may cause measurement deviations or weld deviations.

The weld cross section of the second weld-test may now be compared to the cross section of the *reference-generating weld*. In Figure 9-18 a macrographs of the cross section of the *reference-generating experiment* and the second weld-test,

9. Experiments

respectively, is shown. Both of the cross section images are made when the process is in steady state (SS), 30 seconds after the start, i.e. before the work-piece cross section is beginning to change.

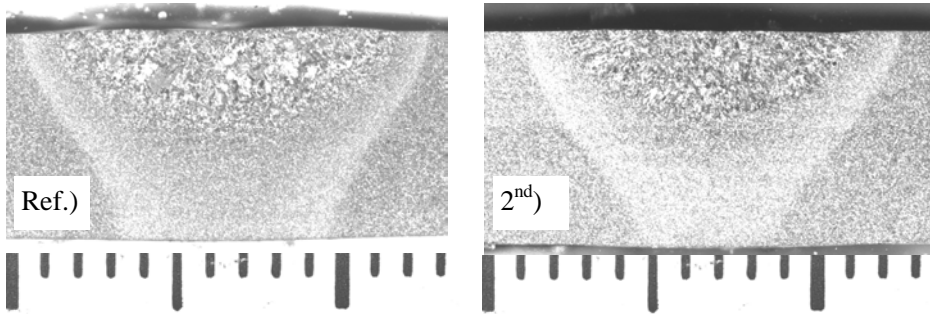


Figure 9-18 Images of the cross section made 30 seconds from the start. That is before the workpiece width starts to narrow down. Ref.) is the *reference-generating experiment* and 2nd) is the *second weld-test*.

In the cross section images of Figure 9-18 the width of the area, which have been melted, is 10.5 mm in the *reference-generating experiment* and 10 mm in the second weld-test, i.e. a deviation of -5%. The width of the HAZ in the top of the cross section is 12.5 mm in the *reference-generating experiment* whereas 11.5 mm in the second weld-test, i.e. a deviation of -9%. The width of the HAZ in the bottom of the cross section is 6.5 mm in the *reference-generating experiment* whereas 4 mm in the second weld-test, i.e. a deviation of -40%. The penetration also deviates a little as the penetration of the *reference-generating experiment* is 3 mm whereas 2.75 mm in the second weld-test.

Why there are these differences in the weld profile of the *reference-generating experiment* compared to the second weld-test at 30 second from start is unknown although it, as discussed above, may be due to small variations in the experimental set-up. It may however be seen that the P-control-system did catch a corresponding error on both of the *outputs*. In Figure 9-16 it is visible that the measured *average temperature* as well as the *approximated width* of the weld at 30 seconds from start are measured to be smaller than the reference values. The P-controller has therefore been trying to correct the error by turning up the *current* and the *weaving width* (Figure 9-17), but as it is seen in Figure 9-18 the result is not perfect. In this situation a PI-controller would have been better as a the integrator function in the PI controller would minimize the proportional error. Due to time constraints only a P-controller was tested experimentally (See Section 2.3).

In Figure 9-19 two close-up images of the top bead of the workpiece, on which the second weld-test was carried through (Figure 9-14), are shown.

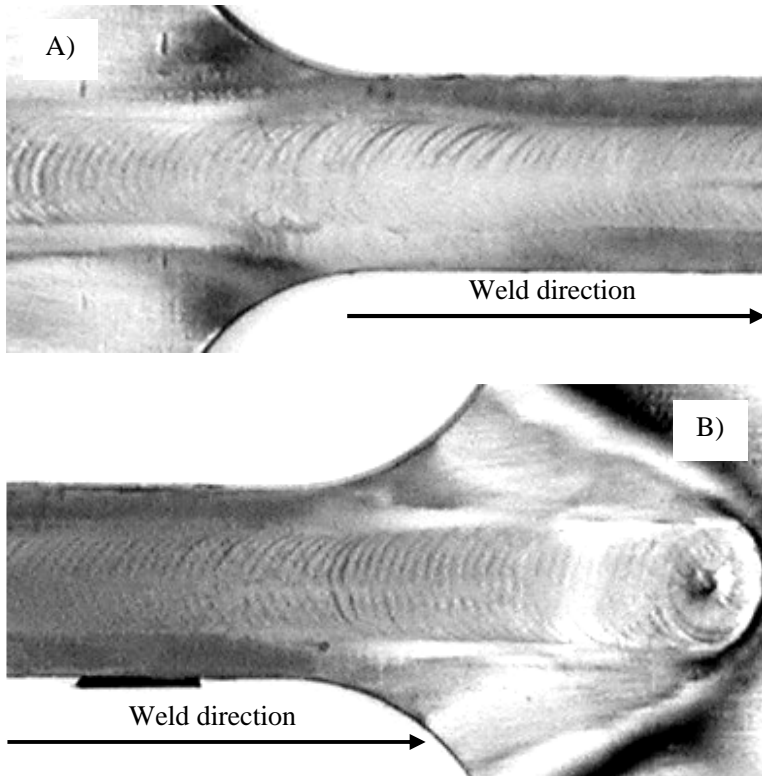


Figure 9-19 Two close-up images of the workpiece of second weld-test (Figure 9-14). A) is a close-up of the weld when the workpiece geometry changes from wide to narrow. B) is a close-up of the weld when the workpiece geometry changes from narrow to wide.

On both of the close-up images of Figure 9-19 it may be seen that the width of the weld only varies little when the workpiece width changes from 150 mm to 15 mm.

In Figure 9-20 the cross section of the *reference-generating experiment* is compared to the cross section of second weld-test made at 70 seconds from the start. That is in the middle of the area where the workpiece width is changed to 15 mm (See Figure 9-14).

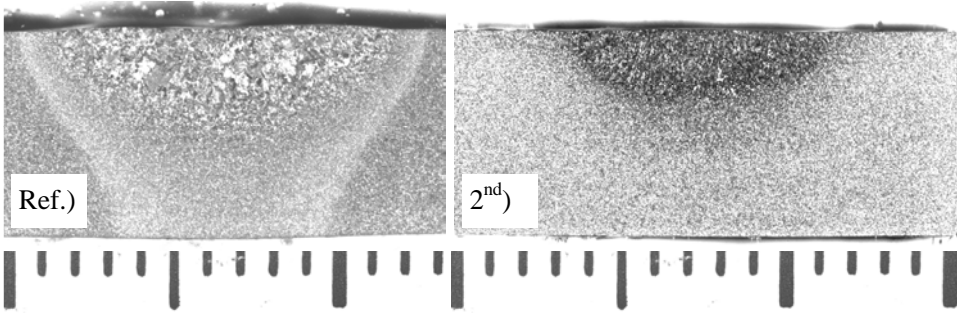


Figure 9-20 Images of the cross section of the *reference-generating experiment* made at 30 seconds from the start (Ref.) and of the second weld-test made at 70 seconds from the start (2nd).

The width of the melt zone, in the area where the workpiece width is only 15 mm, is 8.5 mm which is 2 mm less than the 10.5 mm melt zone width of the *reference-generating experiment*, i.e. a deviation of -20%. The HAZ zone of the two cross sections is completely different because the 15x6 mm cross section area of the second weld-test simply is one big HAZ zone. That is visible in the cross section image of the second weld-test in Figure 9-20, which shows the full 15x6 mm cross section area of the workpiece. The penetration depth of the second weld-test in Figure 9-20 is 0.5 mm less than the penetration depth of the *reference-generating experiment*, i.e. a deviation of -20%.

The fact that the HAZ of the second weld-test in Figure 9-20 is so big was expected due to the limited possibilities for heat dissipation by conduction. Why the melt zone of the second weld-test in Figure 9-20 is smaller than the *reference-generating experiment* is more mysterious, but the reason may be the choice of *output variables*. The *output variable approximated width* of the weld has a proper reaction in this case whereas the *output variable average temperature* has a less proper reaction. The method used to measure the *output variable average temperature* is shown in Figure 3-3.

The *average temperature* is measured by the average emitted radiation within a rectangle behind the tail of the weld pool. To evaluate the effect of the *output variable average temperature* the purpose of the *output variable* must be acknowledged at first. In this chapter the effect of the P-controller is measured on its ability to produce a certain width and depth of the weld pool and heat effected zone. To reach an optimal result in relation to these evaluation criteria's the *output variables* should identify and measure temperatures, which have a distinct effect on the weld pool form. The *output variable average temperature* is not the most proper *output variable* under this criterion. The rectangle behind the weld, in which the average emitted radiation is measured, is highly influenced on the temperature on the side of the tail. Exactly the side of the tail is unusual hot in the second weld-test where the workpiece width is only 15 mm. The measured value of the *average temperature* therefore becomes unusual high even though the weld

pool width and penetration is small. A more reliable output that also would relate better to the weld width and depth might therefore be to measure the weld pool length instead of the average temperature behind the tail.

In general it is important to build up more experience with regard to which surface temperatures that are the optimal to measure in order to obtain a optimal link to the given weld criteria's. That is for example which temperatures are of importance to measure to ensure full penetration in a butt joint, which temperatures to measure to ensure half penetration in a T-joint or which temperatures to measure to ensure full penetration while keeping the cooling rate down etc.

When the *output* variables were chosen (Chapter 3) the main focus was to find a pair consisting of an *input* and *output* variable, which is decoupled from the other pair of *output* and *input* variable. In future tests it may however be wise to pay more attention to obtain outputs that are more linked to the given weld criteria.

The possibilities in designing a *quality reference* based on real-time measured temperatures profiles were discussed in Section 1.3.5.

The result of the second weld-test showed, despite the magnitude of the disturbance, a relative good agreement between the *reference-generating experiment* and the second weld-test. The test revealed that the *output* variable *average temperature* is maybe not the most suited *output* variable to ensure a constant penetration. In the next section the results of the third weld-test is presented.

9.4. Third Weld-test

In the third and last weld-test the workpiece is applied with a disturbance on the workpiece thickness. The thickness of the workpiece is at the middle of the workpiece changed from 6 mm to 3 mm (Figure 9-21). The width is kept constant at 150 mm.

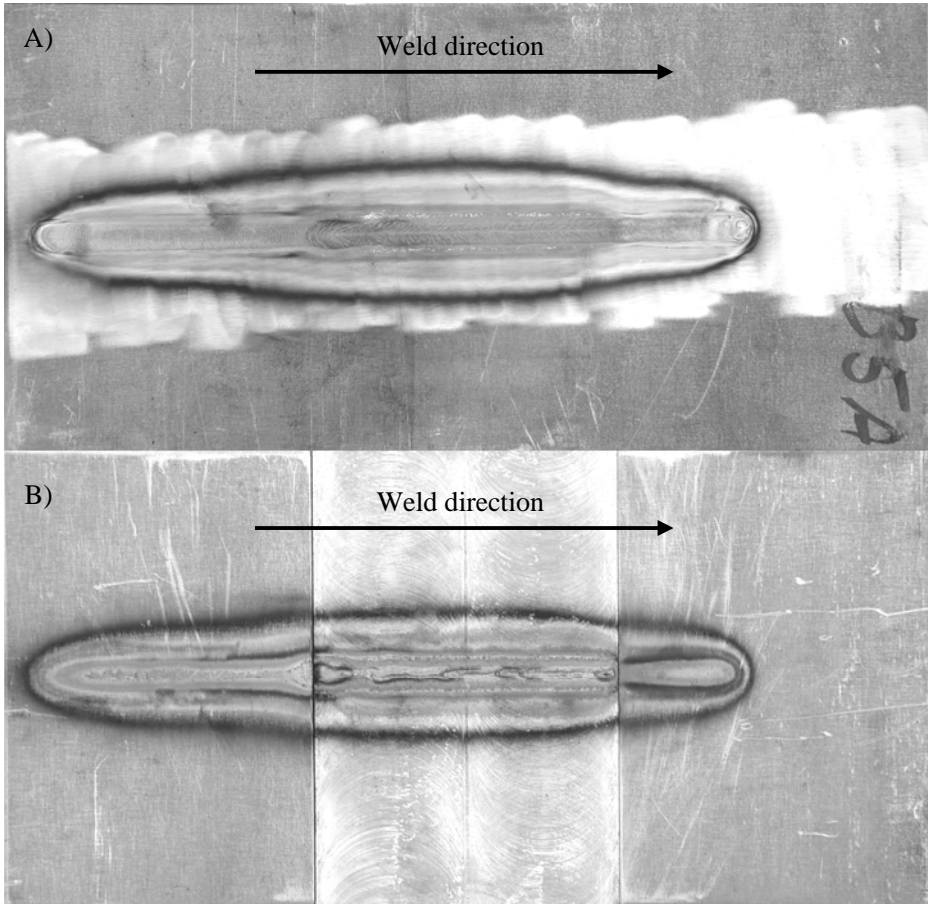


Figure 9-21 The workpiece on which the third weld-test were carried through. A) is the front side of the workpiece and B) is the backside.

The purpose of this test is to see how the control-system reacts on a significant change of the workpiece thickness. The result is compared to the *reference-generating experiment* (Figure 9-5). The experiment is performed with the parameters given in Table 9-1 and based on the controller, which were designed in Section 9.1.

The *output* measured by the temperature imaging system is given in Figure 9-22.

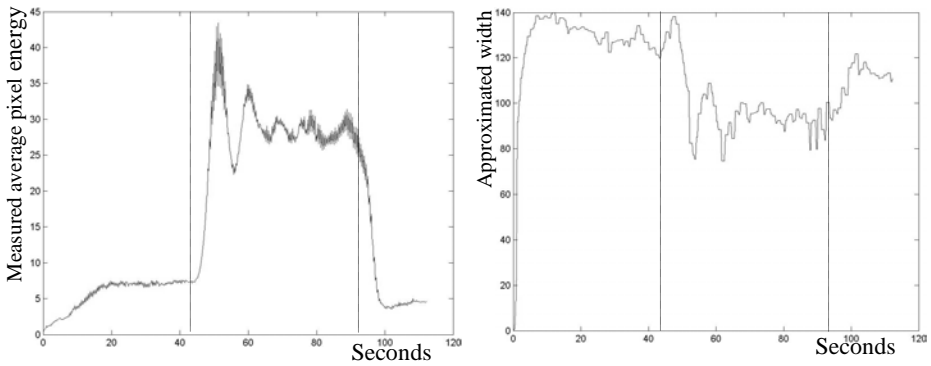


Figure 9-22 Measured *output* of the third weld-test. Left, *average temperature*. Right, *approximated width* of the weld.

The *average temperature* plot on the left of Figure 9-22 should be compared to the reference temperature, which is 7.25. The *approximated width* on the right of Figure 9-22 should be compared to the reference width, which is 147. The time at which the thickness of the workpiece changes from 6 mm to 3 mm is at 43 seconds. The time at which the thickness is changed back to normal thickness is at 92.5 seconds. The dashed lines of Figure 9-22 to Figure 9-24 indicate these steps.

The error between the measured *output* of Figure 9-22 and the reference (Eq. 9.9) is given in Figure 9-16. In Figure 9-17 the *input* values generated by the P-controller are depict.

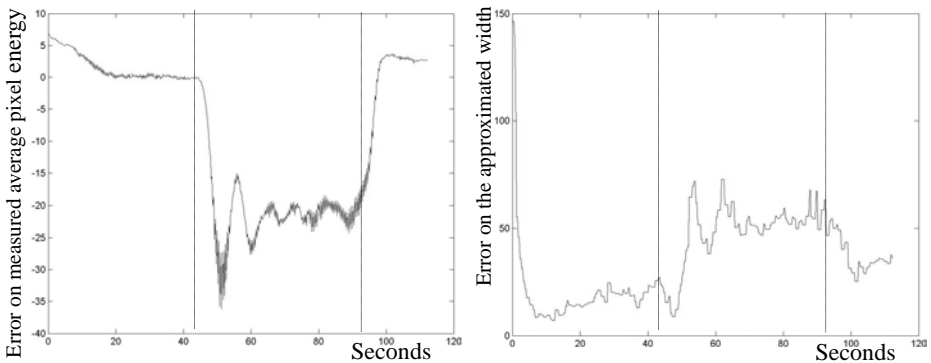


Figure 9-23 The error of the third weld-test. Left, the reference temperature subtracted by the *average temperature*. Right, the reference width subtracted by the *approximated width*.

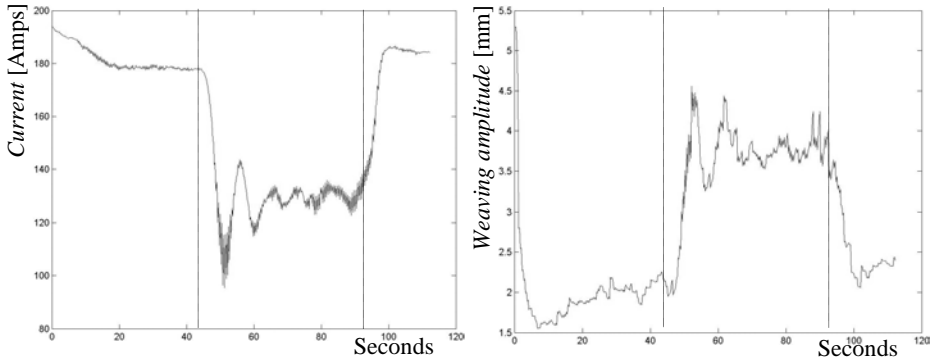


Figure 9-24 The *input* of the third weld-test. Left, the *current* applied to the weld equipment. Right, the *weaving width* applied to the weld equipment.

In the left plot of Figure 9-22 it is visible that the *average temperature* becomes higher when the workpiece thickness is 3 mm instead of the ordinary 6 mm. When evaluating the true temperature change it must however as in the former experiment be taken into account that a very small temperature change may result in quite a large measured pixel energy change (See Figure 7-19). In the right plot it is also clear that the *approximated width* is smaller when the workpiece thickness is 3 mm compared to 6 mm. In Figure 9-24 the *input current* is therefore decreased and the *weaving amplitude* is increased which is a proper response when the workpiece thickness decreases (whether the amplitude of this response is correct is seen in Figure 9-26). The progress before the workpiece thickness is right on the spot besides a small error on the *approximated width*. The *current* and *weaving amplitude* are, just after the workpiece thickness changes from 3 mm back to 6 mm, a bit high, but this was expected, as the accumulated heat in the workpiece, just around and in front of the weld at that position, is low.

In Figure 9-25 and Figure 9-26 cross sections of the third weld-test are compared to cross sections of the *reference-generating experiment*. In Figure 9-25 the cross sections are compared when the process is in steady state (SS), 30 seconds from start, i.e. before the geometrical changes are coming into play.

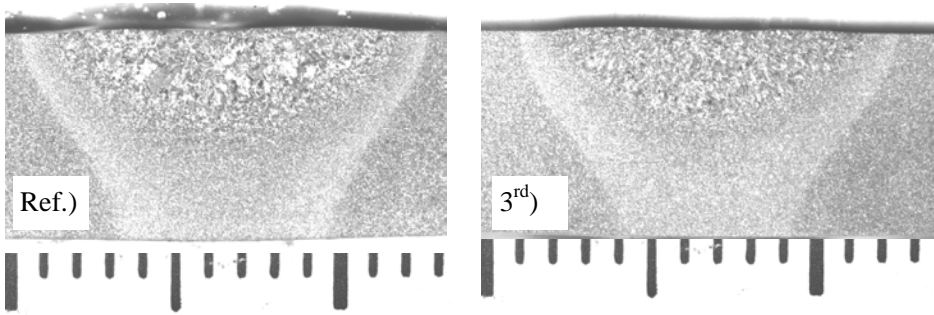


Figure 9-25 Images of the cross section made 30 seconds from the start. That is before the workpiece thickness is decreased. Ref.) is the *reference-generating experiment* and 3rd) is the *third weld-test*.

In the cross section images of Figure 9-25 the width of the area, which have been melted, is 10.5 mm in the *reference-generating experiment* and 9.5 mm in the third weld-test, i.e. a deviation of -10%. The width of the HAZ zone in the top of the cross section is 12.5 mm in the *reference-generating experiment* whereas 11.5 mm in the third weld-test, i.e. a deviation of -9%. The width of the HAZ zone in the bottom of the cross section is 6.5 mm in the *reference-generating experiment* whereas 5 mm in the third weld-test, i.e. a deviation of -30%. The penetration of the *reference-generating experiment* is 3 mm whereas 2.75 mm in the third weld-test.

The weld profile of the third weld-test at 30 second from start is similar to the weld profile of the second weld-test at 30 second from start. The discussion why the weld profile of the third weld-test at 30 seconds from start differs from the weld profile of the *reference-generating experiment* is therefore the same as made in Section 9.3.

In Figure 9-26 the cross section of the *reference-generating experiment* is compared to the cross section of third weld-test made at 70 seconds from the start. That is in the middle of the area where the workpiece thickness is changed to 3 mm (See Figure 9-21).

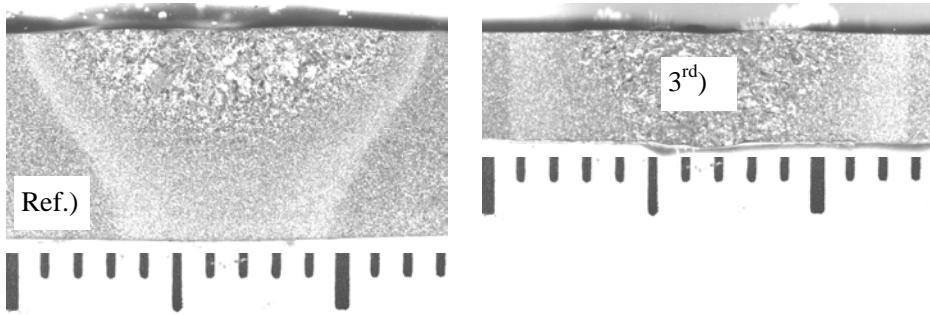


Figure 9-26 Images of the cross section of the *reference-generating experiment* made at 30 seconds from the start, Ref.), and of the third weld-test made at 70 seconds from the start, 3rd).

The width of the melt zone where the workpiece thickness is only 3 mm is 8.5 mm, which is 2 mm less than the 10.5 mm melt zone width of the *reference-generating experiment*, i.e. a deviation of -20%. The width of the HAZ zone in the top of the cross section of third weld experiment (Figure 9-26) is 12 mm, which is 0.5 mm less than the 12.5 mm of the *reference-generating experiment*, i.e. a deviation of -4%. The penetration depth of the third weld-test in Figure 9-26 is the same as the penetration depth of the *reference-generating experiment* that is 3 mm.

Based on the weld criteria's, on which we measure, the weld of the third weld-test where the thickness 3 mm is quite alike the *reference-generating experiment*. The only mentionable difference is the weld width, which deviates with -20%. That difference might have been reduced if the system was allowed a *weaving amplitude* larger than 3 mm (Table 9-1). In Figure 9-24 it is visible that the *weaving amplitude* generated by the P-controller is larger than 3 mm. This large *input* generated by the controller was due to the experimental parameters of Table 9-1 overruled by the on-line weld execution system and changed to a 3 mm *weaving amplitude*.

In Figure 9-27 is shown zoomed-in photos of the workpiece on which the third weld-test is carried out. The photos give a good impression of the dynamic result of the weld combined with a relative plot of the *input* values of Figure 9-24.

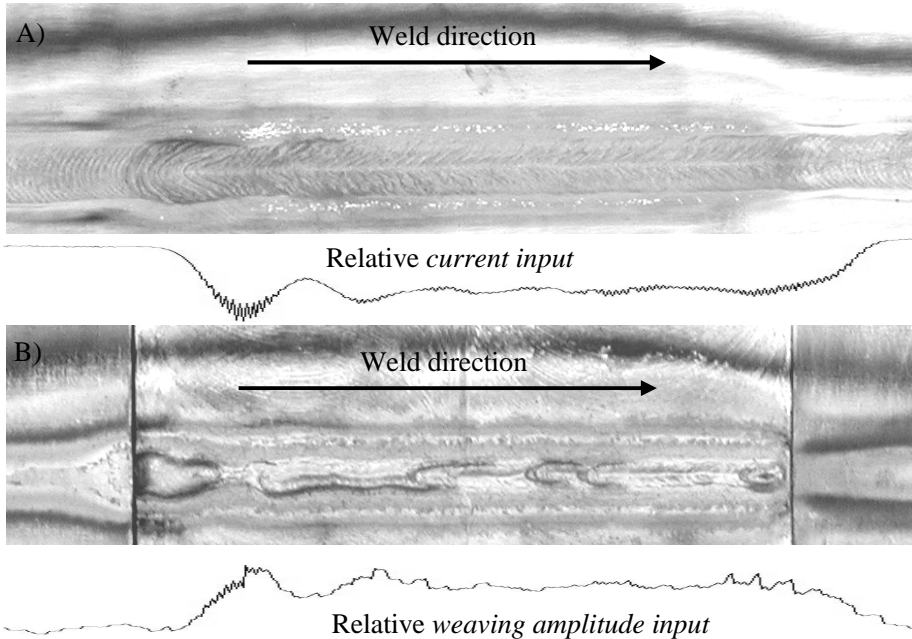


Figure 9-27 The welded area third weld-test. A) is the front side of the workpiece and B) is the backside. The full image is shown in Figure 9-21.

In Figure 9-27 it is visible that the weld is almost falling through due to excess penetration as the workpiece thickness is changed from 6 mm to 3 mm. The change of weld width in relation to the inputs and the workpiece thickness disturbance is also visible.

In all the graphs, related to the *output* variable *approximated temperature* and the *input* variable *current* from the first weld-test to the third weld-test, it is visible that the response is un-balanced. When the *approximated temperature* is lower than the reference temperature the response is small whereas it is large when the *approximated temperature* is larger than the temperature of the reference. The main reason for this is that the choice of the *output* variable *approximated temperature* is un-balanced and unsymmetrical in relation to the *reference-generating experiment*. When the *reference-generating experiment* is in SS the *output* variable *approximated temperature* is only 7.25. Because the temperature imaging system has the potential to measure the *approximated temperature* from 0 to 256 the proportional response when the *current input* is too high has the potential to be much stronger as when the *input* is too low. A more balance and therefore better solution would have been if the *output* variable *approximated temperature* measurements were designed to give an *output* between 100 to 150 during the *reference-generating experiment* or if the *reference-generating experiment* were based on a higher *current input* which also would lead to a more balanced reference value of the *approximated temperature*.

The result of the third weld-test showed, despite the severe disturbance, a relative good agreement between the *reference-generating experiment* and the third weld-test. The result would theoretically have been even better if the on-line weld execution system was not limited to a max *weaving amplitude* of 3 mm.

9.5. Discussion of the experimental results

In Section 9.1 it was shown that the *WAMOS-method* for building dedicated control-systems very well might function fully automatically. In Section 9.2 to Section 9.4 it was shown that the P-controller, which was built based on the *WAMOS-method*, performed convincingly. In the second weld-test the workpiece geometry was applied with a disturbance where the width of the workpiece was changed from 150 mm to 15 mm. In the third weld-test the thickness of the workpiece was changed from 6 mm to 3 mm. Despite these severe disturbances the depth of the weld penetration was kept almost constant at 3 mm. Based on that result it is concluded that the hypothesis of the WAMOS project is proven (Chapter 2).

It was though indicated that a PI-controller would have improved the performance of the WAMOS system. A solution to how to build a PI- and a PID-controller is given in the theory [Franke, 1993] and could be incorporated in the *WAMOS-method*. The main problem in the three weld-tests of Section 9.2 to Section 9.4 is the chosen set of *output* variables. The *output* variables and the temperature regions, which were chosen to be measured, were found not to be optimal. More experience is needed in order to choose a proper set of *output* variables, but it is important to choose a proper *output* set that corresponds optimal to the requirements to the weld result. Despite this positive result of the *WAMOS-method* it is necessary to perform more experiments and to test the system on different geometries to prove robustness of the method.

10. Conclusion

The goal of this project is to develop a method by which real-time control-systems for welding can be designed. The method by which the control-systems are designed must enable welding of thickwalled materials by feeding back the temperatures on the surface of the material.

One important hypothesis for this project is that given the right initial conditions one set of surface temperatures corresponds to only one set of internal temperatures. Hereby a control link from the desired internal temperatures, which is called the off-line *quality reference*, to the on-line control-system and back to the actually archived internal temperature has been established.

An extraordinary goal has been to develop an imaging system based on a CCD-chip-camera. The temperature imaging system must enable measurement under and around the arc. The system must measure temperatures at 1530°C (melting point of metal) and at least 100 degrees down.

In the following the actual contributions of this project are gone through. This is followed by a discussion of the usability of the *WAMOS-method* and the temperature imaging system and by a discussion of possible future steps and possibilities in the system.

10.1. Contributions from and achievements of the project

The main contribution of this project is a method, the *WAMOS-method*, which enables automatic design of dedicated control-systems. This method enables a user automatically to build optimal on-line references and optimal on-line controllers based on a, by the user described, desired temperature distribution (off-line *quality reference*) of the given workpiece.

The off-line *quality reference* is the desired temperature distribution in the workpiece. This temperature distribution is directly linked to the weld quality and properties of the workpiece after the performed welding.

10. Conclusion

To reach the desired welding quality and properties has during the last two decades to a very large degree been based on simple hardness models, experience and experiments. By defining the desired temperature distribution (the *quality reference*) the WAMOS-system facilitates the possibility to define different requests related to the temperature and temperature changes in the weld. It will, as an example be possible:

- To specify the size and the desired position of the heat affected zone (HAZ) or the size of the weld pool.
- To ensure a fully penetrating high strength weld.
- To minimize the heat input in order to minimize distortion.
- To control the thermal cycle and thereby the weld microstructure and properties.

The *WAMOS-method* is presented as a sequential method, which is based on five steps (Section 2.2). Three of these steps are to be continuously repeated for every weld-task and are therefore performed automatically whereas two of the steps are carried out only once per weld-system.

Of the three steps that are to be performed automatically there are three factors that are not directly numerically computable. That is the off-line identification parameter α , the transfer-function numerator, m , and denominator, n , degree and the wish transfer-function matrix $\underline{F}_W(s)$. A suggestion how to select the parameters α , m , and n automatically is therefore given in this report.

To choose $\underline{F}_W(s)$ is usually a compromise between a desired fast reacting control-system and the equipment constraints.

Setting up the wish transfer-function matrix $\underline{F}_W(s)$ in principle is an interactive process and is at the moment not automated. It is though suggested to build the wish transfer-function matrix $\underline{F}_W(s)$ automatically by means of the *off-line preparation system*. In the *off-line preparation system* parameters like workpiece thickness, travel speed and equipment constraints are known. It would therefore stand to reason to define a wish transfer-function matrix $\underline{F}_W(s)$ in the *off-line preparation system*. The wish transfer-function matrix $\underline{F}_W(s)$ should be generated for every *weld-step* along with the *reference-generating simulations* and the *step-input simulations*.

The development of the *WAMOS-method* and the temperature imaging system has been a major task in this project. The *WAMOS-method* and total system is evaluated by various tests. An on-line controller and an on-line reference are built by means of the *WAMOS-method* and this controller and reference is tested in three weld-tests. First an experiment where the controller is tested on a standard workpiece on which no disturbances is applied. This workpiece is similar to the workpiece on which the reference generating *step-input experiments* are carried out. Secondly an experiment on a workpiece where the width halfway is changed

from 150 mm to 15 mm. Thirdly an experiment where the workpiece thickness halfway is changed from 6 mm to 3 mm.

The system performance observed in all three weld-tests was good. The performance of the controller was e.g. measured by comparing the heat affected zone (HAZ) width and the weld pool depth and width of the three weld-test experiments with a reference experiment. The deviations between the reference experiment and the weld-tests were at the top surface below 20% although the artificial disturbances introduced in two of the weld-tests were drastically changing the welding conditions. In the bottom of the weld slightly larger deviations were however observed.

One reason for the observed deviations is that the controller that was built, based on the *WAMOS-method*, is a P-controller. One advantage of a P-controller is that such a controller is simple. A disadvantage of a P-controller is on the other hand that it may introduce a proportional error. This proportional error is one of the main reasons for the deviations. In relation to this it must be mentioned that the theory [Franke, 1993] used in the *WAMOS-method* also describes the possibility to build a PI and a PID-controller.

As remarks to this result it must be mentioned that the controller built for these experiments was not based on a simulated data but generated based on data from a *reference-generating experiment*. This is chosen because it was not within the limits of the project possible to calibrate the temperature imaging system and the finite-element model to correspond each other.

Another reason for the deviation is the chosen set of *output* variables. It is important to choose a proper *output* set variables that correspond optimal to the requirements to the weld result. More experience is needed in order to choose a proper set of *output* variables.

Because the WAMOS generated P-controller in the full geometry of the three weld-test workpieces to a fair extend are capable of achieving the desired weld profile and heat affected zone (HAZ) geometry, the basic hypothesis of this project is supported. It seems therefore to be a fair assumption that, given the proper initial condition, it will be possible to achieve a desired temperature profile within the full geometry of the workpiece by controlling a calculated (time varying) surface temperature profile throughout the process time. This is a key requirement of the *proposed weld-system architecture*.

Despite this positive result of the *WAMOS-method* it is however necessary to perform more experiments and on different geometries to prove robustness of the method.

Together with the developed *WAMOS-method* a low-cost temperature imaging system has been developed. The optical and mechanical design of this system,

have been described in the present report as well as the extensive work performed in order to optimise the position of the camera and in order to gain optimal image profiles. Finally different calibrations of the system have been illustrated.

Two systems were developed: A temperature imaging system, which is dependent on the factor of emittance, and another system, which measures temperatures independent of the factor of emittance. Both of the temperatures imaging systems were tested and they both performed well. It was theoretically as well as experimentally illustrated that the temperature measurements of the emittance independent temperature imaging system were varying less than the emittance dependent temperature imaging system when exposed to emittance changes of the workpiece. Despite the capability of the emittance independent imaging system, it was however decided not to use the emittance independent temperature imaging system in the final experiments. This decision was caused by the difficulty, within the limitations of the present camera, in finding two appropriate wavelength slots, where a proper measuring signal could be achieved by filtering away the background light from the welding process. The camera used was limited to measure wavelengths up to 1100 nm only. The one-wavelength temperature imaging system, which is dependent on the factor of the emittance, was therefore used in three weld-tests elaborated above. The emittance dependent imaging system is capable to measure temperatures from 1350 °C to 1530 °C.

To establish the connection between the off-line finite-element model and the on-line temperature imaging system, off-line simulated surface temperatures were compared to corresponding surface temperature measurements of the emittance dependent temperature imaging system. This comparison demonstrated a promising correspondence between the simulated and actual measured temperatures, but also some inconsistencies were demonstrated which called for time consuming calibration. Because of these inconsistencies and project time restrictions it was decided not to use the *off-line preparation system* for the *reference-generating simulation* when testing the WAMOS-system and hence the *WAMOS-method*. As replacement for the *reference-generating simulation* actual welding experiments, called *reference-generating experiments*, were therefore performed to generate the data needed of the *off-line preparation system*. As the same imaging system therefore was used in both the *off-line preparation system* and the on-line weld execution system it was therefore not necessary to calibrate the emittance dependent imaging system to absolute temperatures. Non-calibrated measurements of the imaging system were therefore used when testing the WAMOS-system.

10.2. Usability of the *WAMOS-method* and System

As mentioned in Chapter 1 the introduction of sensor based closed-loop intelligent welding automation in the welding industry is a natural strategy to pursue in a

more and more globalised world. More specific, there are six main reasons for choosing numerically controlled welding instead of manual welding:

1. The influence of labour cost is greatly reduced, which means that the production may be placed also in high income areas as e.g. Denmark, Europe or USA.
2. Some welding tasks are impracticable without use of numerical welding.
3. By numerically controlled welding, the quality of the weld is improved.
4. By numerically controlled welding, weld quality repeatability is improved.
5. Numerically controlled welding can run at a higher velocity than manual welding.
6. Welding by numerically controlled equipment does not have to be interrupted due to welder fatigue.

The *WAMOS-method* and hence WAMOS-system can be used in a variety of weld processes and welding situations. The limitations of the *WAMOS-method* and the *proposed weld-system architecture* lies in:

1. The model of the off-line preparation system.
2. The capabilities of the on-line weld execution system measurement equipment, which in this case is the temperature imaging system.
3. The weld equipment.

With a proper model and temperature imaging system it will therefore be possible to use this method on literally any type of GMAW, GTAW, laser based welding etc.

Beyond welding, the *proposed weld-system architecture* and the *WAMOS-method* may be used on a variety of other processes. The *WAMOS-method* opens the possibility to define an arbitrary quality, which perhaps in the physical process situation is non measurable. It also lets an off-line simulation system simulate an optimal solution where an output of this solution is physical measurable. This output can then be used in an on-line execution system as feedback. Such architecture is the same as the *proposed weld-system architecture*. It therefore seems straightforward to use the *WAMOS-method* to build the on-line execution controller and the reference for other processes.

Another possibility could be to use the on-line execution system independently of the off-line preparation system. In mass productions it could give an advantage to use this on-line execution system independent of the off-line system. In most industries that use automatic welding the process is controlled in open-loop only. To have an automatic welding system running open-loop, sets high requirements to e.g. the process stability and robustness, the geometry tolerances, material tolerances and the in-process disturbances. If a closed-loop welding control system is used, it would be possible to reduce the tolerance demands of the elements to be welded. Reducing the tolerance demands of the elements to be welded would not only save the factory money but also make it easier for a factory to introduce automatic welding. Most welding systems of today are not very tolerant. In many

industries where manual GMAW or GTAW are used, one of the challenges in changing to today's automatic welding is that automatic welding systems are less tolerant to disturbances and hence rough workpiece tolerances. Introducing an automatic welding system as the on-line system in the WAMOS-system would not require the same change in production tolerances as when introducing traditional automatic welding systems.

10.3. Usability of the Temperature Imaging System

The low-cost CCD-chip based emittance dependent temperature imaging system can like any other temperature vision systems be used for emittance dependent temperature measurement. The limitation of the present CCD camera is that the temperatures to be measured must be fairly high, that is above 1000 °C and it only measures wavelengths up to 1100 nm. The method used to off-filtrate undesired radiation can be used for other joining processes or situations in general where undesired radiation is disturbing the measurements.

The emittance independent temperature vision system has the unique feature to measure the temperature independently of the factor of emittance. This feature can be transferred to ordinary infra read temperature-measuring systems and it is hence possible to measure a wide variety of temperatures independently of the factor of emittance. That is in theory temperatures from below 0 °C to 3000 °C. To measure the temperature independent of the emittance enables a user directly to measure the temperature of many different objects in the one and same picture without knowing the factor of emittance for every object.

10.4. Future Work and Perspectives

The results achieved so far are positive and promising. To continue the work on the *proposed weld-system architecture* and the *WAMOS-method*, the main task is to gain experience in handling this type of system and optimising the system. Suggested focus areas are listed below:

- To calibrate the imaging system and the finite-element model of the *off-line preparation system*, to correspond to each other.
- Gain knowledge in optimal selection of output variables that correspond to the quality reference. It is important to build up experience on how to obtain an optimal link to the given weld criteria's by measured surface temperatures. That is for example,
 - which surface temperatures are of importance to ensure full penetration in a butt joint,

- which temperatures should be measured in order to ensure a desired penetration in a T-joint or
- which temperatures are relevant in order to ensure full penetration while at the same time keeping the cooling rate under control etc..
- Add extra parameters as e.g. filler material. In the present WAMOS-system a simple bead on plate horizontal GTAW welding is carried out, next step is to expand the system to enable filler material, other weld processes, vertical welding etc..
- Expand the *WAMOS-method* and hence WAMOS-system by enabling it to create and take use of a PI- or PID-controller. A PI- and PID-controller will to the contrary of a P-controller aim to eliminate the proportional error which was seen in some of the tests of the WAMOS-system (Chapter 9). How to build a PI- or PID-controller, by means of the same methods as used in *WAMOS-method*, is described in the theory of [Franke, 1993].
- Another way to improve the WAMOS-system might be to apply an observer in the on-line weld execution control-system. The objective of the observer would be to make a mathematical connection between the *output* variables and the desired states e.g. penetration depth or temperature distributions within the workpiece where the temperature can not be observed. An observer could be identified based on the finite-element model and could constitute a part of the *off-line preparation system*.
- Improve the temperature imaging system. It is today possible to buy a camera designed for viewing radiation in the 700-1300 nm spectral region for less than £ 1000. That would give a better possibility to off-filtrate radiating arc 100%. If the camera furthermore was designed with a larger pinhole it would be possible to use a more narrow band pass filter and hence a better off-filtration of the disturbing arc.

Bibliography

[**Agapiou, 1999**]: Agapiou G., Kasiouras C., Serafetinides A. A.: "A detailed analysis of the MIG spectrum for the development of laser-based seam tracking sensors". Optics and Laser Technology 31, 1999 page 157-161.

[**A. I. of P. H.**]: American Institute of Physics Handbook, Second edition. Coordinating Editor: Dwight E. Gray, Ph.D., Office of Science Information Service, National Science Foundation.

[**Andersen, 1997A**]: Andersen H. J., Holm Hans: "Method for Preparation of Laser Welding Control". Proceedings of Seventh International Conference on Computer Technology in Welding, Edited by T. Siewert, NIST Special publication 923 (National Institute of Standards and Technology), San Francisco, 1997.

[**Andersen, 1997B**]: Henrik John Andersen, Hans Holm: "Development of Models for Preparation and Control of Laser Welding". 5th International Conference on Application of Computers in Welding. June 20-24, 1997, San Francisco, USA. Organised by The Welding Institute (UK) and The Edison Welding Institute (USA).

[**Andersen, 2001**]: Henrik John Andersen: "Sensor Based Robotic Laser Welding". Ph.D. thesis, Department of Production, Aalborg University, 2001. ISBN: 87-89867-87-4.

[**Angelis, 1998**]: Ioannis Angelis, Haralampos Sfetsos, Charalabos Doumanidis: "Adaptive Thermal Distribution Control in Scanned Orbital Welding of Piping". PVP-Vol. 374, Fatigue, Environmental Factors, and New Materials ASME 1998.

[**Brüggemann, 1996**]: G. Brüggemann, M. Schröder, J. Ude, T. Benziger: "Prediction of Weld Data Using Process Control Based on Surface Temperature Measurement For Plasma and Laser Welding of the Duplex Steel 1.4462" Welding in the World, Le Soudage dans le Monde, Vol. 38, pp. 369-379, 1996 IIV/IIS.

[**Christensen, 2003**]: K. H. Christensen, T. Sørensen: "A Neural Network Approach for GMA Butt Joint Welding". Proceedings of 11th International Conference on the Joining of Materials - JOM-11, Helsingør, Denmark, May 2003. Also published in 'International Journal for the Joining of Materials', Vol. 15, No. 4, 2003, ISSN 0905-6866.

Bibliography

[CRC, 1979]: CRC Handbook of Chemistry and Physics, A Ready-Reference Book of Chemical and Physical Data, 60th edition 1979-1980, ISBN-0-8493-0460-8.

[Doumanidis, 2001]: Charalabos Doumanidis, Yong-Min Kwak: "Geometry Modeling and Control by Infrared and Laser Sensing in Thermal Manufacturing with Material Deposition". Journal of Manufacturing Science and Engineering, February 2001, Vol. 123 pp. 45-52.

[Doumanidis, 1998]: C.C. Doumanidis: "Thermal Modelling and Adaptive Control of Scan Welding", Welding Research Supplement, 465-s- 476-s, November 1998.

[Doumanidis, 1997]: C.C. Doumanidis: "Scan Welding: Thermal Modelling and Adaptive control", Seventh International Conference on Computer Technology in Welding, NIST Special Publication 923, page 89-100.

[Ericsson, 2001]: M. Ericsson, P. Nylén, G. Bolmsjö: "Three-Dimensional Simulation of Robot Path and Heat Transfer of A TIG-Welded Part With Complex Geometry". 11th International Conference on Computer Technology in Welding NIST Special Publication 973, pp 309-316. Columbus, Ohio, USA, December 6-7, 2001.

[Ericsson, 2002]: M. Ericsson, D. Berglund, P. Nylén: "Three Dimensional Simulation of Robot Path, Heat Transfer and Residual Stresses of a TIG-Welded Part With Complex Geometry". 6th International Conference on Trends in Welding Research. Callaway Gardens Resort, Pine Mountain, Georgia, USA, 15-19 April 2002.

[Fan, 2002]: Haibo Fan, Srikanth Kottigam, Bryan A. Chin: "A Point Infrared Sensing System for Weld Penetration Control in the Presence of Variable Plate Thickness and Variable Joint Gap". 6th International Conference on Trends in Welding Research. Callaway Gardens Resort, Pine Mountain, Georgia, USA, 15-19 April 2002.

[Farson, 1998]: D. Farson, R. Richardson, X. Li: " Infrared measurement of base metal temperature in gas tungsten arc welding". Welding Journal September 1998, page 396 – 401.

[Franke, 1993]: Systemdynamik und Reglerentwurf, ein Zugang über verallgemeinerte Fourier-Reihen von *Dieter Franke, Klaus Krüger und Michael Knoop*. (Methoden der Regelungs- und Automatisierungstechnik) Wien, Oldenbourg, 1993. ISBN 3-486-22239-2.

[Henrikson, 2002]: P. Henrikson, M. Ericsson: „Non-contact Temperature Measurements using an Infrared Camera in Areospace Welding Applications“. 6th International Conference on Trends in Welding Research. Callaway Gardens Resort, Pine Mountain, Georgia, USA. 15-19 April 2002.

[Holm, 2003]: H. Holm, H.C.E. Kjeldsen and J. Klastrup Kristensen: "A reference architecture for the design of an industrial temperature feedback welding control system". Journal of Materials Processing Technology 139 (2003) Page 499–504.

[Hurup, Force]: Kim Hurup, former engineer at FORCE Technology, Parkallé 345, 2605 Brøndby. www.force.dk

[Kalpakjian, 1995]: Manufacturing Engineering and Technology, Third Edition, Seropé Kalpakjian, Illinois Institute of Technology, 1995. ISBN 0-201-84552-0

[Kjeldsen, 2000]: H. C. E. Kjeldsen and H. Holm: "A reference architecture for design of an industrial temperature feedback welding control-system". Proceedings of the Ninth International Manufacturing Conference in China, IMCC'2000 Hong Kong 16 – 17 August 2000, Volume II, page 237 – 238, ISBN: 962-367-292-6.

[Kjeldsen, 2002]: H. C. Kjeldsen, H. Holm and J. Klastrup Kristensen: "New Low-cost Camera Temperature Measurements Compared to Analogous Temperature State Simulations". Published in: "Trends in Welding Research 2002". ISBN: 0871707802

[Klastrup Kristensen, 2005]: Personal communication, 2005.

[Korizis, 1999]: G. Korizis, C. Dumanidis: "Scan Welding: Thermal Modeling and Control of Material Processing". Journal of Manufacturing Science and Engineering, August 1999, Vol. 121, pp 417-424.

[Kovacevic, 1996]: R. Kovacevic, Z.N. Cao, Y.M. Zhang: "Role of Welding Parameters in Determining the Geometrical Appearance of Weld Pool", Transactions of the ASME, Journal of Engineering Materials and Technology, October 1996, Vol 118, pp 589-595.

[Kovacevic, 1995]: R. Kovacevic, Y.M. Zhang, S. Ruan: "Sensing and Control of Weld Pool Geometry for Automated GTA Welding", Transaction of the ASME, Journal of Engineering for Industry, Vol.117, pp 210-222, may 1995.

[Lauridsen, 1991]: Jan K. Lauridsen, Hans Holm: "Pass Shape Models for Computer Aided Off-Line Robot Programming of Multipass TIG-Welding". Manufacturing Systems, Vol. 20 (1991), No.2

[Lauridsen, 1992]: Jan Lauridsen: "Computer Aided Off-line Programming of Multipass TIG-Welding". PhD-thesis, Department of Production, Aalborg University, 1992.

[Lauridsen, 1993]: Lauridsen, Jan Kirkegaard; Holm, Hans: "Geometric Welding Model Based Algorithms for Control of Robotic TIG-Welding". International Conference on Modelling and Control of Joining Processes, Orlando, Florida, 8-10 December, 1993.

[Lenef, 1985]: Lenef,A.L., Gardner,C.S.: “Optical emissions from weld arcs and their effects on the performance of welding robot vision systems”. Applied Optics [APPL.OPT.], vol.24, no.16, 1985, page 2587-2595.

[Lhospitalier, 1999]: Lhospitalier,S., Bourges,P., Bert,A., Quesada,J., Lambertin,M.: “Temperature measurement inside and near the weld pool during laser welding”. Journal of Laser Applications, volume 11, page 32-37.

[Lucas, 2000]: Bill Lucas, Jeremy S. Smith: “Keeping an electronic eye on automated arc welding”. Welding & Metal Fabrication, April 2000, page 6-11.

[Madsen, 1992]: Ole Madsen: “Sensor Based Robotic Multi-Pass Welding”. Ph.D. thesis, Department of Production, Aalborg University, 1992. ISBN: 87-89867-02-5.

[Mills, 1995]: Anthony F. Mills: “Heat and Mass Transfer”, University of California at Los Angeles, 2. print, Chicago, Ill., Irwin 1995. ISBN 0-256-11443-9.

[Moore, 1997]: Kevin L Moore et al.: ”Annual Report, FY97: Advanced Welding Control Project, INEL URC Project No. G22”, July 1997, Measurement and Control Engineering Research Centre, College of Engineering, Idaho State University, Pocatello, Idaho 83209-8060, USA.

[Moore, 1996]: Kevin L Moore et al.: ”Annual Report, FY95/96: Advanced Welding Control Project, INEL URC Project No. G22”, June 1996, Measurement and Control Engineering Research Center, College of Engineering, Idaho State University, Pocatello, Idaho 83209, USA.

[Parenti, 1994]: R. Parenti, P. Verrecchia, G. Bosia, E. Pigone: “Industrialized Real-Time Flame Thermal Mapping System with Off-Line Correction of Spatial Error”. Industrial Electronics, Control and Instrumentation, 1994. IECON '94, 1977 -1980 vol.3.

[Pedrotti, 1995]: F. L. Pedrotti and L. S. Pedrotti, *Introduction To Optics*, Second edition, 1995 ISBN: 0-13-016973-0.

[Poulsen, Unit One]: Per Ove Poulsen, Managing Director Unit One, Sandholmgårdsvej 38, 3460 Birkerød. www.unit-one.dk

[Renier, 1998]: E. Renier, P. Suzeau, F. Truchetet and P. Geveaux: “Spatial and Thermal Measurements Using Thermography CCD During HF Soldering of Metallic Tubes”, Laboratory LE2I, University of Burgundy, 12, rue de la Fonderie, 71200 LE CREUSOT, France, Tel: (22) 3.85.73.10.00, Fax: (33) 3.85.73.10.99, e.renier@gere.u-bourgogne.fr, 1998 IEEE.

[Renier, 1996]: E. Renier, F. Meriaudeau, F. Truchetet: "CCD Technology Applied to Industrial Welding Applications", Electrotechnical Conference, 1996.MELECON '96., 8th Mediterranean, page 1335-1338.

[Sato, 1997]: T. Sato, A. Okubo, T. Oji and Y. Hirata (Osaka University): "Measurement of Molten Pool Temperature Distribution by UV thermal Radiation", Welding International 1998 12 (8) 627-634, Selected from quarterly Journal of the Japan Welding Society 1997 15 (4) 631-638

[Smith, 1996]: Smith, J.S., Howson, K.J., Chinneck, R.J., Lucas, J.: "A Vision System for High Speed Seam Tracking". 6th International Conference on Computer Technology in Welding. Maastricht 1996

[Terp, 1999]: C. B. Terp, H. Holm, J. H. Hoeyer, H. H. Nielsen, J. Dam: "Welding control based on a numerical model and state-space techniques" Proceedings of the Eighteenth IASTED International Conference Modelling, Identification and Control. Innsbruck Austria, 1999, page 265-268

[Weiss, 2004]: Weiss D W, Christensen K H and Klæstrup Kristensen: "Acceleration of Numerical Solution of Inverse Problems in Gas Metal Arc Welding". J. Proc. of Computer Technology in welding and Manufacturing, Sheffield, UK (June 2004).

A. Input File

In this appendix the input file is depicted. The input file contains all the constant figures as workpiece geometry, material figures and other constant equipment constraints. These figures all have in common that they are fed to the *off-line preparation system* at the start of every simulation. Not all the figures in the input file are used. Some of the figures as current, voltage are neglected in the system as they are overruled by the “user request” or “*input variables*” (Figure 4-1) other figures are only usable in the full scale off-line system previously developed by Christian Terp (Chapter 4).

```
!!*****
!!**          input.i          **
!!**          Hans Chr. Kjeldsen Orye          **
!!**          FORCE Technology & Aalborg university          **
!!*****

!set Reference source position = 0e-3 0 0
!set Reference extent         = 5e-3 2.5e-3 0
!set Reference velocity       = 1e-3 0 0
!set Reference intensity      = 1000
!set Welding gun start position = 0e-3 0 6e-3

set time parameters          = dt = 0.25 t in [0,0.25] !25] ![0,61]
set theta                    = 0.75
set Weld velocity            = 4.5e-3 0 0
set Snapshot                 = 10e-3
set Plot pos                 = 100e-3 0 6e-3
set weld stop                = 0.0004
set matlabdump               = false
set save u_max               = false

sub Boundary conditions
  set Extern temperature     = 20
  set Init temperature       = 20
  set Radiation factor       = 0.9
  set Convection              = 15
  set Boundary indicators = n=3 names= cooling reference insulation 1=( 1 2 3 4 5 6 ) 2=( ) 3=( ) !1 2 3 are the planes in the max
  value
                                !for axe x y and z respectively,
                                !4 5 6 are the planes in the minimum value
                                !for axe x y and z respectively.
                                !1=( ) is non isolated, 3=( ) is isolated.

ok

sub Welding parameters
  !set Heat source position = 35e-3 0.00 0.000
  set Heat source position = 0.0e-3 0.0 0.0

set Efficiency arc area = 5e-3 5e-3 {0.5e-3} ! 5 2.25 0.5

!set Efficiency arc area = {5e-3 & 3.875e-3 & 2.75e-3 & 1.1625e-3 & 0.5e-3 } 5 3.875e-3

set Arc efficiency          = 0.7 !0.6
set Arc coeff               = 40.76e-3 0.81e-3 0.09715e-3 0.0662e-3 ;
!set Current                 = 143 ! U [V]
!set Voltage                 = 12.6 ! I [Amp]
set Current                 = 250 ! U [V]
set Voltage                 = 15.0 ! I [Amp]

ok
sub Workpiece
```

Appendix A. Input File.

```
!set Dimensions = [0,0.350]x[-0.100,0.100]x[-8e-3,0]
!set Dimensions = [0,0.350]x[0e-3,50e-3]x[-6e-3,0]
set Dimensions = [0,120e-3]x[-30e-3,30e-3]x[-6e-3,0]
set Element type = ElmT4n3D !ElmB8n3D ! ElmT4n3D
set Elements = [60,30,3]
!set Elements = [40,15,3]
!set Elements = [171,24,3]
set Mesh grading = [1,1,1] ![1,-0.5,-1.8]

set Melt temperature = 1506
set k_coord = 0 53 357 45.5 794 28.8 1778 30 2000 100 ;
!set k_coord = 0 65.2 400 46 700 32.9 800 28.9 1000 27.6 1200 29.7 1500 32.85 ; 1550 164.25 ;
!set c_coord = 0 400 500 700 700 900 745 1100 755 2700 800 700 1500 700;
!set c_coord = 0 400 500 700 700 900 745 1100 755 1700 800 700 1500 700;
set c_coord = 0 456 500 644 667 732 750 800 854 743 984 677 1374 677 1500 733 1794 800 2000 800;
set Density = 7860
ok
sub Static Mesh
!set Static Elements = [2,2,2]
set Static Dimensions = [0,0.120]x[0e-3,10e-3]x[-6e-3,0]
!set Static Elements = [249,15,9]
set Static Elements = [199,9,10]
set Static Mesh grading = [1,-0.5,-1.4]
set Static Element type = ElmB8n3D
ok
! =====

sub SaveSimRes
!set time points for report field plot = [0:61,1]
!set time points for plot = ALL
set field storage format = BINARY
set grid storage format = BINARY
!set times series points = NONE !d=2 n=2 (50e-3,0,0) (50e-3,10e-3,0)
!set line1: start = (0,0,0)
!set line1: stop = (100e-3,0,0)
!set line1: resolution = 31
ok

sub GridRefAdm
set refinement strategy = Absolute !Absolute ! Percent
!set percent refined elements = 1
!set hi limit = 1000000
!set lo limit = 500
set hi limit = 1e99 !Hvis gradienten er højere end hi limit forfines der ikke
set lo limit = 800 !150000 !10000 !250000 !560000 !520000 !560000 !430000 !Gradienter mindre end lo Limit forfines ikke.
set number of refinements = 3 !4! 5! 0 16 !5 ! 1 !Number of Net-forfining 0=ingenforfining 5=anbefalet af Christian
set max refinement levels = 15
!set max nodes = 30000
set max elements = 700000
set start grid for refinement = original ! current
set tolerance = 1e-9
set mixed refinement method = ON
set element order = 1 ! {1&2}
set no of edge refinements = 2 ! 4

ok

sub RefinementIInd_prm
set refinement indicator = Value !Gradient !OwnIndicator ! Gradient ! Value !! ZZ
set error used in stop criterion = OFF
ok

sub LinEqAdmFE
sub Matrix_prm
set matrix type = MatSparse
!set no of additional convergence monitors = 2
ok
sub LinEqSolver_prm
set basic method = ConjGrad
ok
sub Precond_prm
set preconditioning type = PrecRILU
set RILU relaxation parameter = 0.95
ok
sub ConvMonitorList_prm
sub Define ConvMonitor #1
set #1: convergence monitor name = CMRelResidual
!set #1: convergence monitor name = CMRelMixResidual
set #1: residual type = ORIGINAL_RES
set #1: convergence tolerance = 5.0e-1
```

```
!set #1: run time plot      = off
ok

ok

ok

sub Solver #1 NonLinEqSolver_prm
set Solver #1 nonlinear iteration method = SuccessiveSubst
set Solver #1 max nonlinear iterations = 10
set Solver #1 max estimated nonlinear error = 5.0e-1
set Solver #1 nonlinear relaxation prm = 0.5
set Solver #1 adjustments = 1
set Solver #1 continuation parameter = 0.3 0.5 0.6 0.7 ;
ok

sub Solver #2 NonLinEqSolver_prm
set Solver #2 nonlinear iteration method = NewtonRaphson
set Solver #2 max nonlinear iterations = 30
set Solver #2 max estimated nonlinear error = 5.0e-1
set Solver #2 nonlinear relaxation prm = 0.2
set Solver #2 adjustments = 1
set Solver #2 continuation parameter = 0.7 0.8 0.85 0.9 0.925 0.95 1 ;
set Solver no of switches between strategies = 1
set Solver strategy = 1
ok

!sub Optimizer_prm
! set max iterations = 5
! set min linesearch = 1e-3
! set max violation nonlin constr = 1e-1
! set fd perturbation = 1e-6
! set lower bound = -1e4
! set upper bound = 1e4
! set use finite difference = 1
! ok
ok
ok
```


B. Program Code of the Off-line Preparation System

In this appendix the additional program code of the *off-line preparation system* is depicted. This code is programmed in Diffpack. Diffpack is a program language suitable when building finite-element programs. Because Diffpack is based on C++ structure and classes the code is very similar to C++.

```
*****
/**          Hans Christian Kjeldsen Orye          *
/**          FORCE Technology, Denmark             *
/**          hans_chr@mailme.dk                  *
*****

#include <weldsim.h>
#include <realweld.h>
realweld:: realweld () : weldsim() {}

*****
void realweld:: define (MenuSystem& menu, int level) // Defining the menu
/**          *****
{
weldsim:: define (menu, level);
}

*****
void realweld:: scan () // Read input and initializing
/**          *****
{
MenuSystem& menu    = SimCase:: getMenuSystem();
weldsim:: scan ();
}

*****
void realweld:: solveAtThisTimeStep ()
/**          *****
{
weldsim:: solveAtThisTimeStep ();
onlineReference(); // Generating a reference for the online system
}

*****
void realweld:: solveProblem ()
/**          *****
{
weldsim:: timeLoop();
}

*****
void realweld:: computeContVec ()
/**          *****

{
real source_intensity_temp = 0;
real move_size = 0; //the size of the move for each timestep
real dt = tip->Delta(); //Time between each timestep

char * temp2 = ".dat"; //Reference type
int temp3 = tip->getTimeStepNo(); //Reference time step number
char * temp4 = "_outputRealweld-"; //Output type name
String matlabfilenameOutput = aform("%s%s%d%s", casename.c_str(),temp4,temp3,temp2); //Creates the formate of the Matlab
file
```

Appendix B. Program Code of the Off-line Preparation System

```
Os file_output (matlabfilenameOutput, NEWFILE); //Creates a new file

s_o << "\n";
s_o << "*****" << "\n";
s_o << "HCK ----> w_pos i computeContVec i [mm] (before):" << w_pos*1000 << "\n";
s_o << "HCK ----> source_intensity i computeContVec i [mm] (before):" << source_intensity << "\n";

real t = tip->time();

//----- Size of camera image START -----
numOfPiksX = 600;//Number of piksels in the camera in one direction + pendle amplitude
numOfPiksY = 200;//Number of piksels in the camera in the other direction + pendle amplitude
displacementX = 200;//Displacement of the gun position in the image along the x-axe
//----- Size of camera image END -----

//----- Constant control values START -----
source_intensity = voltage * current * arc_eff*0;
//w_pos = source_velocity*t + source_center;
//----- Constant control values END -----

//----- Controller INPUT-FILE START -----
T_ref_1 = 1527; //The reference temperature
T_ref_2 = 644; //The reference temperature

kp11 = 0.1110; //The P-matrix value 1,1
kp21 = -0.4039; //The P-matrix value 1,1
kp12 = 0.0006; //The P-matrix value 1,1
kp22 = -0.0015; //The P-matrix value 1,1

inv_G_zero11 = 0.2068; //The invers value of the identified transfer function in stationary G : inv(G(0))
inv_G_zero21 = -0.1022; //The invers value of the identified transfer function in stationary G : inv(G(0))
inv_G_zero12 = 0.0016; //The invers value of the identified transfer function in stationary G : inv(G(0))
inv_G_zero22 = 0.0056; //The invers value of the identified transfer function in stationary G : inv(G(0))

surf_point_1(1) = 350; //X value of feedback surface point number 1
surf_point_1(2) = 101; //Y value of feedback surface point number 1
surf_point_2(1) = 350; //X value of feedback surface point number 2
surf_point_2(2) = 151; //Y value of feedback surface point number 2
//----- Controller INPUT-FILE END -----

/*
//----- P-Controller SISO 1x1 START -----

if (t >= 5)
{
source_intensity_temp = T_ref_1 * inv_G_zero11 + T_error_1 * kp11;
source_intensity = source_intensity_temp * arc_eff;
if (source_intensity < 0) source_intensity = 0;
}

s_o << "HCK ----> T_error_1:" << T_error_1 << " Kp11:" << kp11 << "\n";
s_o << "HCK ----> T_ref_1:" << T_ref_1 << " inv_G_zero11:" << inv_G_zero11 << "\n";
//----- Controller END -----
*/

/*
//----- P-Controller MIMO 2x2 START -----

if (t <= 5)
{
w_pos(1) = w_pos(1)+1.0e-3;
source_intensity = 250 * voltage * arc_eff;
}
else
{
source_intensity_temp = (T_ref_1 * inv_G_zero11 + T_ref_2 * inv_G_zero21) + (T_error_1 * kp11 + T_error_2 * kp21);
source_intensity = source_intensity_temp * arc_eff;
if (source_intensity < 0) source_intensity = 0;

source_velocity = (T_ref_1 * inv_G_zero12 + T_ref_2 * inv_G_zero22) + (T_error_1 * kp12 + T_error_2 * kp22);
if (source_velocity < 1.5) source_velocity = 1.5;
if (source_velocity > 10) source_velocity = 10;
move_size = source_velocity(1)*dt*1e-3;
w_pos(1) = w_pos(1)+move_size;
s_o << "w_pos:" << w_pos << " move_size:" << move_size << "\n";

Os file_output (matlabfilenameOutput, APPEND);
file_output << T_ref_1 << " " << T_ref_2 << " " << (T_ref_1 - T_error_1) << " " << (T_ref_2 - T_error_2)
<< " " << T_error_1 << " " << T_error_2 << " " << source_intensity << " " << source_velocity << "\n";
*/
```

Appendix B. Program Code of the Off-line Preparation System

```

file_output->close();
}

s_o << "HCK ----> T_error_1: " << T_error_1 << " T_error_2: " << T_error_2 << "\n";
s_o << "HCK ----> T_ref_1: " << T_ref_1 << " T_ref_2: " << T_ref_2 << "\n";
//----- P-Controller MIMO 2x2 END -----
*/

//----- Step input START -----
//Step input on heat intensity
if (t <= 5) source_intensity = 0 * voltage * arc_eff; //voltage * current * arc_eff * 0; //Step input on current
else source_intensity = 250 * 15 * arc_eff; //voltage * current * arc_eff;

//Step input on velocity
if (t <= 100) w_pos(1) = w_pos(1)+1.0e-3;
else w_pos(1)= w_pos(1)+1.25e-3;

//source_extnt(1) = source_extnt(2) = 3e-3;
//source_extnt(3) = 2.5e-3;

//if (t > 0.5) w_pos(2)=0.005; //Step input on w_pos(2)
//----- Step input END -----

s_o << "HCK ----> w_pos i computeContVec i [mm] (after):" << w_pos*1000 << "\n";
s_o << "HCK ----> source_intensity (after):" << source_intensity << " source_intensity not times arc_sff (after): " <<
source_intensity_temp << "\n";
s_o << "*****" << "\n";
}

//*****
void realweld: onlineReference () //Generating Online Reference
//*****
{
real t = tip->time(); //The Present time in the simulation
real dt = tip->Delta(); //Time between each timestep

char * temp1 = "_reference2D-"; //Reference type name
char * temp2 = ".dat"; //Reference type
int temp3 = tip->getTimeStepNo(); //Reference time step number
char * temp4 = "_outputRealweld-"; //Output type name
String matlabfilename = aform("%s%s%d%s", casename.c_str(),temp1,temp3,temp2);
//Creates the formate of the Matlab file
String matlabfilenameOutput = aform("%s%s%d%s", casename.c_str(),temp4,temp3,temp2);

Os file_ref (matlabfilename, NEWFILE); //Creates a new file
Ptv(real) camXYZmid, camXYZ; //Declair Spatial point in the camera coor. system
camXYZmid.redim (3); //Dimension of spatial points
camXYZ.redim (3);

int airTemp = -100;
real dx = 0.0001; //The camera piksel size
real dy = 0.0001; //The camera piksel size
real val; //Temporary temperature variable
real relPosX_ave; //Pixel position along the X-axis relative to welding gun
real relPosY_ave; //Pixel position along the Y-axis relative to welding gun
real T_error_1_temp; //The temperature of temperature point 1, used for calculating T_error_2
//w_pos = source_velocity*t; //ESTIMATED position of the welding gun

Ptv(real) uMinCoor;
Ptv(real) uMaxCoor;
grid->getMinMaxCoord(uMinCoor,uMaxCoor);//Getting min and max coordinates of the plate

//camXYZmid(1) = w_pos(1) + 0.5*dx; //Along the length of the plate(welding direction)
//camXYZmid(2) = w_pos(2) + 0.5*dy; //Along the width of the plate
//camXYZ(3) = uMaxCoor(3); //From the bottom of the plate and up
//int numOfPiksX = 600;//Number of piksels in the camera in one direction + pendle amplitude
//int numOfPiksY = 200;//Number of piksels in the camera in the other direction + pendle amplitude
//int displacementX = 200;//Displacement of the gun position in the image along the x-axe

for (int i = 1; i <= numOfPiksX; i++)
{
relPosX_ave = w_pos(1) + (i -1 -numOfPiksX/2 -displacementX)*dx; //Position of one piksel along the x-axis
camXYZ(1) = relPosX_ave; //Position of one piksel along the x-axis
//s_o << "\n";

for (int j = 1; j <= numOfPiksY; j++)
{
relPosY_ave = source_center(2) + (j -1 -numOfPiksY/2)*dy; //Position of one piksel along the y-axis
camXYZ(2) = relPosY_ave; //Position of one piksel along the y-axis
//s_o << "X:" << camXYZ(1)*1000 << " Y:" << camXYZ(2)*1000 << " ";
}
}
}

```

Appendix B. Program Code of the Off-line Preparation System

```
if ( camXYZ(1) < uMinCoor(1) || camXYZ(1) > uMaxCoor(1) )
    val = airTemp;
else
    if ( camXYZ(2) < uMinCoor(2) || camXYZ(2) > uMaxCoor(2) )
        val = airTemp;
    else
        {
            //s_o << "i"<<i << "j"<< j << " ";
            //s_o << "Foer u->valuePt(camXYZ); ";
            val = u->valuePt(camXYZ);
            //s_o << "Else ";
        }

if (val < airTemp)
    val = airTemp;

//s_o << i<<"X" << " " << camXYZ(1)*1000 << " "; << j << "Y" << camXYZ(2)*1000 << " "; val: << val << " ";
Os file_ref (matlabfilename, APPEND);
file_ref /*<< camXYZ(1) << " " << camXYZ(2) << " " */<< val << " ";
file_ref->close();

/* if ( i == ( 250 ) && j == ( 101 ) ) // it has been: numOfPiksX-20!!!
{
    s_o << "\n";
    s_o << "HCK ----> Pikel number: X: " << 250 << " Y: " << 101 << " Pikel value (val): " << val << "\n";
    s_o << "-----> << "\n";
}
if ( i == ( 300 ) && j == ( 101 ) ) // it has been: numOfPiksX-20!!!
{
    s_o << "\n";
    s_o << "HCK ----> Pikel number: X: " << 300 << " Y: " << 101 << " Pikel value (val): " << val << "\n";
    s_o << "-----> << "\n";
}
if ( i == ( 350 ) && j == ( 101 ) ) // it has been: numOfPiksX-20!!!
{
    s_o << "\n";
    s_o << "HCK ----> Pikel number: X: " << 350 << " Y: " << 101 << " Pikel value (val): " << val << "\n";
    s_o << "-----> << "\n";
}
*/

//----- Generating the ERROR -----

if ( i == ( surf_point_1(1) ) && j == ( surf_point_1(2) ) ) // it has been: numOfPiksX-20!!!
{
    T_error_1 = T_ref_1 - val;
    T_error_1_temp = val;
    s_o << "\n";
    s_o << "HCK ----> Pikel number: X: " << ( surf_point_1(1) ) << " Y: " << ( surf_point_1(2) ) << " Pikel value (val): " << val
<< "\n";
    s_o << "HCK ----> T_error_1: " << T_error_1 << "\n";
    s_o << "-----> << "\n";
}

if ( i == ( surf_point_2(1) ) && j == ( surf_point_2(2) ) )
{
    T_error_2_temp = val;
    s_o << "\n";
    s_o << "HCK ----> Pikel number: X: " << ( surf_point_1(1) ) << " Y: " << ( surf_point_1(2) ) << " Pikel value (val): " << val
<< "\n";
    s_o << "HCK ----> T_error_2_temp: " << T_error_2_temp;
}

/*
if ( i == ( 450 ) && j == ( 101 ) ) // it has been: numOfPiksX-20!!!
{
    s_o << "\n";
    s_o << "HCK ----> Pikel number: X: " << 450 << " Y: " << 101 << " Pikel value (val): " << val << "\n";
    s_o << "-----> << "\n";
}
*/
```

Appendix B. Program Code of the Off-line Preparation System

```
if ( i == ( 500 ) && j == ( 101 ) ) // it has been: numOfPiksX-20!!!
{
    s_o << "\n";
    s_o << "*****" << "\n";
    s_o << "HCK ----> Pikel number: X: " << 500 << " Y: " << 101 << " Pikel value (val): " << val << "\n";
    s_o << "*****" << "\n";
}
if ( i == ( 550 ) && j == ( 101 ) ) // it has been: numOfPiksX-20!!!
{
    s_o << "\n";
    s_o << "*****" << "\n";
    s_o << "HCK ----> Pikel number: X: " << 550 << " Y: " << 101 << " Pikel value (val): " << val << "\n";
    s_o << "*****" << "\n";
}
*/

}
Os file_ref (matlabfilename, APPEND);
file_ref << "\n";
file_ref->close();
}
T_error_2 = T_ref_2 - (T_error_1_temp - T_error_2_temp);
s_o << " T_error_2 = " << T_error_1_temp << " - " << T_error_2_temp << " = " << T_error_2 << "\n";
s_o << "*****" << "\n";

s_o << "\n";
s_o << "*****" <<
"\n";
s_o << "HCK ----> " << "w_pos in [mm]: " << w_pos*1000 << " uMinCoor: " << uMinCoor*1000 << " uMaxCoor: " <<
uMaxCoor*1000 << " source_velocity: "
<< source_velocity << " t: " << t << " source_center: " << source_center << "\n";
s_o << "*****" <<
"\n";
}
```


C. Off-line Identification - Matlab Code

In this appendix the Matlab code developed to perform the off-line identification is illustrated. Based on this code it is possible to generate the *transfer-function matrix*, which consists of one or more transfer-functions. The *input* for this Matlab program is the *output* values, $y(\delta)$, generated from applying one or more step-input on the off-line system. The output of the Matlab program is one or more transfer-functions. The number of transfer-functions is dependent on the number of *input* and *outputs*.

First a main program is illustrated (Section C.1). The main program is used to initiate the sub-program *OI* that performs the off-line identification (Section C.2) and the sub-program *controlMatrix_disc_P_stand* that generates the proportional control gain matrix (Appendix D).

C.1. The main program

In this section the main program that initiates the program that identifies the transfer-functions of the *transfer-function matrix* and the program that generates the k_p gain matrix is illustrated.

```
% *****
%           Hans Christian Kjeldsen Orye           *
%           FORCE Technology, Denmark             *
%           hans_chr@mailme.dk                  *
% *****

% -----
%----- This program is the main program used for generatin Gs and suitable control matrixes. -----
% -----

disp("")
disp("")
disp('-----')
disp('The Control calculation has started.')
disp('-----')

clear; tic;

disp(' ')
disp('-----Off-line Identification-----')
load C:\WAMOS\Temp1.mat %Loading the surface temperature points from the DiffPack simulation.
sim1(:,1)=Output;
clear Output
load C:\WAMOS\Temp2.mat %Loading the surface temperature points from the DiffPack simulation.
sim1(:,2)=Output;
clear Output
load C:\WAMOS\Temp1.mat %Loading the surface temperature points from the DiffPack simulation.
sim2(:,1)=Output;
clear Output
load C:\WAMOS\Temp2.mat %Loading the surface temperature points from the DiffPack simulation.
sim2(:,2)=Output;
clear Output

Output(:,1,1) = sim1(:,1);% Output_temp(:,1); %Step1 current, temp1 current
Output(:,1,2) = sim1(:,2);% Output_temp(:,2); %Step1 current, temp2 weaving
Output(:,2,1) = sim2(:,1);% Output_temp(:,3); %Step2 weaving, temp1 current
Output(:,2,2) = sim2(:,2);% Output_temp(:,4); %Step2 weaving, temp2 weaving

Forskydning11 = 6 %T1 %Step1 current, temp1 current
Forskydning12 = 142.5 %T2 %Step1 current, temp2 weaving
Forskydning21 = 8.5 %T1 %Step2 weaving, temp1 current
Forskydning22 = 105 %T2 %Step2 weaving, temp2 weaving

Output(:,1,1)=Output(:,1,1)-Forskydning11; %T1 %Step1 current, temp1 current
Output(:,1,2)=Output(:,1,2)-Forskydning12; %T2 %Step1 current, temp2 weaving
Output(:,2,1)=Output(:,2,1)-Forskydning21; %T1 %Step2 weaving, temp1 current
Output(:,2,2)=Output(:,2,2)-Forskydning22; %T2 %Step2 weaving, temp2 weaving
```

Appendix C. Off-line Identification - Matlab Code

```
[numberOfOutputTimeStep,NumberOfOutput,NumberOfSimulations]=size(Output) %The exact number of
true output and temperature points

U=([44 0; %Simulation one %U is the power or position etc.
    0 1.5]) %Simulation two

OI_m=([0,0;
       0,0])%Numerator degree "m" in accor. to [Franke, eq.(3.4)] for every output:
       %[out1_sim1 out2sim1 .. .. .; out1_sim2 out2_sim2 .. .. .]
OI_n=([1,1;
       1,1])%Denominator degree "n" in accor. to [Franke, eq.(3.4)] fo every output:
       %[out1_sim1 out2sim1 .. .. .; out1_sim2 out2_sim2 .. .. .]

dt=0.25%

ne=numberOfOutputTimeStep

te=([ne-1,ne-1;
     ne-1,ne-1]*dt)%"te" is the settling time (stationary endpoint)

alpha=([3.5, 3.5; %Small alfa gives small stationary error.
        3.5, 3.5])./te%[Franke, eq. 2.108]. Cell by cell division.

figure(1)
plotNumber=[1 1;
            1 1]%The OI Output to be plotted (0=no plot; 1=plot).

OI; %Offline Identification.

disp(' ')
disp('_____')
disp('-----Control matrix generation-----')
s=tf('s'); %Making s a transfer function variable

a1=1
order1=1
a2=0.2
order2=1
Fw=[a1^order1/(s+a1)^order1 0;
     0 a2^order2/(s+a2)^order2]; %Fw in diagonal matrix form
clear a1 a2 order1 order2

Ip=[1 0 ; 0 1]; %Diagonal matrix

controlMatrix_disc_P_stand; %Generating standard controlmatrix Kp [Franke, (6.14)]

figure(4); hold off;
step(Fw)

disp('-----')
disp('The Control calculation has finished in')
disp(toc)
disp('(seconds.)')
C.106. disp('-----')
```

C.2. Off-line Identification Program

In this section is the program, which identifies the transfer-functions of the *transfer-function matrix* illustrated.

```

%*****
%           Hans Christian Kjeldsen Orye           *
%           FORCE Technology, Denmark             *
%           hans_chr@mailme.dk                   *
%*****

%-----This Program must be runned from control.m-----

disp('----- Start of IO -----')

N=[OL_n+OI_m+1]%[Franke, page 70]
Gs=zeros(max(max(N)),NumberOfSimulations,NumberOfOutput);%Generating a matrix consisting of zeros
Gs_hat=zeros(max(max(N)),NumberOfSimulations,NumberOfOutput);%Generating a matrix consisting of zeros
max_OI_n=max(max(OI_n));
max_OI_m=max(max(OI_m));
ParameterMatrix=zeros(max(max(N)),NumberOfSimulations,NumberOfOutput);%Generating a matrix
consisting of zeros

%-----Plotting Output-----
figure(3);
hold off;
for SimulationNumber=1:NumberOfSimulations;
    for OutputSetNumber=1:NumberOfOutput;
        if (plotNumber(SimulationNumber,OutputSetNumber) == 1)
            for i=1:ne;
                plot(Output(:,SimulationNumber,OutputSetNumber)); hold on;
            end
        end
    end
end
xlabel('Number of Time Step',FontSize',10)
ylabel('Size of Measurement',FontSize',10)
title('Plotting Output',FontSize',11)
figure(1)
clear SimulationNumber OutputSetNumber

%----- Determine the approximation funtion Gs -----
%Calculate the constant term in Gs [Franke, eq. 3.7] for the output temp1 to tempXX
for SimulationNumber=1:NumberOfSimulations;
    for OutputSetNumber= 1 :NumberOfOutput;
        for k=1:N(SimulationNumber,OutputSetNumber);

Gs(k,SimulationNumber,OutputSetNumber)=Output(ne,SimulationNumber,OutputSetNumber)*exp(-
k*alpha(SimulationNumber,OutputSetNumber)*te(SimulationNumber,OutputSetNumber));% [Franke, eq.
3.7]
        end
    end
end

```

```

end
Gs;
%Calculate the other term by use of the Trapezoidal Rule
for SimulationNumber=1:NumberOfSimulations;
    for OutputSetNumber=1:NumberOfOutput;
        for k=1:N(SimulationNumber,OutputSetNumber);
            GsTemp=0;

            %Calculate sumation term in [Franke, eq. 3.9]
            M=ne;
            for ii=1:M-1;
                GsTemp=GsTemp + Output(ii,SimulationNumber,OutputSetNumber)*exp(-
k*alpha(SimulationNumber,OutputSetNumber)*ii*dt);%[Franke, eq. 3.7]
            end

            GsTemp=dt*GsTemp + (dt/2)*( Output(1,SimulationNumber,OutputSetNumber) +
Output(ne,SimulationNumber,OutputSetNumber)*exp(-
k*alpha(SimulationNumber,OutputSetNumber)*te(SimulationNumber,OutputSetNumber)) );

            %add up all the constants to determine Gs

Gs_hat(k,SimulationNumber,OutputSetNumber)=k*alpha(SimulationNumber,OutputSetNumber)*GsTemp
+ Gs(k,SimulationNumber,OutputSetNumber);
        end
    end
end
%Gs_hat is determined
clear GsTemp
Gs_hat;

%----- Generating transferfunctions -----

%Set up of the matrix in [Franke, eq. 3.4]
for SimulationNumber=1:NumberOfSimulations;
    for OutputSetNumber=1:NumberOfOutput;
        Matrix=zeros(N(SimulationNumber,OutputSetNumber));
        %First column
        Matrix(:,1)=1; %[Franke, eq. 3.4], 1
        %From second column to OI_m+1 columns
        for k=1:N(SimulationNumber,OutputSetNumber);
            for m=1:(OI_m(SimulationNumber,OutputSetNumber));
                Matrix(k,(m+1))=(k*alpha(SimulationNumber,OutputSetNumber))^m; %[Franke, eq. 3.4]
            end
        end

        %From after OI_m(SimulationNumber,OutputSetNumber)+1 to N((OutputSetNumber)) columns
        for k=1:N(SimulationNumber,OutputSetNumber);
            for n=1:OI_n(SimulationNumber,OutputSetNumber);
                Matrix(k,(n+
                    OI_m(SimulationNumber,OutputSetNumber)
                    +1))=
(k*alpha(SimulationNumber,OutputSetNumber))^n*Gs_hat(k,SimulationNumber,OutputSetNumber);
                %[Franke, eq. 3.4], n
            end
        end
    end
    OutputSetNumber;
    Matrix; %[Franke, eq. 3.4]

%-----

%Solve the algebraic equations to find b_j and a_i
MatrixInv=inv(Matrix);

```

Appendix C. Off-line Identification - Matlab Code

```

for i=1:(OI_n(SimulationNumber,OutputSetNumber) +OI_m(SimulationNumber,OutputSetNumber)
+1);
    Gs_hat_temp(i,1)=Gs_hat(i,SimulationNumber,OutputSetNumber);
end;
Vector=MatrixInv*Gs_hat_temp;%

clear Gs_hat_temp Matrix MatrixInv;

%Placing the solution in a ParameterMatrix
[numOfElementsInVector,temp]=size(Vector);
for i=1:numOfElementsInVector;
    ParameterMatrix(i,SimulationNumber,OutputSetNumber)=Vector(i);
end;
clear temp
%-----

%-----
% Transform the ParameterMatrix into a transfer function GM
% Set DenTemp and NumTemp
NumTemp(OI_m(SimulationNumber,OutputSetNumber)+1)=0;%IO_m ville måske være det samme
som IO_OutputSetNumber!!!!!!
for i=1:(OI_m(SimulationNumber,OutputSetNumber)+1);
    ii=(OI_m(SimulationNumber,OutputSetNumber)+2)-i;
    NumTemp(i)=Vector(ii);
end
NumEndNum=max_OI_m+2;
for i=1:(OI_m(SimulationNumber,OutputSetNumber) +1);
    Num(SimulationNumber,
        NumEndNum
        OutputSetNumber)=NumTemp(OI_m(SimulationNumber,OutputSetNumber) -i +2);
end

DenTemp(OI_n(SimulationNumber,OutputSetNumber)+1)=1;
for i=1:OI_n(SimulationNumber,OutputSetNumber);
    ii=N(SimulationNumber,OutputSetNumber)+1-i;
    DenTemp(i)=Vector(ii);
end
DenStartNum= max_OI_n +max_OI_m -OI_n(SimulationNumber,OutputSetNumber);
for i=1:(OI_n(SimulationNumber,OutputSetNumber) +1);
    Den(SimulationNumber, DenStartNum +i, OutputSetNumber)=DenTemp(i);
end
clear NumTemp DenTemp
%-----

end
end
ParameterMatrix;

%----- Generating the transferfunction Matrix Ygm -----
disp(' ');
disp('----- Ygm -----');
for SimulationNumber=1:NumberOfSimulations;
    for OutputSetNumber=1:NumberOfOutput;
        Ygm(SimulationNumber,OutputSetNumber)=tf([Num(SimulationNumber,OutputSetNumber)]
        ,
        {[Den(SimulationNumber,OutputSetNumber)]});
    end
end
Ygm

```

```

%----- solving x equations with x unknowns -----
disp(' ');
disp('----- GM -----');
disp('The transfer function to be used for control matrix generation');
GM=inv(U)*Ygm

%----- Plotting G and the simulation output compared with GM -----
disp(' ');
disp('-----Plotting G(s) -----');
t=0:(dt/10):(ne*dt-dt); %Defining the timesteps and timehorizon
figure(1)
for SimulationNumber=1:NumberOfSimulations
    Gtemp=step(GM(SimulationNumber,:),t); %Extracting the GM plot values
    size(Gtemp); size(t); %Just a size control
    for OutputSetNumber=1:NumberOfOutput;

GtempOutputSetNumber(:,1)=Gtemp(:,1,OutputSetNumber)*U(SimulationNumber,OutputSetNumber);
    hold off; subplot(NumberOfSimulations, NumberOfOutput, ( SimulationNumber +
    NumberOfOutput*(OutputSetNumber-1) ) ); step(GM(SimulationNumber,OutputSetNumber));% plot((t-
    dt),GtempOutputSetNumber); %Plotting GM
        clear GtempOutputSetNumber
    end
    clear Gtemp
end

clear t

disp(' ');
disp('-----Plotting Ygm(s) and the simulation output -----');
figure(2); hold off;
for SimulationNumber=1:NumberOfSimulations
    YgmTemp=step(Ygm(SimulationNumber,:),t); %Extracting the GM plot values
    size(YgmTemp); size(t); %Just a size control
    for OutputSetNumber=1:NumberOfOutput;
        YgmTempOutputSetNumber(:,1)=YgmTemp(:,1,OutputSetNumber);
        if (plotNumber(SimulationNumber,OutputSetNumber) == 1)
            plot((t-dt),YgmTempOutputSetNumber);hold on; %Plotting GM
        end
        clear YgmTempOutputSetNumber
    end
    clear YgmTemp OutputSetNumber
end
clear SimulationNumber OutputSetNumber

%generating an output (plotOutput) from "Output" file with the length, ne.
for SimulationNumber=1:NumberOfSimulations;
    for OutputSetNumber=1:NumberOfOutput;
        if (plotNumber(SimulationNumber,OutputSetNumber) == 1)
            for i=1:ne;
                plotOutput(i,OutputSetNumber+
                    (NumberOfOutput*(SimulationNumber-1))
                )=Output(i,SimulationNumber,OutputSetNumber);
            end
        end
    end
end

t=0:dt:(ne*dt-dt); %Defining the timesteps and timehorizon

xlabel('Time in seconds','FontSize',10)
ylabel('Size of Measurement','FontSize',10)

```

Appendix C. Off-line Identification - Matlab Code

```
title('Comparing True Output with the IO generated GM',FontSize,11)
grid on; hold on;

clear plotOutput SimulationNumber OutputSetNumber

disp(' ');
disp('----- end of IO -----')
```

D. On-line Controller – Matlab Code

In this appendix the Matlab code developed to generate the on-line control gain matrix is illustrated. Based on this code it is possible to generate the *transfer-function matrix*, which consists of one or more transfer-functions. The input for this Matlab program is the *transfer-function matrix*, $\underline{G}_M(s)$, which is identified based on off-line identification. The output is the gain matrix \underline{k}_p .

The illustrated program is named *controlMatrix_disc_P_stand* and is initiated by the main program, which is illustrated in Section C.1.

```
%*****
%           Hans Christian Kjeldsen Orye           *
%           FORCE Technology, Denmark              *
%           hans_chr@mailme.dk                   *
%*****

disp(')
disp(')
disp('      ----)
disp('     -----)
disp('    -----)
disp('   -----)
disp('  -----)
disp(' -----)
disp('-----)
disp('Start of program ----controlMatrix_disc_P_stand-----)
disp('-----)

T=dt%Sample time

disp(')
disp(')
disp(')
disp('-----Fw-----)
    Fw%Fw in diagonal matrix form
disp('-----)

disp(')
disp(')
disp(')
disp('-----Fwz-----)
    Fwz=c2d((1/s)*Fw, T, 'zoh') %Z transformed (1/s)*Fw as required in [Franke, (6.11)]. The stepinput 1/s
    is required.
disp('-----)

disp(')
disp(')
```


Appendix D. On-line Controller – Matlab Code

```
disp(' ')
disp('-----Fwz(exp(alfa*T))-----')
disp('-----Fw(alfa)-----')
disp('-----G(alfa) and G(0)-----')
[numOfRows,numOfColumns]=size(Fwz);
for row=1:numOfRows;
    for column=1:numOfColumns;
        %----- Calculating Swz_const "exp(alfa*T)" -----
        numTemp=get(Fwz(row,column),'num');%get the numerator from Fwz and put it in numTemp
        denTemp=get(Fwz(row,column),'den');

        [temp,numSize]=size(numTemp{1});
        for i=1:numSize
            num(1,i)=numTemp{1}(i);%Changes the numTemp from a cell array to a double array
        end

        [temp,denSize]=size(denTemp{1});
        for i=1:denSize
            den(1,i)=denTemp{1}(i);
        end

Fwz_const(row,column)=polyval(num,exp(alfa(row,column)*T))/polyval(den,exp(alfa(row,column)*T));
%Uses polyval to calculate Fwz(exp(alfa*T)). The nominater-result/denominator-result.

clear num den numSize denSize numTemp denTemp
%-----

%----- Calculating Swz_const "alfa"-----
numTemp=get(Fw(row,column),'num');
denTemp=get(Fw(row,column),'den');

[temp,numSize]=size(numTemp{1});
for i=1:numSize
    num(1,i)=numTemp{1}(i);
end

[temp,denSize]=size(denTemp{1});
for i=1:denSize
    den(1,i)=denTemp{1}(i);
end

Fw_alfa(row,column)=polyval(num,alfa(row,column))/polyval(den,alfa(row,column));

clear num den numSize denSize numTemp denTemp
%-----

%----- Calculating GM(alfa) and GM(0)-----
numTemp=get(GM(row,column),'num');
denTemp=get(GM(row,column),'den');

[temp,numSize]=size(numTemp{1});
for i=1:numSize
    num(1,i)=numTemp{1}(i);
end

[temp,denSize]=size(denTemp{1});
for i=1:denSize
    den(1,i)=denTemp{1}(i);
```

```

end

GM_alfa(row,column)=polyval(num,alfa(row,column))/polyval(den,alfa(row,column));
GM_zero(row,column)=polyval(num,0)/polyval(den,0);

clear num den numSize denSize numTemp denTemp

end;
end;
Fwz_const
Fw_alfa
GM_alfa
GM_zero
clear row column numOfRows numOfColumnsdisp(' ')
disp('-----')

disp(' ')
disp(' ')
disp(' ')
disp('-----Ip-----')
Ip
disp('-----')

disp(' ')
disp(' ')
disp(' ')
disp('-----Twz-----')
Twz_const=( (exp(alfa*T)-1) / exp(alfa*T) ) * Fwz_const
disp('-----')

disp(' ')
disp(' ')
disp(' ')
disp('-----Swz-----')
Swz_const=Ip-Twz_const %Complementary connection to Twz
disp('-----')

disp(' ')
disp(' ')
disp(' ')
disp('-----Kp-----')
Kp=( (inv(GM_alfa)*Fw_alfa) -inv(GM_zero) ) *inv(Swz_const)
disp('-----')

disp(' ')
disp('-----inv(G_zero)-----')
inv_GM_zero = inv(GM_zero)
disp('-----')

disp('---Stationary temperature reference value T_ref---')
[numOfRows,numOfColumns]=size(Fwz);
T_ref=zeros(numOfRows);
for row=1:numOfRows;
    for column=1:numOfColumns;

```

Appendix D. On-line Controller – Matlab Code

```
    for i=(te/dt-5):(te/dt);
        T_ref(row,column)=T_ref(row,column) + Output(i,row,column);
    end;
    T_ref(row,column)=T_ref(row,column)/6;
end
end
T_ref
disp('-----')
clear i temp row column numOfRows numOfColumns
```

```
disp('-----Comparing T_ref with U*G_zero-----')
    Must_be_like_T_ref = U*GM_zero
disp('-----')
%clear Must_be_like_T_ref
```

```
%Extra calculations for Simulink:
[numOfRows,numOfColumns]=size(Fwz);
if (numOfRows == 1)
    Gz=c2d( GM, T, 'zoh'); %Z transforming GM
    [a,b,c,d,Ts]=ssdata(Gz);
    P_control
end
if (numOfRows == 2)
    Gz=c2d( GM, T, 'zoh'); %Z transforming GM
    [a11,b11,c11,d11,Ts]=ssdata(Gz(1,1));
    [a21,b21,c21,d21,Ts]=ssdata(Gz(2,1));
    [a12,b12,c12,d12,Ts]=ssdata(Gz(1,2));
    [a22,b22,c22,d22,Ts]=ssdata(Gz(2,2));
    P_control_2x2
end
clear numOfRows numOfColumns
```

```
%disp('-----')
disp('The end of controlMatrix_disc_P_stand program')
disp('-----')
```

E. Camera Tests

In this appendix the result of two tests performed on the CV-M10 camera is described. First, a test on the camera input - output linearity is presented. Secondly, the consequences of overexposing the CCD-chip to radiation, the smears effect, is described.

E.1. Test of Camera Input - Output Linearity

Before calibration of the camera it is tested that the camera output is proportional to the camera input. This is done by capturing images of a constant electrical torch. When capturing the images the shutter of the camera is open for different time intervals. If the input/output proportion of the camera is linear, then the output of the camera should double when the shutter speed is doubled. The achieved input/output proportion can be viewed in Figure E-1.

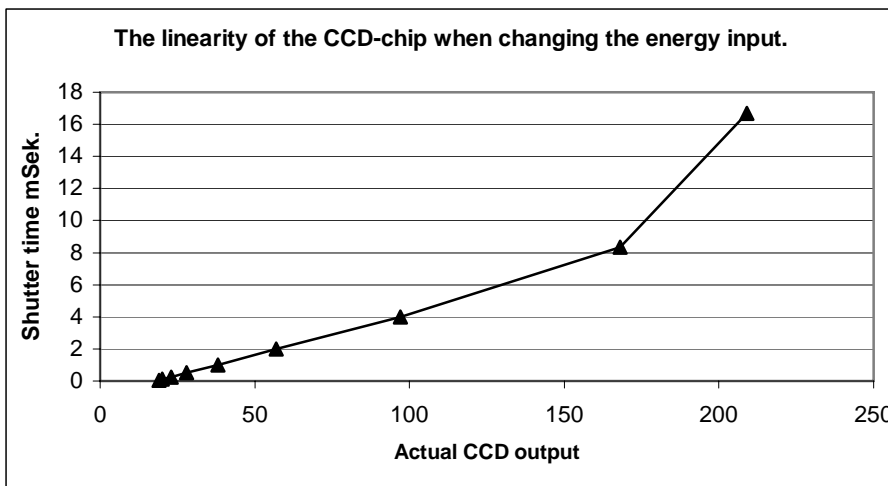


Figure E-1 The proportion between a given input and the received output when changing the shutter time.

The input/output proportion seems proportional, except for the 16 mSek shutter time. The reason for the displacement of the measurement point at 16 mSek is that the maximum CCD output of the camera during these measurements was set to

209. It might be noticed that the actual CCD output at shutter time, zero, is 18. This is due to noise from the surroundings. At a shutter time equal to zero the light inlet to the CCD-chip is remained closed.

E.2. Smears Effect

In this section the consequence of exposing the CCD-chip to too much radiation is illustrated. This effect is called the smears effect and is visible as lines in the image (Figure E-2).

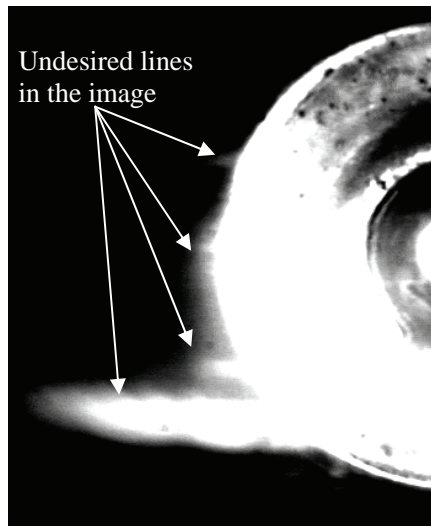


Figure E-2 An exemplification of the smears effect at a shutter time of 1/2000 of a second. In this image a lightning bulb is captured.

The smears effect is the capacity coupling, which arises when the CCD-chip is over-exposed. In the image above (Figure E-2) the effect is seen as light on the left side of the lightning bulb where it is supposed to be dark. This image was captured at a shutter speed of 1/2000 of a second.

Because of the smears effect it is clear that shielding of the Wolfram tungsten electrode is of importance.

F. Spectral Radiance From a GTAW Arc

The undesired radiation from the Argon based GTAW arc is characterized by a unique pattern of spectral lines. The main substance in the plasma of the GTAW welding arc on steel workpiece is argon but also e.g. iron, manganese, tungsten, nitrogen and oxygen typically constitute a small part of the atmosphere and therefore also the emission spectrum. To off-filtrate the majority of the light emitted from the arc, it is important to know the exact pattern of the spectral lines. This pattern has been measured and estimated by means of five different sources:

1. Self-made measurements performed at Aalborg University (AAU) by means of a sensor which is capable of measuring the spectral lines from 190 nm to 850 nm (Section F.1).
2. Self-made measurements at FORCE Technology by means of a sensor, which is capable of measuring the spectral lines from 180 nm to 800 nm (Section F.2).
3. Previously performed measurements generated by FORCE Technology, which show the spectral lines from 200 nm to 1100 nm (Section F.3).
4. Theoretical figures of the spectral radiation in pure Argon (Section F.4).
5. Theoretical figures of the spectral radiation for Argon in air surroundings (Section F.5).

The goal is to identify two ranges of wavelengths where the arc only radiates a minimal portion of light. One of these two ranges of wavelengths is used in the final WAMOS experiments where the WAMOS-system and *WAMOS-method* is tested (Chapter 9). Both of the ranges are used in Appendix I where both the emittance independent and emittance dependent imaging system is calibrated.

F.1. Self-Made Measurements Performed at AAU

At Aalborg University two different spectral pattern measurements were performed:

1. Where the measuring equipment is placed parallel to the surface of the workpiece on which a GTAW arc is active. Here the Wolfram tungsten electrode is visible to the measuring equipment (Section F.1.1).
2. Where the measuring equipment is placed parallel to the surface of the workpiece on which a GTAW arc is active. Because the gas nozzle is tilted 30° (Section F.1.2) the Wolfram tungsten electrode is hidden from radiating directly into the measuring equipment.

All of these measurements were performed by means of a sensor that measured the spectral lines from 190 nm to 850 nm.

F.1.1. Spectral Radiance, Visible Electrode

A sketch of the experimental set-up can be viewed in Figure F-1. Here the Wolfram tungsten electrode is visible for the measuring equipment and the measurements are performed parallel to the surface of the workpiece of which the GTAW arc is active.

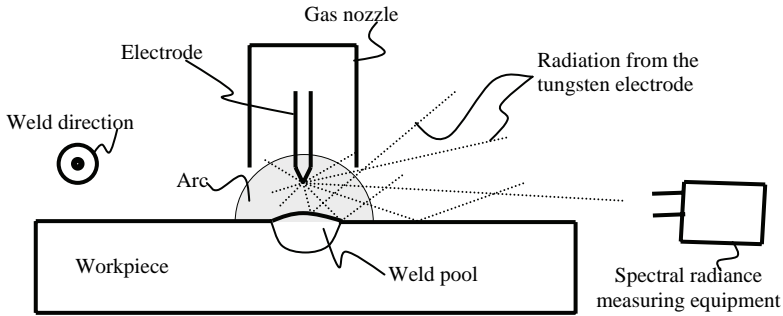


Figure F-1 The set-up for the measurements of Figure F-2. Here the Wolfram tungsten electrode is visible for the spectral radiance measuring equipment.

The spectral lines measured, by means of the above experimental set-up (Figure F-1), are illustrated below (Figure F-2). The measurements were performed by the Physic department at Aalborg University.

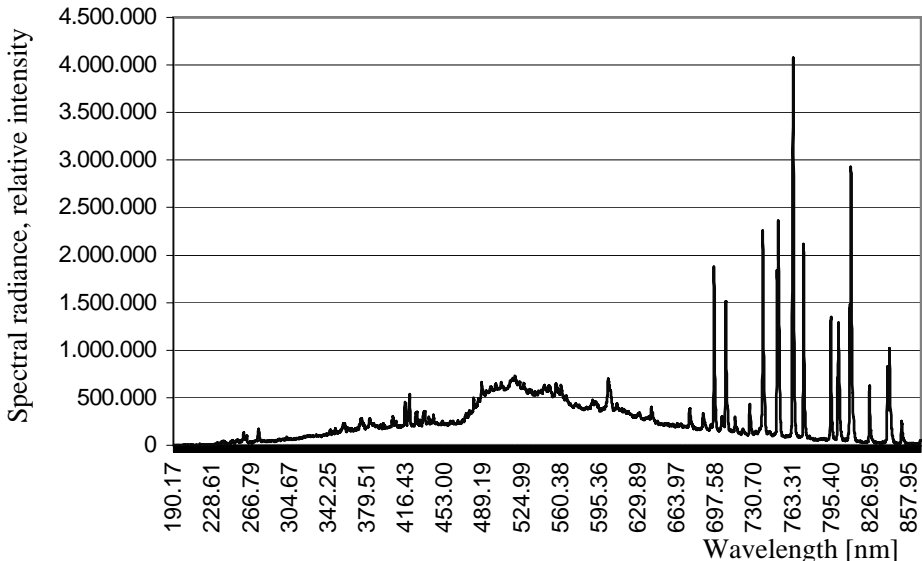


Figure F-2 Spectral irradiation of a 150 amperes GTAW welding arc in 99% argon seen parallel to the plate where the electrode is visible.

F.1.2. Spectral Radiance, Not Visible Electrode

A sketch of the experimental set-up for the measurements of the spectral radiance where the electrode is not visible to the equipment can be viewed in Figure F-3. Again the measurements are made parallel to the surface of the workpiece on which the GTAW arc is active. The electrode is not visible to the measuring equipment due to a 30° rotation of the gas nozzle.

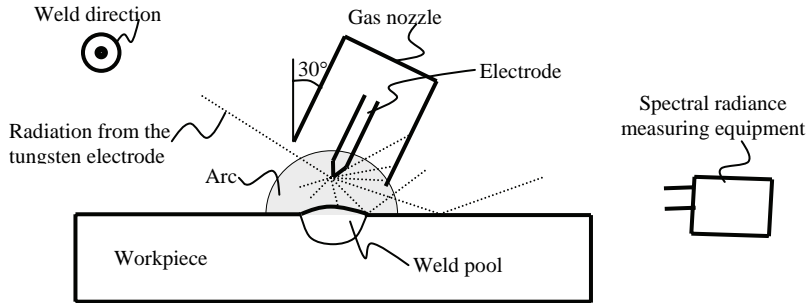


Figure F-3 The set-up for the measurement of Figure F-4. Here the spectral radiance measuring equipment is shielded from direct radiation from the Wolfram tungsten electrode.

The spectral lines measured by means of the above experimental set-up (Figure F-3) are illustrated below (Figure F-4). The measurements were performed by the Physic department at Aalborg University.

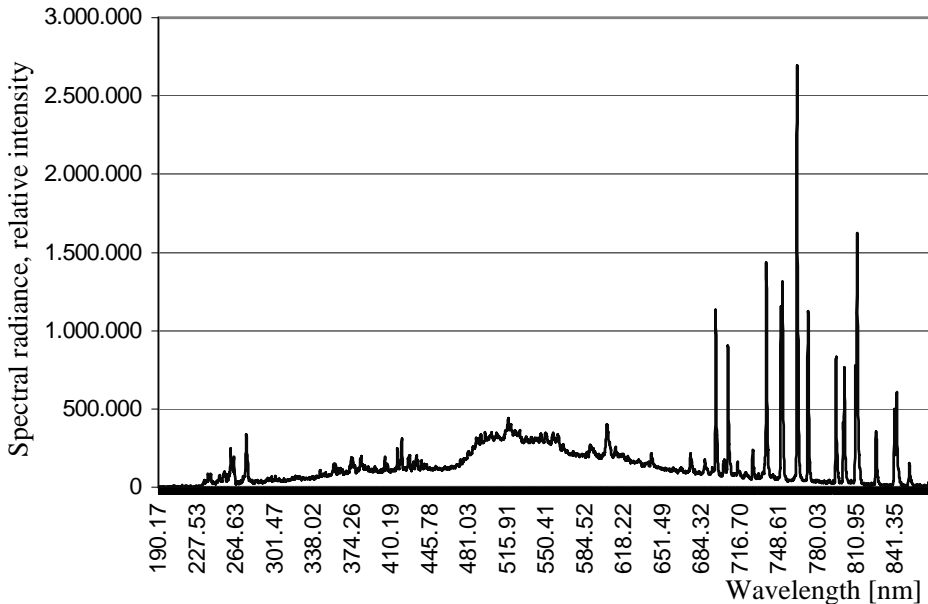


Figure F-4 Spectral irradiation of a 150 amp. GTAW welding arc in 99% argon seen parallel to the plate without the electrode in view.

When comparing the two measurements of the GTAW arc with respectably no visible electrode (Figure F-2) and a visible electrode (Figure F-4), it is easy to see that the experiment with the exposed electrode has a higher energy level for all wavelengths.

F.2. Self-Made Measurements Performed at FORCE

Measurements similar to the spectral radiance measurements performed at AAU have been performed at FORCE Technology. The sensor used at FORCE measured spectral lines from 180 nm to 800 nm. At FORCE twelve measurements were performed. One of these is depict below (Figure F-5). In this experiment the Wolfram tungsten electrode was hidden behind the gas nozzle. The gas nozzle was as earlier hidden due to a 30° rotation of the nozzle (Figure F-3). The measurements were performed by [Hurup] in a distance of one meter from the arc. The exposure time was one second.

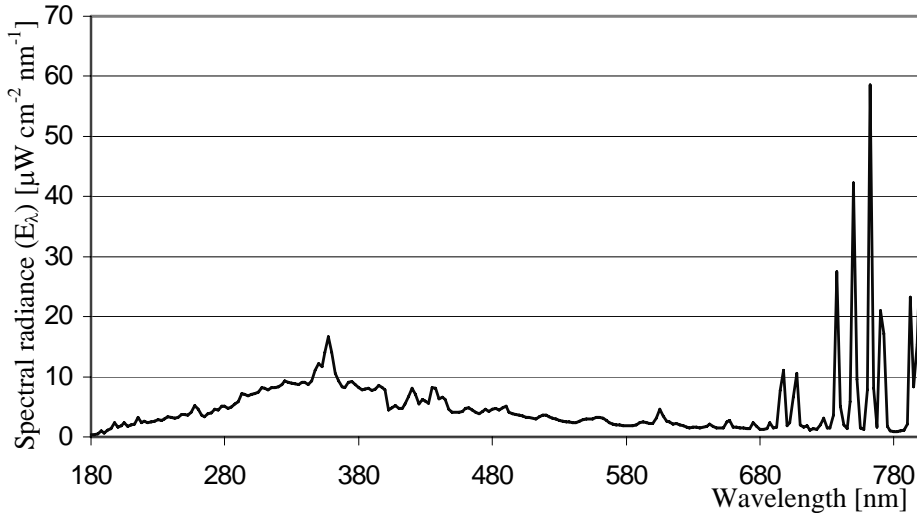


Figure F-5 Spectral irradiation of a 100 amp. GTAW welding arc in 99,9% argon performed parallel to the workpiece without the electrode in view. This is one of the twelve measurements performed at FORCE Technology.

The measurements performed at AAU and FORCE (Section F.1 and F.2) do though not show the spectral radiance above 850 nm. To get information of which spectral lines to expect from a GTAW argon arc above 850 nm a former measurement performed a FORCE was used together with theoretical figures of the spectral radiance in argon.

F.3. Former Measurements Performed at FORCE

FORCE Technology has in a former project measured the spectral radiance of a GTAW welding in the range from 200 nm to 1100 nm. Unfortunately the experimental set-up is not known. The position of the measuring equipment in relation to the welding process is therefore unknown. It is also unknown why the energy level for all wavelengths is displaced with one to two $\mu\text{W} / (\text{cm}^2 \text{nm}^1)$. In general it was not possible to estimate the reliability of this measurement. The measurement though gives a nice view of the spectral radiance for wavelengths up to 1100 nm (Figure F-6).

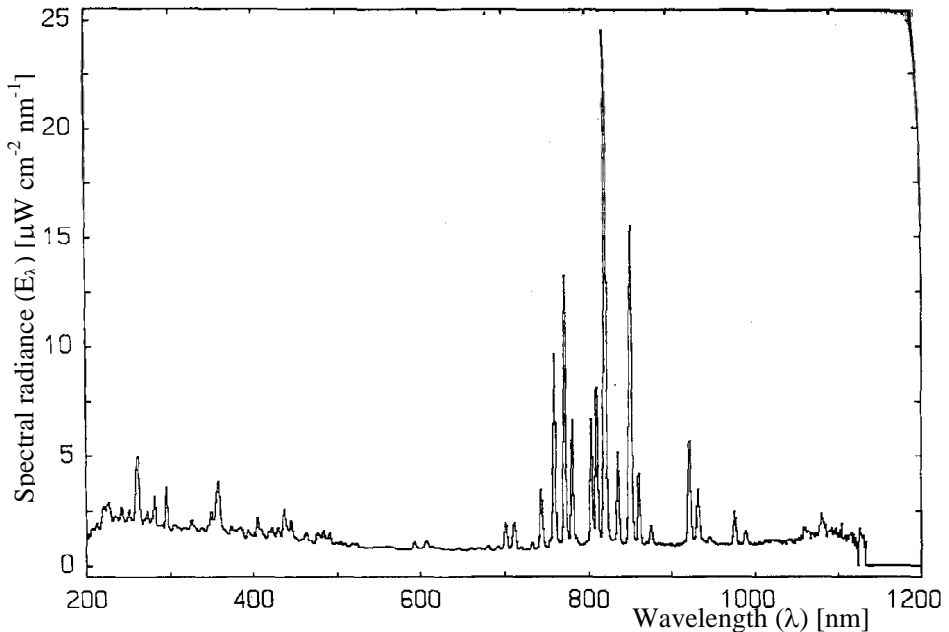


Figure F-6 Spectral radiance for a TGAW welding arc in 99% argon.

According to the above measurement (Figure F-6) it should be possible to find a collection of wavelengths from 500 nm to 700 nm, around 900 nm, around 960 nm and from 980 nm to 1050 nm that does not contain much radiation from the GTAW arc.

F.4. Theoretical Figures of the Spectral Radiation in Pure Argon

At wavelengths from 800 to 1100 nm the Planck's radiation, which is to be measured by the temperature imaging system, is more intensive than for wavelengths below 800 nm (Figure 7.2). Therefore various theoretic literatures discussing the spectral lines in this field have been investigated. Due to

measurements, theory and experiments the position of the band-pass filter in-between 620 nm to 660 and in-between nm 980 nm to 1050 nm was of special interest. One of the references illustrates, by a drawing, the spectral radiation of pure Argon up till 1000 nm [A. I. of P. H.]. Segments of this drawing are shown in Figure F-7 and Figure F-8.

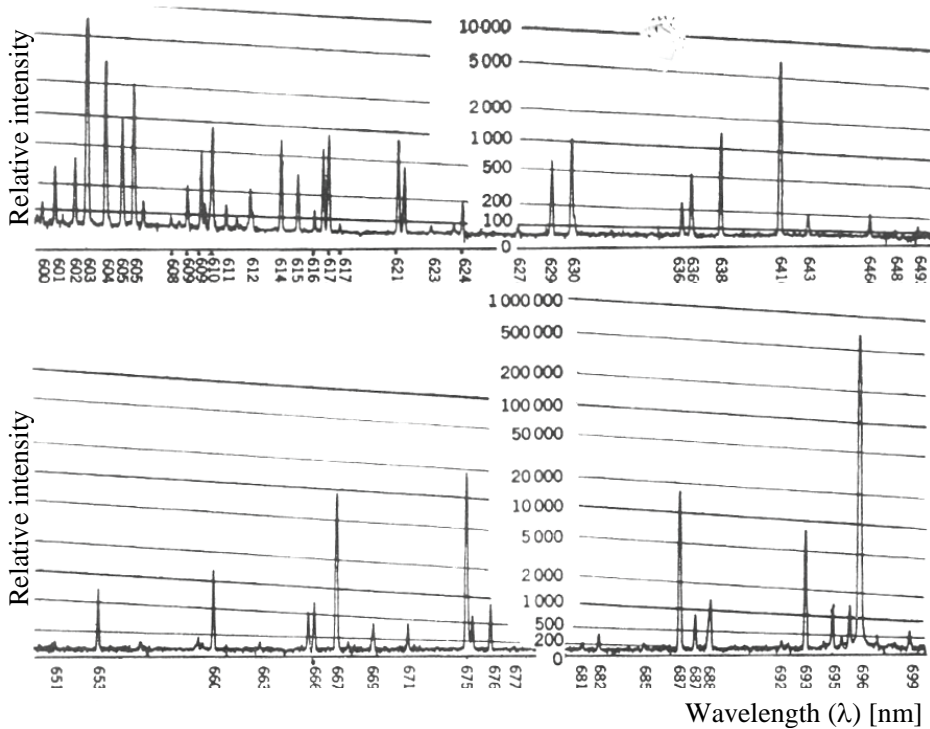


Figure F-7 The theoretic spectrum of pure Argon in the range from 600 nm to 700 nm [A. I. of P. H.]. The scale of the ordinate is relative intensity. This relative scale is comparable to the scale in Error! Reference source not found..

The above spectrum (Figure F-7) shows several small spectral line peaks in the wavelengths between 620 nm to 660 nm. Because the intensities of these spectral lines are low and the distribution of the lines is large this collection of wavelengths contain a range of wavelengths where a pure argon arc would have an only small influence on the temperature measurements. Figure F-2, Figure F-4, Figure F-5 and Figure F-6 also support this.

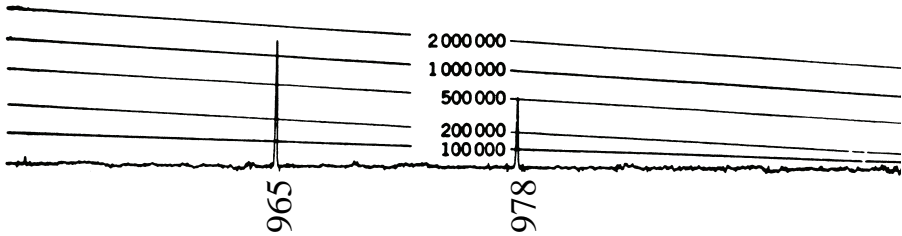


Figure F-8 The theoretic spectrum of pure Argon in the range from 950 nm to 1000 nm [3]. The scale of the ordinate is relative intensity.

In Figure F-8, roughly no radiation is seen above 978 nm. A table in the same reference does, however, show a spectral line at 1047 nm.

Both Figure F-7 and Figure F-8 depicts the spectral lines which in theory is radiated from pure argon. In the next section theoretical figures of the spectral radiance for argon in air surroundings is elaborated.

F.5. Theoretical Figures of the Spectral Radiance for Argon in Air Surroundings

A second reference shows the spectral lines for an argon arc in air surroundings. In Table F-1 the spectral lines for wavelengths between 617 nm to 667 nm is listed and in Table F-2 the spectral lines for wavelengths between 965 nm to 1047 nm is listed [CRC, 1979].

Relative intensity	Wavelength (λ) [nm]
150	617,2
10	617,3
10	621,2
5	621,5
25	624,3
7	629,6
15	630,7
7	636,9
20	638,4
70	641,6
25	648,3
15	653,8
15	660,4
25	663,8
20	663,9

50	664,3
5	666,0
5	666,4
25	666,6
100	667,7

Table F-1 Figures of the theoretic spectrum for Argon in air from [CRC, 1979].

Relative intensity	Wavelength (λ) [nm]
25000	965
4500	978
180	1005
30	1033
100	1047
1600	1047

Table F-2 Figures of the theoretic spectrum for Argon in air from [CRC, 1979].

The two references used above also state that pure iron and tungsten do not contribute with spectral lines above 950 nm.

According to the table above (Table F-2) a weak but undesired spectral line, however, occurs at 1005 nm.

Based on all the above figures one band-pass filter centred at 640 nm with a width of 40 nm (Figure F-9) and one band-pass filter centred at 1010 nm with a width of 40 nm (Figure F-10) was tested in the present welding system.

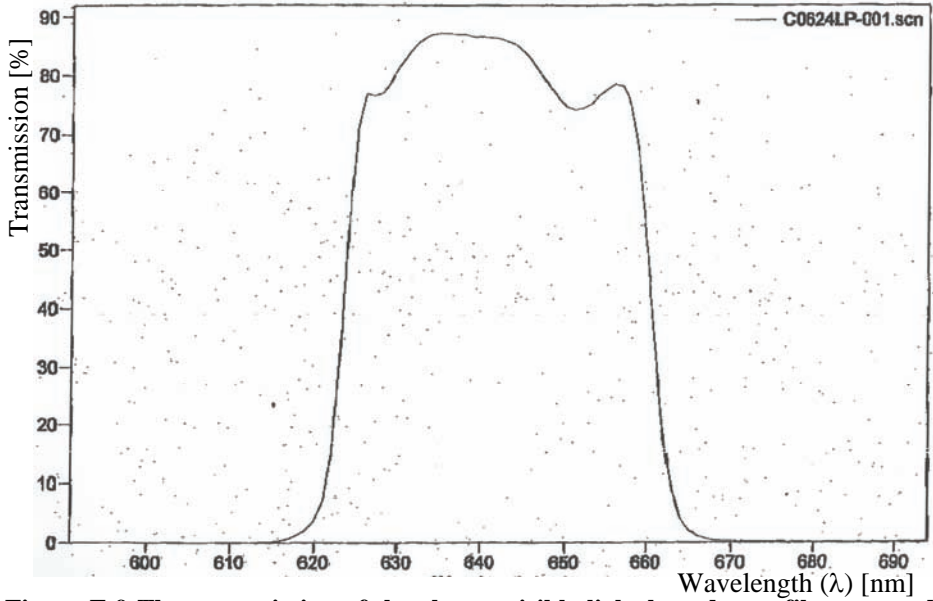


Figure F-9 The transmission of the chosen visible light band pass filter centred at 640 nm and width 40 nm.

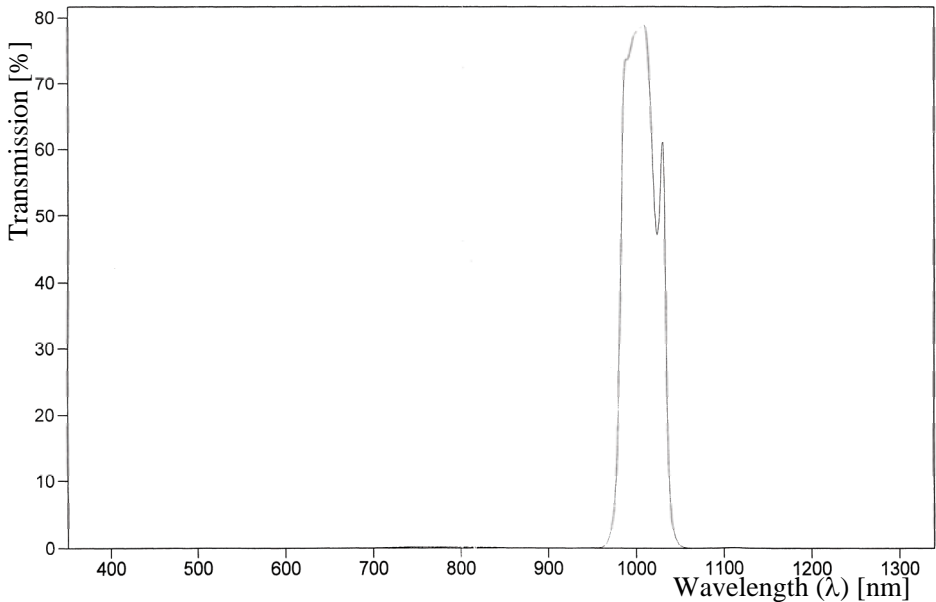


Figure F-10 The transmission of the chosen near infrared band pass filter centred at 1010 nm and width 40 nm.

The tests showed that the band-pass filter centred at 1010 nm gives the best signal to noise ratio. Therefore the filter centred at 1010 nm is used in the final WAMOS welding control experiments. The filter centred at 1010 nm is also used

in Appendix I where the emittance dependent temperature imaging system is calibrated. The emittance independent temperature imaging system is also tested in Appendix I. This test was however performed before the band-pass filters, discussed in this appendix (Figure F-9 and Figure F-10), were chosen. The test of the emittance independent temperature imaging system therefore is based on two former tested band-pass filters. The filter BG38 and filter RG9 (see Appendix I.1).

G. Optical Calculations

During the design of the optical system calculations were performed to ensure that all the elements involved in the system would work together as desired. These calculations were performed in the mathematical program MathCad. The calculations performed in MathCad are illustrated on the following pages.

MathCad is a program that enables the user to combine calculations and graphs with text. A short instructive text have therefore been added to every calculation.

Every calculation is based on following structure: “calculation_name := equation”.

Every result is based on following structure: “calculation_name = the_result”.

Beside the instructive text in the MathCad calculator, every page is introduced with a general description of the action on the actual page.

On the first page Planck's black body radiation equation and the required constants are defined. Two variables are defined: The wavelength λ , which is running from 0 to 2 μm with a step size of 0,001 μm and the temperature, T, which is running from 500°K to 2000°K. Based on the Planck's radiation law and the defined constants a graph that illustrates the energy radiated for different black body temperatures at different wavelengths is calculated.

CCD-Chip calculations.

Radiation energy from a black surface:

$C1 := 3.742 \cdot 10^8$ [$\mu\text{m}^4/\text{m}^2$] where λ is in μm [Mills, 1995, page 491]

$C2 := 1.4389 \cdot 10^4$ [$\mu\text{m} \cdot \text{K}$] where λ is in μm [Mills, 1995, page 491]

$\lambda := 0, 0.001.. 2$ [μm] Wavelength of the radiation

$T := 500.. 2000$ [K] Element temperature

$$E_{\text{picture}}(\lambda, T) := \frac{C1 \cdot \lambda^{-5}}{e^{\frac{C2}{\lambda \cdot T}} - 1}$$

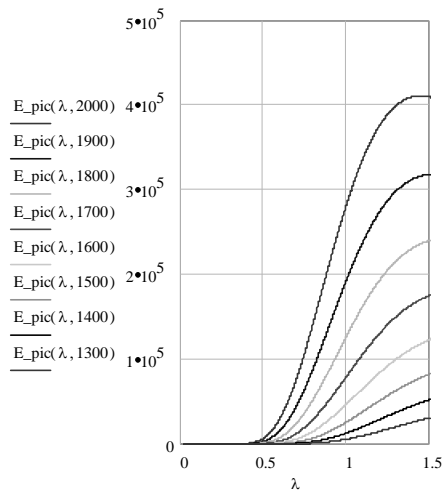
[$\text{W}/(\text{m}^2 \cdot \mu\text{m})$] Radiation from a black element
where λ is in μm [Mills, 1995, page 491]

$$E_{\text{pic}}(\lambda, T) := \begin{cases} E_{\text{picture}}(\lambda, T) \\ 0 \text{ if } E_{\text{picture}}(\lambda, T) < 0 \end{cases}$$

$$E_{\text{pic}}(0.65, 1500 + 273) = 1.219 \cdot 10^4$$

$\varepsilon := 0.7$ Emittance [Mills, 1995, page 15]

$$E_{\text{pic}}(1, 1500 + 273) = 1.119 \cdot 10^5$$



After Planck's law is defined the effect of a pinhole optic is estimated by calculating the proportion of energy, which passes through the pinhole compared to the energy radiated from an object (the workpiece). This in calculation is performed for two pinholes: "Propor_pinhole_filter640" and "Propor_pinhole_filter1010". In the emittance independent temperature imaging system both of the pinholes are used. In the final WAMOS experiments only the pinhole for high wavelengths is used.

The proportion of energy radiated from the object which pass through the pinhole:

$L_{ccd_V} := 4.77$	[mm] Vertical size of the CCD chip (True size= 6.33[mm])		
$L_{ccd_H} := \frac{6.37}{2}$	[mm] Half horizontal size of the CCD chip (True size=8.1[mm])		
$L := 400$	[mm] Distance from lense to object		
$l := 30$	[mm] Distance from lense to CCD-chip		
$L_{obj_V} := \frac{L}{1} \cdot L_{ccd_V}$	[mm] Vertical size of the object	$L_{obj_V} = 63.6$	Theoretical_res := $\frac{L_{obj_V}}{575}$
$L_{obj_H} := \frac{L_{ccd_H}}{L_{ccd_V}} \cdot L_{obj_V}$	[mm] Horizontal size of the object	$L_{obj_H} = 42.467$	Theoretical_res = 0.111
Pinhole_size_lowFilter := 1.5	[mm] Diameter of Pinhole number one (Low wavelengths)		
$v_1 := \frac{Pinhole_size_lowFilter}{L}$	[Degrees] The angle from a point on the object to the two sides of the pinhole opening.		
Propor_pinhole_lowFilter := $\frac{(Pinhole_size_lowFilter)^2}{8 \cdot L^2}$	The proportion of energy radiating from a point which is going through the pinhole. In the calculation it is assumed that the radiating point is right above the pinhole.		
		Propor_pinhole_lowFilter = $1.75 \cdot 10^{-6}$ $v_1 = 3.75 \cdot 10^{-3}$	
Pinhole_size_highFilter := 1.0	[mm] Diameter of Pinhole number two (High wavelengths)		
$v_2 := \frac{Pinhole_size_highFilter}{L}$	[Degrees] The angle from a point on the object to the two sides of the pinhole opening.		
Propor_pinhole_highFilter := $\frac{(Pinhole_size_highFilter)^2}{8 \cdot L^2}$	The proportion of energy radiating from a point which is going through the pinhole. In the calculation we assume that the radiating point is right above the pinhole.		
		Propor_pinhole_highFilter = $7.81 \cdot 10^{-7}$ $v_2 = 2.5 \cdot 10^{-3}$	

Appendix G. Optical Calculations

Here the five tested filters are defined by an approximated equation which approximates each of the filters. The equations are named: “Filter_BG38(λ), Filter_RG9(λ), Filter_RG850(λ), BandpassFilter_640 and BandpassFilter_1010”.

This is followed by a calculation of the proportion between the area of the object to be captured, compared to the area of the CCD-chip. The equation is named: “Propor_obj_to_CCD”.

Finally the shutter speed is defined to 120 of a second.

The equations which describes different filters:

Reflection := 0.92 Reflection coefficient of the filtre

BG38(λ) := Reflection · (68.05 λ^3 - 126.67 λ^2 + 73.28 λ - 12.536) Filter_BG38(λ) := $\begin{cases} \text{BG38}(\lambda) & \text{if } \text{BG38}(\lambda) < 0 \\ 0 & \text{if } \lambda > 0.8 \end{cases}$ Compound approximation of the BG38 filtre

Line1(λ) := Reflection · (22.2 λ - 15.5) Three approximated tendency lines for the RG9 filtre

Line2(λ) := Reflection · (-0.45 λ + 1.3)

Line3(λ) := Reflection · (-4.5 λ + 5.23)

Filter_RG9(λ) := $\begin{cases} 0 & \text{if } \text{Line1}(\lambda) > 0 \\ \text{Line1}(\lambda) & \text{if } \text{Line1}(\lambda) > \text{Line2}(\lambda) \\ \text{Line2}(\lambda) & \text{if } \text{Line2}(\lambda) > \text{Line3}(\lambda) \\ \text{Line3}(\lambda) & \text{if } \text{Line3}(\lambda) < 0 \end{cases}$ Compound approximation of the RG9 filtre

Line1(λ) := Reflection · (17.2 λ - 14.2) Two approximated tendency lines for the RG850 filtre

Line2(λ) := Reflection · (0.1 λ + 0.88)

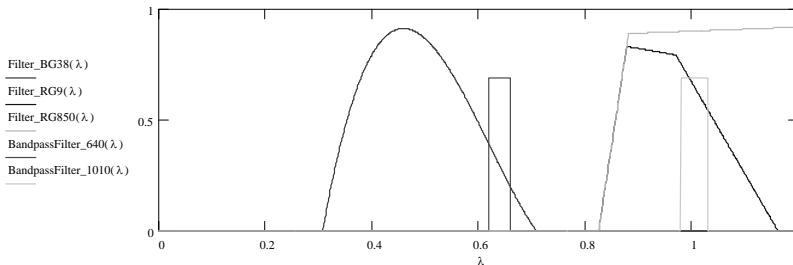
Filter_RG850(λ) := $\begin{cases} 0 & \text{if } \text{Line1}(\lambda) > 0 \\ \text{Line1}(\lambda) & \text{if } \text{Line1}(\lambda) > \text{Line2}(\lambda) \\ \text{Line2}(\lambda) & \text{if } \text{Line2}(\lambda) < 0 \end{cases}$ Compound approximation of the RG850 filtre

Line1 := Reflection · 0.7

BandpassFilter_640(λ) := $\begin{cases} 0 & \text{if } \lambda > 0 \\ 0 & \text{if } \lambda > 0.62 \\ \text{Line1} & \text{if } \lambda > 0.66 \end{cases}$

Line1 := Reflection · 0.75

BandpassFilter_1010(λ) := $\begin{cases} 0 & \text{if } \lambda > 0 \\ 0 & \text{if } \lambda > 0.98 \\ \text{Line1} & \text{if } \lambda > 1.03 \end{cases}$



The proportion between the area of the pictured object and the area of the CCD chip:

Propor_obj_to_CCD := $\frac{L_{\text{obj_V}} \cdot L_{\text{obj_H}}}{L_{\text{ccd_V}} \cdot L_{\text{ccd_H}}}$ [mm²] Area of picture
 [mm²] Area of CCD chip

Propor_obj_to_CCD = 177.778 The calculated proportion

Shutter speed:

Shutter_speed := $\frac{1}{120}$ [sec] Shutter speed [CV-M10 manual].

At this page the CCD-chip sensitivity is described by the equation “Sensitivity_CCD(λ)” and the sensitivity is illustrated by a graph.

The total amount of Joule measured at the CCD-chip at different temperatures is calculated for both the low band-pass filter ($E_{chip_filter640}(T)$) and a high band-pass filter ($E_{chip_filter1010}(T)$). Both of the equations are illustrated by a graph where the saturation level of the CCD-chip as well as the noise level of the CCD-chip is also added. In the emittance independent temperature imaging system (Appendix H) both of these two filters are used. In the final WAMOS experiments only the high-pass filter is used.

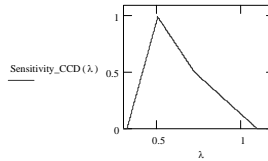
Equations which describes the CCD-chip sensitivity:

Line1(λ) := 5.45 λ - 1.75
 Line2(λ) := -2.25 λ + 2.13
 Line3(λ) := -1.35 λ + 1.48
 Sensitivity_CCD(λ) := 0

Three approximated tendency lines for the relative CCD-chip sensitivity

if Line1(λ) > 0
 | Line1(λ)
 | if Line1(λ) > Line2(λ)
 | | Line2(λ)
 | | if Line2(λ) < Line3(λ)
 | | | Line3(λ)
 | | | 0 if Line3(λ) < 0

Compound approximation of the relative CCD-chip sensitivity



Measured Joule on the CCD-chip:

When using BandpassFilter 640:

λ_{1_high} := 0.67 [μ m]
 λ_{1_low} := 0.6 [μ m]

$$E_{chip_filter640}(T) := \int_{\lambda_{1_low}}^{\lambda_{1_high}} (E_{pic}(\lambda, T) \cdot \epsilon \cdot \text{Shutter_speed} \cdot \text{Propor_pinhole_lowFilter} \cdot \text{BandpassFilter_640}(\lambda) \cdot \text{Propor_obj_to_CCD} \cdot \text{Sensitivity_CCD}(\lambda)) d\lambda$$

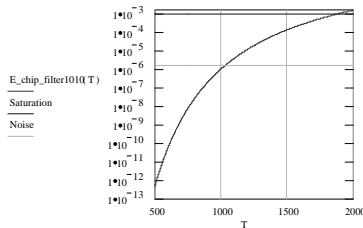
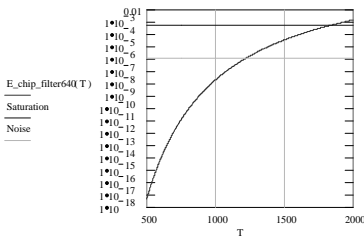
When using BandpassFilter 1010:

λ_{2_high} := 1.05 [μ m]
 λ_{2_low} := 0.95 [μ m]

$$E_{chip_filter1010}(T) := \int_{\lambda_{2_low}}^{\lambda_{2_high}} (E_{pic}(\lambda, T) \cdot \epsilon \cdot \text{Shutter_speed} \cdot \text{Propor_pinhole_highFilter} \cdot \text{BandpassFilter_1010}(\lambda) \cdot \text{Propor_obj_to_CCD} \cdot \text{Sensitivity_CCD}(\lambda)) d\lambda$$

Saturation := $60 \cdot 10^{-9} \cdot 10^4$ [J/m²] Saturation level

Noise := $121 \cdot 10^{-12} \cdot 10^4$ [J/m²] Noise level

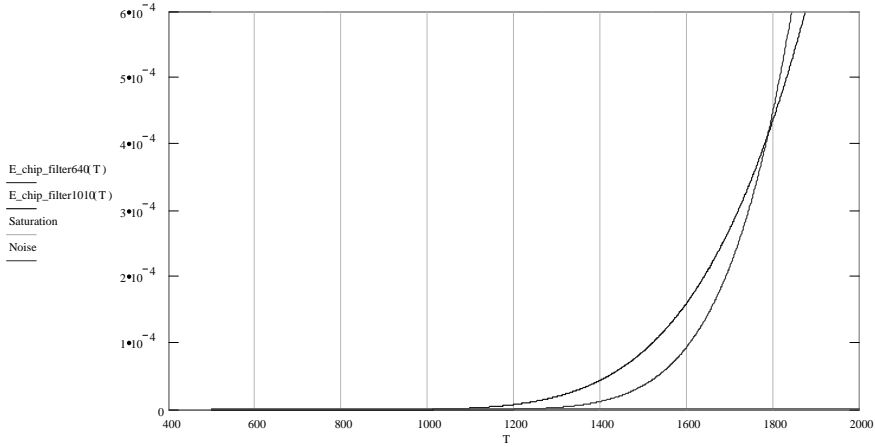


Shutter_speed = 8.33*10 Pinhole_size_lowFilter = 1.5 Pinhole_size_highFilter = 1 L = 400 l = 30 ϵ = 0.7

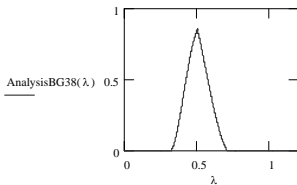
Appendix G. Optical Calculations

Here the energy measured by the CCD-chip behind the band-pass filter centred at 640 as well as behind the band-pass filter centred at 1010 nm are illustrated together in one graph for temperatures from 500 °K to 2000 °K. The noise level is the bottom line and the saturation level of the chip is the top line.

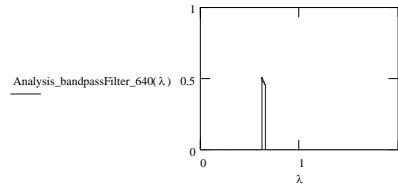
Below this graph five graphs are calculated which each shows the CCD-chip characteristic combined with the filter characteristic for each of the five filters that have been tested during the WAMOS project.



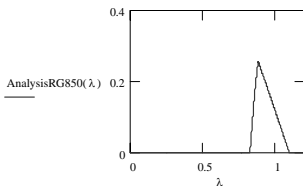
AnalysisBG38(λ) := Filter_BG38(λ) · Sensitivity_CCD(λ)



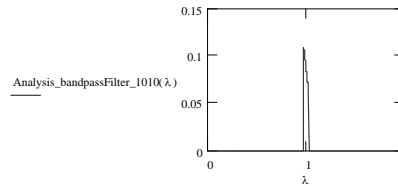
Analysis_bandpassFilter_640 (λ) := BandpassFilter_640(λ) · Sensitivity_CCD(λ)



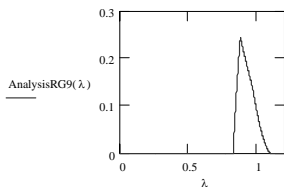
AnalysisRG850(λ) := Filter_RG850(λ) · Sensitivity_CCD(λ)



Analysis_bandpassFilter_1010 (λ) := BandpassFilter_1010(λ) · Sensitivity_CCD(λ)



AnalysisRG9(λ) := Filter_RG9(λ) · Sensitivity_CCD(λ)



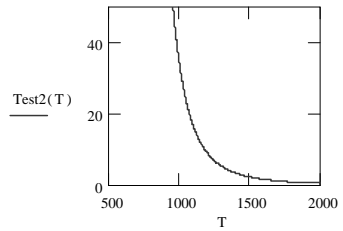
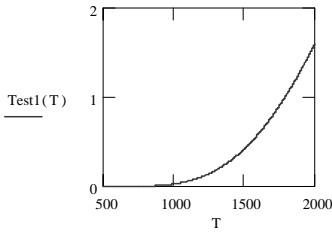
On this page a suggestion to how to perform emittance independent measurements is tested. The suggestion is to divide the two measured pixel energy levels and use this result as an estimator for the absolute temperature of the object which is measured. The two pixel levels are both measurements of the emitted radiation from the same object just measured in two different wavelengths.

Emittance independent measurements

The effect of dividing the two measured energy levels (E_chip_filter640(T) / E_chip_filter1010(T)):

$$\text{Test1}(T) := \frac{E_{\text{chip_filter640}}(T)}{E_{\text{chip_filter1010}}(T)}$$

$$\text{Test2}(T) := \frac{E_{\text{chip_filter1010}}(T)}{E_{\text{chip_filter640}}(T)}$$



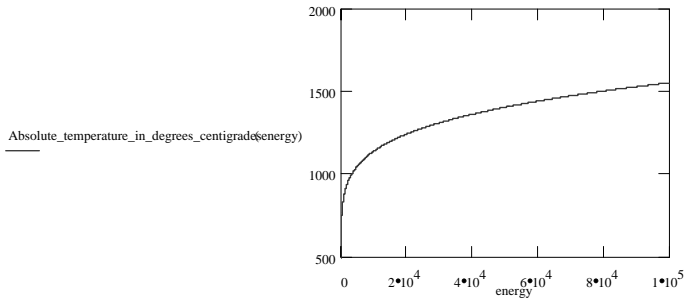
Appendix G. Optical Calculations

Finally, to get a sense of how the CCD-chip energy is converted to a temperature, an estimation of the how the pixel energy level is transferred to the energy, E , is made. This estimation is based on Planks black body radiation equation.

An estimation of the how the pixel energy level is transferred to the energy E in Planks black body radiation equation.

energy := 1.. 1·10⁵

$$\text{Absolute_temperature_in_degrees_centigrades}(\text{energy}) := \frac{C2}{\ln\left(\frac{\varepsilon \cdot C1}{\text{energy}} + 1\right)} - 273$$



H. Emittance Independent Temperature Imaging System

Due to Planck's law it is possible to determine the temperature of an object by means of the radiation emitted from the object. Planck's law is defined as [Mills, 1995, page 491]:

$$E = \varepsilon \cdot \frac{C_1}{\lambda^5} \cdot \frac{1}{e^{\frac{C_2}{\lambda T}} - 1} \quad \text{H.1}$$

where,

E = the energy emitted from an object due to the following parameters.

ε = the emittance (between 0 and 1).

$C_1 = 3.742E8 \mu\text{m}^4/\text{m}^2$ when λ is in μm [Mills, 1995, page 491].

$C_2 = 1.4389E4 \mu\text{m} \cdot \text{K}$ when λ is in μm [Mills, 1995, page 491].

λ = the wavelength of the radiation. Due to the camera this factor is between 0.4 and 1.1 [μm].

T = the temperature to be measured [$^\circ\text{K}$]. In this application it is between 1623 $^\circ\text{K}$ and 1805 $^\circ\text{K}$ (1350 $^\circ\text{C}$ to 1530 $^\circ\text{C}$).

To calculate the absolute temperature based on Planck's law; the energy emitted from the object, E , must be measured, the wavelength, λ , of the measured energy must be known, and the factor of emittance, ε , must be known.

The factor of emittance, ε , is a number between 0 and 1, where 1 is defined as a black body. A piece of metal, which is painted black, is well at absorbing radiation. Just as good as it is at absorbing light it is good at emitting light. Whereas a white painted piece of metal is poor at absorbing light and poor at emitting light. A black piece of metal that is 1000 $^\circ\text{C}$ will emit three times as much radiation as a white piece of metal. This is due to the factor of emittance, ε , which for a black surface is approximately 0,9 whereas it is 0,3 for a white surface.

Today it is possible to buy much commercial equipment, which can measure the temperature of a surface by means of the radiation, emitted from a surface. Based on the writer's knowledge all these different commercial equipments are however dependent on the user setting the factor of emittance. None known equipment is independent of the factor of the emittance, ε .

This WAMOS-system is meant for use in the heavy metal industry such as ship-yards. This results in some special demands to the temperature imaging system. In the heavy metal industry the nature of the workpiece surface to be welded are changing substantially do to rust, dust, oil etc. Such changes in the surface characteristic also change the coefficient of emittance, ε . To measure correct temperatures based on conventional vision systems therefore becomes difficult and will require some restrictions to the nature of the surfaces on which the weld is performed.

Because of the changing character of the metal surfaces in the heavy metal industry a temperature imaging system that is independent of the nature of the surface would be desirable. It has therefore been a goal to develop a temperature imaging system that is independent of the factor of emittance, ε .

In the effort to find a way to measure the temperature from emitted radiation independently of the factor of emittance, it was natural to look at Planck's law of radiation (Eq. H.1). During this process it was discovered that it theoretically is possible to measure the temperature independent of the factor of emittance. This is if the temperature that is to be measured is not too high (e.g. below 3000°C). Both, how this is possible and the mathematical proof for this is demonstrated in the following sections.

H.1. Proof of How to Perform Temperature Measurements Independent of the Factor of Emittance

It is discovered that it should be possible to measure the absolute temperature of an object independently of the factor of emittance. This is if the radiation emitted from an object is measured in two different wavelengths (λ_1 and λ_2). If the radiation emitted from a specific point is captured e.g. by two vision systems that measures the radiation of the same point but in two different wavelengths, then Planck's law opens the possibility to measure the temperature independently of the factor of emittance, ε . The proof for this is shown below:

When a hot object is measured in the wavelength λ_1 Planck's law gives [Mills, 1995, pages 491]:

$$E_1 = \varepsilon \cdot \frac{C_1}{\lambda_1^5} \cdot \frac{1}{e^{\frac{C_2}{\lambda_1 T}} - 1} \quad \text{H.2}$$

where,

E_1 = the energy emitted from a given area due to the following parameters.

ε = the emittance (between 0 and 1) To be neglected in this proof.

$C_1=3.742E8 \mu\text{m}^4/\text{m}^2$ when λ is in μm [Mills, 1995, page 491].

$C_2=1.4389E4 \mu\text{m}\cdot\text{K}$ when λ is in μm [Mills, 1995, page 491].

λ_l = one of the two wavelengths in which the radiation is measured. Because of the present camera this factor is between 0.4 and 1.1 μm .

T = the temperature to be measured [$^{\circ}\text{K}$].

When the same measurement is performed on the same object but in a different wavelength, λ_2 , the equation is:

$$E_2 = \varepsilon \cdot \frac{C_1}{\lambda_2^5} \cdot \frac{1}{e^{\frac{C_2}{\lambda_2 \cdot T}} - 1} \quad \text{H.3}$$

Isolating C_1 in Eq. H.3 gives:

$$C_1 = \frac{E_2 \cdot \lambda_2^5}{\varepsilon} \cdot \left(e^{\frac{C_2}{\lambda_2 \cdot T}} - 1 \right) \quad \text{H.4}$$

Now inserting Eq. H.4 in Eq. H.2:

$$E_1 = \varepsilon \cdot \frac{E_2 \cdot \lambda_2^5}{\varepsilon \cdot \lambda_1^5} \cdot \frac{e^{\frac{C_2}{\lambda_2 \cdot T}} - 1}{e^{\frac{C_2}{\lambda_1 \cdot T}} - 1} \quad \text{H.5}$$

which gives:

$$\frac{E_1 \cdot \lambda_1^5}{E_2 \cdot \lambda_2^5} = \frac{e^{\frac{C_2}{\lambda_2 \cdot T}} - 1}{e^{\frac{C_2}{\lambda_1 \cdot T}} - 1} \quad \text{H.6}$$

If the maximum wavelength of the camera, which is 1.1 μm , was used and if the maximum temperature to be measured is 1800 $^{\circ}\text{K}$ then the exponential parts of Eq. H.6 would be no less than:

$$e^{\frac{C_2}{\lambda_2 \cdot T}} = e^{\frac{1.4389 \cdot 10^4}{1.1 \cdot 1800}} = 1432 \quad \text{H.7}$$

Where,

$C_2=1.4389\text{E}04$ [Mills, 1995, p.491]

$\lambda=1.1$ (μm) The maximum measurable wavelength of the camera.

$T=1800$ $^{\circ}\text{K}$ The maximum temperature to be measured by the camera.

Because -1 is small compared to 1432, -1 of Eq. H.6 is neglected:

$$\frac{E_1 \cdot \lambda_1^5}{E_2 \cdot \lambda_2^5} = \frac{e^{\frac{C_2}{\lambda_2 \cdot T}}}{e^{\frac{C_2}{\lambda_1 \cdot T}}} \quad \text{H.8}$$

Taking ln to this expression (Eq. H.8) gives:

$$\ln\left(\frac{E_1 \cdot \lambda_1^5}{E_2 \cdot \lambda_2^5}\right) = \frac{C_2}{\lambda_2 T} - \frac{C_2}{\lambda_1 T} \quad \text{H.9}$$

$$\Downarrow$$

$$\ln\left(\frac{E_1 \cdot \lambda_1^5}{E_2 \cdot \lambda_2^5}\right) = \frac{C_2}{T} \cdot \left(\frac{1}{\lambda_2} - \frac{1}{\lambda_1}\right) \quad \text{H.10}$$

$$\Downarrow$$

$$T = \frac{C_2 \cdot \left(\frac{1}{\lambda_2} - \frac{1}{\lambda_1}\right)}{\ln\left(\frac{E_1 \cdot \lambda_1^5}{E_2 \cdot \lambda_2^5}\right)} \quad \text{H.11}$$

Based on Eq. H.11 it is possible to calculate the absolute temperature by means of two measurements of the energy emitted from an object. Because the energy is measured in two different wavelengths (λ_1 and λ_2), this measurement is independent of the factor of emittance, ε .

When performing the temperature measurements C_2 , λ_1 and λ_2 are known constants. Eq. H.11 is therefore simplified to the function T , which is a simple function of E_1 and E_2 :

$$T\left\{\begin{matrix} E_1 \\ E_2 \end{matrix}\right\} = \frac{C_a}{\ln\left(\frac{E_1}{E_2} \cdot C_b\right)} \quad \text{H.12}$$

Where $C_a = C_2 \cdot \left(\frac{1}{\lambda_2} - \frac{1}{\lambda_1}\right)$ and $C_b = \frac{\lambda_1^5}{\lambda_2^5}$.

Based on the above equation (Eq. H.12) it is clear that the temperature, T , is based on the proportion of the measured energy E_1 and E_2 . Therefore the camera system is supposed to measure the emitted energy of one point in two different wavelengths.

Because the temperature estimation theoretically is based on a proportion, a table containing different proportions and their matching temperature could give us the absolute temperature. Using a table, that contains proportions and their respective absolute temperatures, would give a simple and applicable system where the camera system measures the two energy levels. These energy levels are to be divided and based on this proportion the absolute temperature is achieved from the table. The table could be generated based on physical or theoretical calibration.

In the following sections the optical design of the camera, which enables temperature measurements independent of the factor of emittance, is given. In the next appendix (Appendix I) the calibration process of the emittance independent temperature imaging system as well as for the emittance dependent temperature imaging system is described. The emittance dependent temperature imaging system measures the temperature based on one wavelength only.

H.2. Optical Design of the Emittance Independent Camera

In the section above it was verified that it theoretically is possible to measure the absolute temperature independent of the factor of emittance. In this section the actual optical design of the emittance independent temperature imaging system is described.

To measure the temperature independent of the factor of emittance, every point on the object on which the temperature is desired, must be measured in two different wavelengths. E.g. if two different cameras measures the radiation from the same object but in different wavelengths, then every pixel value of camera one must be compared to its corresponding pixel of camera two. This demands that the pixel value of one given pixel of camera one, must be compared with the value of the corresponding pixel of camera two, where both of the pixels measures the radiation from the exact same point.

To measure the radiation of an object in two different wavelengths can be done by means of two separate cameras or by means of one camera. The use of two cameras would cause that the two images of the same object are captured from different positions. This results in difficulties in comparing the measurements performed by each of the two cameras (Figure H-1).

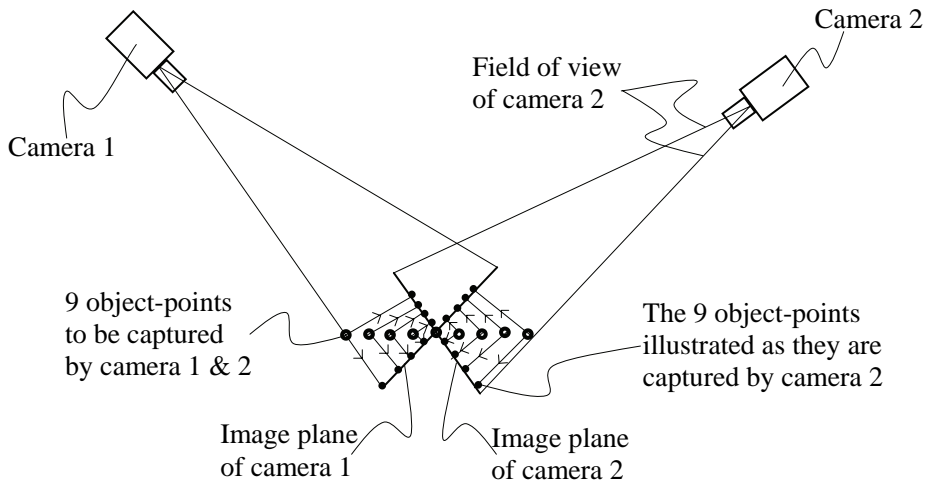


Figure H-1 Illustration of the difficulty in comparing measurements performed by one camera with the corresponding measurements performed by the other camera when the measurements are not performed from the same position.

The contrary, to measure the emitted radiation of an area by two different cameras, is if the emitted radiation is measured in two different wavelengths by the one and same CCD-chip. If the radiation from an area is measured in two different wavelengths by the same chip then no or only minimal geometrical manipulation of the captured images is needed, in order to compare the different pixel values of the two wavelengths. To measure the two different filtered images at one chip also has the advantage that this arrangement is more stable than two individually placed cameras are.

In the process of choosing between an emittance independent temperature imaging system, that is based on one or two cameras, a list of advantages and disadvantages is made (Table H-1).

	One camera	Two cameras
Advantages	<ul style="list-style-type: none"> + Only one camera and one frame grabber is needed. + Very stable optical set-up. + Minimal geometrical manipulation of the images. + No need to time synchronise the two cameras. + Handy on a robot. 	<ul style="list-style-type: none"> + Standard optics might be used.
Disadvantages	<ul style="list-style-type: none"> ÷ A special dual optic has to be designed. 	<ul style="list-style-type: none"> ÷ Requires two camera and two frame grabbers. ÷ The relative position of the

		<p>two cameras must be VERY stable.</p> <p>÷ Unless the two cameras are placed close together, it will require heavy geometrical manipulation of the two grabbed images to calculate the absolute temperature values.</p> <p>÷ Requires that the cameras are time synchronised.</p> <p>÷ Less handy than one camera</p>
--	--	---

Table H-1 A list of advantages and disadvantages in relation to the choice to perform emittance independent temperature measurements by means of one or two cameras.

To use one camera requires a non-standard and quite advanced optical set-up with more lenses and filters in one and same optic. Beside the non-standard optical set-up, the system based on one camera, is more simple, handy and robust than a system based on two cameras. It is therefore chosen to base the emittance independent temperature imaging system on the one-camera set-up.

The chosen and tested design of the emittance independent temperature imaging system is illustrated below (Figure H-2).

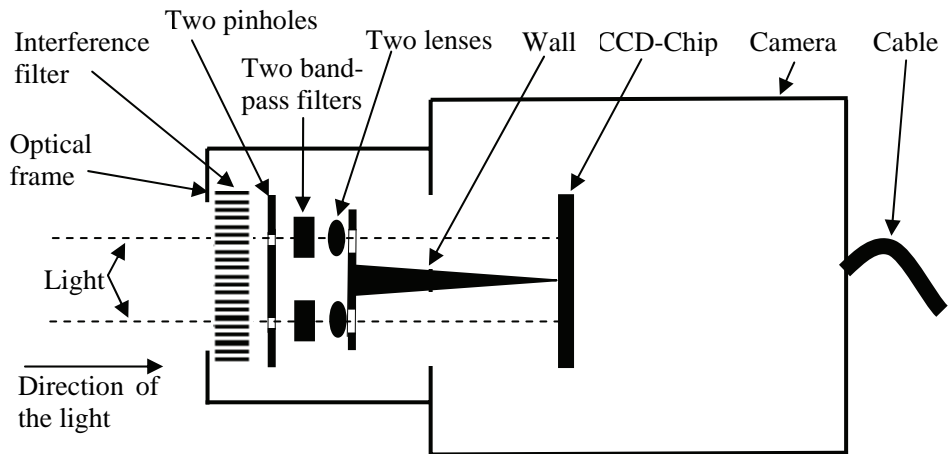


Figure H-2 The optical set-up of the emittance independent camera. The interference filter was in the actual experiments, though, placed in front of the optical frame.

The emittance independent one-camera set-up has the same basic structure as the emittance dependent camera system (Chapter 7). The optical set-up is based on an interference filter, a pinhole, a band-pass filter and a lens. The emittance

independent system does however contain two of each of these optical elements. This is though with the exception of the interference filter that covers both of the light sources at once.

The light emitted from an object passes among others through the interference filter and through each of the two pinholes. After the emitted light has passed the pinholes the light is limited to two small areas of light that passes through each of their band-pass filter and lens. The lenses are placed in a lens holder on which a wall is attached. The purpose of the wall is to ensure that the light focused by one of the lenses only radiates on its half-side of the CCD-Chip. All the optical parts are attached in the optical frame and the frame is mounted on the camera.

The camera used for this emittance independent system is the same as used in the emittance dependent system (Chapter 7). The camera is a CV-M10 RS Progressive Scan Monochrome camera. The datasheets of the chosen camera can be viewed in Enclosure B.

The camera with the optical frame mounted is illustrated in Figure H-3.



Figure H-3 The CV-M10 RS Progressive Scan Monochrome camera with the optical frame mounted.

The total weight of the camera inclusive the designed optic is 0.5 kg. The optical frame is mounted on the camera by a standard C-mount thread. To ensure that the optical frame is fixed on the exact same position, in relation to the CCD-chip of the camera, an optical frame holder was constructed to avoid any rotation of the optical set-up.

Below an image of the camera and all the optical elements are shown (Figure H-4). In the following, the optical elements are described one by one in the order as shown in Figure H-4.

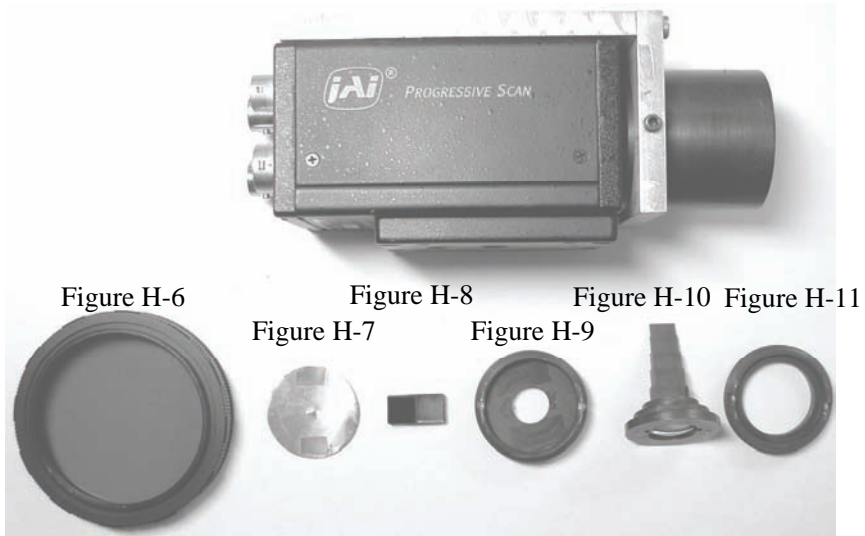


Figure H-4 The camera and all the elements of the emittance independent optical design.

The optical element on the left side below in the image (“Figure H-6”) of image Figure H-4 is the outermost part of the optical design and the following elements on the right (“Figure H-7 → Figure H-11”) are respectively placed deeper and deeper into the optical frame. All the optical elements except the pinhole optic are black coated. This is to minimise reflection of diffuse light.

The most outer part of the optical design is the interference filter. The purpose of the interference filter is to eliminate some of the reflected radiation of the Wolfram tungsten electrode. By Brewster’s law [Pedrotti, 1995] it is possible to calculate an angle θ where the reflected radiation is fully polarized and therefore theoretically may be fully blocked by an interference filter (Figure H-5). This angle θ is approximately 56 degrees when the atmosphere is Argon and the reflection plate is Iron.

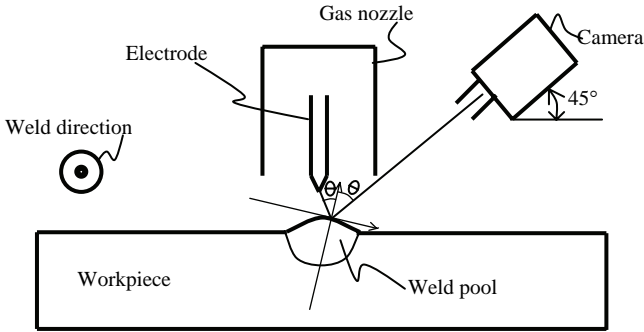


Figure H-5 When the angle θ is 56 degrees the reflection is in theory completely off-filtrated by use of an interference filter.

In the emittance independent optical set-up the interference filter is positioned in front of the optical set-up (Figure H-6).



Figure H-6 The interference filter is placed in front of the optical set-up.

After the interference filter the emitted light has to pass through two pinholes. The purpose of the pinholes is twofold:

1. To ensure that the light which passes through the band-pass filter and the lens is passing through the centre of the filter and the centre of lens only. This is to avoid diffuse light on the CCD-chip.
2. To level the amount of light on each half sides of the chip. The camera cannot differentiate the exposure from the one half of the chip to the other. Changing the size of the two pinholes individually does the differentiation in exposure.

In Appendix G the diameter of both the pinholes is calculated. The diameter of the pinhole in the side where the band-pass filter is penetrable for wavelengths around 640 nm is 1.5 mm (the right hole in Figure H-7). The diameter of pinhole in the side where the band-pass filter is penetrable for wavelengths around 1010 nm is 1.0 mm (the left hole in Figure H-7).



Figure H-7 Left, the pinhole optic. Right, the pinhole optic placed in the optical frame. The diameter of the left hole is 1 mm where the diameter of the right hole is 1,5 mm.

After the pinhole optic the two small light spots now passes through their respective filters (Figure H-8).

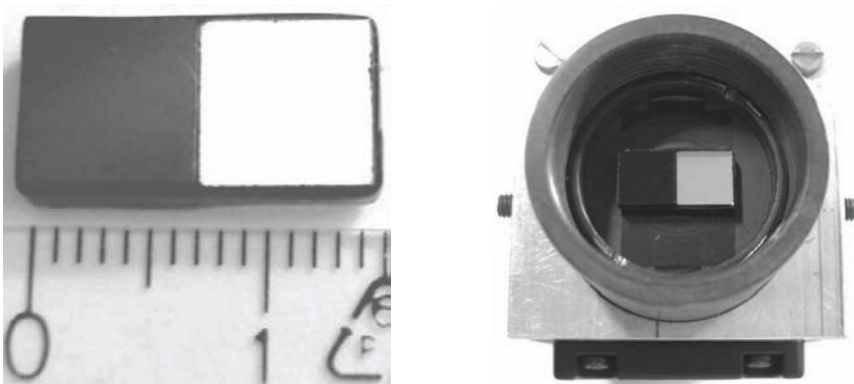


Figure H-8 Left, the band-pass filter for low and high wavelengths. Right, the band-pass filters placed in the optical frame.

The black band-pass filter is penetrable at 1010 nm and the bright band-pass filter is penetrable at 640 nm. The choice of band-pass filters is described in Appendix F.

After the light is filtrated in their respective wavelengths the light passes through the lenses. The lenses are placed in a lens holder, which is fixated between two lock nuts. The upper lock nut is illustrated in Figure H-9.

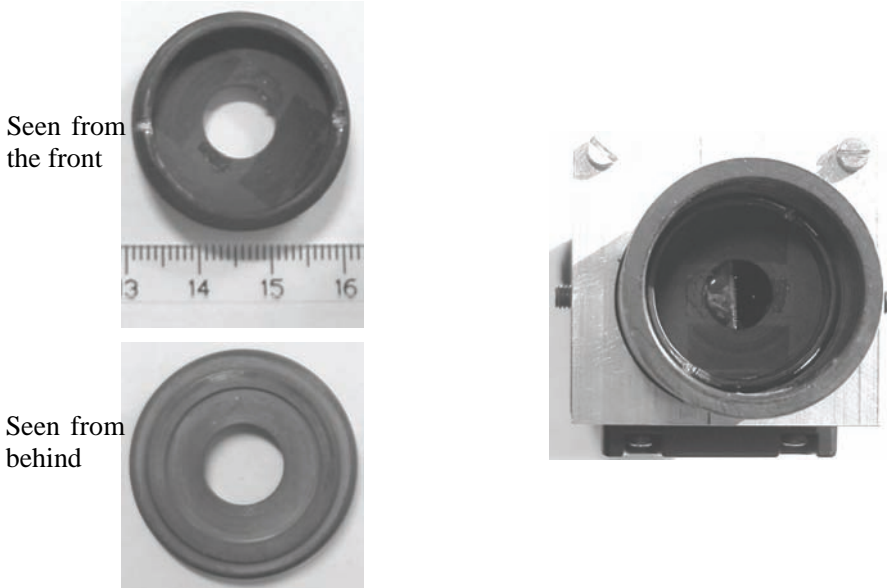


Figure H-9 Left, the upper lock nut. Right, the lock nut placed in the optical frame.

The two lenses are plane convex lenses with a diameter of 12.5 mm. The lens used for light around 640 nm is coated for the visual range whereas the lens used for light around 1010 nm is coated for the near-infrared range.

The CCD-chip has a width of 6.37 mm. One half of this width is used to capture the light from one of the lenses and the other half of the CCD-chip captures the light of the other lens. Because the diameter of each lens is 12.5 mm the lenses are too wide to be placed beside each other. To ensure that both of the lenses are able to focus the light on each of their half part of the CCD-chip, a portion of the lenses is cut off.

The lenses are respectively focusing light in the 640 nm range and light in the 1010 nm range. Because of the different wavelengths the focal length of the lenses changes. The difference in focal length from a wavelength of 640 nm to wavelength of 1010 nm is 0.5 mm. The lens, which focuses the light in the 640 nm range, is therefore positioned 0.5 mm closer to the lens than the lens meant for the 1010 nm light.

The lens holder not only holds the two lenses in their respective positions it also works as a wall. The wall is meant to avoid that light from each of the lenses does not fall on the wrong side of the CCD-chip (Figure H-10).

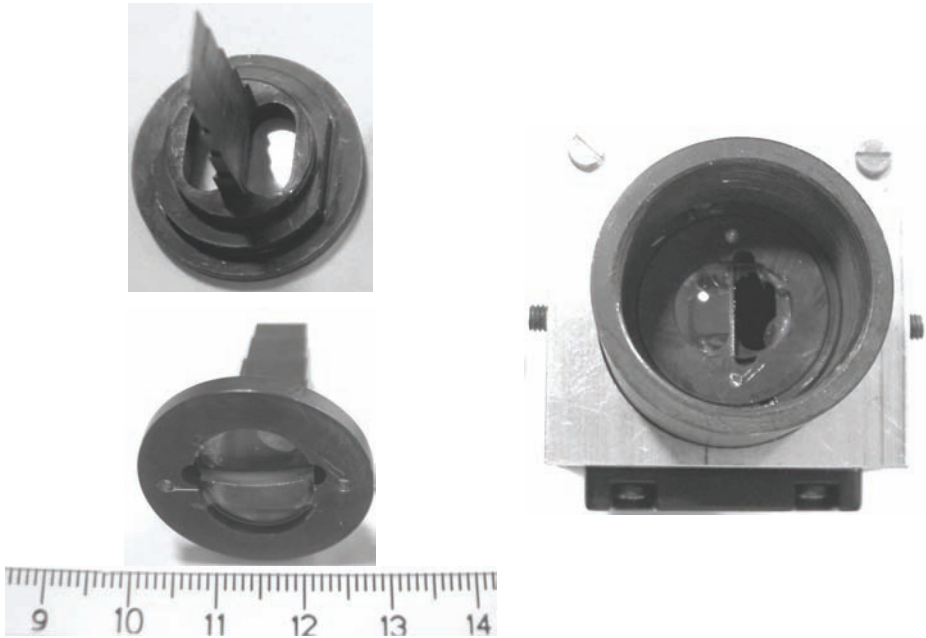


Figure H-10 Left, a coated lens holder with the two lenses. Right, the lens holder with the lenses is placed in the optical frame.

The lower lock nut that together with the upper lock nut fixates the lens holder is illustrated in Figure H-11.



Figure H-11 Left, the lower lock nut. Right, the lower lock nut placed in the optical frame.

After the light has passed the lenses, the light has direct access to the CCD-chip. Figure H-12 shows the CCD-chip in the bottom of the optical frame.

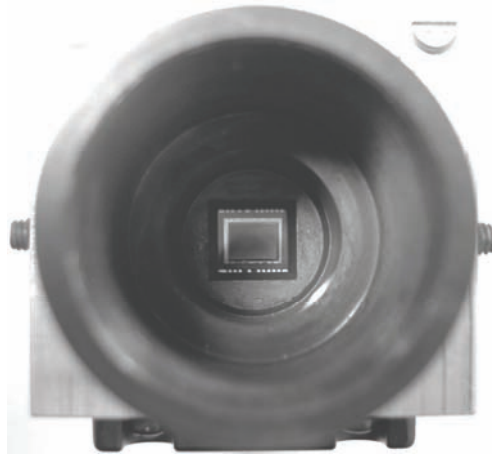


Figure H-12 The CCD-chip.

The CCD-chip captures the image every time the camera is triggered. The image is then by software (Chapter 7.5) divided into two images. One image that depicts the temperature measured in wavelengths around 640 nm and one image that depicts the temperature measured in wavelengths around 1010 nm. During tests of the camera it though turned out that the band-pass filter penetrable around 640 nm does not off-filtrate the undesired radiation of the argon arc satisfactorily. The temperature measurements carried through during the test of the WAMOS-system are therefore not based on the emittance independent measurements. The more simple emittance dependent temperature imaging system that measures the emitted radiation within wavelengths around 1010 nm only, have instead been used. To minimise the variation in the factor of emittance of the workpieces all the workpieces used in the experiments are brushed with a metal brush.

In this appendix the possibility to measure the temperature by means of a temperature imaging system that is independent of the factor of emittance was verified theoretically and the optical design of the temperature imaging system was demonstrated.

In the next appendix (Appendix I) both the emittance independent and emittance dependent temperature imaging system are calibrated and the possibility to measure the temperature independently of the factor of emittance is verified experimentally. In Section 7.5 the software that controls the camera and processes the images is introduced and briefly described. In Appendix J physical measurements generated by the emittance dependent temperature imaging system, that is in calibrated in Appendix I, is compared to the corresponding off-line simulations.

I. Calibration of the Temperature Imaging System

In this appendix the emittance dependent and independent temperature imaging system is calibrated to measure absolute temperatures. The calibration was performed by means of three different methods:

1. **Calibration in a furnace** and by means of thermocouples.
2. **Calibration on a non-moving weld** and by means of thermocouples.
3. Combined theoretical and physical **calibration on a moving weld**.

The first two methods turned out to be inadequate for calibration of the temperature imaging systems, whereas the third method performs satisfactorily. The emittance dependent temperature imaging system is therefore calibrated by means of the third method.

Because one of the two filters of the emittance independent temperature imaging system does not off-filtrate the argon arc adequately the emittance independent system is calibrated by means of the first method only. In the first method no argon arc is present.

Neither the emittance dependent or the emittance independent imaging system is used in calibrated form when the *WAMOS-method* and WAMOS-system is tested:

- The calibration of the emittance independent temperature imaging system is only used to test the possibility to perform surface measurements independently of the factor of emittance.
- The calibrated emittance dependent system is only used in Appendix J where the absolute temperature measurements of the temperature imaging system is compared to corresponding off-line simulations. To compare physical temperature measurements of the temperature imaging system to corresponding off-line simulations, it is advantageous that the temperature imaging system measures in absolute temperatures. The emittance dependent temperature imaging system therefore is calibrated to measure absolute temperatures.

All the experiments performed to test the WAMOS-system use a non-calibrated emittance dependent surface temperature-measuring imaging system. When testing the WAMOS-system and *WAMOS-method* off-line simulations of the *off-line preparation system* are not used. The *off-line preparation system* is not used

because experiments (See Appendix J, Appendix L or [Kjeldsen, 2002]) showed deviations between the surface temperatures profiles, which were calculated by the finite-element model and the surface temperature profiles measured by the developed imaging system.

As replacement for the *reference-generating simulation*, actual welding experiments are performed to generate the data needed of the *off-line preparation system*. In these actual welding experiments, the temperature imaging system measures the surface temperatures on which the on-line model is to be built as well as the *reference* needed for the on-line system. The actual weld experiments (*reference-generating experiments*) used as substitute for the *off-line preparation system* is presented in Chapter 3.3.

Because the temperature imaging system is used as a substitute for the *off-line preparation system* it is not necessary to calibrate the emittance dependent temperature imaging system to absolute temperatures. To use absolute temperatures, when the on-line control-system compares the actual archived surface temperature profiles to the temperature profiles of the *reference-generating experiment*, would not be of any use only serve as an extra complexity. Non-calibrated measurements of the temperature imaging system are therefore used when the WAMOS-system is tested.

In the following three sections the three used calibration methods are presented and applied on the respective two temperature imaging systems.

I.1. Calibration In a Furnace

The intention with a calibration by means of a furnace was to heat up a small plate of metal to different temperatures while the emitted radiation of the metal plate is measured by the temperature imaging system and compared to thermocouple measurements (Figure I-1).

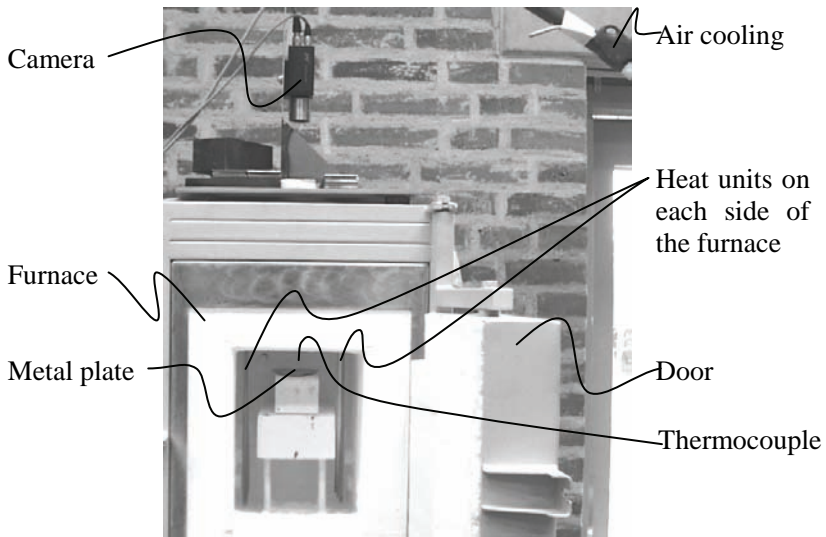


Figure I-1 The furnace calibration set-up at Aalborg University, Fibigerstraedet 14.

The camera is placed on top of the furnace where it through a long small hole in the top of the furnace can measure the emitted radiation of the metal plate within the furnace.

The calibration of the emittance independent temperature imaging system was not performed with the band-pass filters chosen in Appendix F but with two earlier tested band-pass filters. The two filters used, during the test of the emittance independent temperature imaging system, are the band-pass filter BG38 and the high-pass filter RG9. The characteristics of the band-pass filters are depict below (Figure I-2). The characteristics depict takes account for both the characteristic of the respective band-pass filter and the characteristic of the CCD-chip.

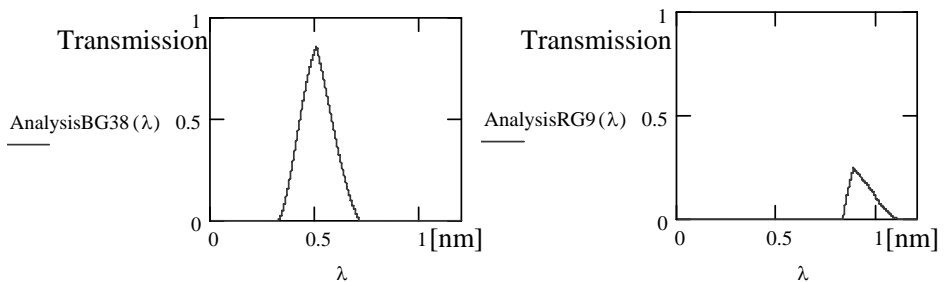


Figure I-2 The characteristic of the BG38 and the RG9 filter. For both graphs the sensitivity of the CCD-chip has been taken into account. A transmission of 1 is the same as 100% transmission.

It is visible that the RG9 filter off-filtrate more light than the BG38 filter. This is mainly due to the low sensitivity of the CCD-chip at long wavelengths, which in this graph is taken into account.

The calibration in the furnace based on the two above filters was performed in two attempts. In the first attempt an iron plate similar to the workpiece, on which the WAMOS welding experiments are performed, was heated up. In the second attempt a platinum plate was heated up.

I.1.1. Calibration By Means of an Iron Plate

In the first calibration attempt an iron plate similar to the workpieces used for the welding experiments was used. This iron plate was placed in the middle of the furnace and heated up to certain temperatures while the emittance independent temperature imaging system measured the radiation emitted from the plate. This radiation was measured in the two wavelengths defined by the band-pass filters above (Figure I-2).

In Figure I-3 and Figure I-4 measurements of the iron plate grapped by the emittance independent temperature imaging system at a temperature close to melting is depict. The two images below (Figure I-3 A and B) are raw measurements of the temperature imaging system. Measurement A is captured by use of the band-pass filter BG38 which penetrates radiation with small wavelengths. Measurement B is captured by use of the high-pass filter (RG9). In Figure I-4 the proportion between the two measurements is depict (B/A). The pixel values of this proportion image (Figure I-4 B/A) are the values that are to be inserted as the proportion (E_1/E_2) of equation H.12. See Eq. I.1.

$$T \left\{ \frac{E_1}{E_2} \right\} = \frac{C_a}{\ln \left(\frac{E_1}{E_2} \cdot C_b \right)} \quad \text{I.1}$$

Based on the proportion E_1/E_2 it is possible to calculate the absolute temperature.

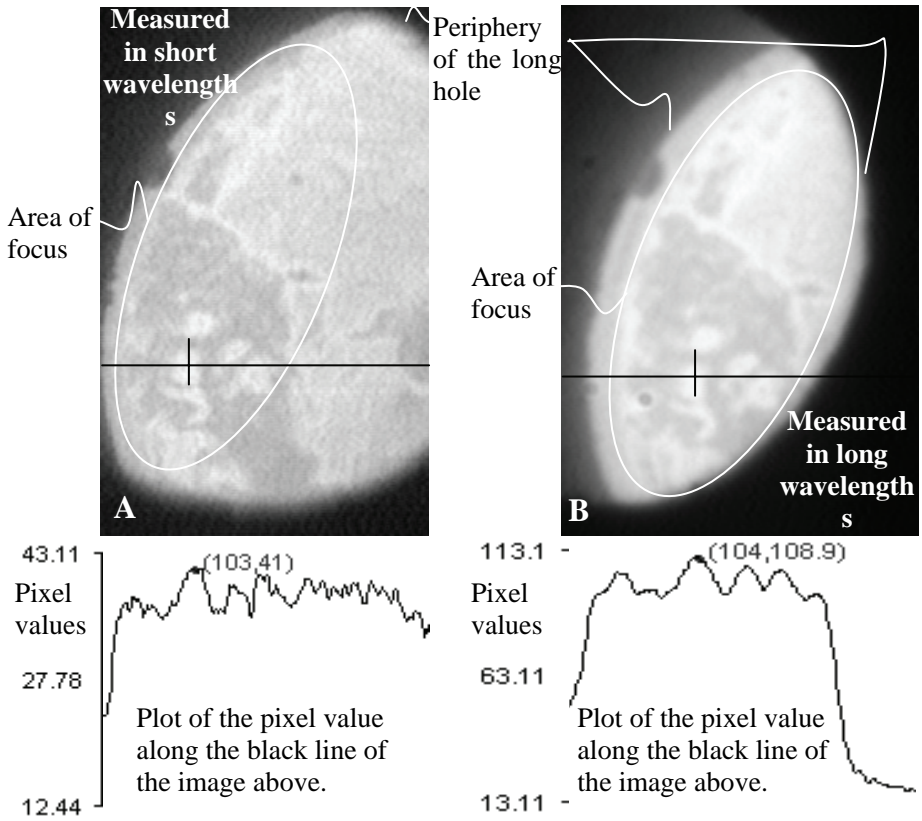


Figure I-3 Two measurements of the one and same iron plate measured in two different wavelengths.

On Figure I-3, A and B, it is visible that measured radiation of the iron surface changes from one area to another. This is though the temperature of the surface should be uniform. Variation in the factor of emittance is the reason for this variation in measured radiation. It is on Figure I-4 B/A clear that this variation is minimized.

The variations of the emittance occur due to oxide scales on the surface of the iron plate. These iron scales arise because the iron plate is disposed to oxygen. When Figure I-3 is compared to Figure I-4 the effect of the emittance independent temperature imaging system is demonstrated.

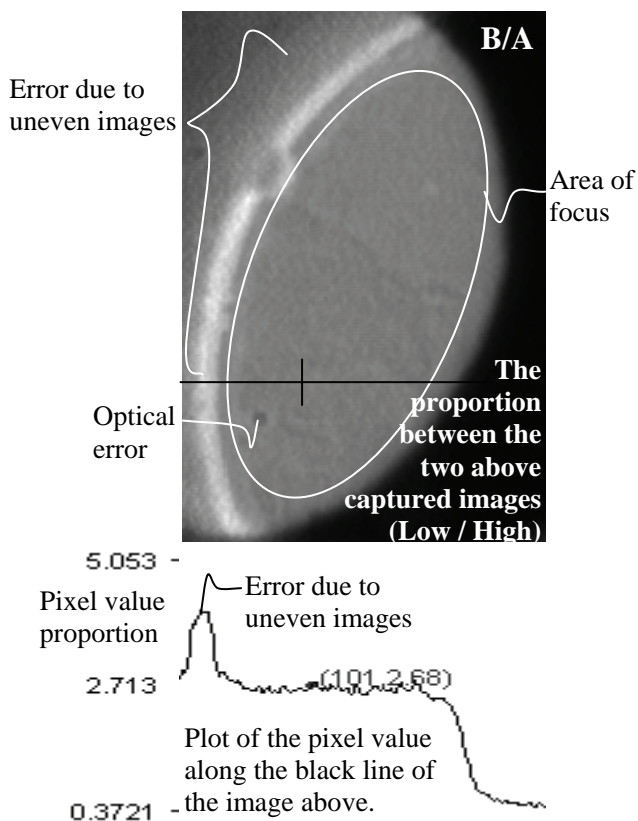


Figure I-4 The proportion of the two images of Figure I-1.

The same experiment as performed on the iron plate was performed on a platinum plate. The reason for changing from an iron to a platinum plate was that the iron plated started melting when the temperature in the furnace was measured to 1325°C. The temperature was measured with thermocouples just above the plate (Figure I-1). Knowing that the melting point of the plate is 1530°C gave cause for some reflections. The conclusion was that the dark surface of the iron plate (high factor of emittance) absorbed more radiation than the more reflecting surface of the thermocouple. Shielding the plate and thermocouple from direct radiation from the heat units did however not change the picture. It was therefore chosen to exchange the iron plate with a platinum plate. Platinum has like the thermocouple a low factor of emittance together with a higher melting point than iron. It is therefore regarded as more suitable for the calibration at temperatures from 1350°C to 1530°C.

I.1.2. Calibration By Means of a Platinum Plate

In the second calibration attempt, by means of the furnace, a platinum plate was heated up (Figure I-1). A set of measurements of the emitted radiation of the

platinum plate captured by the emittance independent temperature imaging system is illustrated in Figure I-5.

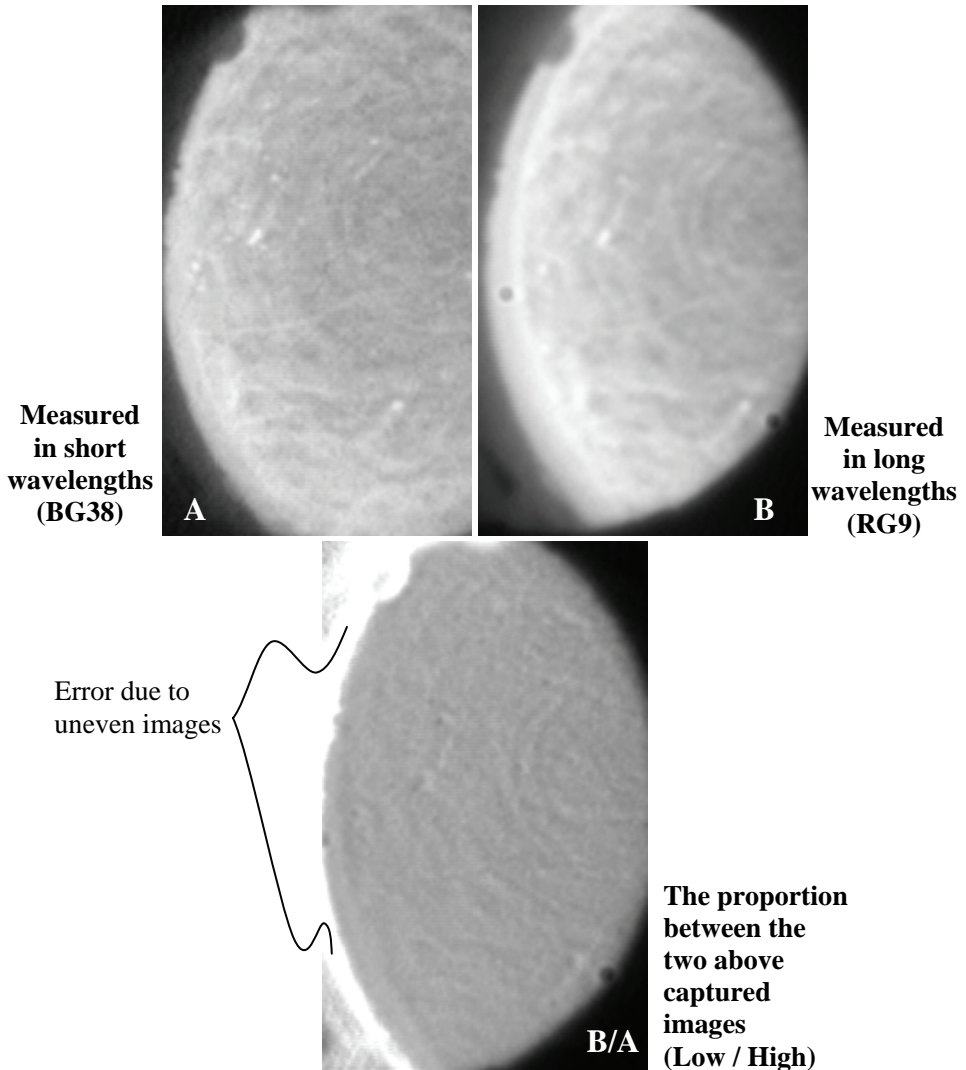


Figure I-5 Two measurements of the emitted radiation of the platinum plate (A and B) and the proportion of the two measurements (A/B).

Measurement A (Figure I-5) is captured by use of the BG38 band-pass filter and measurement B is captured by use of the high-pass filter R9. The image below measurement A and B is the proportion (B/A) of measurements A and B. In the calibration process this proportion is compared to the temperature of the thermocouple that is positioned just above the platinum plate. The proportion was measured from temperatures at 1275°C to temperatures at 1550°C. These temperatures were fixed by the thermocouples. Based on this calibration procedure

the measured figures could be placed in a table and used as absolute calibration figures.

To test the calibration figures the proportions are inserted in Eq. H.12. One extra constant, C_c , is however added (Eq. I.2).

$$T \left\{ \frac{E_1}{E_2} \right\} = \frac{C_a}{\ln \left(\frac{E_1}{E_2} \cdot C_b \cdot C_c \right)} \quad \text{I.2}$$

Where, C_a and C_b are two known constants (Appendix H.1), E_1/E_2 is the proportion of the two measurements of the emittance independent temperature imaging system (B/A). C_c is a correction constant that corrects a constant error of the proportion, E_1/E_2 .

The constant error, C_c , of the measured proportion, E_1/E_2 , is due to different penetrate abilities to the light of the two optics of the emittance independent camera optic. The different penetrate abilities comes from two different sizes of the pinholes, from two different penetrate abilities of the two filters and from the sensitivity of the CCD-chip.

The pinhole in front of the optic with the BG38 band-pass filter has a diameter of 1.5 mm whereas the pinhole for the optic with the RG9 highpass filter is 1 mm (Appendix H.2). The area proportion between these two pinholes is 2.25.

The difference in penetrate ability and the difference in sensitivity for the CCD-chip is illustrated in Figure I-2. The areas under the two of those graphs are clearly different. The area of the BG38 band-pass filter is approximately 5 times larger than the area of the RG9 highpass filter.

Multiplying the two proportions above gives the constant error, C_c :

$$C_c = 2.25 \cdot 5 = 11.25 .$$

Based on the temperatures measured by the thermocouples and the measured proportions that are inserted into Eq. I.2, it is possible to compute a graph (Figure I-6). This graph has the thermocouple-measured temperatures on the abscissa, named "Thermocouple-measured temperatures", and the calculated temperatures (Eq. I.2) on the ordinate, named "Emittance independent temperatures".

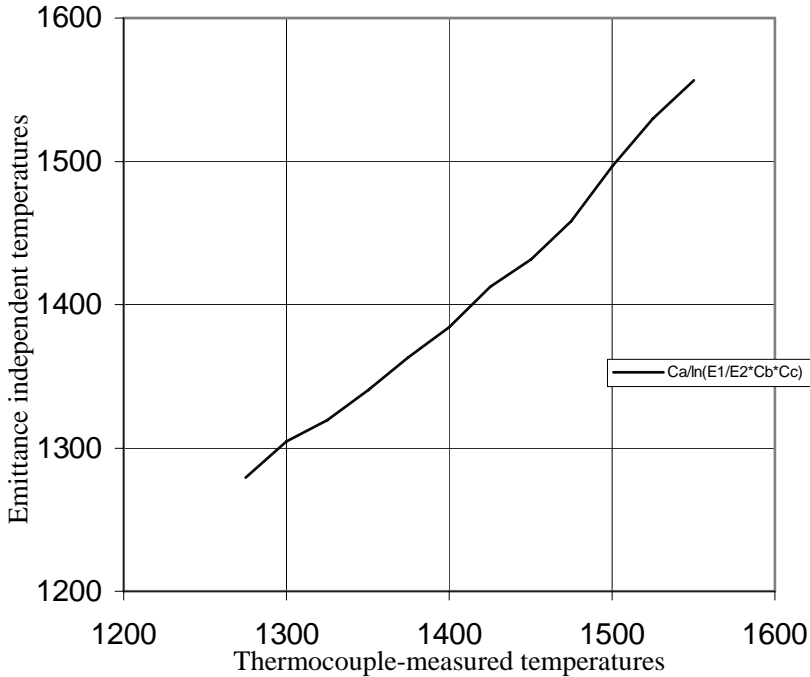


Figure I-6 The emittance independent temperature measurements of a platinum plate compared to thermocouple measured temperatures.

In the graph above (Figure I-6) the physical thermocouple measurements are compared to the theoretical and physical calibrated emittance independent temperature figures of the temperature imaging system. The figure shows a good accordance between the thermocouple temperature measurements and the emittance independent temperature measurements. This coherence substantiates the validity of the theoretical and physical possibility to perform emittance independent temperature measurements.

It is, however, to be mentioned that the value of λ_1 and λ_2 that constitute a part of C_a and C_b (Eq. I.2) are set to respectably 0.87 nm and 0.55 nm. Varying λ_1 and λ_2 has a distinct influence on the result of Eq. I.2 and therefore also on the graph (Figure I-6).

In Appendix H the possibility to measure the temperature by means of a temperature imaging system independently of the factor of emittance was verified theoretically. In this section the possibility was verified experimentally.

In the following section the possibility to calibrate the emittance dependent temperature imaging system based on a non-moving weld is discussed. The following two sections only deals with the emittance dependent temperature imaging system.

I.2. Calibration On a Non-moving Weld

The reason for a calibration on a non-moving weld was to calibrate the emittance dependent temperature imaging system in its true environment. The intention why the weld was not moving was to create a symmetrical heat conduction and to enable simple thermocouple measurements of the workpiece. By a symmetrical heat conduction it is possible to compare measurements of the camera all around the peripheral of the weld. Watching the temperature around the weld where the temperature profile is symmetrical enables the possibility to see the effect of undesired reflection of the electrode due to the angle of reflection.

Despite the good intentions it turned out that the weld process created many oxide scales on the surface around the weld. Because of these oxide scales the emitted radiation of the workpiece changed significantly. The test results on the non-moving weld were therefore not useful for calibration of the emittance dependent temperature system.

The arrangement of the test elements is depict below (Figure I-7).

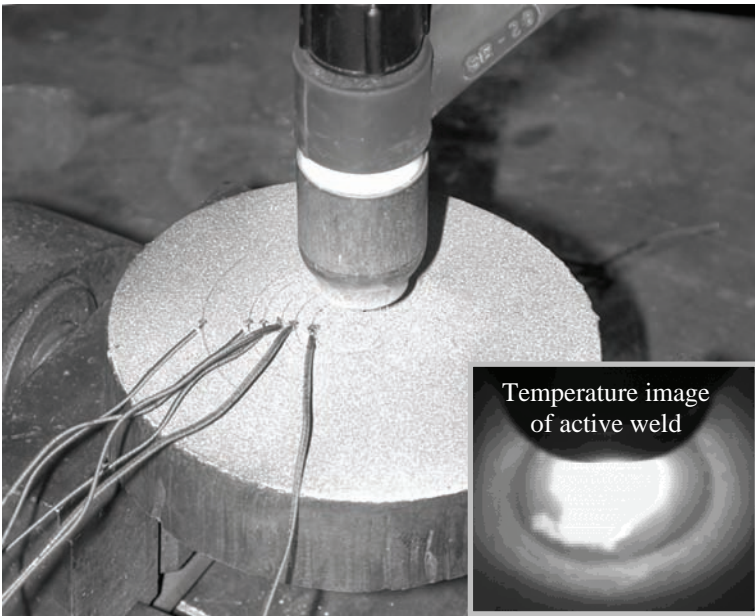


Figure I-7 The arrangement of the calibration test on the non-moving weld.

The workpiece is of a thickness of 20 mm. The large thickness is to avoid burning through. The round shape of the workpiece is to facilitate symmetrical heat convection. The six wires are all thermocouples that are placed in different lengths from the centre of the weld pool.

This calibration method failed due to lack of gas protection causing oxide scales. It was therefore decided to calibrate the emittance dependent temperature imaging system based on a weld process that is running as analogous to the weld process to be controlled as possible. This is described in the following section.

I.3. Calibration on a Moving weld.

When calibrating the emittance dependent temperature imaging system on a moving weld it is more difficult to measure one or more reference temperatures, e.g. measured by means of thermocouples, than on a non-moving weld. It was therefore decided to use the melting point as a temperature reference. By means of one reference temperature and Planck's law it is possible to calibrate the temperature imaging system. The melting point of the workpiece is 1530 °C. The position and the measured vision value of the melting point can be identified from stored camera measurements after an ended calibration welding. The position of the melting point is on the boarder of the weld.

Based on the emitted radiation of the workpiece it is by Planck's law possible to calculate the absolute temperature (Eq. I.3 and I.4):

$$E = \varepsilon \cdot \frac{C_1}{\lambda^5} \cdot \frac{1}{e^{\frac{C_2}{\lambda T}} - 1} \quad \text{I.3}$$

↓ For temperatures below 1800 °C

$$T = \frac{C_2}{\lambda} \cdot \frac{1}{\ln\left(\frac{\varepsilon \cdot C_1}{E \cdot \lambda^5} + 1\right)} \quad \text{I.4}$$

where C_1 , C_2 , and λ are known constants and ε is dependent on the surface of the given workpiece (Eq. I.5):

$$T = C_A \cdot \frac{1}{\ln\left(\frac{\varepsilon}{E} \cdot C_B + 1\right)} \quad \text{I.5}$$

If ε/E of Eq. I.5 is changed to $C_C / \text{Value}_{pixel}$, C_C is the constant which is to be identified to calibrate the system. Value_{pixel} is the value measured by the temperature imaging system at the identified melting point. C_C is a correction constant that describes the difference in emitted energy compared to the measured temperature value, Value_{pixel} , of the temperature imaging system. The factor of emittance, ε , constitute a part of the correction constant C_C (Eq. I.6):

$$T = C_A \cdot \frac{1}{\ln\left(\frac{C_C}{Value_{pixel}} \cdot C_B + 1\right)} \quad \text{I.6}$$

This correction constant C_C is the constant that is to be identified in calibration process of the emittance dependent temperature imaging system.

As C_A and C_B are based on known constants and the $Value_{pixel}$ is known for the temperature $T = 1530^\circ\text{C}$ the calibration constant, C_C , is computable (Eq. I.7).

$$C_C = \frac{Value_{pixel}}{C_B} \cdot \left(e^{C_A \frac{1}{T}} - 1\right) \quad \text{I.7}$$

In a calibration test on a workpiece similar to the one used in the final experiments (Chapter 9) the measured value of the temperature imaging system was measured to 142. The calibration constant C_C is by equation I.7 calculated to 0,0333.

Based on the calculated constant, C_C , and equation I.6 it is now possible to draw the relation between measured pixel values and the absolute temperature (Figure I-8).

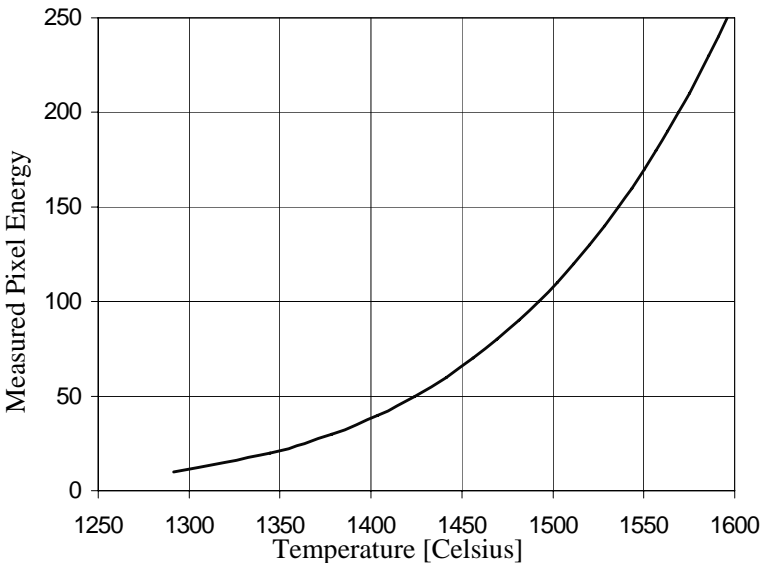


Figure I-8 illustrates the relation between measured pixel value and the corresponding calibrated absolute temperature.

This calibration is used in the following appendix where measured surface temperatures of an actual performed weld experiment are compared to surface temperatures of a corresponding simulated weld experiment.

J. Temperature Measurements Compared to Off-line Simulations

In this appendix measurements performed by the temperature imaging system, which is dependent on the factor of emittance, are compared to thermal finite-element simulations. The finite-element simulations are made by the *reference-generating system* which constitute a part of the *off-line preparation system*. The comparison is made on the basis of the width of the weld and the gradients at the side of the weld pool, only, as these are regarded as crucial parameters in avoiding welding defects like e.g. lack of fusion and/or penetration. The calibration of the finite-element model of the *off-line preparation system* has been based on macro cross sections, which the simulation model has been calibrated to fit in the height and width. The calibration of the finite-element model is performed under the conditions listed in Table J-1 except that the welding *current* was 143 amps.

The experiment performed to compare the measurements of the temperature imaging system to the simulated temperatures was made under the following conditions (Table J-1).

Current	250 [A]
Travel speed	4.5 [mm/sec] (no weaving)
Material type	Grade S235
Plate thickness	6 [mm]
Work angle and Travel angle	0 [°]
Tip to plate distance	2.7 [mm]
Camera position	Behind the welding process
Camera angle	45 [°] to the plate

Table J-1 Constant weld parameters used in the present welding experiment.

The camera images to be shown in the following are calibrated and visualized from 1200 to 1600 °C. To avoid undesired reflected radiation at the side of the weld the camera has been placed behind the weld process.

The calibrated image of the welding that is compared to the simulated temperature profile is shown below (Figure J-1).

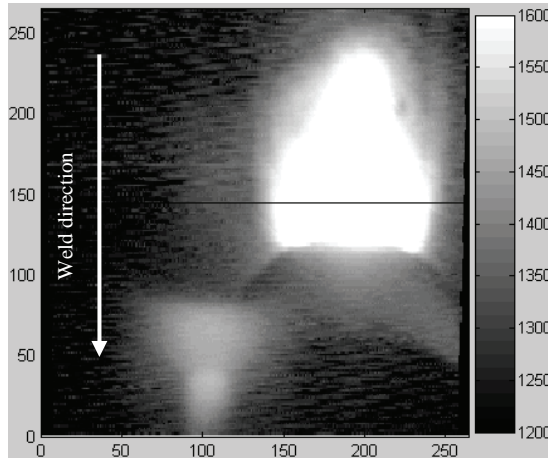


Figure J-1 Calibrated image taken by the temperature imaging system. The scale of the abscissa and the ordinate is 0.1 [mm]. The temperature scale at the right goes from 1200 to 1600 °C.

The temperature profile along the black line in the figure above (Figure J-1) is plotted below in Figure J-2. This picture is based on ten plots generated from ten images taken in a row at 10 Hz. One plot is lying below the nine other plots. This plot was made approximately 0.05 second after the arc was turned off. The temperatures below 1375 °C is dominated by noise due to the sensitivity of the camera. The scale of the abscissa is 0.1 mm and the scale of the ordinate is in °C.

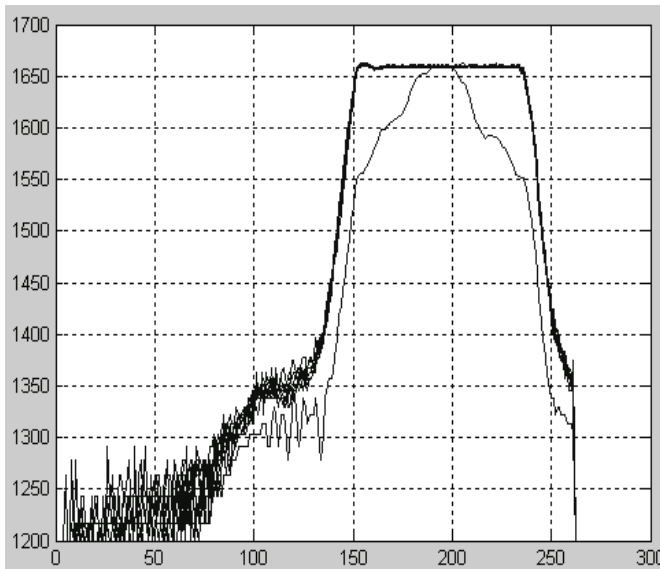


Figure J-2 The temperature distribution across the weld along the black line sketched in Figure J-1.

The width of the weld at 1530°C, which is set to be the melt temperature, is when the arc is on measured to be 10.0 mm and 8.7 mm 0.05 sec, after the arc has been shut off. The distance in direction at the black line from where the temperature is 1500 to where it is 1400 °C is in both cases measured to be 0.9 mm. This measure is here designated the gradient. Here, it is obvious that the arc despite the filtration has a certain impact on the measurement.

The analogous but simulated weld temperature profile is illustrated below in Figure J-3 and Figure J-4.

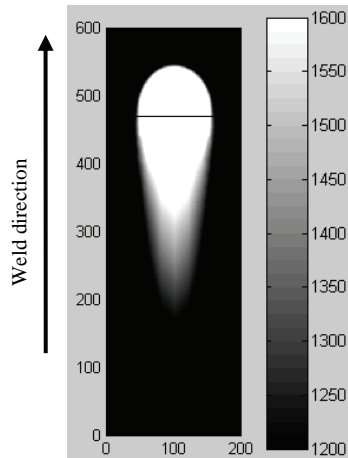


Figure J-3 Simulation of the welding to be compared i.e. according to the parameters in Table J-1. The scale of the abscissa and the ordinate is 0.1 mm. The temperature scale at the right goes from 1200 to 1600 °C as in Figure J-1.

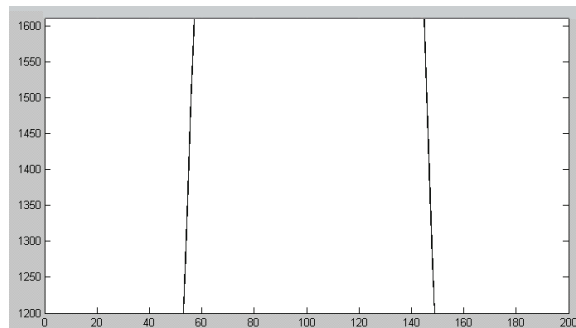


Figure J-4 The temperature distribution across the weld along the black line sketched in Figure J-3. The scale of the abscissa is 0.1 mm and the scale of the ordinate is in degrees Celsius.

The width of the modelled weld at 1530°C is here measured to be 8.7 mm. The distance from where the temperature is 1500°C to where it is 1400°C is measured to be 0.15 mm and is as before designated the gradient (Figure J-4).

The width of the simulated weld (8.7 mm) and the width actual weld measured by the camera (8.7 mm 0.05 sec after the arc has been shut off) is equal. The width measured by the camera is, however, rather disturbed by the arc and approximately 0.05 second after turning off the arc the measured width of the weld shrinks from 10 to the 8.7 mm. Macro cross sections of the workpiece made subsequently shows that the width of the weld is 8.7 mm.

The gradients measured as the distance from where the temperature is 1500°C to the where the temperature is 1400 °C was for the simulated weld measured to be 0.15 mm and for the physical welding, measured by the temperature imaging system, measured to 0.9 mm. Because the gradient does not change after the arc is turned off this inconsistency is not due to the disturbing arc (Figure J-2). The error might come from either undesired radiation from the electrode or an incorrect simulation model.

Though deviations for both the developed camera and for the finite-element simulation of the *off-line preparation system* were identified, a promising correspondence was demonstrated. The deviation was concluded to be due to a lacking filtration of the arc and limitations to the simulation model of the *off-line preparation system*.

K. Journal Paper (2003)

This paper was at the Ninth International Manufacturing Conference in China, IMCC'2000 Hong Kong 16 – 17 August 2000 presented by Hans Christian Kjeldsen Orye. This paper is published in Journal of Materials Processing Technology 139 (2003) Page 499–504.



Journal of Materials Processing Technology 139 (2003) 499–504



www.elsevier.com/locate/jmatprotec

A reference architecture for the design of an industrial temperature feedback welding control system

H. Holm^{a,*}, H.C.E. Kjeldsen^a, J.K. Kristensen^b

^a Department of Production, Aalborg University, Fibigerstraede 16, 9220 Aalborg East, Denmark

^b The Division of Welding and Production Technology, The FORCE Institute A/S, Park Alle 345, 2605 Brøndby, Denmark

Abstract

This paper describes a provisional not fully developed architecture of a thermal feedback system for closed-loop control of robotic arc welding. The architecture is based on an off-line planning system for welding and an on-line welding control system, where the off-line planning system builds the reference to be followed by the on-line closed-loop system. The main aim of this architecture is to develop a method by which thermal feedback welding control systems can be designed. This control system is meant for control of welding of thick-walled sheet metal geometries and the system feeds back the temperatures on the surface of the geometry. The temperature is fed back by an infrared CCD-array camera.

© 2003 Elsevier Science B.V. All rights reserved.

Keywords: Finite element; Process model; On-line control system; Off-line control system; IR vision; CCD camera; Weld quality; Robotic welding

1. Introduction

Although automated welding systems have been commercially available for some time, full automation of this process has not yet been achieved because of difficulties concerning control and sensor technologies.

To obtain full automation of the automated welding process planning of torch and power trajectories is needed. The reason is that by such planning, programmes for numerically controlled welding machines (welding robots and power sources) can be produced without involving the machinery in the programming work. Hereby production can continue to use the equipment to carry out the planned programs, while plans for succeeding seams to be welded are being produced.

It has to be mentioned that manually performed welding trajectory planning has proven to be so time-consuming that planning of such trajectories in most industrial applications has to be carried out automatically. To avoid trajectory planning becoming a bottleneck in the production and to keep the total production costs on a competitive level, the availability of sufficiently good mathematical welding process models is crucial.

One way to achieve a successful method for the preparation of machine welding could be to carry out research

to obtain a comprehensive understanding of human welding control. This strategy seems to encompass so many difficult obstacles that most researchers have avoided it.

Some researchers have without much success tested a strategy by which attempts have been made to establish mathematically based systems, which are meant to imitate human motions, without actually understanding the principles behind human welding control. Due to the difficulties and lack of success of the two above mentioned strategies a third strategy was chosen.

Here the trajectory (i.e. the course) of torch motions as well as of power and filler material applied to the material to be welded is planned in such detail that sufficient information is available for the creation of a program to control a numerically controlled machine. By this strategy a system is to carry out the planning of the torch motion and the planning of the electrical arc power and filler material flow to be applied to the material to be welded. The planning must be carried out such that a desired geometric weld quality is achieved.

The planning of the motion as well as the power and material flow trajectories is done by means of a mathematical, computer-applied model of the weld geometry, which is fed with some power (heat) process properties and quality criteria, which correspond to the chosen geometry and power model.

In situations, where welding execution is to be carried out by a closed-loop (sensor feedback) welding

* Corresponding author.

E-mail address: r9hh@iprod.auc.dk (H. Holm).

disturbance-compensating system, the planning encompasses trajectories, which serve as references, that can be followed by the welding control system.

A very important reason for carrying out welding under closed-loop (sensor feedback) disturbance compensation control is that without that type of control one will have to ensure acceptable weld quality despite disturbances such as apparent geometric groove disturbances and too much material and heat. The unnecessary high heat input in the workpiece has an undesired influence on expansions and contractions, with the result that stress is built into the workpiece, which causes costly workpiece distortions. Therefore, it is desirable to be able to control the energy induced into the workpiece best possible.

Related to this strategy three authors have been identified [1–5], who all have worked with two-dimensional finite difference thermal diffusion modelling in order to use it for the preparation of trajectories for manual welding. None of them, however, have tried to make the trajectory planning automatic.

One of these authors has developed a thermal feedback control based on applications of a time series model [1]. This method is also divided into an off-line and an on-line method. The off-line method is based on numerical models, and it is capable of determining optimal heat distribution and cooling. The optimal distribution is successfully used in the on-line system where a thermal camera determines the deviation between the actual and the desired surface heat profile. The system then determines which weld weave pattern and heat input minimises the deviation.

The above mentioned welding system gives improved welding results with a minimised heat input, but the system is designed for specific types of welding tasks.

As robotic welding systems do not incorporate the adaptive skills of a human welder, the main problem in robotic welding is the control of the welding process itself.

In this paper a new architecture for a complete welding control system is presented. This system is based on a combined off-line planning control system and an on-line surface temperature feedback control system as described previously for the chosen strategy. The off-line environment, which is to be capable of coping with any arbitrary geometry is presently being developed [6] and it will make it possible to use the control techniques developed for state space control systems, e.g. optimal control, and the flexibility of the finite element (FE) models. The off-line control system will continuously adapt the control variables to the states of the workpiece. This will be done through the use of a reference heat profile of the heat-affected zone and of the weld pool. This will then be compared with the achieved heat distribution in a FE model. The off-line planning system will then use optimal control to compute a dynamic trajectory of welding control variables. The on-line system performs the welding process, based on knowledge from the off-line system.

Based on the idea of having an off-line planning system containing heavy mathematical models and a fast

on-line system which carry out the work while at the same time it is capable of coping with small environmental changes, this paper presents a reference architecture of the forthcoming development of welding process control systems.

2. Method

The proposed method is expected to enable on-line control of the weld quality of the internal of thick-walled workpieces. This is expected to be possible even though the temperatures in the interior of the workpiece cannot be measured during the process, such that they can be fed back. It is, however, possible to measure the temperatures from the surfaces of the workpiece during the process. The surface on which the welding process is carried out has therefore been chosen as the surface for the temperature feed back of the process. Consequently, a camera is planned to be mounted on the welding robot. This surface temperature feedback is achievable by means of a CCD-chip based camera, which is able to measure the absolute temperature independently of the emittance [7].

The reason why on-line control of the internal of thick-walled workpieces becomes possible by feeding back the surface temperature is because of the off-line generated surface temperature reference (Fig. 1). The surface temperature reference is generated by an off-line planning system, which uses a FE model to simulate the process by calculating the temperatures of the internal of the workpiece. As reference for the off-line system a desired temperature profile is defined, a control reference, which enables the future user to obtain a desired welding quality during the welding process. This temperature profile could define the desired temperatures on the back side of the workpiece, i.e. the side of the workpiece where measurement of the surface temperatures to ensure full penetration is normally not possible. The defined reference temperature profile for the off-line system represents the quality to be gained firstly by the off-line planning system and successfully by the on-line system.

When controlling the temperatures inside the workpiece by simulating the process using the FE method the theoretical temperatures in all the node points are known, also the nodes on the surface. The temperature of the nodes on that surface, where the arc touches the workpiece and where temperatures can be measured by the CCD-camera, are saved as output from the off-line system and are used as the reference temperature input in the on-line system. In the on-line system the off-line generated surface temperature is used as temperature reference and compared to the surface temperatures measured by the temperature-measuring CCD-camera.

The architecture of the welding control system, which is to be explained in more detail in the following, is based on an automated tungsten inert gas (TIG) welding process.

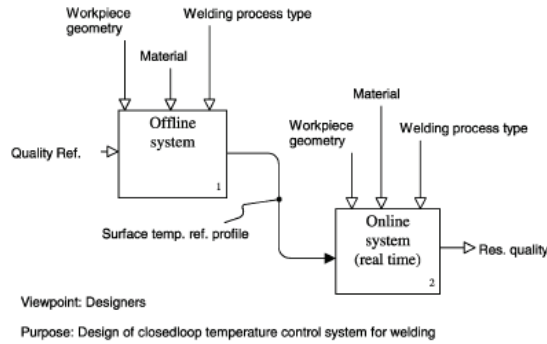


Fig. 1. The overall architecture of the complete welding control system.

Now, the new architecture for the off-line planning control system and an architecture for the real-time surface temperature feedback control system are presented as well as the connection between the two control systems, which carries the reference temperature trajectory from the simulation control system to the real-time physical welding feedback control system.

2.1. Off-line system

The off-line planning system is based on a reference model, a controller and a FE model. The reference model, which serves as input is composed of a quality reference (for instance specified in ISO standard terms), the workpiece geometry and material data. The output is a surface temperature reference, which is to be used by the on-line closed-loop system (Fig. 2).

This off-line planning system contains all the necessary elements for planning the trajectories of motion and power used as input for an on-line open loop control system (execution system). This is the case as the off-line system is capable of generating a full reference for an on-line open loop execution system.

Because the off-line system is capable of simulating a selected output of the welding control system, it is also capable of generating a reference for the on-line closed-loop system (execution system), which receives a sensor feedback on the selected output of the system. Information on the properties of the system is represented in the temperature trajectories, which serve as input trajectories. As the off-line reference generating system generates the reference temperatures based on knowledge of the internal workpiece temperatures, it is natural to store some of these temperatures as reference for the on-line closed-loop system. The

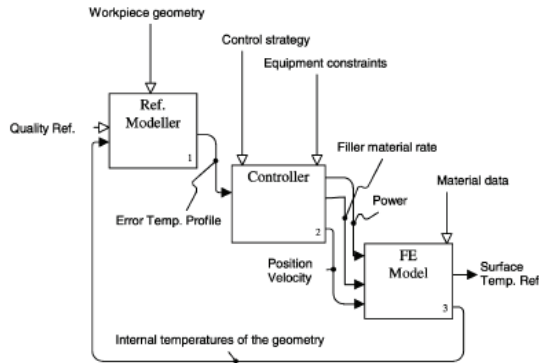


Fig. 2. The architecture of the off-line system.

simulated temperatures to be stored are the temperatures of the surface of the workpiece, as these temperatures are comparable with the temperatures measured by the camera in the on-line closed-loop sensor feedback execution system. By feeding, this temperature information from the off-line planning system is transferred to the on-line closed-loop system. The knowledge lying implicitly in the heavily calculated states of the off-line system is transferred to and used in the on-line system. When comparing the on-line sensor feedback with a signal based on knowledge of the off-line system, more information is exploited than that when it represented in the feedback signal.

The controller for the off-line planning system could take many different forms. Presently, the controller is based on a simple search algorithm, which search for the largest error between the desired reference temperatures and the achieved temperatures. The controller includes equipment constraints as maximum velocity and acceleration of the robot to be controlled in the on-line system, and constraints relating to the welding equipment. Based on the search algorithm and the different constraints, the controller finds its path through the weld task and minimises the error in accordance to the defined temperature reference input, derived from, e.g. the ISO standard terms. The output of the controller is the position, the velocity and the welding power.

Instead of sending the position and the velocity to the robot and the power to the welding equipment as in the physical system, a FE model is fed with this input. The purpose of feeding a FE model with the input is to simulate the controlled welding process. As the FE model's control-input is the input which brings the welding process as close as possible to its desired state, the best input possible for the real welding system has been generated in the form of the output from the simulated controller. Hereby, an off-line planning system has been built for the closed-loop on-line, physical system.

One of the key parts in this system is the model. To plan a welding trajectory based on this system requires a model that describe the process sufficiently well. The question as to what is sufficiently well will have to be answered by testing the model at different stages. Presently, a non-linear model has been developed. The model is based on a non-linear model of the heat conduction, on a linear model of the radiation and convection, and on a simplification of the model of the weld pool to heat conduction in solid material. The heat source is modelled as a Gaussian heat distribution.

Because of the chosen modelling method and the architecture of the system, it is possible to use this off-line system with an arbitrary workpiece geometry. This control system is continuously adapting the control variables to the states of the workpiece. This is done through the use of the reference heat profile of the internal weld pool, which is compared with the achieved heat distribution in the FE model. The off-line system will then use optimal control to compute a new set of adapted welding control variables.

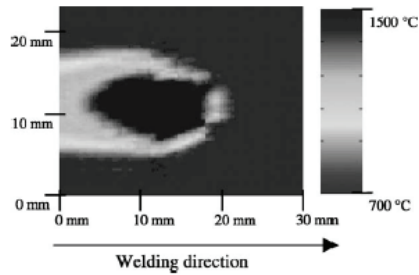


Fig. 3. A preliminary example of a surface temperature profile generated by the off-line system at the time step (k) used as reference temperature profile in the on-line system [6]. This temperature profile is to be compared with the temperature profile measured by the CCD-camera.

The off-line system does not use a predefined weaving pattern but creates its own arbitrary weaving path due to the optimal control strategy.

Using this architecture for the off-line process planning system enables use for planning and programming of open loop robotic welding execution as well as of closed-loop robotic welding execution.

Since a FE programme carry out the simulation, the trajectories of the temperatures of the surface where the arc touches the workpiece constitute part of those temperatures, which are simulated.

To ensure the specified penetration requirements the simulated welding temperature on the surface (the front side of the plate) (Fig. 3) appears as a result. These simulated surface trajectories form good temperature reference trajectories for a physical closed-loop welding control system (the on-line system), which feeds back measured temperatures from the surface of the workpiece (Fig. 4), where the arc touches the workpiece and where CCD-camera measuring is possible.

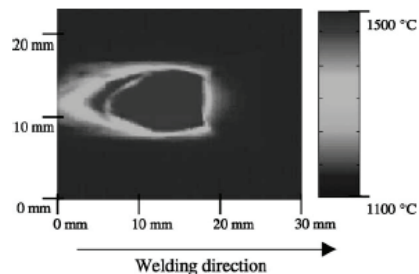


Fig. 4. A preliminary example of a temperature profile measured by the CCD-camera at the time step (k). This temperature profile is to be compared with the surface temperature profile generated by the off-line system at time step (k).

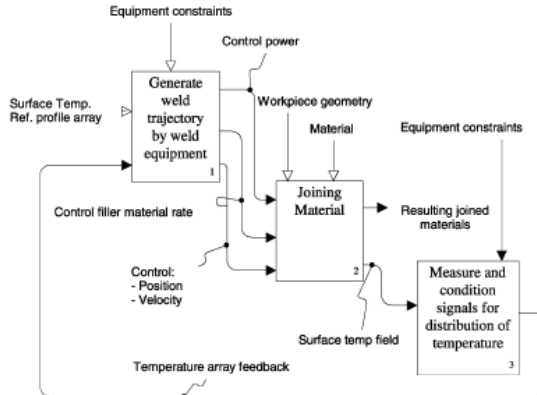


Fig. 5. The architecture of the on-line system.

In future it is expected that the two pictures in Figs. 3 and 4 will, after adjustments and calibrations, be comparable, but as the system is not yet developed far enough the figures cannot illustrate this yet. Please note the different grey scales in Figs. 3 and 4.

2.2. On-line system

Based on the reference surface temperature profile from the off-line system of that surface which can be measured by a CCD-camera, the on-line system controls that the robot and the welding equipment fit to the surface temperature profile of the physical welding system and to the reference surface temperature profile provided by the off-line system. For design of this on-line control system (Fig. 5) can be used exactly the same method as used for the design of the off-line control system by which the trajectory planning has been done. The only difference is that the feedback and the output in the on-line system are temperature profiles of the surface of the material. In the off-line system the feedback was the temperature profiles of the internal of the material.

The on-line control system is based on a controller that generates the weld trajectory by the weld equipment, and on a camera that measures the temperature profile of the surface of the workpiece.

In the off-line system a FE model of the heat conduction was used. As a FE model can be represented as a state space model, a simple version of the off-line model is used for the design of the on-line state space control system for real-time closed-loop control of welding. When using a simplification of the FE model this approach assures a fast real-time control system based on structured laws of physics. Besides the state space model, the controller contains the necessary equipment constraints.

The on-line control system real-time controls the position, the velocity of the robot and the welding power of the welding equipment as well as the filler material flow rate. This requires a real-time connection to the robot and the welding equipment. As the system runs, the material is joined and the camera is real-time measuring the surface temperature distribution. This temperature profile is continuously fed back to the controller, where it is compared with the reference temperature trajectory.

The camera is a standard 768×574 pixel CCD-chip based camera, which has been changed to an emittance independent temperature-measuring camera. The camera is capable of measuring a temperature from 1000 to 1500 °C.

2.3. Connection between the two control systems

The advantage of the system, the combination of the off-line and the on-line system. The off-line system is a heavy control system based on advanced physical FE calculations whereas the on-line system is a fast real-time system based on the knowledge from the off-line system. The off-line system is thus used for a twofold purpose. One is to prepare the welding by generating the temperature control reference. The other is to serve as a tool for design of the control laws by which the on-line real-time control system is to be operated.

It is believed that if the on-line system can obtain the same surface temperature profile as calculated by the off-line system, then the temperature isotherms in the internal of the plate will be just as calculated in the off-line model as long as the model is sufficiently accurate. Therefore, one of the most critical bottlenecks in the system is the model, which has to be adequately precise.

3. Expected results

The aim is to obtain a method for the generation of control systems, which are capable of controlling automatic welding of welds with varying positions in space. This method is to a large extent expected to reduce the number of physical welding experiments. The reason is that the number of experiments necessary for FE model validation is much smaller than the necessary number of experiments for creation of an equivalent set of regression models.

4. Conclusions

The reason why the method enables a flexible production is that the temperature control reference is created by an automatic off-line programming system. The off-line programming system is much more flexible towards changes in workpieces than any known method today. It is, hence, very flexible in customer tailored production. Because a FE model forms the basis for the automatic off-line robot programming system and for the generation of the reference for the temperature control system. A FE model yields large flexibility in its range of validity towards changes in the geometry as a model is automatically generated once a product

has been constructed in a 3D CAD-system and imported to the FE environment.

References

- [1] C.C. Doumanidis, Thermal modelling and adaptive control of scan welding, *Weld. J.* (1998) 465–476.
- [2] K.L. Moore, et al., Annual Report, FY95/96: Advanced Welding Control Project, INEL URC Project No. G22, Measurement and Control Engineering Research Center, College of Engineering, Idaho State University, Pocatello, ID, USA, June 1996.
- [3] K.L. Moore, et al., Annual Report, FY97: Advanced Welding Control Project, INEL URC Project No. G22, Measurement and Control Engineering Research Center, College of Engineering, Idaho State University, Pocatello, ID, USA, July 1997.
- [4] R. Kovacevic, Y.M. Zhang, S. Ruan, Sensing and control of weld pool geometry for automated GTA welding, *Trans. ASME, J. Eng. Ind.* 117 (1995) 210–222.
- [5] R. Kovacevic, Z.N. Cao, Y.M. Zhang, Role of welding parameters in determining the geometrical appearance of weld pool, *Trans. ASME, J. Eng. Mater. Technol.* 118 (1996) 589–595.
- [6] C.B. Teap, H. Holm, J.H. Hoeyer, H.H. Nielsen, J. Dam, Welding process control based on a numerical model and state-space techniques, in: *Proceedings of the IASTED International Conference on Modelling, Identification and Control, 1999*, pp. 265–268.
- [7] H. Dissing, J. Christensen, M. Smith, T.S. Jensen, T. Schmidt, Testing a finite element welding model, Six Term Project Report, Department of Production, Aalborg University, Denmark, June 2000.

L. Conference Paper (2002)

This paper was at the 6th International Conference on Trends in Welding Research 15-19. April 2002 presented by Hans Christian Kjeldsen Orye. This paper is published in: "Trends in Welding Research 2002". ISBN: 0871707802.

New Low-cost Camera Temperature Measurements Compared to Analogous Temperature State Simulations

H. C. Kjeldsen

FORCE Technology, Broendby, Denmark hck@force.dk or hans_chr@mailme.dk

H. Holm

Aalborg University, Aalborg East, Denmark i@hh@iprod.auc.dk

J. Klastrup Kristensen

FORCE Technology, Broendby, Denmark jek@force.dk

Abstract

This paper describes a newly developed low-cost charge-coupled device (CCD) camera for surface temperature measurements in connection with the gas tungsten arc welding (GTAW) process. The purpose of the camera is to capture the surface temperature profile of the weld in progress in order for the control system to compare it to an analogous temperature profile state obtained by simulation. An offline planning system, which performs the state simulation, by use of a finite element system that models the internal and surface temperature profile of a given workpiece. A promising correspondence is demonstrated between the surface temperature profile measured by the camera and the offline simulated surface temperature profile. Based on this correspondence it is believed possible to use a real-time system for control of the welding process, which is based on an offline generated temperature trajectory reference generated by a finite element model based trajectory planning system.

Introduction

The camera to be described in this document is meant for generating the temperature feedback used in a real-time thermal feedback welding control system primarily for the gas tungsten arc welding process (GTAW). This thermal feedback welding control system has been built in order to test a proposed control method for welding of thick walled metal, where the temperatures from the surface of the geometry are fed back [1]. To understand the purpose of and the requirements to the camera, the system in which the camera interacts is briefly presented. The presentation of this system is also to be used for estimating the possibility of building a real-time welding control system, which is driven by an offline generated temperature trajectory reference.

The thermal feedback welding control system can be divided into two sub-systems as shown in Figure 1:

- An *offline* planning system.
- An *online* control system (in which the surface temperature profile feedback is used).

Offline planning system. The offline system is a closed loop planning system, which calculates the optimal path and heat input based on a previously defined quality reference defined by temperatures. The offline system is based on a Finite Element model, which for each time step calculates the internal temperatures of the geometry to be welded. The calculated internal temperatures of the relevant positions are fed back and compared to the quality reference temperatures, while the temperatures at that surface (where the welding arc is active) are stored. After the simulation is completed

the stored surface temperature profiles are used as input surface temperature reference profiles for the online control system.

The offline system does not use a predefined weaving pattern but creates its own thermal quality determined weaving path due to an optimal control strategy.

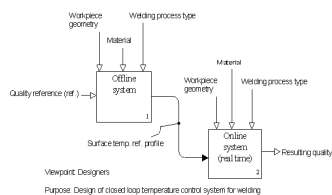


Figure 1. Overall architecture of the proposed method for thermal feedback welding control.

Online control system. The online system is a control system comparable with the offline system. The main difference is that the online system does not have a control loop around a Finite Element model, but instead it has a loop around temperatures measured from the actual process. The purpose of the online system is to enable coping with disturbances during welding.

The newly developed low-cost CCD camera, which captures the surface temperature profile around and underneath the electric arc, generates the feedback in the online feedback system. The camera delivers this feedback to the controller where it is compared to the surface temperature reference profile previously generated by the offline system. Based on the error between these two temperature profiles, the controller generates a new path and heat input for the coming time step. This loop continues till the welding is completed.

The CCD camera is developed to fulfill the difficult task of measuring the surface temperature profile under and around the electric arc. The camera is based on a conventional and very cheap CCD chip based black and white camera. By replacing the conventional CCD chip filter with a dedicated and more suitable filter, and by developing special designed optics for heat measurements, it is possible to obtain surface temperature profile images. In the following, the specially developed optical system for the low-cost CCD camera is described. This enables measurement of the surface temperature profile under and around the very strong electric arc, is described.

Camera design

The camera described below is designed to measure temperatures just outside the melt pool, which are temperatures from roughly 1300 °C to the melt temperature, approximately 1510 °C.

Choice of camera. The temperature of an object may be determined from the electromagnetic radiation emitted from the object within the spectrum illustrated in Figure 2.

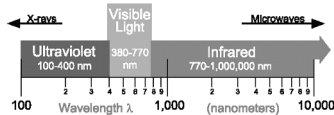


Figure 2. The electromagnetic spectrum.

Planck's Law describes the connection between the radiation from an object and the temperature of the object (Eq. 1).

$$E_1 = \epsilon \cdot \frac{C_1}{\lambda_1^5} \cdot \frac{1}{e^{\frac{C_2}{\lambda_1 T}} - 1} \quad (1)$$

Where E is the energy emitted from the object at a wavelength (λ), ε the emittants, T the absolute temperature and C₁ and C₂ constants.

According to (Eq. 1) the peak in the radiation moves towards smaller wavelengths (higher energy) as the temperature rises. This can also be seen in Figure 3, which illustrates Eq 3.

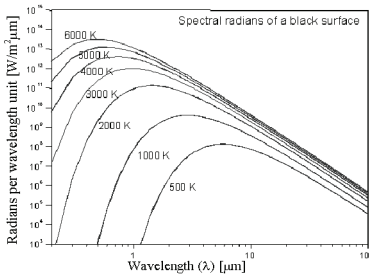


Figure 3. Intensity of the emitted radiation of a black surface as a function of wavelength and temperature.

It follows from Figures 2 and 3 that a significant emission is occurring within the visible region once the temperature is above approximately 1000 °K. It is therefore chosen to base the measurements on a charge-coupled device (CCD) chip based camera, because it is very cheap and capable of measuring visible and near-infrared light. The theoretical sensitivity for a silicon-based chip is shown in Figure 4, but though the sensitivity is theoretically highest at approximately 1100 nm, real CCD chips are typically not very sensitive at wavelengths above 700 nm.

The camera finally chosen was a CV-M10 RS Progressive Scan Monochrome camera. The main reason for choosing this CCD camera is its ability to measure relatively long wavelengths compared to other CCD cameras at the same price level. The nominal sensitivity of the camera including a lens optimized for visible light is

shown in Figure 5. Here, the camera seems to have virtually no sensitivity above 1000 nm.

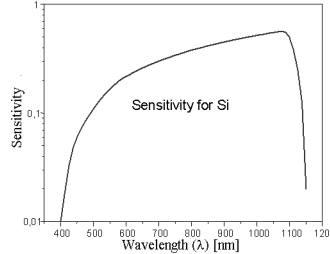


Figure 4. Theoretical sensitivity for silicon.

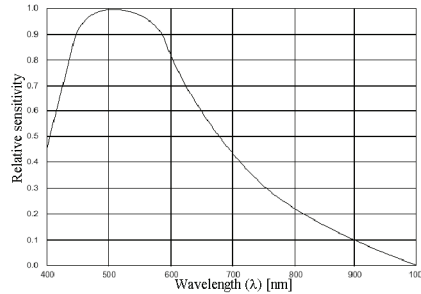


Figure 5. Nominal spectral sensitivity characteristic of a CV-M10 RS Progressive Scan Monochrome camera. The curve includes lens characteristics, but excludes light source characteristics.

However, when measuring the actual response characteristics of the camera without lens, a slightly different response was found, as can be seen in Figure 6. Most notable is that the relative sensitivity was found to be approximately 20% higher at 700 nm. The long wavelength cut-off was therefore also estimated to be of higher temperature than the 1000 nm stated in the camera datasheet (Figure 5).

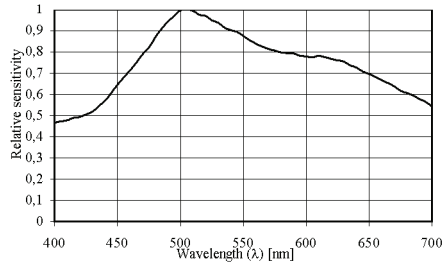


Figure 6. True spectral sensitivity characteristics of the CCD chip in a CV-M10 RS Progressive Scan Monochrome camera (without lens characteristics).

Optical design. The most difficult task in the development of a low-cost CCD camera for surface measurements of a GTAW

welding process is the optical design. The main purpose of the optics is to focus the waves radiated from the desired surface area of the plate on to the chip, and to off-filtrate the not desired radiation sources. In the design of the optics one has to be aware of three main radiation sources. Radiation from:

1. The plate on which the welding process is running (desired).
2. The arc (noise).
3. The tungsten electrode tip (noise).

The radiation from the plate surface on which the welding process is active is the desired radiation. Based on that radiation it is in principle possible to estimate the temperature of the plate. However, as the light from the arc and the electrode is far more intensive than the light from the plate it therefore becomes a very important issue to off-filtrate the not desired light, which originates from the tungsten electrode tip and the arc.

The undesired radiation from the arc is characterized by a unique pattern of spectral lines typical of the atoms or ions forming the arc-plasma. Each line corresponds to a jump between two electronic energy levels and a large part of the emission occurs in the visible and ultraviolet range. The main substance in the plasma of GTAW welding of steel is argon but also e.g. iron, manganese, tungsten, nitrogen and oxygen typically constitute a small part of the atmosphere and therefore also the emission spectrum. Because the arc radiation is characterized by this pattern of spectral lines, it should in theory be possible to find a set of wavelengths where the arc does not contain spectral lines.

To gather knowledge of the spectral radiance of the present process, different sources were used:

- Self made measurements by two different sensors both capable of measuring the spectral lines from 150 nm to 800 nm. These measurements are not figured in this paper.
- Earlier measurements made at FORCE Technology, which show the spectral lines from 200 nm to 1100 nm (Figure 7).
- Theoretical figures of the spectral radiation.

Earlier measurements made at FORCE Technology show the spectral lines from 200 nm to 1100 nm. These measurements show low radiation activity from 500 nm to 700 nm, around 900 nm, around 960 nm and from 980 nm to 1050 nm, as shown in Figure 7.

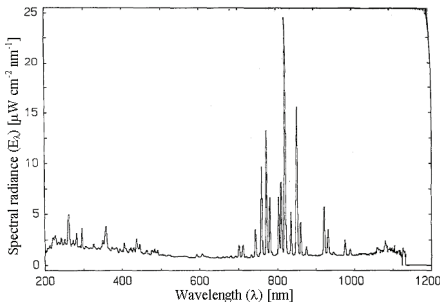


Figure 7. Spectral radiance for a TIG welding arc in 99% argon.

As the conditions for the above measurements were not ideal for the present application, additional measurements have been made in this work. Based on these results, the wavelength range from 500 to 700 nm showed not to be a proper area in which to place

a band pass filter due to rather low signal to noise ratio. As the signal is stronger at wavelengths from 800 to 1100 nm (Figure 3), various theoretic literature discussing the spectral lines in this field has been investigated. Due to measurements, theory and experiments the position of the band pass filter in-between 980 nm and 1050 nm was of special interest. One of the references illustrates, by a drawing, the spectral radiation of pure Argon up till 1000 nm [3]. The drawing is shown in Figure 8. This figure shows roughly no radiation above 978 nm. A table in the same reference does, however, show a peak at 1047 nm.

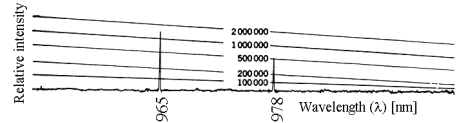


Figure 8 The theoretic spectrum of pure Argon in the range from 950 nm to 1000 nm [3]. The scale of the ordinate is relative intensity.

A second reference showing the spectral lines for an argon arc in air surroundings gives the results shown in Table 1 [4].

Relative intensity	Wavelength (λ) [nm]
25000	965
4500	978
180	1005
30	1033
100	1047
1600	1047

Table 1. Figures of the theoretic spectrum for Argon in air from [4].

The two references used above also state that pure iron and tungsten do not contribute with spectral lines above 950 nm. It has, therefore, been chosen to use a band pass filter centred at 1010 nm with a width of 40 nm, as shown in Figure 9. According to the table above (Table 1) a weak but undesired spectral line does, however, occur at 1005 nm.

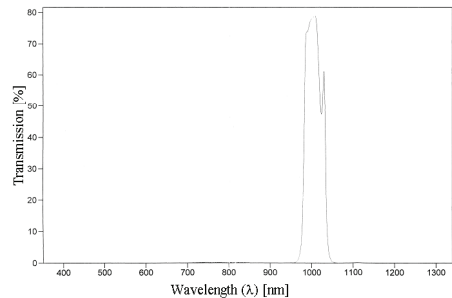


Figure 9. The transmission of the chosen near infrared bandpass interference filter at 1010 nm and width 40 nm.

The purpose of the band pass filter is to block the undesired radiation from the arc. The radiation is neither desired from the arc, nor from the electrode. However, the radiation from the tungsten electrode tip is not characterized by spectral lines as the arc radiation, but by a Planck blackbody radiation. The temperature at the tip of the electrode is during the welding process approximately 3000 °C.

The radiation from the electrode tip will, therefore, always at any wavelength be stronger than the radiation from the plate (Figure 3). It is, therefore, not possible to use the same filtration technique as used to off-filtrate the undesired plasma radiation from the arc. However, if the stick out of the electrode is small and the position of the camera is high the gas nozzle will shield the camera from direct radiation from the electrode, as shown in Figure 10. This will protect the camera from direct radiation from the electrode and minimize the risk of smears effect* on the chip.

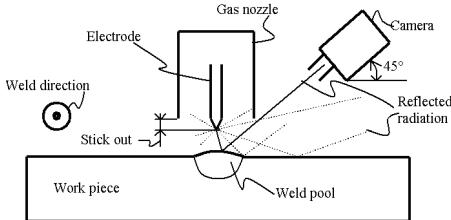


Figure 8. Direct radiation from the electrode tip is shielded by the gas cup.

However, the welding bead and the plate surface will reflect a substantial part of the radiation into the camera. To minimize the noise from the undesired reflection from the electrode, one must pick the position of the camera with thoughtfulness. When measuring on the temperature in front or at the tail of the welding pool, the camera should be placed at the side of the welding gun orthogonal to the welding direction (Figure 10). At this position the noise from reflection of the electrode (and the arc) is minimal. Opposite, when measuring the temperature at the side of the weld-pool one should place the camera in front of or behind the gun to avoid most reflection.

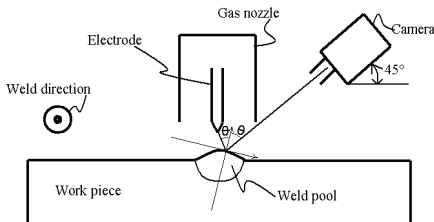


Figure 9. When the angle θ is 56 degrees the reflection is in theory completely off-filtrated by use of an interference filter.

To minimize the undesired reflected radiation from the electrode even further, an interference filter only passing through light with a selected polarization has been applied to the optical setup. This eliminates some of the reflected radiation and by Brewster's law [5] it is possible to calculate an angle θ where the reflected radiation is fully polarized and therefore theoretically may be fully blocked by the interference filter. This angle θ is approximately 56 degrees when the atmosphere is Argon and the reflection plate is Iron (Figure 9). To obtain the highest effect

* Smears effect is the capacity coupling, which arises when the CCD chip is over-exposed. The "smears" effect is visible as lines in the images.

possible of the interference filter, the angle of the camera should therefore be 34 degrees. Such a sharp angle would, however, give very deform images. It is therefore chosen to place the camera in an angle of 45 degrees.

Behind the interference filter and band pass filter a proper lens is placed, which is coated to allow penetration of a small amount of infrared waves. Finally, to minimize the amount of diffuse waves in the optical setup, a 1 mm pinhole has been placed in front of the optic. The distance from the lens to object (the weld pool) is in this setup 400 mm.

Calibration. By measuring the radiation at the border of the weld pool where the temperature is expected to be approximately 1510 °C, one camera calibration fix temperature point is given. The additional calibration is based on the theoretical radiation (Eq. 1) fitted to this fixed temperature point.

Results and Discussion.

In the following, the images generated by the developed camera are compared to thermal simulations generated by the Finite Element planning system. The comparison is made on the basis of the width of the weld and the gradients at the side of the weld-pool, only, as these are the crucial parameters in avoiding welding defects like e.g. lack of fusion and/or penetration. The calibration of the Finite Element model in the offline planning system has therefore also been based on macro cross sections which the simulation model has been calibrated to fit the height and the width of a welding current of 143 A. In this comparison no interference filter was used.

The experiment to be compared was made under the following conditions (Table 2).

Current	250 [A]
Travel speed	4.5 [mm/sec] (no weaving)
Material type	Grade S235
Plate thickness	6 [mm]
Work angle and Travel angle	0 [°]
Tip to plate distance	2.7 [mm]
Camera position	Behind the welding process
Camera angle	45 [°] to the plate

Table 2. Constant weld parameters used in the present welding experiment.

Below, a picture taken by the camera is figured (Figure 12). This picture is taken under the above given conditions (Table 2), but from the side of the welding process. In this picture the white area is the area where the camera pixels are saturated. The tail of the weld pool can be seen to the left. The black cone in and below the weld is the gas nozzle and the white light above is undesired reflected radiation, mainly from the electrode.

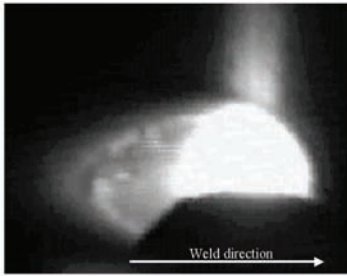


Figure 10. Image taken from the side of the welding. This picture has not yet been calibrated to fit a temperature scale.

The camera images to be shown in the following are calibrated and visualized from 1200 to 1600 °C, and to avoid undesired reflected radiation at the side of the welding the camera has been placed behind the welding process.

The calibrated image of the welding to be compared to the simulated temperature profile is shown below (Figure 13). Figure 10

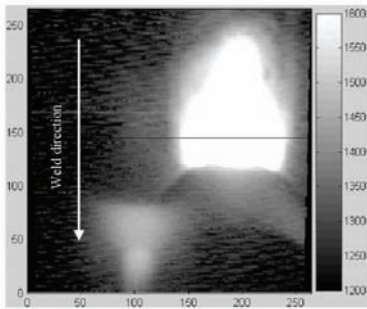


Figure 11. Calibrated image taken by the described camera. The scale of the abscissa and the ordinate is 0.1 [mm]. The temperature scale at the right goes from 1200 to 1600 °C.

The temperature profile along the black line in the figure above (Figure 13) is plotted below in . This picture is based on ten plots generated from ten images taken in a row at 10 Hz. One plot is laying below the nine other plots. This plot was made approximately 0.05 second after the arc was turned off. The temperatures below 1375 °C is dominated by noise due to the sensitivity of the camera. The scale of the abscissa is 0.1 mm and the scale of the ordinate is in °C.

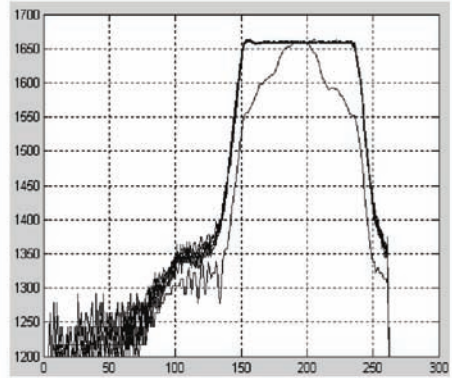


Figure 12. The temperature distribution across the weld along the black line sketched in Figure 13.

The width of the weld at 1510 °C, which is set to be the melt temperature, is when the arc is on measured to be 10.2 mm and 9.1 mm 0.05 sec after the arc has been shut off. The distance in direction at the black line from where the temperature is 1500 to where it is 1400 °C is in both cases measured to be 0.65 mm. This measure is here designated the gradient. Here, it is obvious that the arc despite the filtration has a certain impact on the measurement.

The analogous but simulated weld temperature profile is figured below in Figures 15 and 16.

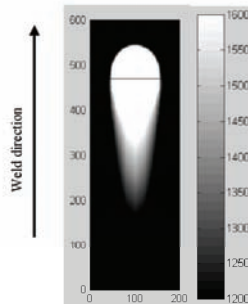


Figure 13. Simulation of the welding to be compared i.e. according to the parameters in . The scale of the abscissa and the ordinate is 0.1 mm. The temperature scale at the right goes from 1200 to 1600 °C as in .

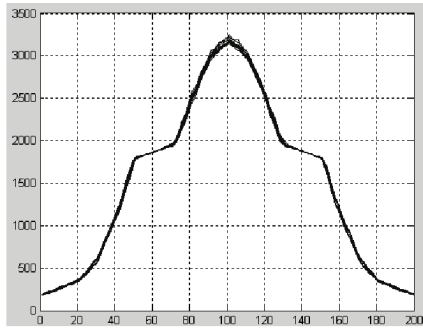


Figure 12. The temperature distribution across the weld along the black line sketched in Figure 15.

Figure 12 is based on ten plots generated from ten images taken in a row at 10 Hz. The scale of the abscissa is 0.1 mm and the scale of the ordinate is in degrees Celsius. Remark that the temperature scale unlike the previous figures goes from 0 to 3500 °C. The shape of the curve above 1800 °C is mainly due to the form of the heat-source and weld pool models.

The width at 1510 °C of the modelled weld is here measured to be 11.5 mm. The distance from where the temperature is 1500 to where it is 1400 °C is measured to be 0.15 mm and as before designated the gradient.

The width of the simulated weld (11.5 mm) and the width measured by the camera (10.2 mm) is fairly equal. The width measured by the camera is, however, rather disturbed by the arc and approximately 0.05 second after turning off the arc the measured width of the weld shrinks to 9.1 mm, which is in complete accordance with a macro cross sections made subsequently. It is therefore concluded that the filtration used in the camera is only partly sufficient for measuring the width of the weld-pool measuring close to the centre of the arc.

The gradients measured by the distance from where the temperature is 1500 to the temperature is 1400 °C was for the simulated weld measured to be 0.15 mm and for the welding measured by the camera measured to 0.65 mm. This inconsistency might be due to the disturbing arc, but measuring the gradient after the arc has been turned off did not seem to change the gradient (Figure 11). Based on a similar comparison of the gradients at the tail of the weld-pool, it was found that the deviation seemed to be due to the simulation model mainly. The deviation probably arises due to the values used for the heat conduction in the simulation model, which does not take into account the actual melting phase transition. The next step to be taken is, therefore, to improve the model by a more sophisticated weld-pool model and hereby achieve a more true view of the dynamic temperature distribution.

The noise from the arc was acknowledged to be a problem close to the centre of the arc where the intensity of the arc is highest. Camera measurements of the temperatures behind the tail of the weld-pool were in this paper, because of limited calibration of the simulation model, not compared to the simulation. However, measurements of the gradients and temperatures behind the tail of the weld-pool showed that the disturbance of the arc behind the tail was minimal.

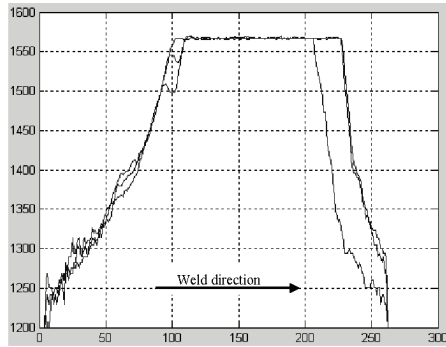


Figure 13. The temperature distribution along the centre of the welding taken with the camera positioned on the side as in Figure 12.

The figure above () is based on three plots generated from three images taken in a row at 10 Hz. The last plot is laying below the two other plots. This plot shows the temperatures approximately 0.05 second after the arc was turned off. In the present plot the temperatures below 1250 °C are dominated by noise due to the sensitivity of the camera. The scale of the abscissa is 0.1 [mm] and the scale of the ordinate is in Degrees Celsius. The figure shows that the arc has a large impact on the temperature measurement in front of the weld, but virtually no effect on the temperatures behind the molten tail. Based on the present camera it is therefore recommendable to build a controller based on temperature feedback of areas behind the molten tail of the weld-pool.

Summary and Conclusion

A camera was developed capable of measuring the temperature profile of GTAW welding in the range close to the arc. The purpose of the camera is to capture the surface temperature profile of the weld in progress in order for the control system to compare it to an analogous temperature profile state obtained by simulation. An offline planning system which, by use of a finite element system models the internal and surface temperature profile of the given work-piece, performs the state simulation.

Though deviations for both the developed camera and the simulation were identified, a promising correspondence was demonstrated. The deviation was concluded to be due to a lacking filtration of the arc and limitations to the simulation model of the offline planning system. It was shown that measurements behind the tail of the weld-pool could be made with virtually no disturbance from the arc. Based on the correspondence between the simulated and the measured surface temperature profile it is estimated possible to build a real-time system for control of the welding process, which is based on offline generated temperature trajectory reference as it was described in the introduction. Although the potential of the technique for real-time control of robotic arc welding looks good, further research and development work is needed to assess its viability.

References

1. H. C. Kjeldsen and H. Holm, *A reference architecture for design of an industrial temperature feedback welding control system*, Innovation and Technology for the New Millennium, Proceedings of the Ninth International Manufacturing Conference, Vol. 2, pp.237-238 (2000)
2. C. B. Terp, H. Holm, J. H. Hoeyer, H. H. Nielsen and J. Dam, *Welding Process Control Based on a Numerical Model and State-Space Techniques*, IASTED International Conference Modelling, Identification and Control, 265-268 (1999).
3. *American Institute of Physics Handbook*, Second edition.
4. *CRC Handbook of Chemistry and Physics*, A Ready-Reference Book of Chemical and Physical Data, 60th edition 1979-1980, ISBN:0-8493-0460-8.
5. F. L. Pedrotti and L. S. Pedrotti, *Introduction To Optics*, Second edition, ISBN: 0-13-016973-0.
6. C. C. Doumanidis (1998), *Thermal Modelling and Adaptive Control of Scan Welding*, Welding Journal November, 465-476.
7. Kevin L Moore et al., *Annual Report, FY95/96: Advanced Welding Control Project, INEL URC Project No. G22*, June 1996, Measurement and Control Engineering Research Center, College of Engineering, Idaho State University, Pocatello, Idaho 83209, USA.
8. Kevin L Moore et al., *Annual Report, FY97: Advanced Welding Control Project, INEL URC Project No. G22*, July 1997, Measurement and Control Engineering Research Center, College of Engineering, Idaho State University, Pocatello, Idaho 83209-8060, USA.
9. R. Kovacevic, Y.M Zhang, S. Ruan, *Sensing and Control of Weld Pool Geometry for Automated GTA Welding*, Transaction of the ASME, Journal of Engineering for Industry, Vol.117, pp 210-222 May 1995.
10. R. Kovacevic, Z.N. Cao, Y.M. Zhang, *Role of Welding Parameters in Determining the Geometrical Appearance of Weld Pool*, Transactions of the ASME, Journal of Engineering Materials and Technology, October 1996, Vol 118, pp 589-595.

M. Examples of Joints

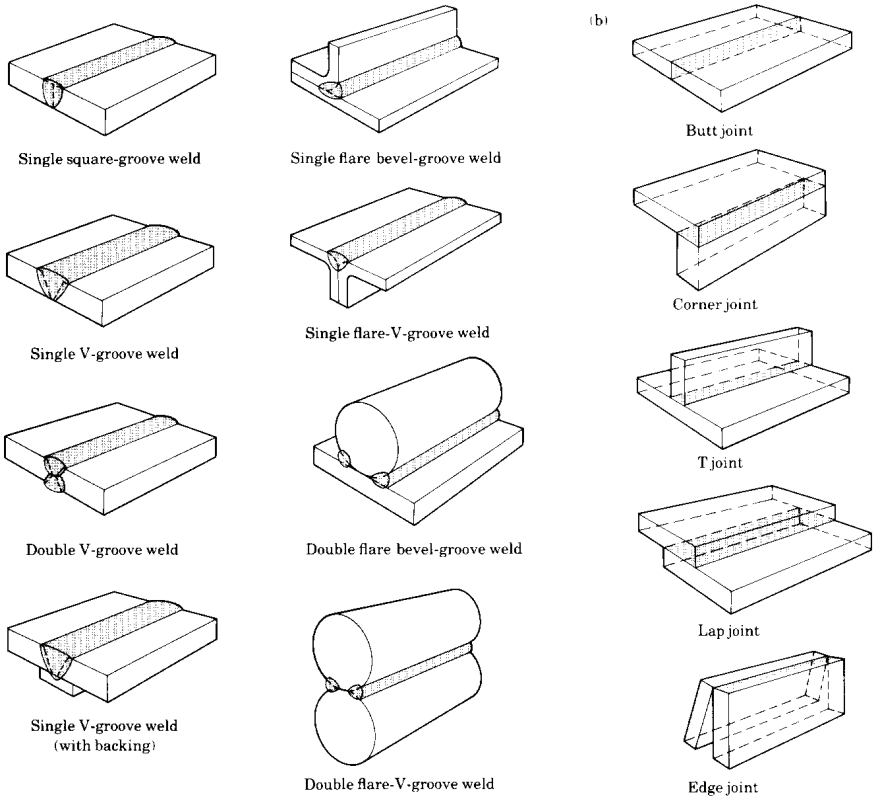


Figure M-1 Examples of joints [Kalpakjian, 1995, p.857].

N. Data Sheets of the Chosen Camera



CV-M10 BX/RS ***Progressive Scan Monochrome Camera***



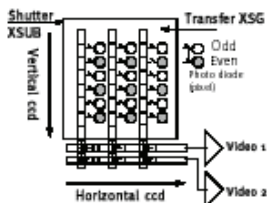
- CCR and EIA versions. EIA versions meet VGA format
- 1/2" Hyper HAD CCD with square pixels
- High resolution – horizontal 600 TV lines, vertical 575 TV lines
- Full frame read-out from a single frame shutter pulse
- Single channel progressive full frame in 1/25 sec. or 1/30 sec.
- 2-channel interlaced or 2-channel non-interlaced in 1/50 sec. or 1/60 sec.
- Fast asynchronous reset – frame or field shutter
- Shutter 1/60 to 1/20,000 or 1/20,000 to 1/800,000 sec.
- Long-time integration 2 to 16 fields
- Internal, external, HD, VD or random synchronization
- Set-up by RS 232C (RS version) or switches (BX version)
- RS 232C interface
- Windows 95/NT set-up software
- Software includes DLL and LIB files for easy integration

The leading manufacturer in high performance camera solutions

CV-M10 BX/RS CAMERA SERIES

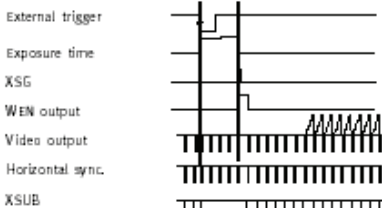
Progressive scan CCD sensor

In the progressive scan CCD sensor the number of vertical transfer cells are equal to the total number of sensing photo diodes. The integrated charge in the diodes for both odd and even fields is at time XSG transferred as a full frame to the vertical register. From here the frame is read out with the double vertical speed to two horizontal registers. A full frame as a result of the same shutter pulse can be read out as two fields, each through its own output. By combining the two fields from output 1 and 2 in a frame grabber 50 or 60 frames are achieved. In non-interlaced scan mode, output 1 will be a progressive full frame (Line 1 - 2 - 3 - 4 etc.). It will take $\frac{1}{25}$ or $\frac{1}{30}$ second.



Asynchronous triggered shutter

The shutter function in the CCD sensor is done by draining all photo diodes in parallel with the XSUB pulse synchronized to HD. A last XSUB is generated from the negative external trigger pulse. This pulse will reset and synchronize HD in the camera. The selected exposure time will then start, and an image will be charged in the photo diodes. The selected shutter time will stop with a XSG and video enable pulse out 1 HD long (WEM). The WEM pulse indicates the beginning of the video read-out. The composite video signal is without V-sync. The WEM pulse indicates the start and top of the image. The video frame or field has to be read out prior to supplying a new trigger pulse.



Frame grabber interface – single channel mode

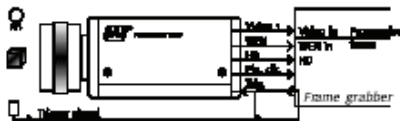
This application shows a typical set-up for capturing a fast moving object and transfer it to a frame grabber as a full progressive scanned frame. It will take $\frac{1}{25}$ or $\frac{1}{30}$ second. The frame grabber needs an input for the WEM pulse for vertical sync.

The horizontal sync. is taken from the HD out or separated from the composite video signal from the camera.

A trigger sensor will detect the arrival of an object in the field of view and start the selected shutter time. By using the pixel clock (user option) to synchronize the frame grabber total jitter-free operation is achieved.

Set-up
Asynchronous trigger shutter.
Non-interlaced scan.
Video 1 output.

Result
1 full progressive scanned frame in frame grabber in $\frac{1}{25}$ sec. or $\frac{1}{30}$ sec.



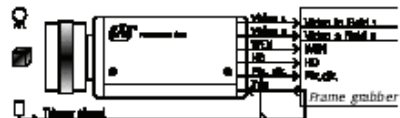
Frame grabber interface – dual channel mode

This set-up shows an application where a progressive scanned frame consisting of 2 interlaced fields as a result of one shutter pulse is transferred to 2 field stores. The 2 fields need to be combined in the computer. This set-up makes use of the optional pixel clock output from the camera for a jitter-free image digitizing.

With this set-up a full progressive scanned frame is transferred to the computer in $\frac{1}{50}$ second.

Set-up
Asynchronous trigger shutter.
If necessary through the frame grabber.
Interlaced scan.
Video 1 and video 2 output.

Result
2 interlaced fields in 2 field grabbers in $\frac{1}{50}$ second.
The pixel clock provides jitter-free image acquisition.
For applications with sub-pixel accuracy.



Software control for CV-M30 RS Camera

The unique WindowsNT based camera control tool makes it easy to control the M30 RS camera from a standard PC. The program includes an on-screen help function. Supplied DLL and LIB files with documentation allow easy integration of the camera control in custom application.

System requirements:

- 486 processor
- 1 MB free disk space
- Windows 95/NT (incl. DLL)
- Windows 3.1 (excl. DLL)
- Up to 9 com ports available
- 9600 bps



Interface cable (PC to camera)

CAMERA 6 PIN	COM PORT ON PC 9 PIN	25 PIN D
1 CD	8	
4 DTR	20	
6 DSR	6	
1 TXD	2 RXD	3
2 RXD	3 TXD	2
3 GND	5 GND	7
4	7 RTS	4
5	8 CTS	5
6	9 CI	22

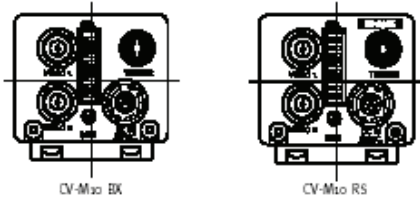
Connection description

Male Hirose HR30-7P-6P

Pin 1 TXD (RS only)
 Pin 2 RXD (RS only)
 Pin 3 Ground
 Pin 4 N.C.
 Pin 5 Trigger input
 Pin 6 WEN pulse output



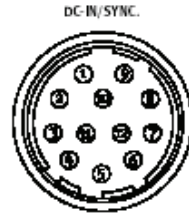
Back view



Connection description

Male Hirose HR10A-10P-12P

Pin 1 Ground
 Pin 2 +12V DC power
 Pin 3 Ground
 Pin 4 Video 1 output
 Pin 5 Ground
 Pin 6 Ext. HD (HD output)*
 Pin 7 Ext. VD (VD/output)*
 Pin 8 Ground
 Pin 9 Video-2 output (pixel clock output)*
 Pin 10 Ground
 Pin 11 +12V DC power
 Pin 12 Ground

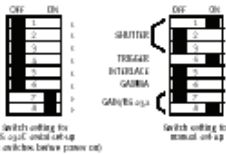


* Option

Setting switch

CV-M30 RS CV-M30 BX

SW 1 on rear panel



SW 2	SW 3	SW 4
0: OFF	0: OFF	0: OFF
1: 1/2000	1: 1/2000	1: 1/2000
2: 1/1000	2: 1/1000	2: 1/1000
3: 1/500	3: 1/500	3: 1/500
4: 1/250	4: 1/250	4: 1/250
5: 1/125	5: 1/125	5: 1/125
6: 1/60	6: 1/60	6: 1/60
7: 1/30	7: 1/30	7: 1/30
8: 1/15	8: 1/15	8: 1/15
9: 1/8	9: 1/8	9: 1/8
10: 1/4	10: 1/4	10: 1/4
11: 1/2	11: 1/2	11: 1/2
12: 1	12: 1	12: 1
13: 1/2	13: 1/2	13: 1/2
14: 1/4	14: 1/4	14: 1/4
15: 1/8	15: 1/8	15: 1/8
16: 1/16	16: 1/16	16: 1/16
17: 1/32	17: 1/32	17: 1/32
18: 1/64	18: 1/64	18: 1/64
19: 1/128	19: 1/128	19: 1/128
20: 1/256	20: 1/256	20: 1/256
21: 1/512	21: 1/512	21: 1/512
22: 1/1024	22: 1/1024	22: 1/1024
23: 1/2048	23: 1/2048	23: 1/2048
24: 1/4096	24: 1/4096	24: 1/4096
25: 1/8192	25: 1/8192	25: 1/8192
26: 1/16384	26: 1/16384	26: 1/16384
27: 1/32768	27: 1/32768	27: 1/32768
28: 1/65536	28: 1/65536	28: 1/65536
29: 1/131072	29: 1/131072	29: 1/131072
30: 1/262144	30: 1/262144	30: 1/262144
31: 1/524288	31: 1/524288	31: 1/524288
32: 1/1048576	32: 1/1048576	32: 1/1048576
33: 1/2097152	33: 1/2097152	33: 1/2097152
34: 1/4194304	34: 1/4194304	34: 1/4194304
35: 1/8388608	35: 1/8388608	35: 1/8388608
36: 1/16777216	36: 1/16777216	36: 1/16777216
37: 1/33554432	37: 1/33554432	37: 1/33554432
38: 1/67108864	38: 1/67108864	38: 1/67108864
39: 1/134217728	39: 1/134217728	39: 1/134217728
40: 1/268435456	40: 1/268435456	40: 1/268435456
41: 1/536870912	41: 1/536870912	41: 1/536870912
42: 1/1073741824	42: 1/1073741824	42: 1/1073741824
43: 1/2147483648	43: 1/2147483648	43: 1/2147483648
44: 1/4294967296	44: 1/4294967296	44: 1/4294967296
45: 1/8589934592	45: 1/8589934592	45: 1/8589934592
46: 1/17179869184	46: 1/17179869184	46: 1/17179869184
47: 1/34359738368	47: 1/34359738368	47: 1/34359738368
48: 1/68719476736	48: 1/68719476736	48: 1/68719476736
49: 1/137438953472	49: 1/137438953472	49: 1/137438953472
50: 1/274877906944	50: 1/274877906944	50: 1/274877906944
51: 1/549755813888	51: 1/549755813888	51: 1/549755813888
52: 1/1099511627776	52: 1/1099511627776	52: 1/1099511627776
53: 1/2199023255552	53: 1/2199023255552	53: 1/2199023255552
54: 1/4398046511104	54: 1/4398046511104	54: 1/4398046511104
55: 1/8796093022208	55: 1/8796093022208	55: 1/8796093022208
56: 1/17592186044416	56: 1/17592186044416	56: 1/17592186044416
57: 1/35184372088832	57: 1/35184372088832	57: 1/35184372088832
58: 1/70368744177664	58: 1/70368744177664	58: 1/70368744177664
59: 1/140737488355328	59: 1/140737488355328	59: 1/140737488355328
60: 1/281474976710656	60: 1/281474976710656	60: 1/281474976710656
61: 1/562949953421312	61: 1/562949953421312	61: 1/562949953421312
62: 1/1125899906842624	62: 1/1125899906842624	62: 1/1125899906842624
63: 1/2251799813685248	63: 1/2251799813685248	63: 1/2251799813685248
64: 1/4503599627370496	64: 1/4503599627370496	64: 1/4503599627370496
65: 1/9007199254740992	65: 1/9007199254740992	65: 1/9007199254740992
66: 1/18014398509481984	66: 1/18014398509481984	66: 1/18014398509481984
67: 1/36028797018963968	67: 1/36028797018963968	67: 1/36028797018963968
68: 1/72057594037927936	68: 1/72057594037927936	68: 1/72057594037927936
69: 1/144115188075855872	69: 1/144115188075855872	69: 1/144115188075855872
70: 1/288230376151711744	70: 1/288230376151711744	70: 1/288230376151711744
71: 1/576460752303423488	71: 1/576460752303423488	71: 1/576460752303423488
72: 1/1152921504606846976	72: 1/1152921504606846976	72: 1/1152921504606846976
73: 1/2305843009213693952	73: 1/2305843009213693952	73: 1/2305843009213693952
74: 1/4611686018427387904	74: 1/4611686018427387904	74: 1/4611686018427387904
75: 1/9223372036854775808	75: 1/9223372036854775808	75: 1/9223372036854775808
76: 1/18446744073709551616	76: 1/18446744073709551616	76: 1/18446744073709551616
77: 1/36893488147419103232	77: 1/36893488147419103232	77: 1/36893488147419103232
78: 1/73786976294838206464	78: 1/73786976294838206464	78: 1/73786976294838206464
79: 1/147573952589676412928	79: 1/147573952589676412928	79: 1/147573952589676412928
80: 1/295147905179352825856	80: 1/295147905179352825856	80: 1/295147905179352825856
81: 1/590295810358705651712	81: 1/590295810358705651712	81: 1/590295810358705651712
82: 1/1180591620717411303424	82: 1/1180591620717411303424	82: 1/1180591620717411303424
83: 1/2361183241434822606848	83: 1/2361183241434822606848	83: 1/2361183241434822606848
84: 1/4722366482869645213696	84: 1/4722366482869645213696	84: 1/4722366482869645213696
85: 1/9444732965739290427392	85: 1/9444732965739290427392	85: 1/9444732965739290427392
86: 1/18889465931478580854784	86: 1/18889465931478580854784	86: 1/18889465931478580854784
87: 1/37778931862957161709568	87: 1/37778931862957161709568	87: 1/37778931862957161709568
88: 1/75557863725914323419136	88: 1/75557863725914323419136	88: 1/75557863725914323419136
89: 1/151115727451828646838272	89: 1/151115727451828646838272	89: 1/151115727451828646838272
90: 1/302231454903657293676544	90: 1/302231454903657293676544	90: 1/302231454903657293676544
91: 1/604462909807314587353088	91: 1/604462909807314587353088	91: 1/604462909807314587353088
92: 1/1208925819614629174706176	92: 1/1208925819614629174706176	92: 1/1208925819614629174706176
93: 1/2417851639229258349412352	93: 1/2417851639229258349412352	93: 1/2417851639229258349412352
94: 1/4835703278458516698824704	94: 1/4835703278458516698824704	94: 1/4835703278458516698824704
95: 1/9671406556917033397649408	95: 1/9671406556917033397649408	95: 1/9671406556917033397649408
96: 1/19342813113834066795298816	96: 1/19342813113834066795298816	96: 1/19342813113834066795298816
97: 1/38685626227668133590597632	97: 1/38685626227668133590597632	97: 1/38685626227668133590597632
98: 1/77371252455336267181195264	98: 1/77371252455336267181195264	98: 1/77371252455336267181195264
99: 1/154742504910672534362390528	99: 1/154742504910672534362390528	99: 1/154742504910672534362390528
100: 1/309485009821345068724781056	100: 1/309485009821345068724781056	100: 1/309485009821345068724781056
101: 1/618970019642690137449562112	101: 1/618970019642690137449562112	101: 1/618970019642690137449562112
102: 1/1237940039285380274899124224	102: 1/1237940039285380274899124224	102: 1/1237940039285380274899124224
103: 1/2475880078570760549798248448	103: 1/2475880078570760549798248448	103: 1/2475880078570760549798248448
104: 1/4951760157141521099596496896	104: 1/4951760157141521099596496896	104: 1/4951760157141521099596496896
105: 1/9903520314283042199192993792	105: 1/9903520314283042199192993792	105: 1/9903520314283042199192993792
106: 1/1980704062856608439838586784	106: 1/1980704062856608439838586784	106: 1/1980704062856608439838586784
107: 1/3961408125713216879677173568	107: 1/3961408125713216879677173568	107: 1/3961408125713216879677173568
108: 1/7922816251426433759354347136	108: 1/7922816251426433759354347136	108: 1/7922816251426433759354347136
109: 1/15845632502852875518708694272	109: 1/15845632502852875518708694272	109: 1/15845632502852875518708694272
110: 1/31691265005705751037417388544	110: 1/31691265005705751037417388544	110: 1/31691265005705751037417388544
111: 1/63382530011411502074834777088	111: 1/63382530011411502074834777088	111: 1/63382530011411502074834777088
112: 1/126765060022823004149669554176	112: 1/126765060022823004149669554176	112: 1/126765060022823004149669554176
113: 1/253530120045646008299339108352	113: 1/253530120045646008299339108352	113: 1/253530120045646008299339108352
114: 1/507060240091292016598678216704	114: 1/507060240091292016598678216704	114: 1/507060240091292016598678216704
115: 1/1014120480182584033197356433408	115: 1/1014120480182584033197356433408	115: 1/1014120480182584033197356433408
116: 1/2028240960365168066394712866816	116: 1/2028240960365168066394712866816	116: 1/2028240960365168066394712866816
117: 1/4056481920730336132789425733632	117: 1/4056481920730336132789425733632	117: 1/4056481920730336132789425733632
118: 1/8112963841460672265578851467264	118: 1/8112963841460672265578851467264	118: 1/8112963841460672265578851467264
119: 1/16225927682921344531157702934528	119: 1/16225927682921344531157702934528	119: 1/16225927682921344531157702

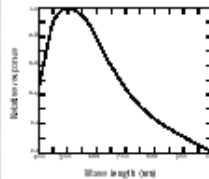
Specifications for CV-M10

Specifications	Remarks	CV-M10C	CV-M10E
Scanning system		625 lines 25 frames/sec.	525 lines 30 frames/sec.
CCD sensor		Monochrome 1/2" Hyper HAD II progressive scan CCD	
Sensing area		6.4 mm (H) x 4.8 mm (V)	
Picture elements		782 (H) x 582 (V)	659 (H) x 494 (V)
Video output elements		767 (H) x 575 (V)	648 (H) x 486 (V)
Cell size		8.3 x 8.3 μm	9.0 x 9.0 μm
Resolution (horizontal)		600 TV lines	500 TV lines
Resolution (vertical)		575 TV lines	486 TV lines
Sensitivity		0.8 Lux, F1.4	
SN ratio		35 dB (AGC off, Gamma 1)	
Video output		Composite VBS signal 1.0 Vpp, 7.5 Ohm	
Video 1 interlaced O-E-O		1 frame 1/25 sec.	1 frame 1/30 sec.
Video 2 interlaced E-O-E		1 frame 1/25 sec.	1 frame 1/30 sec.
Video 1+2 interlaced		1 progr. fr. 1/50 sec.	1 progr. fr. 1/60 sec.
Video 1 non-interlaced		1 progr. fr. 1/25 sec.	1 progr. fr. 1/30 sec.
Synchronization		Int. X-tal, Ext. HDV/D or random trig.	
HDV/D sync. input		1V, 75 Ohm	
Trigger input		12 μsec. 4 msec. 4V, 75 Ohm	
HDV/D or HDV/D output	option	4V	
Pixel clock output	option	4V	
Controls and functions	BK	RS	
	SW	SW	RS 232
Shutter mode - Full version only	*	*	Off - Normal - High - Long time exp.
Gamma	*	*	0.45 - 1
Gain	*	*	Fixed - Manual - Auto.
Scanning	*	*	Non-interlaced - Interlaced
Reset mode	*	*	Normal - Random trig.
Shutter normal	*	*	1/50 to 1/10,000 sec. in 8 steps
Shutter high	*	*	1/20,000 to 1/800,000 sec. in 8 steps
Long time integration	*	*	2 - 4 - 6 - 8 - 10 - 12 - 14 - 16 fields
Manual gain	*	*	Potentiometer on rear plate
Gain 1		*	Relative 0 - 255
Gain 2		*	Relative 0 - 255
Set-up 1		*	Relative 0 - 255
Set-up 2		*	Relative 0 - 255
White clip 1		*	Relative 0 - 255
White clip 2		*	Relative 0 - 255
V sub (Full version only)		*	Relative 0 - 255
File		*	Load to and from file
Memory		*	Restore and store user set-up
Memory		*	Restore factory set-up
Operating temperature			-5°C to +45°C
Power			12V DC ±10%, 0.5 Amp.
Lens mount			C-mount
Dimensions			40 x 50 x 80 mm (HxWxD)
Weight			245 g

Ordering Information

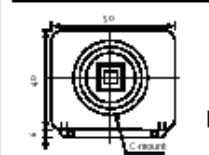
- CV-M10BK 1/2" Monochrome Progressive Scan Camera, CCR.
- CV-M10E 1/2" Monochrome Progressive Scan Camera, EIA.
- CV-M10RS 1/2" Monochrome Progressive Scan Camera, CCR, RS 232C.
- CV-M10RS 1/2" Monochrome Progressive Scan Camera, EIA, RS 232C.
- Cable for RS 232C Interface.

Spectral Sensitivity



Dimensions

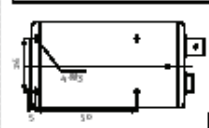
Front view



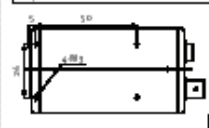
Side view



Bottom view



Top view



JAI Corporation, Japan
 German Industry Center
 3-18-1 Nakano, Midori-ku
 Yokohama,
 Kanagawa 226-0005, Japan
 Phone +81 45 993 5400
 Fax +81 45 993 0142
 www.jai-corp.co.jp

RIAS, Denmark
 Camera Solutions
 Produktionsvej 1, 2600 Glostrup
 Copenhagen, Denmark
 Phone +45 4471 8858
 Fax +45 4475 0850
 www.jai.dk

JAI UK Ltd., England
 Audley House
 Northridge Road
 Bredbourne
 Heris WPA, WY, England
 Phone +44 1432 879 659
 Fax +44 1432 879 288



THE MECHANIC COMPANY

Visit our web site on www.jai.dk